Republic of Iraq
Ministry of Higher Education
and Scientific Research
University of Babylon
College of Engineering
Department of Mechanical Engineering

Improving the Performance of a Double Pipe Heat Exchanger Using (MgO-CMC/Water) Nanofluid with a Two-phase Flow

A Thesis
Submitted to the College of Engineering / University of Babylon in Partial Fulfillment of the Requirements for the Degree of Doctorate of Philosophy in Engineering / Mechanical Engineering / Power

By

Mustafa Mohammed Gabir Radaid

Supervised by

Prof. Dr. Dhirgham A. AL Khafaji

2023 A.D **1444 A.H**

بسم الله الرحمن الرحيم

انَّ الَّذينَ آمَنُوا وَعَمِلُوا الصَّالِحَاتِ إِنَّا لَا نُضِيعُ
أَجْرَ مَنْ أَحْسَنَ عَمَلًا

صدق الله العلي العظيم

سورة الكهف (30)

DEDICATION

TO

My Mother, Wife and Children

My Supervisor

To everyone who helped me

With Respect and Love

Supervisors Certificate

*I certify that this thesis entitled (**Improving the Performance of a Double Pipe Heat Exchanger by Using (MgO – CMC / water) Nanofluid with a Two-phase Flow**) and submitted by the student (**Mustafa Mohammed Gabir Radaid**) was prepared under my supervision at the Department of Mechanical Engineering/College of Engineering/University of Babylon as a part of the requirements for the degree of Doctorate of philosophy in Mechanical Engineering.*

Signature:
Supervisor: **Prof. Dr. Dhirgham A. Alkhafaji**
Date: / /

Head of Department Certificate

I certify that this thesis mentioned above has been completed in Mechanical Engineering in the College of Engineering/ University of Babylon

Signature:
Head of Department: **Asst. Prof. Dr. Samer Abdulhaleem**
Date: / /

Examination Committee Certification

We certify the we have read thesis entitled "Improving the Performance of a Double Pipe heat Exchanger Using (MgO-CMC/Water) Nanofluid with a Two-phase Flow" and as an examining committee, examined the student "Mustafa Mohammed Gabir", in its content and that in our opinion it meets the standard of thesis for the degree of Doctorate of Philosophy in Mechanical Engineering

Prof. Dr. Dhirgham A. Alkhafaji
Supervisor
Date:

Asst. Prof. Dr. Rehab Noor Mohammed
Member
Date:

Prof. Dr. Nizar Jawad Hadi
Member
Date:

Prof. Dr. Hameed Kadhem Hamzah
Member
Date:

Prof. Dr. Hayder K. Rashid
Member
Date:

Prof. Dr. Ahmed Waheed Mustafa
Chairman
Date:

Approval of Mechanical Engineering Department
Asst. Prof. Dr. Samer Abdulhaleem
Date:

Approval of the College of Engineering
Prof. Dr. Laith Ali Abdul-Rahaim
Date:

ACKNOWLEDGMENTS

First of all, I would like to praise and thank ***GOD*** *for helping me to complete this thesis.*

I wish to express my gratefulness to my supervisor ***Prof. Dr. Dhirgham A. AL Khafaji*** *for his continuous supervision, positive discussions and important ideas through this research work.*

I would like to present my gratitude to all staff of ***the Department of Mechanical Engineering****, University of Babylon for their cooperation and help to complete this work.*

Special thanks to ***my mother and my wife*** *for their love and support during the period of preparing this work.*

Mustafa Mohammed
2023

ABSTRACT

A nanofluid with different concentrations of Magnesium oxide (MgO) and carboxymethyl cellulose (CMC) is examined in a horizontal direction U-bend double pipe heat exchanger to improve the performance for parallel and counter flow under the effect of single and two-phase flow. The study contributes for volume flow rate (8, 10, 12 and 14) L/min for pure water, Water-CMC fluid at CMC concentrations (0.2% and 0.5%) by weight, Water-MgO fluid at MgO nanoparticles concentrations (0.125%, 0.25%, 0.5% and 1%) by volume, and Water-MgO-CMC fluid generate at the same previous concentrations.

When 24 L/min of water injected with (360, 420 and 460) L/hr of air in annular side, a two-phase flow recognized three types of flow regimes, bubbly, slug flow and stratified flow.

The experimental work is done by using a double pipe heat exchanger with U bend made out of two concentric pipes. The inner pipe is Copper pipe with inner and outer diameters of 20 and 22 mm, respectively, and the outer pipe is a Perspex with inner and outer diameters of 45 and 50 mm respectively. The experimental study also includes a preparation of the nanofluid and the measurement of hot fluid properties.

A CFD simulation is built based on the volume of fluid (VOF) model for multiphase flow using the commercial code ANSYS Fluent 2020 R1. This code is used to predict the temperature, pressure, velocity, and void fraction of two-phase flow along the U-bend double pipe heat exchanger. This study is numerically accomplished numerically by solving a set of partial differential equations, namely, the conservation of mass, momentum and energy. These equations are linearized, discretized, and solved by a finite volume method to obtain a detailed solution, including the required parameters in flow field, and validate with experimental data.

The results indicate that the convection heat transfer coefficient (h) increases by increasing CMC particles weight concentrations, MgO particles volume concentrations, and hot fluid volume flow rate. The convection heat transfer coefficient for parallel flow enhances from (2532.4) at a minimum flow rate of 8 L/min to (2771.71) at a maximum flow rate of 14 L/min. Moreover, adding 1% MgO vol. and 0.5% CMC wt. the convection heat transfer coefficient increases from (5062.57) at a minimum flow rate of 8 L/min to (5545.24) at a maximum flow rate of 14 L/min. The friction factor increases with the increase of CMC particles weight concentration, MgO particles volume concentration, and decreases with increasing a hot fluid volume flow rate.

Depending on the two-phase flow effect, the convection coefficient increases about 8% when air flow rate increases, and the effectiveness of heat exchanger increases about 9%. The overall heat transfer coefficient of a counter flow is 4-6% higher than that of a parallel flow with the addition of 1% MgO vol. and 0.5% CMC wt. to pure water.

Finally, a comparison is carried out between the numerical and experimental results for Newtonian fluid (pure water) at flow rate 8, 10, 12, and 14 L/min. There is an excellent agreement between the numerical and experimental results (with maximum deviation of 7% in Nusselt Number) of the present work along with quite good agreements in the trends and values of the results that extracted from CFD simulation of the present work with and obtained by significant researchers.

List of Contents

Chapter 3: Experimental Study

Chapter 4: Numerical Work

Chapter 5: Result and Discussion

Nomenclatures

Symbol	Meaning	Unit
A	Cross sectional area	m^2
C_p	Specific heat	J/kg.°C
C	Thermal capacity	J/kg s
D	Diameter	m
D_h	hydraulic diameter	m
d	inner pipe diameter	m
h	Convection heat transfer	$W/m^2.^oC$
k	Thermal conductivity	W/m.°C
L	Length of inner pipe	m
$\dot{m}$	Mass flow rate	kg/sec
P	Pressure	Pa
Q	Heat transfer rate	W
R	Radius	m
S	Entropy	J
T	Temperature	°C
U	Overall heat transfer coefficient	W/m.°C
v	Velocity	m/s
$\dot{V}$	Volume flowrate	m^3/s
n	Nanoparticles shape factor	-------

Greek Symbols

Symbol	Meaning	Unit
μ	Dynamic viscosity	(Pa.s)
φ	Nanoparticle's concentration	(%)
Δ	Denotes a difference or gradient	-------
ε	Effectiveness	-------
ρ	Density	(kg/m^3)

Subscripts

Symbol	Description
1-phf	One phase flow
2-phf	Two-phase flow
a	Air
ave	Average
bf	Base fluid
Calib	Calibration
CF	Counter flow
c	Cold fluid
cr	Critical
en	Environment
f	Fluid
h	Hot fluid
y	Hydraulic
i	Inner pipe
in	Inlet
max	Maximum
min	Minimum
nf	Nanofluid
Out	Outlet
p	Solid particle
PF	Parallel flow
re	Reading
s	Surface
Vf	Void fraction

Dimensionless Numbers

f	Friction Factor	$f = \frac{\Delta P}{\frac{L_i}{D_i} \times (\frac{v^2 \rho_{nf}}{2})}$
e	dimensionless exergy loss	$e = \frac{E}{T_e C_{min}}$
Nu	Nusselt number	$\mathrm{Nu} = \frac{h\,D}{k}$
Pr	Prandtl number	$Pr = \frac{\mu\,Cp}{k}$
Re	Reynolds number	$Re = \frac{\rho v D}{\mu}$

Abbreviations

Symbol	Description
CFD	Computation Fluid Dynamic
LMTD	Logarithmic Mean Temperature Difference
ANSYS	Analysis System

CHAPTER ONE

INTRODUCTION

CHAPTER ONE

INTRODUCTION

1.1 General Overview

One of the most popular forms of heat exchanger is the double-pipe model. Principle work of this type is that the hot fluid flows inside the inner pipe, where the cold fluid flows through the annular or vice versa. The direction of the fluid flow can be either parallel or counter through the heat exchanger.

With the help of the heat exchanger's heat transfer mechanism, heat is transported from one body or fluid stream to another. In order to compute the transfer of energy efficiently under controlled circumstances, designing a heat exchanger equipment is involved using heat transfer equations [1].

These types of heat exchanger are employed in sustainable energy application, industrial, and commercial field because of their various sizes, ease of use, manufacturing, and compactness. Conventional fluids, such as water, ethylene glycol, steam and refrigerant are commonly used as heat transfer working fluids. To improve this mechanism the heat transfer coefficient must be enhanced taking into account size and cost of the heat exchanger [2].

1.2 Heat Exchanger Improvement Techniques

Many techniques have been offered to enhance the heat transfer mechanism in a heat exchanger. Generally, these techniques are divided into three primary kinds as shown in table (1-1) [3].

1.2.1 Active Techniques

This method entails using an additional external need to enhance thermal energy transfer. Common models include reciprocating plungers, magnetic fields that implemented different types of turbulent flow, shear force-producing vibrations in the flow, and effects on electromagnetic fields. There are various factors to take into account when enhancing this method in double pipe heat exchangers [7].

Table (1-1): Sample of techniques used in research.

Authors	Structure	Technique
Zhen Zhang [4]	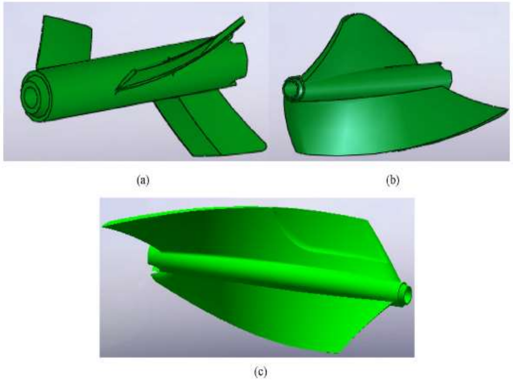	Active
Yadav [5]	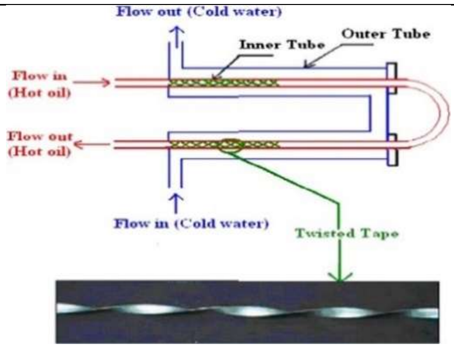	Passive
Duangthongsuk [6]		Compound

1.2.2 Passive Techniques

In a double pipe heat exchanger, they define this as the transfer of heat energy without the use of additional external force, and the condensation process demonstrates this method. The main principle of this approach is the changes in geometrical style, surface shape, and various types of addition [8].

1.2.3 Compound Technique

To improve results for various applications, compound techniques promote thermal energy exchange in double pipe heat exchangers. This style emphasizes the combination of active and passive technique. Hence, better modes from both active and passive techniques, such as fins, coils, and turbulators, should be used to acquire the best results from this technique [9].

1.3 Two Phase Flow

Engineering applications of two-phase flow have persisted over time, and with that, the demand for more precise data and a deeper comprehension of the phenomenon has grown. The simultaneous flow is related to a two-phase flow, such as the movement of air and water [10].

Gas-liquid two-phase flow is best described as the interactive motion of two different kinds of media. They are extremely important in many industrial applications. The knowledge of non-boiling two-phase, two-component (liquid and permanent gas) heat transfer is required. When a gas-liquid mixture flows in pipe, a variety of flow pattern may occur, depending primarily on flow rates, the physical properties of the fluids, and pipe inclination angle that reported [11].

Numerous significant technical applications, such as nuclear reactors, chemical plants, solar collectors, oil wells and pipelines, frequently use gas-liquid two-phase systems. Typically, when there is variation in pipe temperature with a slug or intermittent flow, which may actually be more harmful than a high absolute temperature, heat transfer coefficient must be understood for safety purposes.

1.3.1 Flow Phases

A phase is a simple state of matter, which can be a liquid, gas or solid flows in the pipe. A simple phase is the single substance (usually pure), while the complex phase has different matters, which are almost mixed. Multiphase flows can be subdivided into four categories which are illustrated [12] as: gas-solid, gas-liquid, liquid-solid, and three-phase flow.

Two-phase flow is categorized as follows [13,14]:

1. According to the matter of phase:
   - i. One component in two phases. (Steam-water flow)
   - ii. Two components in two phases. (Water-Air Flow)
2. According to the external wall state:
   - i. Adiabatic flow.
   - ii. Heating flow.
   - iii. Cooling flow.

1.3.2. Arrangement Two-Phase Flow in Pipe

Two-phase mixtures may be arrangement according to the position of pipe or duct which carries the flow which was presented [13] as:

1. Horizontal flow
2. Vertical flow (upwardly or downwardly).
3. Inclined flow (upwardly or downwardly).

1.3.3. Flow Patterns

When the two-phases flow together in the same stream (channel or pipe), many shapes of flow will be noticed, which are generally called "flow patterns". These patterns are dependent on many factors such as: pipe geometry, position of pipe, flow rate of phases, angle of inclination, nature of phases, and etc.

To predict which of the flow patterns exist in certain conditions in the flow, many investigators drew maps to locate that depending on flow conditions, geometry and position of pipe or duct, and types of phases when these flow through a pipe or duct. These maps of flow pattern which are described by chart have many lines to separate the consequent flow patterns [14].

1.3.4 Flow Patterns in Horizontal Systems

Flow patterns of gas and liquid in a horizontal tube are strongly influenced by gravity that acts to stratify the liquid to the bottom of the tube and the gas to the top. Co-current gas-liquid flow in horizontal pipes displays similar patterns to those for vertical flow; however, asymmetry is caused by the effect of gravity, which is most significant at low flow rates. The sequence of flow regimes identified [15] is shown in Figure (1-1). In the bubbly regime the bubbles are confined to a region near the top of the pipe. On increasing the gas flow rate, the bubbles become larger and coalesce to form long bubbles giving what is known as the plug flow regime. At still higher gas flow rates the gas plugs join to form a continuous gas layer in the upper part of the pipe. This type of flow, in which the interface between the gas and the liquid is smooth, is known as the stratified flow regime. Owing to the lower viscosity and lower density of the gas it will flow faster than the liquid. As the gas flow rate is increased further, the interfacial shear stress becomes sufficient to generate waves on the surface of the liquid producing the wavy flow regime. As the gas flow rate continues to rise, the waves, which travel in the direction of flow, grow until their crests approach the top of the pipe and, as the gas breaks through, liquid is distributed over the wall of the pipe. This is known as the slug regime and should not be confused with the regime of the same name for vertical flow. At higher gas flow rates an annular regime is found as in vertical flow. At very high flow rates the liquid film may be very thin, the majority of the liquid being dispersed as droplets in the gas core. This type of flow may be called the spay or mist flow regime. It may be noted that similar flow regimes can be seen with immiscible liquid systems. If the densities of the two liquids are close the flow regimes for horizontal flow will more nearly resemble those for vertical flow. Two-phase, two components (air-water), adiabatic and horizontal flow are the cases under consideration in the present study.

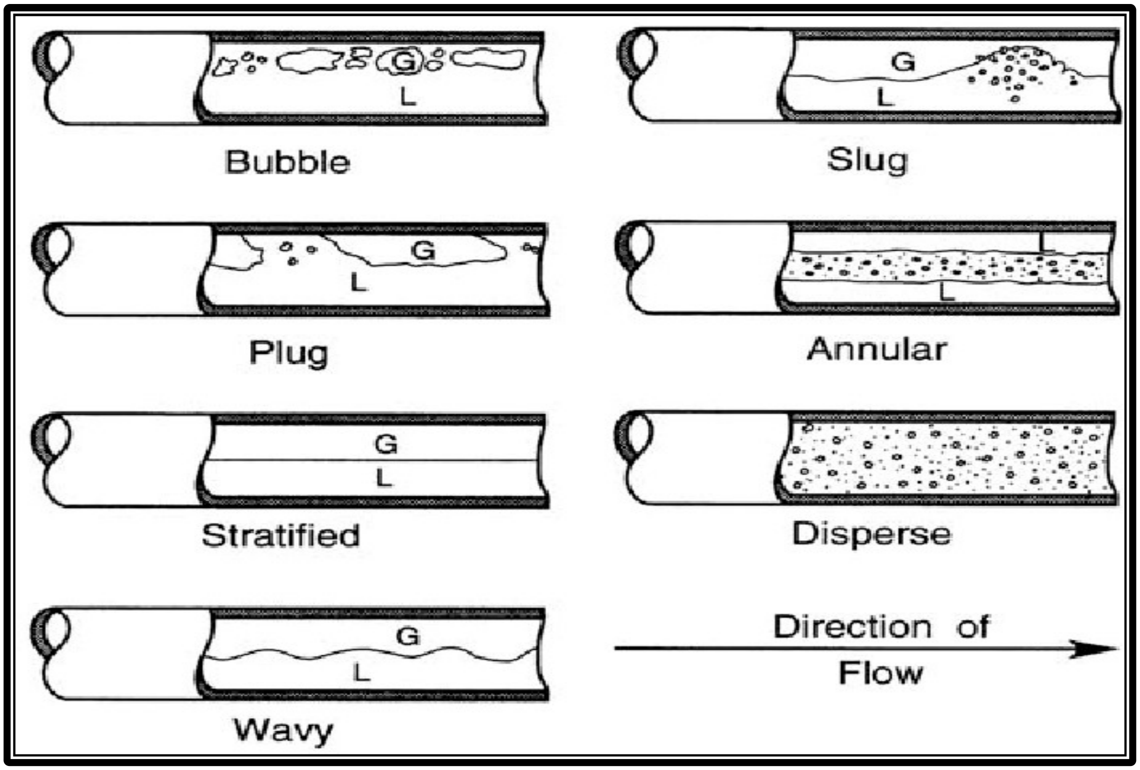

Figure (1-1): Flow Patterns in the horizontal flow **[15]**.

1.4 Nanofluid Concept and Applications

When non-metallic or metallic nanoparticles with a typical size of less than 100 nm are dispersed in a fluid, they create a nanofluid, which is essential in heat transfer and fluid flow engineering applications. Typically, metals, carbides, oxides, or carbon nanotubes are nanoparticles utilized to create nanofluids. Base fluids also consist of coolants such as ethylene or tri-ethylene glycols, water, oil, biofluid, polymer solutions, and other lubricants.

Nanofluids are used in a variety of applications, such as grinding, lowering boiler flue gas temperatures, chillers, chiller systems, fuel cells, pharmaceutical operations, hybrid engines, and car engine cooling [16]**.**

There are two methods, used for the preparation of nanofluids, single-step method and two-step method. By using chemical solvents, a single-step process combines the creation of nanoparticles with their dispersion into a base fluid in one step [17].

The most popular technique for making nanofluids involves two steps and allows for large-scale production, whereas a single step only allows for the dispersion of dry powders in a fluid. Processing is done in the two step using high-shear mixing, ball milling, ultrasonic agitation, intense magnetic force agitation, and homogenization [18].

1.5 Nanofluids Thermophysical Characteristics and Stability

The increase in the properties of nanofluid such as the thermal conductivity, density, and viscosity lead to increase the effectiveness of heat transfer process. When nanofluid flows in a pipe, the heat transfer from fluid to wall of pipe by forced convection is considered. It is predicted that the increase in thermal conductivity using nanofluid will be equal to the increase in heat transfer coefficient with employing the nanofluid.

Nanoparticle form, concentration, and aggregation in nanofluids, and the duration of the sonication process used to prepare them are the key factors determining nanofluids' thermophysical characteristics [19].

The rheological and thermophysical properties of the resulting nanofluids are greatly influenced by the consistency of the fluid-borne nanoparticles. Due to particle collisions brought on by Brownian motion, clusters form in the base fluid. Many internal forces between the nanoparticles and the base fluid, such as the attraction between the particles caused by the Van der Waals forces, regulate the cluster forms or aggregation [20].

The impact of methods for creating nanoparticles on the thermophysical behavior and stability of nanofluids. Importantly, the study pointed out that there doesn't seem to be a common approach to stability measurements. Once the aggregates' density rises above the base fluid's, they start to crystallize and eventually compromise the stability of the nanofluids [21].

Utilized nanoparticles' volume and size, the mixture's temperature, and the usage of surfactants all have an impact on the values of Nanofluids' thermophysical characteristics [22].

1.6 Heat Transfer Mechanisms of Nanofluids

Since 1995, when nanofluids were first introduced, numerous mechanisms have been proposed as possible explanations for the improved heat transmission of nanofluids. It is difficult to fully comprehend the nanoscale impacts that underlie the enhanced heat properties noted in the literature because of the size and volume of interacting with the base fluid are particles.

The main benefit of using nanofluids is that they have better heat transfer capabilities than conventional heat transfer fluids, increasing their thermal conductivity. The type, size, concentration, and kind of base fluid, as well as the thermophysical features of the nanoparticles and the base fluid, are factors that affect the thermal conductivity augmentation [23]. Investigated the mechanisms that would make it easier to simulate nanofluid flow, they emphasized the considerable influence of forces like drag, Brownian motion, lift, Van der Waals, thermophoresis, rheological behaviors of nanofluids and electrostatic double-layer forces on the thermal. When particles in a fluid move at random and uncontrollably because of collisions between slower-moving and faster-moving particles, this phenomenon is known as Brownian motion. Thermal diffusion causes Brownian motion, which is exacerbated by greater temperatures, smaller particle size, and low viscosity [24]. There are three different kinds of collisions that result from the nanofluids' increasing temperature: collisions between base fluid molecules, base fluid molecule-nanoparticle collisions, and nanoparticle-nanoparticle collisions as a result of Brownian motion. They came to the conclusion that, among the three different types of collisions, Brownian motion's impact on a thermal conductivity augmentation is the less [25].

the effect of nanolayers on the thermal conductivity of nanofluids. Their results proved that the thermal model is enhanced as a result of accounting for this factor. was the first to introduce the idea of nanolayers and their effect in nanofluid thermophysical behavior. The nanolayer is known as the solid-like structure or the interfacial layer between the solid surface and the first layer of the fluid in contact with the solid surface. A structured, layered arrangement of the fluid molecules around the surface of the nanoparticles was observed. These layers behaved like solids and act as a thermal bridge for the heat transfer process enhancing the overall thermal conductivity of the fluid. In the solid–solid interface, this layer acts as a barrier of heat transfer due to incomplete contact between solid surfaces. However, it is not the case for the solid–liquid interface as the aligned interfacial shell in the nanoparticle suspension would make heat transfer across the interface effective [26].

The major cause of the thermal conductivity gain seen with nanofluids, as supported by the scientific community, the random collision of particles within the fluid is still occurring. Studying how the nanolayer affected the thermal conductivity of fluids containing nanoparticles, a rise in nanolayer thickness and a decrease in particle size were shown to increase the effective heat conductivity [27]. The researchers came to the conclusion that altering the nanolayer structure would be a useful way to create more thermally conductive nanofluids. The nanoclusters are another element that affects the thermophysical behavior of nanofluids. It is important to note that robust Van der Waals interactions in nanoparticles drive them to aggregate into nanoclusters that provide rich zones of highly thermally conductive nanoparticles, which increase the fluid's bulk thermal conductivity [28].

1.7 Advantages and Disadvantages of Nanofluids

There are several advantages and disadvantage of nanofluids are summarized in table (1-2).

Table (1-2): Main advantages and disadvantages of nanofluids.

Advantages		Disadvantages
1	The suspended nanoparticles concentration in the base fluid increases the surface area of contact viscosity, density, and effective thermal conductivity of the fluid.	High cost of nanofluids and the higher production cost of nanofluids are among the reasons that may hinder the application of nanofluids in industry.
2	The dispersion of nanoparticles flattens the transverse temperature gradient of the fluid.	Suffers from the problem of agglomeration at the bottom of the tank. It cannot use for long term due to aggregation and sedimentation.
3	The turbulence and mixing of fluctuation of the fluid increase the temperature distribution of the base fluid.	In the case of using non-spherical particles, the length should be in microns and effect of corrosion and erosion take into account
4	Smashing the sublayers that are generated near the wall through the pipe.	Lower specific heat in compartion with the base fluid and higher viscocity causes higher pumping power
5	The collision between particles, fluid and wall surface increases the temperature distribution in the base fluid.	Problems in production process

1.8 Using Dispersed Medium

One of the major concerns for the design of any heat exchanger types or thermal devices depended on fluid flow. Heat exchanger is very important device used in various thermal application. As is well known, the principle of operation of the heat exchanger depends on the heat transfer from hot fluid to cold fluid. To improve this principle, several techniques must be used, as presented in section (1-2). To make these techniques more effective, a nanofluid is added as a working fluid. It has been observed when nanofluids are used, the deposition of nanoparticles occurs in the base fluid. This separation causes many problems, including a decrease in heat transfer improvement, as it worked at the beginning of its addition to the system. Therefore, nanoparticles must be kept suspended in the base fluid to obtain the best heat transfer and prevent deposition problem, which is done by using a dispersed medium. A dispersed medium has two media or more that do not mix together. Clearing, the two media have very different nature.

1.9 Nano Particles Types

Nano particles can sub divided in three types [28]:

1. Metal types like as (Gold, Silver, Copper, Aluminum, and Iron.
2. Metal oxides like as (Alumina (Al_2O_3), Copper oxide (CuO), Iron oxide (Fe_2O_3), Titanium dioxide (TiO_2), Zinc oxide (ZnO), and Magnesium oxide (MgO).
3. Non-metal like as carbon nanotubes are also utilized due to their extremely high thermal conductivity in the longitudinal (axial) direction.

The Magnesium oxide (MgO) is select in this study due to various reason. Firstly, MgO nanoparticles have been identified as a potential nano-powder for increasing the thermal performance of various systems. Secondly, MgO nanoparticles have anomalous thermal conductivity, which in turn can enhance the conduction heat transfer within the system. Finally, MgO nanoparticles using in thermal system which need to high pressure and temperature.

1.10 Objective of the Thesis

The present work aims to study the effect of two-phase flow on heating transfer characteristics in a double pipe exchanger containing a pure water as a cold fluid and various hot fluids. The hot fluids are pure water, water-CMC fluid, water-MgO fluid, and water-MgO-CMC fluid. Cold fluid flows through the annular side of the pipe while heated fluid flows inside. The Carboxymethyl cellulose (CMC) added to nanofluids to prevent nanoparticles from deposition. Exploring the impact of nanofluid volume fraction and two-phase flow on enhancing heat transfer rate. The current work's strategy is:

1. Numerical work focuses on Computational Fluid Dynamics (CFD) (ANSYS FLUENT code 2020 R1) used to predict water and nanofluid flow (with and without air injection) and temperature fields in a double-pipe heat exchanger and comparison with the experimental work. This is numerically accomplished by solving the Navier Stokes equations for momentum and energy.
2. Experimental work includes many steps such as:
    a) Manufacturing double-pipe heat exchangers.
    b) Setting up the experimental rig that contains all the necessary apparatuses and required instruments.
    c) Preparing different hot fluid (water-CMC, water-MgO, water-MgO-CMC) and measurement of its physical properties.
    d) Measuring the temperature of cold and hot fluids at their entrance and outlet.
    e) Measuring the pressure of cold- and hot-fluid inlets and outlets.
    f) Experimenting with different hot fluid flows in the inner pipe to determine the heat transfer properties in the double-pipe heat exchanger for counter and parallel flow configurations.
    g) Studying the effect of two-phase flow on the heat transfer enhancement.
    h) Using experimental data, establishing a correlation to assess the Nusselt number and friction factor in order to forecast an increase in heat transmission.

1.11 Layout of the Thesis

The scope of this research can be summarized in the following stages:

1. Chapter one deals with an introduction of the problem.

2. The literature review is done on two phases, nanofluids, and heat transfer flow as reported in chapter two.
3. Chapter three deals with the experimental approaches that are used to solve the problem.
4. Chapter four is devoted to the Computational Fluid Dynamics (CFD) that are used to predict temperature, pressure, velocity, and void fraction of two phases flow along the U-bend double pipe heat exchanger.
5. Chapter five presents the result and discussion, which is divided into two parts: experimental and theoretical results. Also, this chapter deals with comparison experimental and theoretical results.
6. Chapter six illustrates the conclusions from this work and the suggestions for further work.

2

CHAPTER TWO

LITERATURE REVIEW

Chapter Two

Literature Review

2.1. Background

Heat exchangers were used in a variety of industrial processes to exchange heat energy between two fluids. As a result, the development of these devices is essential to the reduction of operation costs and the improvement of energy efficiency. The use of heat exchangers in industries processing allows for the fluid temperature to be more precisely controlled, which in turn leads to improve product quality. The chemical, petrochemical, biochemical, and nuclear sectors are the most common types of businesses that utilize heat exchanger, namely as the cooling jackets in commercial reactors. Cooling jackets or coils are responsible for producing the two-phase flow, and the coolant that is used has saturation properties (temperature and pressure) that are comparable to those of the system [29]. Bubbles may form in the liquid bulk even when flow conditions are present, and this can lead to gas-liquid dispersion. Because of the shear forces that are produced either by the liquid itself or by the equipment, such as the impeller, or by contact with the wall, the flow hydrodynamics cause the bubble to break apart and spread throughout the liquid. By heating the pipes to a temperature that is somewhat near to the temperature at which the liquid is saturated, bubbles that can be used in the gas-liquid dispersion may be produced. By vapor cooling liquids in condensers at temperatures close to subcooling, it is possible to make a gas-liquid combination that is analogous to that produced in stirred reactors [30]. Because of changing in the flow properties and physical properties of the bulk fluid in the presence of dispersant, forced convection takes on new characteristics [31]. With increasing a working fluid thermal conductivity, nano-scale components were disseminated into the working fluid using this technology. Nanoparticles were mixed into the working fluid to increase the heating transfer coefficient under forced convection conditions. Heat transfer characteristics are improved by a greater dispersion of high conductivity nanoparticles in the fluids [32]. The distribution of nanoparticles in a working fluid alters its viscosity, density, and heat capacity in addition to modifying the flow conditions. Thermal conductivity is affected by temperature, particle size, pH, and nanoparticle concentration [33]. The static model [34] assumed that nanoparticles were stationary in bulk liquid, with the nanofluid having a homogeneous distribution of nanoparticles that flowed along the stream line inside the bulk fluid. The stream line flow structure is deformed by turbulent flow, which also results in an uneven distribution of nanoparticles [35], while dynamic models were linked with assumptions of random nanoparticle movement within bulk fluid.

2.2. Previous Studies Related to Heat Transfer in Two Phases Flow

Cioncolini and Thom [36] analyzed the estimation of the fraction of responsible liquid in adiabatic two phases annular move in vertical pipes. In this investigation, of eight gas liquid mixtures and 19 various sizes, spanning from 5 to 57.1 mm, an experimental data bank of 1504 points was created. Nine empirical correlations were examined against this data bank. It was discovered that the correlations of Sawant, Mishima, and Ishii of Oilman, Pots, and Trompe reproduced the data as the best. A fresh correlating strategy that draws on both dimensional analysis and physical intuition and is capable of giving film some atomization process more physical context, was suggested, and it outperformed all previously used techniques, which also serves as the governing, served as the foundation for the new correlation.

Kashinsky et al. [37] concluded that gas is introduced into a liquid in a rectangular channel with increasing surface liquid velocity at various inclination angles to decrease the rate of heating transfer and shearing stress. Increasing liquid velocity breaks up the bubbles to generate fragments, which is the most logical explanation for this discovery. In general, heating transfer enhancement rises with rising laminar Reynolds numbers and begins to decline in turbulent areas. At higher gas phase flow rates and higher liquid flow rates, single-phase flow transfers heat more quickly than two-phase flow does.

Dizaji and Jafarmadar [38] investigated air bubbles were introduced into the water stream in a horizontal twin pipe heat exchanger to study the influence on gas-liquid dispersion bubbly flow. Result demonstrated influence of gas bubbles improved heat exchange. Reduced heat transfer enhancement by raising the Reynolds number, and heat transfer was increased by injecting bubbles more on the shell side than the tube side. While air bubbles injected on the shell's side would increase turbulence, bubbles injected inside the tube served as an insulator.

Vidal [39] presented a no-slip technique to forecast the friction factor and, by extension, the frictional pressure are dropping for two-phase flowing. The method is more accurate than other ways that have been published since it is based on the mixed Reynolds number redefinition. Unfortunately, due to the homogenous hypothesis, that method disregarded pertinent two-phase flowing data. Through the use of the void fraction and flow pattern parameters, two-phase flow phenomenology is introduced in this work, changing the mixture Reynolds number. To compare predictions and experiments, data from the open literature were used. This information took into account a variety of two-phase horizontal flow situations for refrigerants and air-water mixes. In order to confirm that the new results are more accurate, the proposed-method predictions were also compared with a model from the literature and homogenous approaches. The enhanced friction factor method is presented in detail in this publication.

Abid et al. [31] studied employing a variety of liquids, including water, water containing 60% ethanol, water containing 35% glycerol, and water containing 65% glycerol, researchers were able to determine the impact of the physical characteristics of the liquid phase on the heating transfer coefficient in a bubble column. They came to the conclusion that viscosity, surface tension, thermal conductivity, and specific heating all have an impact on bubble size depending on the type of liquid. Greater viscosity liquids produced big bubble sizes that increased the heat transfer coefficient, whereas lower viscosity liquids produced small bubble sizes that decreased the heating transfer coefficient.

Junior and Lima [40] illustrated that Gas-liquid flow in pipes may take the shape of an annular pattern where the fluid flows as a thin layer near the pipe wall and the gas flows as a core in the pipe central. This flowing pattern was frequently observed during boiling and condensation processes, for instance, in the petroleum, cooling, and steam production sectors. The interfacial friction parameter was one of the crucial final elements in annular flow for defining the interfacial shearing stress and, as a result, the pressure gradient. To estimate the interfacial friction parameter, numerous correlations were established in the literature. The primary goal of this research was to compare some of these connections to experimental data that was also gleaned from the literature. Each correlation's characteristics and constraints as well as its precision in connection to experimental data were noted. Despite the fact that the correlations studied had diverse characteristics, the results show that they produced generally excellent results. However, further analysis incorporating more correlations and sets of experimental data is still required.

Aliyu et al. [41] presented that it is crucial for correct modeling of pipeline systems' pressure drop and convection coefficient are used to illustrate gas-liquid interfacial friction in annular regime. Throughout the past 50 years, several empirical relationships have been discovered. However, they were only applicable for pipelines with inner diameters between 10 and 50 mm, were limited to velocity ranges for each phase, and mainly applied for air pressures. In this investigation, they experimented with 11-29 m/s and 0.1-1.0 m/s surface gas and liquid ranges for long flow stream with a 101.6 mm internal diameter. A broad database compiled and used to examine documented interfacial friction factor relationships. For various fluids types used to form two phases flows in pipes with an inner diameter of 16 to 127 mm, the database includes measurements important parameters for various implemented fluids types. Up to 6 bar of experimental pressure was used in eleven experiments. Many published correlations and the big pipe data showed significant disparities, especially for films area at low allowable shearing stress. So, using large database, the interfacial friction parameter showed a correlation. In order to properly express and accommodate required boundary settings of experimental, fluid types characteristics, operation pressures and the correlation incorporates dimensionless values.

Wang and Guo [42] elaborated that by using conformal transformation theory, the inner flow field's velocity boundary layer and exterior flow field over the wave interface were both achieved, providing an explanation of shear stress at the wave contact at the most basic level. The wave interface's parameters, such as wave height, wave length, and the ratio of ascending to descending semi period wave lengths, were taken into consideration while calculating the viscous drag coefficient. These elements significantly affect the gradient of velocity over the wave interface, which is what determines how the local shear stress is distributed differently. Also, the influence of fluid flow was investigated, providing evidence that the sooner the fluid flow separated from the wave interface, The turbulent perturbation was made and the resulting lower drag force was larger the depression.

Ribeiro et al. [43] studied air-oil two phases flow in vertical pipe. The viscosity of this type is high about 0.2 kg/m.s using 0.6 cm pipe diameter. The air-oil two phases flow velocity employed at ranges 22.37-59.06 m/s and 0.05-0.16 m/s, respectively. The two-fluid model was a method that is used to find different parameters and take into account friction coefficient. This model was very important to know the types of flow regime

2.3. Previous Studies Related to Effect of Nanofluid on Heating Transfer.

For reasons of economy and safety, improving heat transmission in industrial processes becomes a more difficult problem. Researchers are interested in understanding the heat transfer phenomenon in solid-liquid dispersion (nano-fluid) systems for effective heat exchanger design. A noteworthy method for improving heat transfer is nanotechnology, in which materials at the nanoscale are disseminated throughout the process fluid to increase the fluid's thermal conductivity. When forced convection is present, to increase the heat transfer coefficient and enhance heat transmission, nanoparticles are added to the process fluid. By improving the dispersion of high conductivity nanoparticles in the fluid, the heating transfer characteristics are improved, increasing the heat transfer coefficient [44]. Several physical characteristics of the process fluid, such as viscosity, and heat capacity and density, as well as flow conditions, are also impacted by the dispersion of nanoparticles in the fluid. Temperature, nanoparticle size, pH, and concentration all affect thermal conductivity. The static model of thermal conductivity presumes that the nanoparticles in the bulk fluid are stationary in which nano-fluid is a bulk fluid that contains uniformly distributed nanoparticles that flow in a straight line [45]. Despite the assumption that nanoparticles would move randomly within bulk fluid when combined with dynamic models, flow turbulence deforms the stream line flow structure and causes an unequal distribution of nanoparticles [46]. Maxwell-Granett modified models are used to present the effects of nanoparticle shape, nanoparticle size, particles-particle interaction, and interfacial thermal resistance [47]. Effective medium theory (EMT), which is represented by the following equation, can be understood by simple correlation:

$$\frac{Keff}{Kbf} = \frac{Kp+2Kbf+2\Phi(Kb-Kbf)}{Kp+2Kbf-\Phi(Kb-Kbf)} \quad \textbf{(2.1)}$$

The four mechanisms of nano-fluid conduction are Brownian motion is brought on by nanoscale convection, bulk fluid particle collisions, heat transport of nanoparticles in bulk fluid, and collisions between nanoparticles by [48]. They suggested using convection at the nanoscale for known thermal conductivity. There are different correlation models to find effective nanofluids thermal conductivity.

Tables 2.1: Effective nano-fluid thermal conductivity correlations of different models.

Investigators	correlation	Model type
Maxwell-Granett model[1904] [47]	$\frac{Keff}{Kbf} = \frac{Kp + 2Kbf + 2\Phi(Kb - Kbf)}{Kp + 2Kbf - \Phi(Kb - Kbf)}$	Static model
Hamilton and Crosser [1962] [49]	$\frac{Keff}{Kbf} = \frac{Kp + 2(n-1)Kbf + \Phi(n-1)(Kb - Kbf)}{Kp + 2(n-1)Kbf - \Phi(Kb - Kbf)}$ Where $n = \frac{3}{\Psi}$	Static model
Corcione, 2011 [46]	$\frac{Keff}{Kbf} = 1 + 4.4\, Rep^{0.4} Pr^{0.66} (\frac{T}{Tfre})^{10} (\frac{Kp}{Kbf})^{0.05} \Phi^{0.66}$ *Where* $Rep = \frac{2\rho\, Kb\ T}{\pi\, \mu^2\, dp}$, $Pr = \frac{Cp\, \mu}{Kbf}$ *and Kb= 1.38* $*10^{-23}$ *J/k*	Dynamic model

Li and Xuan [50] moderated equation to increase heat exchange rate utilizing Cu nanoparticles as shown in the equation below and is applicable at ranges of $0<\Phi<2\%$, $10^4<Re<2.5*10^4$.

$$Nu = 0.0059\, Re^{0.9238} Pr^{0.4} (1 \ + 7.68.\, \Phi^{0.6886} Ped^{0.001}) \quad \textbf{(2.2)}$$

Maiga et al. [51] developed Al_2O_3/ethylene glycol nanoparticles to be used to construct a correlation for heat transfer rate enhancement that is appropriate at ranges of $6.6 \le Pr \le 13.9$, $0< \Phi<10\%$, $10^4 \le Re \le 5*10^5$, as shown in Equation:

$$Nu = 0.085\, Re^{0.71} Pr^{0.35} \quad \textbf{(2.3)}$$

Buongiorno [52] developed a correlation for Al_2O_3 nanoparticle-based heating transfer rate enhancement that is relevant for ranges of

$\delta = 15.5\,, 5000 < Re < 65000, 0 < \Phi < 3.6\%$, as presented in the following equation:

$$Nu = \frac{\left(\frac{f}{8}(Re-10\quad)\right)}{1+\delta\left(\frac{f}{8}\right)^{0.5}(Pr^{0.6667}-1)}\mathrm{Pr} \tag{2.4}$$

As previously stated, the fluid-particle interaction, particle-particle collision, particle-tube wall collision, Brownian motion of particles, and shear lift forces all have an impact on the forced convection parameters of nanofluids. These forces deform the heat boundary layer by increasing the amount of turbulent flow. Figure summarizes the several parameters that improve a nanofluid flow's ability to transmit heat (2-1). Many studies investigations, nanoparticles that are thought of as nanoscale solids suspended in bulk fluid have been utilized. This section summarizes prior studies that are pertinent to the current work. Some of the previously reported studies include:

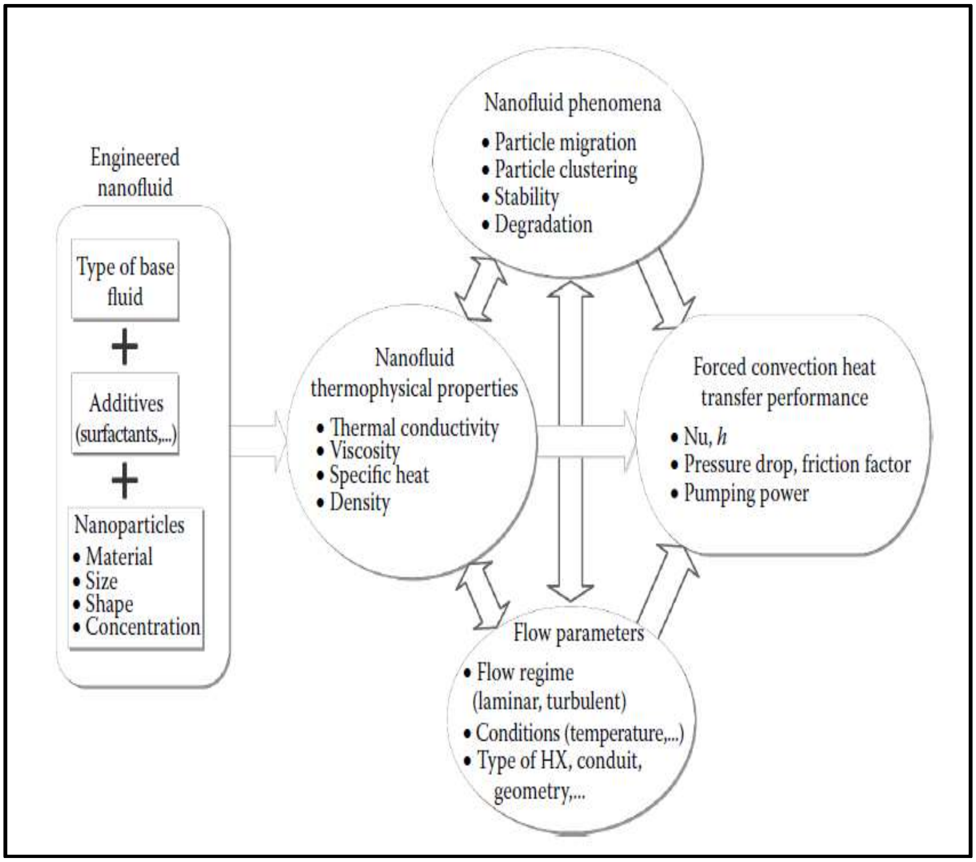

Figure 2.1: effective factors in heat transfer enhancement parameters of nanofluid flow forces **[52]**.

Duangthongsuk and Wongwises [53] used TiO_2 nanoparticles with a 21 nm diameter and a 0.2 vol% concentration to improve heating transfer in a horizontal pipe. The findings demonstrated that 6–11% improvement was achieved, and that with increasing hot fluid flow rate and falling nanofluid temperature, the heating transfer coefficient rose. Also, results showed that nanofluid had a friction factor that was similar to that of water without nanoparticles and that it had no discernible effects on pressure drop.

Zamzamian et al. [54] studied the improvement of heating transfer in heat exchangers using CuO/ethylene glycol and Al_2O_3/ethylene glycol nanofluid. The influence of nanoparticle size, concentrations, and temperature was examined, along with forced conversation heat transfer. The findings were in good agreement with correlations from earlier research. Outcomes demonstrated that the convection coefficient rises by 0.02–0.5 for two reasons firstly increase concentrations of nanoparticles and secondly the temperature of nanofluid.

Darzi et al. [55] presented the effects of using 20 nm Al_2O_3 nanoparticles diameter on the heat performance and pressure drop of heat exchanger experimentally. At temperatures ranging from 27 to 55 ºC. It was determined what a nanofluid's effective viscosity. The Reynolds values used in the experiments ranged from 5000 to 20,000, with varying nanoparticle concentrations up to 1% by volume. The results show that there is a strong possibility for improving heat exchanger thermal performance by adding nanoparticles to the tested ranges when the pressure drop penalty is minimal. Based on the Reynolds number and nanoparticle concentration, an empirical connection for Nusselt number change was developed.

Aghayari et al. [56] examined the improvement of gamma-AL_2O_3 nanoparticles at volume fractions range 0.1%–0.3% in a nanofluid were studied for their thermal transfer coefficient and Nusselt number. Several parameters at counter flow direction flow like as heat transfer coefficient and Nusselt number were examined in relation to temperature and nanoparticle concentration. The agreement between experimental findings and genuine theoretical data depend on semiempirical equations is satisfactory. The experimental findings demonstrate that the heating transfer coefficient and Nusselt number increase by 19%-24. The heating transmission coefficient has also been found to rise with operation temperature and nanoparticle concentration.

Albadr et al. [57] presented counter-flow shell and tube design rig and used Al_2O_3 nanoparticles has 30 nm diameter and added at 0.3-2 by volume percent range to the thermal fluid. According to the findings, a little increase in heating transfer coefficient was brought about by increasing concentrations of nanofluid. When the nanoparticles concentrations grew, the bulk fluid's viscosity increased higher, which raised the friction factor.

Maddah et al. [58] studied heating transfer and total heat transfer were experimentally by using a titanium dioxide nanofluid- and twisted-tape-equipped double-pipe heat exchanger. Cold and hot water served as the working fluids on both the shell and tube sides, with the inner tube having an 8 mm diameter and the outer tube a 16 mm diameter. The twisted tapes had dimensions of 1 mm (d), 5 mm (W), and 120 cm (L) and were fabricated from a sheet of aluminum. Nanoparticles of titanium dioxide were made with a concentration of 0.01% (v/v) and a size of 30 nm. Researchers looked at the total heat transfer coefficient, fluctuations in the turbulent flow regime's (Re=2300) heat transfer under various flow conditions. Heating transfer coefficient increased by 10–25% when utilizing twisted tape and nanofluid compared to when without using them. As operational temperature and mass flow rate rise, so does the heating transfer coefficient, as was also found. The experimental results also showed that compared to a non-twisted control, a 0.01% TiO_2/water nanofluid with twisted tape showed a slightly greater friction factor and pressure drop. The empirical correlations for the friction factor shown strong agreement in experimental outcomes.

Sahin et al. [59] investigated the impact of CuO nanofluid on improving heating transfer in a horizontal pipe employing CuO nanoparticles with a size of 33 nm and concentrations between 0 and 4 vol% and Re between 400 and 20,000. With a volume fraction of 0.005 nanoparticles and Re=16,000, a 20% gain in heat transfer was the greatest. The lowest enhancement was 5% with Re=20,000 and a volume proportion of nanoparticles of 0.02.

Pandiarajuse et al. [60] used MgO nanofluids as a heat pipe with a flat plate's working fluid. Powdered MgO was made using wet chemical techniques. The solid state of created nano powders was characterized using Fourier transform infrared spectroscopy (FTIR), X-ray direction (XRD) techniques, ultraviolet spectroscopy (UV), and scanning electron microscopy (SEM). The ethylene glycol and binary mixture of water was added to the nano powders to create nanofluids. Using a transient hot-wire arrangement, the thermal conductivity of the generated nanofluids was determined. Using the Box-Behnken response surface method, a total of 17 tests were run. In order to statistically validate all of the necessary components, their mutual expectations, and their quadratic terms, analysis of variance was performed (ANOVA). For different temperatures, volume fractions, and solution ph, MgO nanofluids' optimum stability and heating conductivity were predicted, and the results were compared to actual data. The findings showed that by increasing the particle concentration and pH of MgO nanofluids at certain regions, thermal conductivity was increased and made stable at the appropriate temperature.

Asadi and Pourfattah [61] explored the properties of ZnO- and MgO-engine oil nanofluids, which are employed as coolants and lubricants, and their capacity for heat transmission. The viscosity and heating conductivity tests were carried out at a range of temperatures (from 15 °C to 55 °C) and solid concentrations (from 0.125% to 1.5%). The nanofluids displayed Newtonian behavior over the tested temperature and solid concentration ranges. The results also demonstrated that samples containing ZnO exhibit a higher increase in dynamic viscosity than samples containing MgO. The same temperature and solid concentration range were used to assess thermal conductivity as well. At temperatures of 55 oC and solid contents of 1.5%, maximum increases of around 28% and 32%, respectively, engine oil nanofluids containing ZnO and MgO were observed. Additionally, the effectiveness of the nanofluids for heat transfer was assessed using a variety of figures of merit, and it was discovered that using the ZnO-engine oil nanofluid is advantageous in a restricted temperature range whereas using the MgO-engine oil nanofluid is advantageous exclusively in laminar flow regimes.

Rao and Sankar [62] conducted experimental investigation for the calculation of the friction factor and CuO nanofluid convective heating transfer flowing through a double pipe U-bend heating exchanger under turbulence. Several volume concentrations (0.01%, 0.03%, and 0.06%) and varying mass flowing rates (8, 10, 12, and 14 LPM) were used to move the CuO nanofluid across the inner pipe of the U-bend heating exchanger. With a constant mass flow rate of 8 LPM, hot water was forced through the annulus tube. The findings show that as Reynolds number and particle volume concentrations rise.

Pattanayak et al. [63] analyzed the utilizing a double-pipe counter-flow heating exchanger, Al_2O_3, CuO, TiO_2, and ZnO-based nanofluids' abilities to transport heat were examined at different volumes (0.025%, 0.05%, 0.075%, and 0.1%) were examined. The manufactured double-pipe heat exchanger was made up of a copper inner tube and an unplasticized polyvinyl chloride outer tube. Dimensionless quantities like the Prandtl number, the Reynolds number, and the Nusselt number, as well as the efficiency of a heat exchanger, were estimated using the computed density, viscosity, and thermal conductivity. Transmission electron microscopy scanning, and electron microscopy were utilized to characterize nanoparticles that had been prepared using a high-energy ball milling process. The nanofluids' stability was ensured by the addition of polyvinyl alcohol at a concentration of 3 percent as a surfactant. As the experimented volume concentration increased, it was found that the Reynolds number decreased, yet the thermal conductivity, viscosity, and friction factor all rose. With an inaccuracy of just 11.4%, there is a correlation between the experimentally observed data for the information for all of these nanofluids, including the Nusselt number. TiO_2-water nanofluids were found to be the most effective of all the nanofluids examined.

Shirazi [64] investigated the using modified spiral bands and Al_2O_3 nanoparticles as flow turbulators, heat transfer phenomena are seen in heat exchangers. Findings are validated using established relationships. The results demonstrate that for various hollow tape widths, the tube with cross-hollow twisted tape inserts exhibits the optimum exegetics performance. The clearance, or the width difference between the tube and the twisted tape, has an effect on the efficiency of heat transmission as well. With decreased clearance, the exegetics become more effective. When there are four unilaterally twisted tapes, the tube performs at its best exegetically. The outcomes demonstrated that boosting nanofluid concentration improves executive function.

Jassim and Ahmed [65] experimentally investigated and compared the effects of two distinct nanofluids (Al_2O_3/water and Cu/water) at various volume concentrations and flow rates on the efficiency of a double pipe heating exchanger. The effects of altering the hot-side inlet temperature are also examined at the selected concentrations. For each Reynolds number, the concentration of the nanoparticles on a volume basis varies from 0.26% to 0.83% in the nanofluid that is pumped on the shell-side of the heat exchanger. Findings showed that the base fluid's nanoparticle content had a significant potential for transferring energy. The Nusselt number noticeably increases as the mass-flow of the nanofluid is increased, according to observations of the experimental results. Al2O3 and Cu both have enhancements of up to 13% and 23% for the Re and concentration ranges indicated above. According to experimental findings, the efficacy has significantly increased (up to 7% for aluminum oxide and 10% for copper). Also, with an increase in the hot-side inlet temperature, performance improves. While using nanoparticles, it has been found that a proportionate relationship exists between the concentration and the amount of heat loss from the shell-side (cold fluid) to the atmosphere. Also, it is observed that copper nanofluid leaks less heat than aluminum oxide nanofluid.

Ali and Jalal [66] determined the impact of inner pipe twisting on a double pipe heating exchanger's overall performance. The fluid-to-fluid heat exchange is explored in both parallel and counter flow directions. Together with the initial elliptical pipe, three other pipes are investigated for the heating transfer rate and pressure drop. These three pipes have 3, 5, and 7 twists per unit length. Using water as the working medium, with Reynolds numbers (Re) ranging from 5000 to 26,000, all experiments are carried out in a turbulent flow regime. The outcomes show that all of the investigated twisting pipes enhance heat exchanger performance in both flow directions.

Ding et al. [67] compared the use of numerical simulations to examine the heating transfer and flowing properties of TiO_2-H_2O nanofluids in corrugated and smooth double-pipe heating exchangers with 0.0, 0.1, 0.3, and 0.5, w% of TiO_2. The findings showed that TiO_2-H_2O nanofluids significantly improved heating transmission as compared to deionized water, and that as the mass fraction of TiO_2 rose, the heat exchange capacity gradually increased. The corrugated pipe heating exchanger disrupted the boundary layer and created vortices in the corrugated zone, which hampered fluid flow on both the pipe side and shell side. This enhanced the ability to transmit heat more effectively than a smooth double-pipe heating exchanger, however, it also made the pipe's fluid flow resistance higher. In general, it was discovered that using corrugated pipes and nanofluids considerably increased the double-pipe heat exchanger's ability to transmit heat.

2.4. Previous Numerical Studies Related to The Effect of Nanofluid on Heat Transfer.

Akhtari et al. [68] analyzed using both experimental and computational methods, of the heat transfer of an Al_2O_3/water nanofluid moving across double pipes and shell and tube heating exchangers in laminar flow conditions. The properties of heat transmission were analyzed, and the effects of key factors including nanofluid temperature, nanoparticle concentration, and hot and cold volume flowing rates were looked into. According to the findings, when the hot and cold volume flowing rates, particle concentrations, and nanofluid inlet temperature rise, both double pipe and shell and tube heat exchangers have improved heat transfer efficiency. This was the case regardless of whether the heat exchangers were double pipe or shell and tube designs. According to the findings, in double pipe and shell and tube heat exchangers, the heat transfer coefficients of nanofluid are greater by 13.2% and 21.3%, respectively, than those of water in the heat exchangers when compared with the heat transfer coefficients of pure water. In a shell and tube heating exchanger, nanofluid performs 26.2% better than a twin pipe heating exchanger in terms of heating transfer efficiency. The modeling of heating transfer in the aforementioned heat exchangers was accomplished by the use of a method known as computational fluid dynamics. The calculated global heating transfer coefficients of the nanofluids show a high degree of concordance with the experimentally determined values.

Khedkar et al. [69] demonstrated the ability of TiO_2-water nanofluids to transport heat in a heat exchanger with 13 concentric tubes. Copper concentric inner tubes measuring 1000 mm in length make up the heating exchanger. The nanofluids are a mixture of TiO_2 nanoparticles and water as the base fluid. In a concentric tube heating exchanger, the outcomes of cooling nanofluids versus using base fluids as coolant are compared. On a Concentric tube heat exchanger, the impacts of the hot fluid input flow rate, Reynolds number, and nanofluid composition are examined. Compared to water, which is also used as a cooling medium, nanofluids have higher average heat transfer rates, and these rates increase as the composition of the nanofluids changes. This study's findings are technologically significant for concentric tube heat exchangers' 20 effective design, which boosts cooling effectiveness in low heat flux cooling systems.

Davarnejad and Jamshidzadeh [70] investigated the use of computational fluid dynamics to study the turbulent heat transfer characteristics of a magnesium oxide-water nanofluid in a cylinder tube. The k-ε turbulence model was used for the two-dimensional modeling. The base fluid was pure water, with nanoparticle volume fractions of 0.0625%, 0.125%, 0.25%, 0.5%, and 1%. The used Reynolds numbers were between 3000 and 19000. Single phase and Volume of Fluid (VOF), and mixed models were all utilized. The findings demonstrated a strong agreement between the experimental data accessible in the literature and the simulation data. Simulation in this study and experimental work both show that when the volume percentage of nanofluid increased, the Nusselt number (Nu) rose. Although the friction factor of nanofluid increasing, it had little impact on the increase in heat transmission as compared to the Nusselt number (Nu). It was found that two phase models, especially in higher volume percentages of nanoparticles, were more reliable than the others in forecasting heat transport.

Ali F.H. et al [71] presented a rotating outer circular cylinder and a concentric inner sinusoidal cylinder that were kept at constant hot and cold temperatures, were utilized for mixed convection issues. A fluid made of water and copper nanoparticles was placed in the empty distance between the walls of the cage and the cylinders. The governing equations are modelled in COMSOL 5.2 a, a finite element solver for partial differential equations based on the Galerkin technique, and are constructed for velocity, pressure, and temperature formulation. The solid volume fractions are (0.02, 0.04, and 0.06), Re is (1, 25, 100, 200, and 300), Ra is (less than 104) and the inner cylinder corrugation frequencies are (N = 3, 6 and 9), are the governing parameters taken into consideration. The calculations show that the average and local Nusselt numbers, stream and isothermal lines, and nanoparticle volume fraction all play a significant influence in the formation of the annular enclosure's

Rao and Sankar [32] performed CFD simulation for using the single phase fluid approach method, The Reynolds number range of 3000 to 22000 was used to estimate the convective heating transfer and friction parameter of CuO/water nanofluid flowing in a twin pipe U-bend heating exchanger. The ANSYS 14.0 work bench was used to develop the U-bend heat exchanger prototype. Cast iron and stainless steel were chosen as the inner and annulus tube materials in this investigation. In this investigation, particle volume concentrations of 0.1% and 0.3% were employed. CuO/water nanofluid has a mass flow rate that ranges from 0.134 to 0.267 kg/sec while the mass flowing rate of hot fluid is still constant. In a heat exchanger, the temperature of nanofluids is kept at 333 K. The findings showed that as volume % and Reynolds number increased, Nusselt number increased and friction factor decreased. The numerical results show that for a nanofluid with a concentration of 0.3%, the Nusselt number augmentation is 18%, and friction penalty that is 1.14 times that of water.

Tijerina et al. [72] evaluated the separate experiments, laminar convective heat transfer was used to study straight conventional tubes (L = 5.34 m, dt = 10 mm) and straight microtubes (L = 0.3 m, dt = 0.5 mm) flow of nanofluids with constant temperature and heating flux. Al_2O_3, TiO_2, SiO_2, ZnO, and CuO, nanoparticles were used in place of water, ethylene glycol, and turbine oil to test a variety of process variables. In the present study, six alternative combinations of base fluids, geometries, and nanoparticle concentrations are taken into account. The single-phase dispersion model (SPD), in addition to the single-phase model, was employed to evaluate the efficacy of the estimated results (SPH). The findings revealed that as the Reynolds number grows, the Nusselt number (Nu) climbs as well (Re). Moreover, the Nu considerably increased with increasing nanoparticle concentrations (up to 16% at volume fraction b = 4%, Re = 950). To enable a wide range of technical applications, for a variety of process conditions, straight traditional tubes and straight microtubes are used to flow nanofluids, and heating transfer correlations are generated for each of these configurations (25 Re 1500, 0 B 10, 6 Pr 500).

Kaska et al. [73] conducted CFD model using commercial software that uses the SIMPLE algorithm and finite volume approach. A new idea for a hybrid nanofluid is water mixed with aluminum nitride (AlN) and alumina (Al_2O_3) nanoparticles as the base fluid to improve heat transmission. The simulation methods were carried out using volume fractions of 1, 2, 3, and 4% and Reynolds numbers varying from 5000 to 17000. The diameter of the nanoparticles is fixed at 35 nm, and 7000 w/m^2 of heat is supplied along the elliptical tube. With the help of experimental data that was previously published in the literature, computational results were validated. The findings demonstrated that the distribution of hybrids Al-Al2O3 nanoparticles in water as a base fluid considerably improves thermal transfer.

Naik et al. [74] demonstrated heat transfer increase employing various nanofluids comprising nanoparticles (Al_2O_3, Cu, Ag, TiO_2, SiO_2, Fe) volume percentage (0.02 0.05). CFD (Computational Fluid Dynamics) is used for numerical simulations, while Solid Works is used to construct the model. The governing equations are discretized by using finite volume method and solved using SIMPLE. The results showed that the heating transfer rate increases as the flow rate increases. Also, it has been discovered that as operating temperature and nanoparticle concentration rise, the heat transfer rate rises.

Bendaraa et al. [75] investigated the way nanofluids behave thermally in a double-pipe heating exchanger. The lubrication unit of a thermoelectric power station is to be cooled using a counter-flow design. The goal of this research is to compare the heat performance of an exchanger with deionized water and a nanofluid depend on an alumina suspension. They performed numerical tests in a usage built on the COMSOL to evaluate the thermal performance of the investigated configuration. These studies serve to show the applicability of this theory. As a consequence, the discovered that the nanofluid's volume fraction increases the exchanging coefficient overall, the efficiency and power of the exchanger, as well as the convective heating transfer coefficient. It is stated that a 1% increase in volume percentage can improve the exchanger's power, efficacy, and overall exchange coefficient by 17.62%, 1.473%, and 10.80%, respectively. Also, it is noted that when nanofluid concentration rises, the temperature pinch points at the intake and outflow decrease, indicating that nanofluids are more effective at lowering temperatures than traditional fluids.

2.5. Previous Studies Related to Impact of Nanofluid-CMC on Heating Transfer

In the laboratory, **Semmar et al. [76]** used polymers like carbopol and carboxymethyl cellulose can be dissolved in water to replicate the thermo-rheological behavior of complicated fluids. Then, with high accuracy, their thermophysical characteristics must be known. Thermal balance and the description of temperature field development in unstable settings are made possible, in particular, by the research of specific heat at constant pressure. In this study, results on the direct determination of the specific heating of two solutions at temperatures between 20 and 90 °C are presented. The specific heat was more temperature dependent for carboxymethyl cellulose solutions than for Carbopol solution. Additionally, the examination of the concentration dependence of the specific heat demonstrates a molecular energy contribution. As a result, the surplus of the specific heat value of the water may be close to 8%.

Semmar et al. [77] used adiabatic calorimetry to investigate the impact of thermal and mass concentration on two extremely viscous solutions' specific heat capacities. The development of specific heat capacities with temperature is contrasted to pure water, and the absolute measurements were automated to run continuously over the temperature range (CPE). 290–360 K, with an average heating rate of 8104 K/s. For both carboxy-poly-ethylene and carboxy-methyl-cellulose (CMC) solutions. The increase in temperature brought on by CPE solutions is comparable to the growth of Cp in pure water, with a variable value. At 83 g/l concentration, CMC solutions exhibit the same temperature behavior. Lower concentrations respond much differently to temperature. We provide a correlation to take temperature and concentration parameters into account, making it simpler to use these data.

Reddy and Rao [78] determined experimentally TiO_2 nanofluid flowing in a dual pipe heating exchanger with and without helical coil inserts: heating transfer coefficient and friction parameters**.** The studies made use of Reynolds numbers between 4000 and 15,000 and volume concentrations between 0.0004% and 0.02%. The basic fluid is created using 40% ethylene glycol and 60% distilled water. The heating transfer coefficient and friction parameter increase by 10.73% and 8.73%, respectively, when compared to base fluid moving in a tube, as 0.02% volume concentration of nanofluid is utilized. The heating transfer coefficient and friction factor in a tube with a P/d = 2.5 helical coil insert are increased by 13.85% and 10.69%, respectively, for 0.02% nanofluid compared to base fluid. The observed heating transfer coefficient and friction parameter values are compared to those in the available literature. Generalized correlations for friction factor and Nusselt number are developed based on experimental data. The findings are presented graphically and in tabular form. Furthermore, conducted is an uncertainty analysis, and the experimental error is in the 10% range.

Kholiya et al. [79] established of using the Vinet-Tait-Birch-Murnaghan , and Shanker equations of states, a straight forward model calculate the pressure for MgO under high compression, the high-pressure behavior of solids is studied (EOSs). Stacey's development of the basic thermodynamics for solids in the limit of extreme compression is also addressed in relation to these EOSs. It is found that the results from the current model, Birch-Murnaghan EOSs, Vinet, and Tait, are in agreement with the experimental proof of MgO's high-pressure compression behavior. In the ultrahigh pressure zone, it has also been found that the present design and the Stacey requirement is met by the Birch-Murnaghan EOS.

Qiao et al. [80] developed Maize starch, polyvinyl alcohol, and borax are used to create a starch adhesive. During the preparation process, water resistance was increased by including a certain amount of water-soluble carboxymethyl cellulose, and a specific amount of pre-polymerized poly-methylene poly-phenylene isocyanate was used as a cross-linking agent. Mechanical testing apparatus was used to evaluate the bonding strength of three-layer plywood in accordance with the National Standard of the People's Republic of China, GB/T 17657-2013, and water resistance was evaluated using hot pressing. Scanning electron microscopy (SEM), differential scanning calorimetry (DSC), and thermogravimetric analysis (TGA), were used to evaluate adhesion cure. The results showed that the interface compatibility between starch adhesive and pre-polymer, bonding strength of the starch adhesive, solids content, and initial viscosity, were all improved. The optimal CMC content was 0.375% as the adhesive's curing temperature decreased.

Akbari et al. [81] modelled Hydrodynamic and heat-transfer properties of non-Newtonian nanofluids. The researchers used alumina at volume fractions of 0.5 and 1.5 as the solid nanoparticle in a numerical simulation of a laminar forced non-Newtonian nanofluid flow with a 0.5 weight percent CMC solution in water as the base fluid. A two-dimensional microchannel with a Reynolds number range of 10 Re 1000 was numerically solved using a Cartesian coordinate scheme. The rectangle-shaped geometric area under study had its top and bottom walls affected by a constant heat. Researchers looked into the effects of Reynolds number, non-Newtonian nanofluids, and nanoparticle volume fraction. The impact of non-Newtonian nanofluid motion on pressure drop, the Nusselt number, dimensionless temperature, and heating transfer coefficient is discussed in this study. The findings showed that increases the volume percentage of solid nanoparticles and decreasing their diameter will enhance heat transmission, which is particularly relevant in the Reynolds parameter. The outcomes of the added factors are graphed and compared for various parameters.

Das et al. [82] explored the stability and Al_2O_3-water nanofluids properties are examined, along with the effects of surfactants on those qualities. Further investigated are solid volume fractions (0.1–2.0%) and the impact of temperature (20–60 °C). Many surfactants are used to test the stability of nanoparticle suspensions, with sodium dodecylbenzene sulfonate (SDBS) offering the better stabilization. Rod-shaped particles with diameters between 20 and 70 nm are visible in TEM pictures. Adding SDBS surfactant lowers particle clustering and the suspension's polydispersity index, according to DLS experiments. Solid volume percentage increases and heating conductivity increases (0.1–2.0%), whereas the viscosity of Al_2O_3-based nanofluids in water rises with solid volume fraction (0.1-1.0%) and decreases with heat. The obtained values for viscosity and heating conductivity are contrasted with those of other current models. Lastly, a sensitivity analysis was performed, and the results that, at a given thermal, particle loading increases the sensitivity of thermal conductivity. The findings provide a comprehensive thermophysical feature database of water-based Al_2O_3 nanofluids for usage in a variety of engineering applications.

Arya et al. [83] studied the MgO/ethylene glycol nanofluid counter current corrugated plate heating exchanger's thermo-hydraulic performance. In order to conduct heat exchange with water. In ethylene glycol, MgO nanoparticles were diluted to 0.1%, 0.2%, and 0.3% concentrations. After that, a counter-current flow of the nanofluids was introduced to the heat exchanger. The test rig provided circumstances for determining how several operational factors, such as mass concentration, pressure drop, input temperature of the nanofluid, fluid flow, affected the heating transfer coefficient, and thermal performance index of the heat exchanger. It has been demonstrated that mass concentration and flowing rate raise the heating transfer coefficient. Nonetheless, both of them cause the system's pressure to fall. With wt% = 0.3, it was discovered that the thermal transfer and pressure drop were both 35% and 85% higher. Surprisingly, input thermal was found to have no influence on pressure drop readings and only slightly increase the heating transfer (up to 9.8% at wt% = 0.3). The thermo-hydraulic performance index of the heating exchanger was observed for increasing by 34% with the introduction of MgO nanoparticles.

Suppiah et al. [84] examined Halloysite nanotube content's impact on films made of carboxymethyl cellulose and halloysite nanotube's thermal characteristics and moisture content. Solvent casting was used to make the carboxymethyl cellulose and HNT-based bio-nanocomposite films. The thermogravimetric analysis (TGA) findings showed that the thermal stability of CMC/HNT bio-nanocomposites was enhanced by the incorporation of Halloysite nanotube (HNT) nanofiller. The outcomes demonstrated that the thermal degradation temperatures (Td1 and Td2) and the amount of residue left after burning at 800 degrees Celsius rose as the amount of HNT filler increased. This demonstrated the effective incorporation of the HNT nanofiller into the CMC matrix in the bio-nanocomposites. The moisture content of the CMC/HNT bio-nanocomposite films dropped as the amount of HNT increased.

Gupta and Varshney [85] used the carboxymethyl cellulose (CMC) complexed with lithium tetrafluoroborate method to produce a solid polymer electrolyte that conducts lithium ions. Using an ac impedance analyzer, the ionic conductivity at room temperature was determined to be 8.2 106 S cm1. Conductivity increased even further thanks to the plasticizer, reaching up to 3.7 103 S cm1 at ambient temperature. Fourier transform infrared (FTIR) spectroscopy and X-ray diffraction (XRD) were used to analyze the structure. According to the XRD results, the electrolyte film is amorphous. The complexation of the salt and plasticizer with the polymer matrix was verified by FTIR spectroscopic analysis. The glass transition and melting temperatures of pure CMC and CMC-based polymer electrolyte sheet were assessed using differential scanning calorimetry.

Arya et al. [86] looked at a double-pipe heat exchanger's capacity to use MgO-ethylene glycol as a heating transfer fluid. Two processes were used to create the nanofluid, containing 0.1, 0.2, and 0.3% by weight. The test rig supplied the environment for determining the system's friction factor, pressure drop, and convective heating transfer coefficient. Experimental research was done to examine the effects of several operational factors on the heat transfer coefficient and pressure drop, including flow rate, nanoparticle mass concentration, and fluid intake temperature to the heat exchanger. When wt%=0.3, the heating transfer coefficient inside the heating exchanger may be 27% higher than the base fluid. (Ethoxylated Glycol). When MgO nanoparticles were present, the pressure loss increased by 35% at wt% = 0.3. According to the 64/Re equation, the system's friction factor decreased nonlinearly as the Reynold number rose. When the mass concentration of nanoparticles rose, the friction factor rose as well, with the nanofluid with a mass concentration of wt%=0.3 showing the largest rise in friction factor (32%). Similarly, it was discovered that the input temperature had no impact on the system's friction factor or pressure drop, but did have a little impact on the heat transfer coefficient. Also, experimental studies of a MgO-ethylene glycol nanofluid's thermo-physical characteristics at various thermal were carried out.

Svetlov et al. **[87]** examined the procedure of heat exchange that is performed on wet sodium carboxymethyl cellulose. It was determined how to go about determining the thermal conductivity coefficient of a medium that included wet dispersion particles. The thermophysical characteristics of sodium carboxymethyl cellulose were investigated and characterized. Research was done to determine how a material's thermal conductivity coefficient is affected by the amount of moisture it contains and its density. In order to determine the heating conductivity coefficient of sodium carboxymethyl cellulose at various densities of the wet material, an empirical equation was derived by processing the experimental data. The coefficient was calculated using this equation.

Arya et al. [88] investigated to assess a double-pipe heating exchanger's prospective use of MgO/water-ethylene glycol nanofluids. Experimental measurements were made of the heating exchanger's total heating transfer coefficient, the working fluid's inlet temperature, the pressure drop, indicator of the nanofluid's hydraulic performance, and the friction factor. The asymptotic particulate fouling model was used to study and model of inside the heating exchanger, where nanoparticle fouling has occurred. Findings indicated that when Re = 10500 and wt.% =0.3 in the turbulent domain, MgO nanoparticles can improve the heating transfer coefficient by 39%. Moreover, the inclusion of MgO nanoparticles increased the pressure drop and the friction factor values. At Reynolds number = 10500 and weight percentage = 0.3, the former was improved by 33.8%, while the latter was improved by 37%. The creation of a porous particle fouling layer on the interior wall inner of tubes results in a fouling thermal resistance that changing asymptotically with time, according to the results. Overall, the combination of MgO/water and ethylene glycol exhibits excellent potential for application as a coolant in heating exchangers.

Ali et al. [89] examined the MgO-oil based nanofluid's ability to transfer heat in a tiny counter-flow double pipe heating exchanger. The basis fluid for the nanofluid was maize oil, and the MgO particles were nanoscale. The heat exchanger had a length of 500 mm and was constructed of 316 stainless steels. In the inner tube, the nanofluid serves as the heating medium while the annulus is filled with cold water. The commercial software ANSYS FLUENT 17.0 was utilized for numerical analysis. The results of using nanofluids as a hot medium are contrasted with those of using pure oil as the base fluid. Researchers have looked at the impacts of hot nanofluid input flow rate and nanoparticle concentration. It is discovered that the typical heating transfer rates for nanofluids are greater than those for pure maize oil. The total heating transfer coefficient and heating transfer rate are both positively impacted by increasing MgO content and nanofluid intake flow rates. In contrast, the pumping power increases as the pressure drop increases.

Akinpelu et al. [90] investigated the thermophysical properties of three metal oxides during drilling operations at various temperatures, including titanium dioxide (TiO_2), aluminum oxide (Al_2O_3), and copper oxide (CuO) dispersed in a CMC water mixture. Each oxide's nanoparticles were assessed at a maximum concentration of 0.4 volume percent at less than or equal to 0.4 concentration in water. The established governing equations were reduced to a set of Ordinary Differential Equations, which were then numerically solved utilizing the shooting method and the Runge Kutta Scheme (order 4). The results demonstrated that the metal oxides improved the heat transfer properties of the CMC/water combination. Moreover, the increase in conductivity with TiO_2 in CMC water is the least and the biggest with CuO in CMC water combination. As the volume percent of nanoparticles in the dispensing medium grew, viscosity and thermal conductivity increased as well. When these results were compared to earlier research, they were found to be in perfect agreement.

Hasan et al. [91] studied and minimized oil fouling in a twin pipe heating exchanger using a surface active agent to facilitate the flowing of a dispersion fluid with varying amounts of dispersed oil fractions in water. Under turbulent flow circumstances, for both hot and cold fluids, the effect of the dispersed oil fraction (5%vol and 10%vol) and temperature (35 C - 55 C) on the oil fouling rate was investigated and addressed. To minimize the fouling rate in turbulent flow, different quantities of alkylbenzene sulfonate were used as a surfactant. It was discovered that when the fluid temperature lowers, the fouling thermal resistance (Rf) rises. Because of increased oil deposition, for all temperatures, the Rf increases as the fraction of dispersed oil increases. A considerable reduction in Rf was seen after adding 0.2%vol to 0.5%vol of alkylbenzene sulfonate, based on the oil fraction and Reynolds number. As Reynolds number fell, the mitigation percentage rose, reaching as high as 96%.

Yanjiao et al. [92] presented of creating boron nitride/ethylene alcohol (BN/EG) nanofluids in two steps. Investigations were done on how dispersant affected stability, thermal conductivity, and viscosity. The results demonstrated that the addition of anionic and cationic dispersants rapidly reduces the stabilization of BN/EG nanofluids, which has minimal practical application value. Non-ionic dispersants, on the other hand, may increase stability and fluidity while also increasing heat conductivity.

2.6. Motivation

From the literature can be concluded that the works focused on the heating transfer enhancement using different techniques and nanofluid in heating exchanger. It can be noted increasing Reynolds number, nanofluid concentrations, mass flow rates lead to enhance the convection heat transfer.

The objective of this study is to investigate the impact of single and two phases flow on the heat transfer characteristics of double pipe heat exchangers containing various hot fluids types. The hot fluids are pure water, the water-Cmc fluid, the water-MgO fluid and the water-MgO-Cmc fluid. The water-Cmc fluid results from mixing pure water with Cmc at two concentrations 0.2% and 0.5% by weight. The water-MgO fluid results from mixing pure water with MgO nanoparticles at four concentrations 0.125%, 0.25%, 0.5% and 1% by volume. The water-MgO-Cmc fluid present main fluid in this work result from mixing pure water with each previous concentration of MgO and Cmc. Besides, the influence of the two phases flow and mixed nanoparticles with surfactant together will be studied for the first time considering the influence of heat exchanger design and flow conditions which fill the gap in the previous publications. Also, there is no experimental work implements this case which can lead to illustrate the complex phenomenon in full-details.

In this study, the impact of using two phases flow in annular side and different hot fluids flow in inner pipe, will be carried out experimentally. The hot fluids heated to 50 ^{o}C and using a high technique equipment in measuring the parameter such as pressure sensor and temperature data logger. The CFD simulation carried out by using the commercial code ANSYS Fluent 2020 R1 to find temperature, pressure and velocity distributions for nanofluid flow under effect of single and two phases flow.

2.7 Summary of important investigation

Based upon the comprehensive review and according to the author's knowledge there is many works on heat transfer effected by two phases, nanofluids and nanofluids with surfactant in heat exchanger application as indicated in table (2-2).

Table (2-1): The scope of literature review.

Author	System	parameters	Results
Rao and Sankar	CuO nanofluids flow in a double pipe U-bend heat exchanger under turbulent flow conditions	- Flow rate - NPS conc.	the Nusselt number of nanofluids increases with increase of Reynolds number and particle volume concentrations. The Nusselt number enhancement is about 18.6% at 0.06% volume concentration when compared to base fluid with a pumping penalty of 1.09-times
Pattanayak et al.	double-pipe counter-flow heat exchanger	- NPS types - NPS conc.	The thermal conductivity, viscosity, and friction factor all increased, but the Reynolds number decreased. There exists a link between the experimentally measured data for the Nusselt number and the data for all these nanofluids, with an error of just 11.4%. It was discovered that TiO_2-water nanofluids were the most efficient of all the nanofluids tested.
Jassim and Ahmed	of a double pipe heat exchanger	- Nanofluid types - NPS type - Re	raising the nanofluid's mass-flow Nusselt number. For the aforesaid Re and concentration range, Al_2O_3 and Cu enhancements are up to 13% and 23%, respectively. Experimental findings demonstrate a significant efficiency boost (up to 7% for aluminum

			oxide and 10% for copper). Increased hot-side inlet temperature boosts performance. Nanoparticles increase heat leak from the shell-side (cold fluid) to atmosphere according to concentration. The heat leak in aluminum oxide nanofluid is higher than in copper nanofluid.
Akhtari et al.	double pipe and shell and tube heat exchangers, under laminar flow conditions	hot and cold volume flow rates, nanofluid temperature, and nanoparticle concentration	The heat transfer coefficients of nanofluid in double pipe and shell and tube heat exchangers are 13.2% and 21.3% greater than those of pure water. Nanofluid outperforms twin pipe heat exchangers by 26.2% in shell and tube heat exchangers. The heat exchangers were modeled using computational fluid dynamics (CFD). Nanofluid global heat transfer coefficients match experimental values.
Khedkar et al.	a concentric tube 13 heat exchanger	- Flow rate - Tubes number - NPS conc.	The average heat transfer rates for nanofluids as a cooling medium are greater than those for water, which is also utilized as a cooling media, and this rises with nanofluid composition. This study's findings are technologically significant for the efficient design of concentric tube heat exchangers to improve cooling performance in low heat flux cooling systems.

Davarnejad and Jamshidzadeh	turbulent heat transport behavior of a Magnesium Oxide-water nanofluid in a circular tube using computational fluid dynamics (CFD)	- Re - NPS conc. - Flow types (single, two phase, three phase flow)	Simulations matched experimental data in the literature. The Nusselt number (Nu) grew as nanofluid volume % increase in experimental work and simulation (this research). Nanofluid friction increased, but Nu had a greater impact on heat transfer increment. Two-phase models predicted heat transfer better, particularly at higher nanoparticle volumes.
Rao and Sankar	a double pipe U-bend heat exchanger, CFD	- Re - NPS conc. -	The results revealed that as volume fraction and Reynolds number increased Nusselt number increased, and friction factor decreased. Based on the numerical results, the Nusselt number enhancement for 0.3% nanofluid is 18% with a friction penalty of 1.14-times compared to water results.
Dew and Shrivastava	Pipe	- -NPS conc.	Analysis reveals that copper-oxide nano fluid has the greatest heat transfer when compared to other nano fluids. CuO nano fluid has 8% greater heat transmission than Al_2O_3, and CuO has 39.90% more heat transfer than Fe_2O_3.
Naik et al.	Pipe	- NPS types - NPS conc.	The findings demonstrate that the heat transfer rate rises with increasing flow rates. It has also been found

			that the heat transfer rate increases with increasing operating temperature and nanoparticle concentration.
Reddy and Rao	twin pipe heat exchanger with and without helical coil inserts	- NPS conc. - Based fluid conc. - Flow rate	In a tube with a P/d = 2.5 helical coil insert, 0.02% nanofluid increases heat transfer coefficient and friction factor by 13.85% and 10.69%, respectively. Heat transfer coefficient and friction factor estimates are compared to literature. Experimental data generates generalized correlations for Nusselt number and friction factor. Graphics and tables show the results. Experimental error is 10% after uncertainty analysis.
Das et al.	stability and characteristics of Al2O3-water nanofluids, as well as the influence of surfactants on those properties	temperature (20-60 °C) and solid volume fractions (0.1-2.0%)	the sensitivity of thermal conductivity rises with particle loading at a given temperature. The findings offered a complete thermophysical property database of water-based Al_2O_3 nanofluids for use in a variety of engineering applications.
Arya et al.	counter-current corrugated plate heat exchanger using MgO/ethylene glycol nanofluid	- Flow rate - NPS Conc.	Flow rate and mass concentration promote convective heat transfer. Both increase system pressure drops. Heat transfer coefficient and pressure drop rose 35% and 85% at wt.% = 0.3. Intriguingly, input temperature increased heat transfer coefficient by 9.8% at wt.% =

			0.3 but did not affect pressure drop readings. MgO nanoparticles improved heat exchanger thermo-hydraulic p
Arya et al.	MgO-ethylene glycol as a heat transfer fluid in a double-pipe heat exchanger.	The nanofluid was made in two steps at weight concentrations of 0.1, 0.2, and 0.3%.	The friction factor rose as the mass concentration of nanoparticles increased, with the greatest friction factor augmentation of 32% belonging to the nanofluid with mass concentration of wt.%= 0.3. Similarly, input temperature was shown to have just a little impact on the heat transfer coefficient and no effect on the system's friction factor or pressure drop. The thermo-physical characteristics of a MgO-ethylene glycol nanofluid were also investigated experimentally at different temperatures.
Arya et al.	MgO/water-ethylene glycol nanofluids in a double-pipe heat exchanger.	- Inlet temperature - MgO conc. - Re	Results also revealed that the formation of porous particulate fouling layer on the internal wall of the inner tube creates a fouling thermal resistance which changes asymptotically with time. Overall, MgO/water-ethylene glycol shows a great potential to be used as a coolant within a heat exchanger.

Ali et al.	a MgO-oil based nanofluid in a tiny counter-flow double-pipe heat exchanger.	- Flow rate - NPS conc.	The average heat transfer rates for nanofluids are found to be greater than those for pure corn oil. The enhancement of both MgO concentration and nanofluid intake flow rates has a favorable effect on the total heat transfer coefficient and heat transfer rate. In contrast, as the pressure drop grows, so does the pumping power.
Akinpelu et al.	thermophysical characteristics of three metal oxides, Titanium Oxide (TiO_2), Aluminum Oxide (Al_2O_3), and Copper Oxide (CuO) dispersed in a Carboxyl methyl cellulose (CMC) water combination	- Deferent drilling temperatures - CMC conc. - NPS conc.	The results revealed that the metal oxides improved the heat transmission performance of the CMC water combination. Furthermore, the conductivity increase with TiO_2 in CMC water combination is the least and the greatest with CuO in CMC water mixture. Viscosity and thermal conductivity rose as the volume percent of nanoparticles in the dispensing medium increased. These findings were compared to previous research and found to be in excellent accord.

3

CHAPTER THREE

EXPERIMENTAL WORK

CHPTER THREE

EXPERIMENTAL WORK

3.1 Motivation

Experimental measurements provide the most practical and dependable information for thermo-physics properties, temperature distribution, flow rates, and other parameters at defined experimental points. The present work includes the design and build up of the experimental rig in Laboratories of the Department of Mechanical Engineering for postgraduate students. The main objective of this work is to analyze and improve heat transfer in a U-bend double pipe heat exchanger under the effect of a single and two-phase flow by using different hot fluid types. There are two cycles for fluids flow impalement in this work hot and cold cycle. The hot cycle presents worm fluid flow inside the inner pipe whereas a cold fluid presents the applied of cold fluid in annular side. The hot cycle is filled by different hot fluids like pure water, the water-CMC fluid, the water-MgO fluid, and the water-MgO-CMC fluid. While, the cold cycle had been filled by pure water as single phase or added air to pure water to generate two-phase flow.

3.2 Experimental Apparatus:

Where the mean apparatus presents are:

1. Test section (double pipe heat exchanger with U-bend).
2. The hot cycle represents hot fluid flow in inner copper pipe. This cycle consists of two tanks, heater, pump, flow meter, control valves, pipes and fitting.
3. The cold fluid cycle consists of two pass one for water and another for air.
4. The water pass has tank, pump, water flow meter, control valves, pipes and fitting.

5. The air pass has compressor, reservoir, air flow meter and pressure regulator.
6. Mixing chamber to mix water and air to get two phases flow, the place of this chamber is in the cold fluid cycle.
7. The electric control boards.
8. Instrument for measuring temperature and pressure.

Figure (3-1) shows the schematic diagram of test rig assembly used in this experimental work. Figure (3-2) presents the setup of test rig. Some of these parts are locally manufactured, all fitting are connected carefully to avoid any leakage. Multi-layer insulator is used to isolate the test section and prevent any heat dissipation in order to get an accurate result. The test rig had the following parts;

1. Test section with U-bend shape
2. Hot fluid cycle
3. Cold fluid cycle
4. Tanks
5. Electrical heater
6. Centrifugal Pumps
7. Control valves
8. Piping system
9. Air stream
10. Air compressor
11. Air reservoir
12. Pressure regulator
13. Mixing chamber
14. Check valve
15. Electric control panel
16. Measuring devices

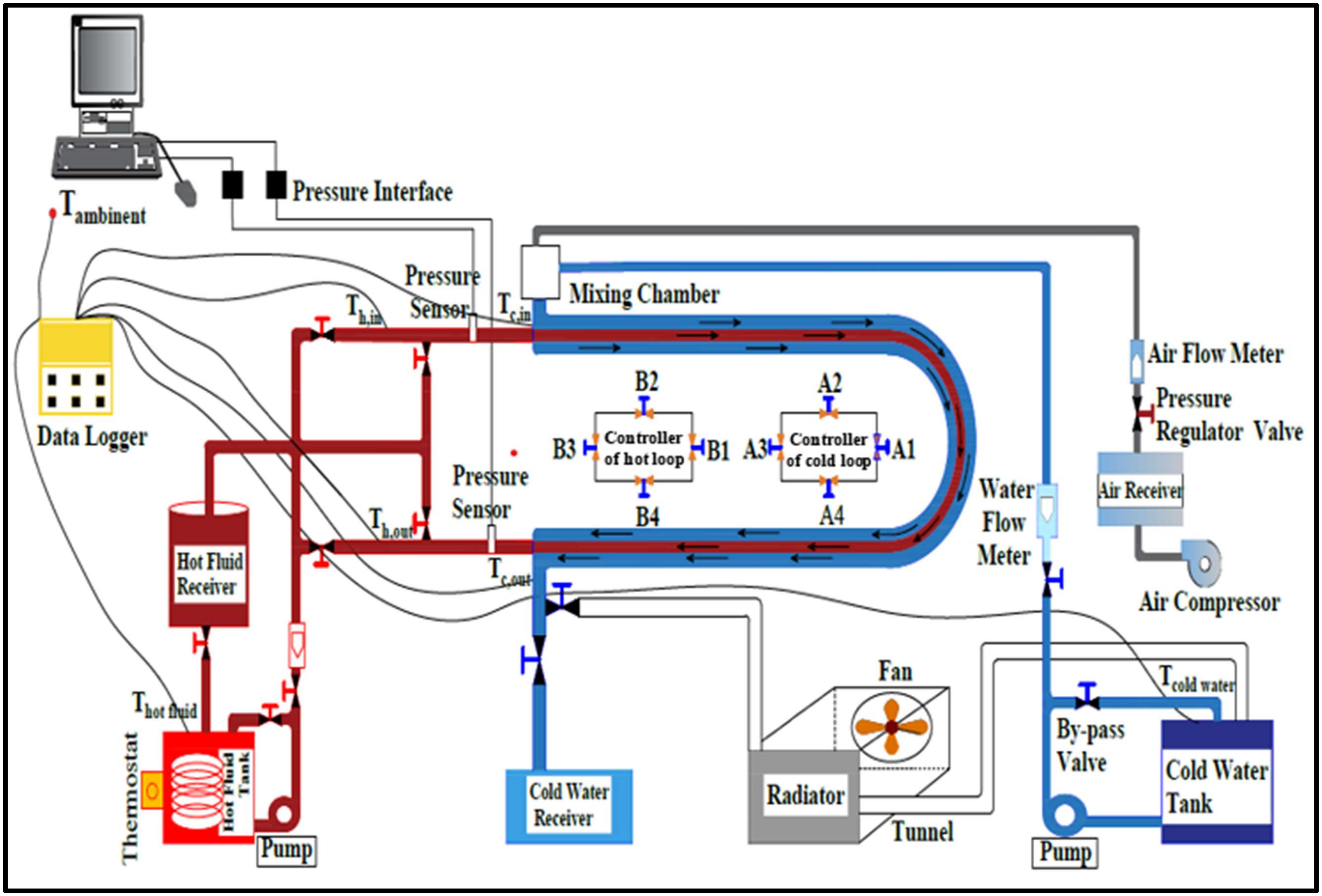

Figure (3-1): Schematic diagram of design rig.

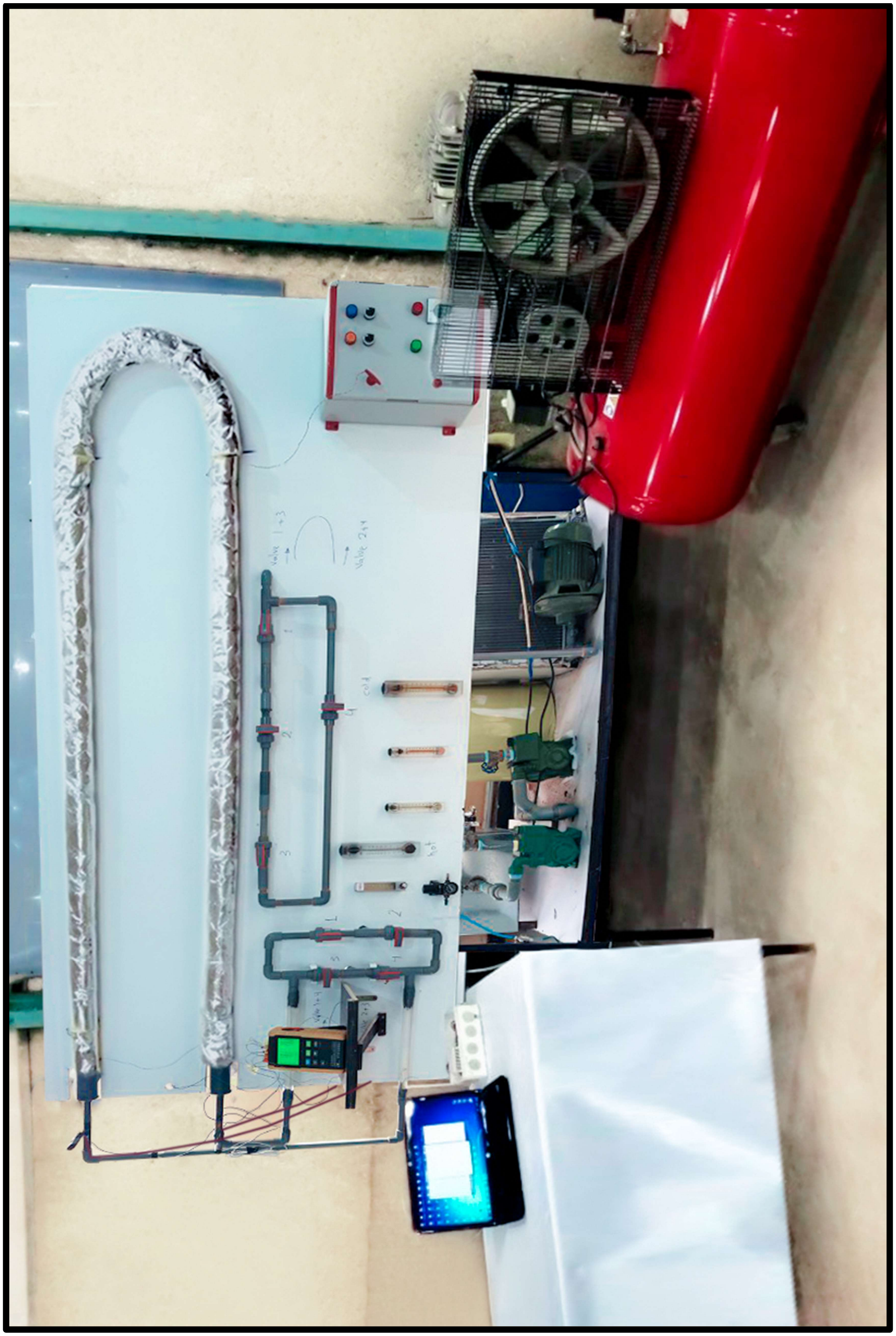

Figure (3-2): Photo of experimental designed rig.

3.2.1. The Test Section

The test section of rig that is implemented in the present work for a double pipe heat exchanger is built up from two concentrated pipes with U-bend. The inner pipe made of copper with inner and outer diameter of 0.02 m & 0.022 m respectively. The outer pipe made of Perspex has inner and outer diameters of 0.045 and 0.05 mm, respectively. The schematic diagram and dimensions of the test section are shown in figure (3-3).

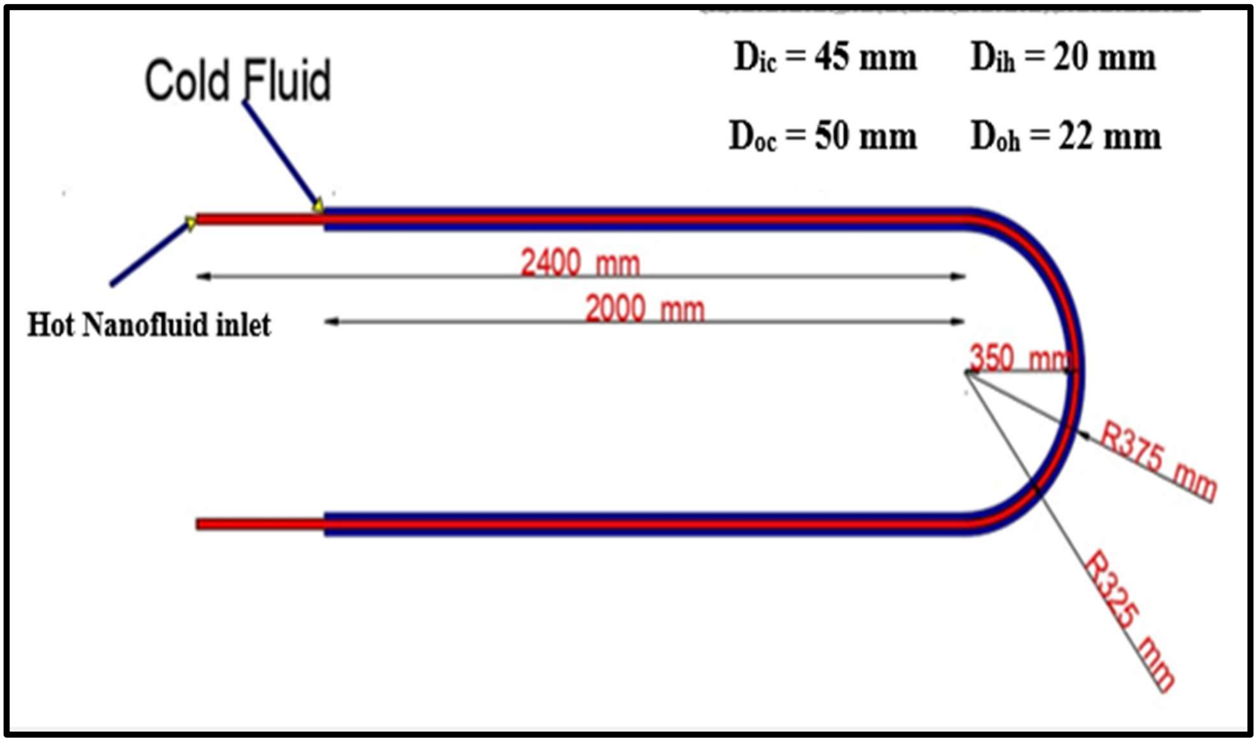

Figure (3-3): Schematic diagram of the test section.

3.2.2. The Hot Flow Cycle

It is the inner cycle where the hot working fluid flow from the hot fluid tank through the inner copper pipe to accumulate hot fluid tank and then returns to the start point. This cycle consists of two tanks, two heaters, hot fluid pump, hot fluid flow meter, control valves, and piping system as indicated with a red color in figures (3-1) and (3-3)

3.2.3. The Cold Flow Cycle

It is the outer cycle where the cold fluid flow from cold water tank through the annular side between copper and Perspex pipes to the accumulate tank or to the outside. The cold fluid in this cycle either single phase or two phases. This fluid is represented by a blue color in figures (3-1) and (3-3).

3.2.4. Tanks

There are four different tanks used for containment hot fluid and cold fluid in a current work. The first, hot fluid tank is used for the purpose of containing and preparing a hot fluid to the hot flow cycle and it is manufactured from a stainless-steel metal. Two heaters are used to heat the working fluid. This tank filled with working fluid and used to feed the system with the required amount of hot working fluid through the pump. The hot fluid tank has dimensions of (1200 X 60 X 60) mm with 4 mm thickness as shown in figure (3-4). The accumulation hot fluid tank is the second tank in the hot flow cycle that used for accumulating and re-circulating of hot working fluid returning from cycle. It has a capacity of 100 liter, as shown in figure (3-5). The hot working fluid that is accumulated in second tank returns to the first tank after open the valve between them.

The third tank, the cold-water storage with a yellow color, as depicted by figure (3-4). This tank is made from galvanized steel sheet with cylindrical shape with dimension of 0.5 m and 1.2 m of diameter and height, respectively. Finally, the accumulated cold-water tank has the same dimensions and a color of the previous tank. It is used for the purpose of receiving cold fluid that passed through annular side. For the purpose of delivering hot fluid and cold water, a set of measuring devices and fitting are used. The pure water thermo-physical properties are shown in **appendix A.**

3.2.5 Electric Heater

It is a device used to heat the working fluid electrically. The hot fluid temperature is recorded using 12-channel temperature recorder device, as shown in figure (3-6). There are two heaters in the test rig. Each heater of (1200 W) power is located horizontally in lower side for the hot tank, with thermostat to keep the working fluid temperature 50 °C.

3.2.6 The Circulating Pump

It is a device utilized to pump and circulate the working fluid as shown in the schematic diagram of figure (3-1). There are two pumps used for the purpose of fetching hot and cold fluids from reservoir and suppling team the right path. One of these pumps is connected to the hot cycle and used to pump and circulate the hot fluid through the inner pipe of the designed rig. Another pump used to supply water at the entrance of the annuls side of the test rig. The two pumps have the same specifications and they are manufactured by Marquees company, see figure (3-7).

3.2.7 Control Valves

They are used to control the fluid flow coming from tanks. The opening or closing of the control valves is usually done manually, as shown in the schematic diagram figure (3-1).

3.2.8 Piping System

Piping system contained valves, a bypass pipe line to control on flow of hot and cold fluid. Check valve connected at the inlet port of the cold fluid to prevent backflow in case of two phases flow. The feed line of liquid contains a valve to control the flow supply through the pipes and flow meter, as shown in figure (3-1). The amount of water that delivered through this system could be measure by a water flow meter. The piping system classifies into two branches one for cold fluid and the other is for hot fluid. For hot and cold pipes has controller to control on the flow direction. The control system is shown in Figure (3-8).

3.2.9 Compressor

It presents a source for accumulate and deliver air which is then mixed with water in a mixing chamber to form two-phase flow. The physical properties of air as listed in **appendix A**. The air passage must have a reservoir after compressor to accumulate a large amount of air and supply it at steady and fixed flow rate during the test rig run. The compressor of model BS 5169 IIIE is made by IR company. This type of compressor is manufactured to push air as a positive displacement mechanism. The specifications of this model are: 150 L/s max air flow rate, the operation temperature range between (-10 to 120) °C, and the maximum pressure of delivered air of 16.5 bar. The compressor is shown in figure (3-9).

Figure (3-4): Hot tank of nanofluid.

Figure (3 - 5): Accumulated hot nanofluid tank.

Figure (3 -6): Heaters.

Figure (3 -7): Centrifugal pump

Figure (3-8): Pipe controller.

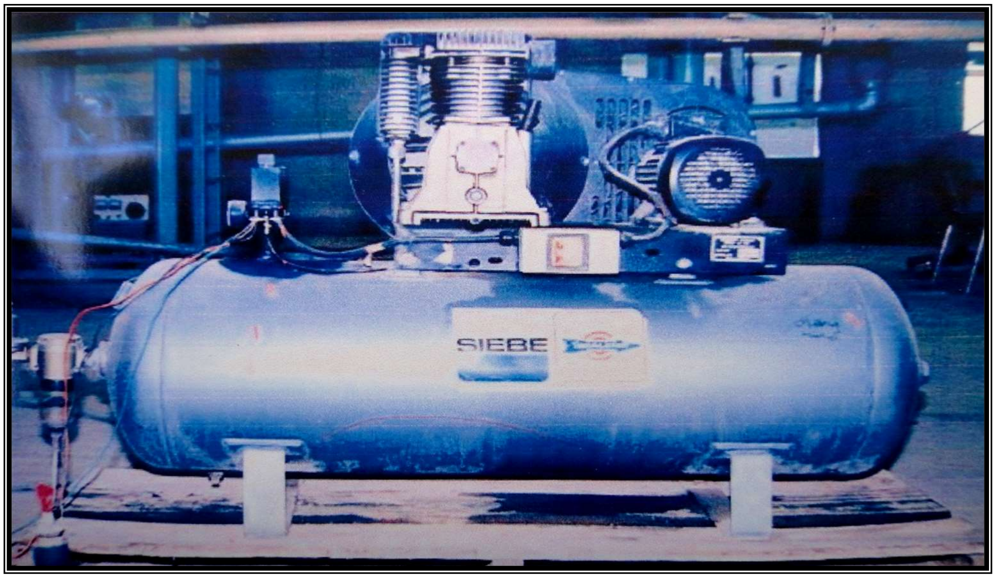

Figure (3-9): Compressor.

3.2.10 The Air Stream

This is the amount of air flow rate required to mix with cold water and produce air-water two phases flow. This process needed to several air devices for supply, storage, regulator (pressure and flow rate), and connect them all literally and technically, as shown in the schematic diagram of figure (3-1) which appears with gray color.

3.2.11 Air Reservoir

Is used to collect the air coming from a compressor under a pressure of 3 bar in order to provide the air to the flow meter, as illustrated by figure (3-10).

3.2.12. Pressure Regulator

In this work, a pressure regulator (Startz Electric RA2000) is used with a range of (0 – 10 bar), as shown in figure (3-11) to control the air pressure and the air flow coming from air reservoir. The pressure in all tests is kept a constant at (1.2 bar). The calibration operation for this device is done in Central Organization for Standardization and Quality Control as shown in **appendix B**.

3.2.13. Check Valve

The mechanism of this item is depending on a circle piece of iron with spring to allow flow in a one direction only and prevent a reverse flow as shown in figure (3-12). Reverse flow occurs in a two-phase flow when the one phase has a pressure higher than the other.

3.2.14. Mixing Chamber

This equipment is used to get a good mixing of air-water. It is a mild steel chamber with two inputs, one is for water and the other is for air, while, there is one output for mixed phases (air-water). Figure (3-13) shows a schematic represents of the mixing chamber.

Figure (3-10): Reservoir.

Figure (3-11): Pressure regulator.

Figure (3-12): Check valve

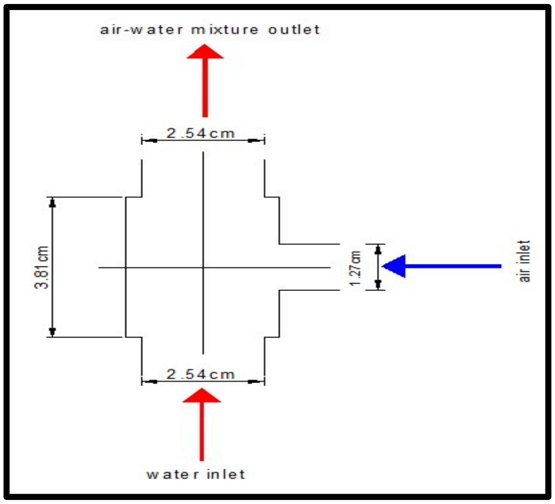

Figure (3-13): Schematic diagram of mixing Chamber.

3.2.15. The Control Panel

Figure (3-14) shows a control board which contains the following components:

1- Switches; to turn on and turn off the circulating pumps (oaring and blue).
2- Selector switch; To turn on and turn off the electrical heater (red).
3- Regulator switch to control the cooling fan speed (green).

Figure (3-14): Control Panel

3.2.16. Measuring Systems

3.2.16.1. Liquid Flow Meter

A standard liquid flow meter type (ZYIA) is used. The flow rate is in the range of (2 to 35) L/min, as shown in figure (3-15). A check valve is used to prevent the back flow in the line of cold water. The flow entered the bottom of the tapered vertical pipe and caused the float to move upward. The weight and buoyancy force balanced the float rose to a point in the pipe. It is connected vertically to measure hot nanofluid and cold-water flow rates that exist from the pump before entering the double pipe heat exchanger.

3.2.16.2. Air Flow Meter Air flow meter is a measurement device, with an air flow rate of rang (350 to 3500) L/hr as shown in figure (3-16). The mechanism of this devise depends on the air pressure that push float tapered vertical tube to the required level of the flow rate depending on buoyancy forces.

Figure (3-15): Liquid flow meter

Figure (3 -16): Air flow meter

3.2.16.3. Temperature Measurement

The temperatures at different positions in the test rig are measured by using data logger with SD card as shown in figure (3-17). This operation called a paperless recorder to save temperatures values at different positions and times.

There are seven channels with type K thermocouples (chromium$^-$-aluminum$^+$) are used. The temperature ranges from (-100 to 1300 °C) of thermocouple type K. Thermocouples are fixed in different positions along the rig pipe as presented in table (3-1). Table (3-2) presents accuracy of thermocouples type K. Figure (3-18) shows the calibration certificate of temperature recorder device.

Calibration Certificate

This certificate guarantee that the product has been inspected and tested in accordance with the published specifications.

The instrument has been calibrated by using equipment which already calibrated to standards traceable to international standards.

ISO 9001:2000 SGS

UKAS QUALITY MANAGEMENT 005

CE

The Art of Measurement

CAL9712

Figure (3-17): Temperature recorder device. **Figure (3-18):** Calibration certificate.

Table (3- 1): Thermocouple's position.

Channels No.	Position
1	hot tank
2	cold tank
3	inlet cold fluid
4	outlet cold fluid
5	inlet hot fluid
6	outlet hot fluid
7	ambient

Table (3- 2): Thermocouples specification.

Sensor type	Resolution	Range	Accuracy
Type K	0.1°C	(-50.1°C to 100°C)	± (0.4 % +1°C)
		(-50.0°C to 999.9°C)	± (0.4 % +0.5°C)
	1°C	(1000°C to 1300°C)	± (0.4 % +1°C)

3.2.16.4. Pressure Transducer

The pressure of hot fluid that flowed in the inner pipe of the heat exchanger measured by a pressure transducer setup (PTS) technique. This technique is dependent on the connected pressure sensors at the inlet and the outlet of the inner pipe as shown in Figure (3-19). This operation is done by connected sensor with pressure interface and then to computer. The pressure sensor type and model are pointed in figure (3-19). The measured value of pressure is converted the current and voltage by sensor, then transform to computer. This signal is processed using a pre-installed program in the same computer. Pressure sensor operates between (0 to 20 Mpa) that implemented in this work with type KELLER. Table (3-3) represents the specifications of the pressure transducer.

Figure (3-19): Photograph of (a) Data logger (b) Transformer (c) Pressure transducer.

Table (3-3): Specifications of pressure sensor.

Operating pressure range	(0 to 1) bar
Sensor Output	Current (4 to 20 mA)
Hysteresis	0.5%
Body Material	Stainless Steel
Pressure Sensor Type	Piezo resistive Transmitter
Operating Temperature	(-20°C to +80°C)
External Diameter	17mm
External Length (height)	76mm

3.2.16.5. Interface System

This device has two jobs, receiving single from sensors and then sending it to the computer. The signal that transformed is processed by a free software setup on computer as shown in figure (3-2). This operation means transform analog signal to digital signal and saved data in computer. The interface system specifications are tabulated in table (3-4) and figure (3-20).

Table (3-4): Specifications of interface system.

Supply voltage	Over USP line (5 V dc, +/- 5%)		
Power consumption	1 W		
Accuracy	+/- 0.2%		
Environment temperature	Operation: -10 to 55°C		Storage: -20 to 65°C
Dimension	Height:112mm	Width:72mm	Depth:26mm
Sampling period	750 ms		

3.3. Calibration of Measuring Devices3.3.1. Calibration of Temperature Recorder Device: The thermocouples of the data logger are calibrated against a mercury thermometer. The calibration is performed only for channels 1 and 7. The recorded values of the two devices are shown in **appendix C**. The other channels from number two to six are calibrated by using the value of accuracy $\pm(0.4\% + 0.5\ ^{o}C)$ as shown in table (3-5) for type K thermocouple according to the reading temperature range $(-50$ to $999.9\ ^{o}C)$.

3.3.2. Pressure Measuring System Calibration This process is done in two steps. At the begging holes are made at the inlet and the outlet of inner pipe and then the U-tube manometer is attached to these holes, and calculating the difference in pressure at various flow rates. Then pressure sensors are also connected to the inlet and the outlet of the inner pipe and measuring pressure values at the same previous flow rate. The information of this process is represented in **appendix C**.

$$P_{Calib} = 0.1656 + 1.1748P_{re} - 0.0393P_{re}^2 \quad (3\text{-}2)$$

Where P_{calib} is calibrated pressure value, while P_{re} is the pressure measurement by pressure sensor. The recorded values of the two devices are shown in **appendix C.**

3.3.3. Liquid Flow Meter Calibration

The flowmeter can be calibrated using the conventional method, this method is done by using stop watch and scaled tank to measure the amount of water at each selected value of water flow rate. The calibration values and curve presented in **appendix C.** A check valve that is located directly after the flow meter to prevent the back flow.

$$Q_{Calib} = 0.8845 + 1.1309\,Q_{re} - 0.0005\,Q_{re}^2 \quad (3\text{-}3)$$

Where (Q_{calib}) is calibrated discharge value, while (Q_{re}) is the flow meter measurement.

3.3.4. Calibration of Air Flow Meters:

The calibration of air flow meter done by using orifice and U-tube manometer. The values of air discharge that is taken from air flow meter and orifice could be seen in **appendix C**. The pressure values at each air flow from flow meter and orifice gives calibration response.

A. Orifice Characteristic

The orifice that is implemented in this calibration has inner and outer diameter 14 and 45 mm, respectively. The air flow rate is computed by straight pipe. There are two pressure taps one for inlet and another at outlet, these taps located at pipe diameter upstream and downstream respectively as shown in figure (3-20). The following equation derived from Bernoulli's equation as presented by **Holman [93]** used to measure air flow rate by orifice when consider flow is incompressible.

$$\boldsymbol{Q_{theory}} = \boldsymbol{U_2 A_2} = \frac{A_2}{\sqrt{1-\left(\frac{A_2}{A_1}\right)^2}} \sqrt{\frac{2(\Delta P)_G}{\rho_G}} \tag{3.4}$$

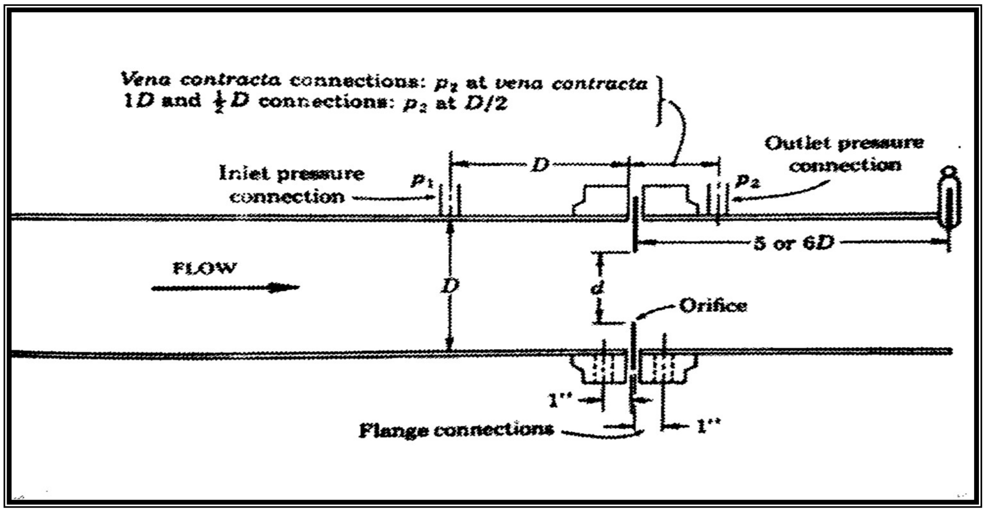

Figure (3-20): Location of outlet pressure connection for orifice taps **[93]**.

B. U-Tube Manometer

The pressure drops between two flow point after and before the orifice measure by U-tube manometer to calibrate the air flow meter. The liquid used in the manometer is mercury. A comparison between measured discharge by orifice and measured discharge by air flow meter has been made for every air flow rate, the values of discharge are calibrated, as shown in **appendix C**. The calibration curve for air flow meter represents in **appendix C**, which is used for different air flow rate.

3.4. Preparations of MgO Nanofluids.

There are many techniques that adopted for the preparation of nanofluids. The nanoparticle used to the preparation of nanofluid is MgO with a mean diameter less than 50 nm. Nanoparticle's volume concentrations used in this study are (0.125 %, 0.25 %, 0.5% and 1%). The properties of nanoparticle are given in **appendix D**. The following procedure represents the steps that used in the present work to mix distilled water and nanoparticle to prepare a nanofluid.

3.4.1. Steps for Preparing a Nanofluid

1. XRD Examine : The selected nano-powder has been tested using x-ray diffractometer (XRD). To Ensure that MgO nanoparticle is less than 50 nm should be examined by X Ray Diffraction (XRD) device shown in figure (3-21). The average grain size of MgO nanoparticles is found to be between 43 to 50 nm with a purity of 99.99% XRD pattern which is pointed in figure (3-22).

2. The Magnesium Oxide nanoparticles (MgO) have been selected in the present work having a BT-9300Z particle size less than 50 nm. Nanoparticles size has been measured using particle size analyzer as indicated in Figure (4-23).

Figure (3-21): XRD diffractometer

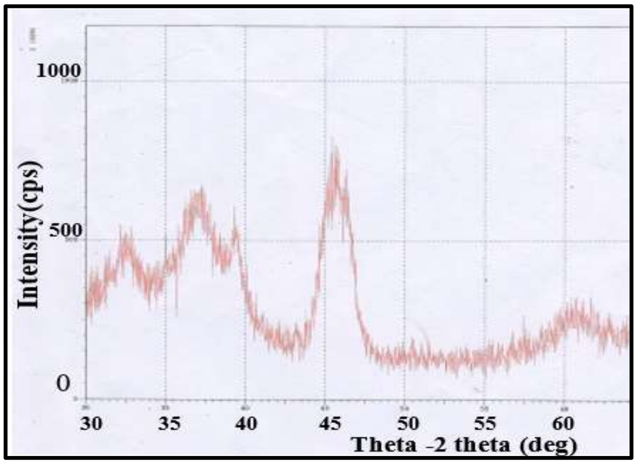

Figure (3-22): XRD pattern of MgO nanoparticle.

Figure (3-23): BT-9300Z particle size analyzer

3. Nanofluid Preparation

The best nanofluid produced from mixing MgO nanoparticles with a pure water by using ultrasonic cleaner model JTS-1018. This operation done in several steps. First step is by filling up the bath with more than of three quarters by water and putting containers of nanofluid, then connecting a basket to prevent any damage. Second step includes sending sound waves in the water-MgO fluid by increasing frequency from 50 Hz to 40 kHz. The time intervals to remain the water-MgO fluid in the ultrasonic cleaner about six hours to complete mixing process of the water-MgO fluid, this time increase with increasing nanoparticles concentration. The ultrasonic cleaner is shown in figure (3-24) and their specifications are given in the Table (3-5).

Table (3-5): Specifications of ultrasonic cleaner bath

Model	**JTS-1018**
Tanks working dimension (mm)	L_1= 406, W_1=305, H_1=460
Overall dimension (mm)	L_1= 586, W_1=485, H_1=680
Ultrasonic frequency	40 kHz
Ultrasonic power	720 Watt (variable)
Digital timer control	1-30 min
Capacity	54 liters
Temperature control range (ºC)	< 90 ºC
Ultrasonic power output	800 W

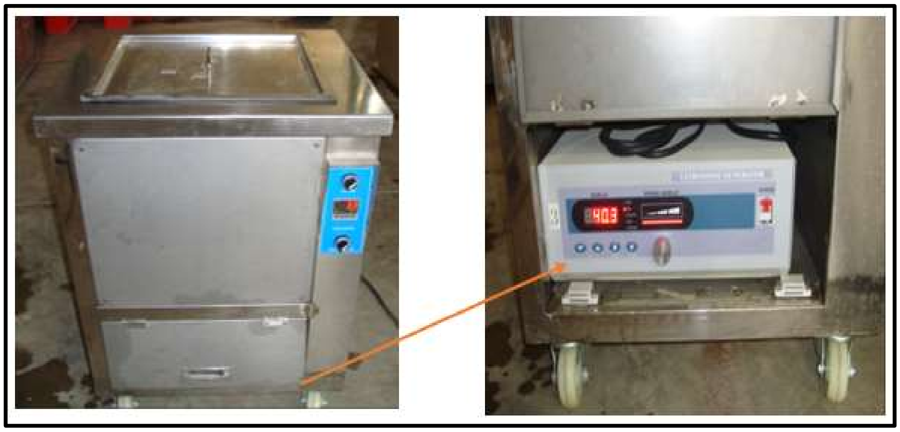

Figure (3-24): Ultrasonic cleaner

4. Volume Concentrations

The required volume fraction of MgO nanoparticles calculated by mixture law. This law dependent on mass and density of pure water and MgO nanoparticles. The mass of MgO nanoparticles for each concentration can be found using a sensitive electronic balance as shown in figure (3-25).

The mass of MgO nanoparticles added to thirty liters of pure water. Adding the weight of nanoparticles to thirty liter of the distilled water in order to calculate the concentrations. According to the following equation reported by [95].

Figure (3-25): Electronic weighting machine

$$\varphi\,\% = \frac{Volume\ of\ MgO}{Volume\ of\ MgO \quad Volume\ of\ Water} \qquad (3\text{-}5)$$

$$\varphi\,\% = \frac{(m_p/\rho_p)}{(m_p/\rho_p) + (\,m_{bf}/\rho_{bf}\,)} \qquad (3\text{-}6)$$

There are four volume concentrations in experiment are implemented as, (0.125 %, 0.25 %, 0.5% and 1%). The measured mass of MgO nanoparticles for each concentration presented in **appendix D**.

5. The water-MgO fluid is taken to magnetic stirrer device to complete mixing process and reduced agglomeration of MgO nanoparticles. The interval time of this operation about one hour.

6. The mixture of water-MgO fluid took to ultrasonic device to complete mixing of nanofluid. This operation is done in six hours.

7. The above steps can be used to prepare the Water-MgO fluid at each concentration require as 0.125%, 0.25%, 0.5% and 1%.

3.4.2. Nanofluid Property Measurements.

3.4.2.1. Measurement of Density

Sample volume with different concentrations of nanofluid weights and this weight is divided by volume. Measurements are repeated three times and then the average is taken to get an accurate measurement, as shown in figure (3-26). The measurement is carried out in the Laboratories of Babylon University. The results of experimental measurements of density are given in **appendix D**. There is a little difference of the density measurements with the empirical relation (3-7) used by **Zan Wu et al. [95],** and the differences are given in table (3-14).

$$\rho_{nf} = (1-\varphi)\rho_{bf} + \varphi\rho_p \qquad (3\text{-}7)$$

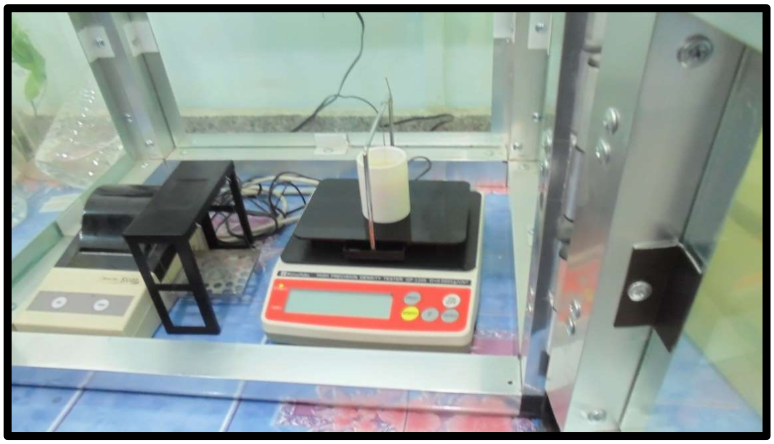

Figure (3-26) Measurement of the Nanofluids Density

3.4.2.2. Measurement of Specific Heat

Specific heat is measured by using (ESD – 201) type, as shown in figure (3-27). This device composed of a metal vessel with the capacity of 10 liters, and the vessel is isolated by polyester material from the outside. There is a mixer inside the vessel rotated by electric motor in order to distribute the temperature. The mercury thermometer is put in a small hole at top of the device to measure the temperature of nanofluid inside the vessel. The results of experimental measurements of specific heat are shown in **appendix D**. There is a little difference of the specific heat measurements with the empirical relation (3-8) used by **Zan Wu et al. [95],** and the differences are given in table (3-15).

$$Cp_{nf} = \frac{(1-\varphi_p)Cp_{bf}\rho_{bf}+\varphi_p Cp_p\rho_p}{\rho_{nf}} \qquad (3\text{-}8)$$

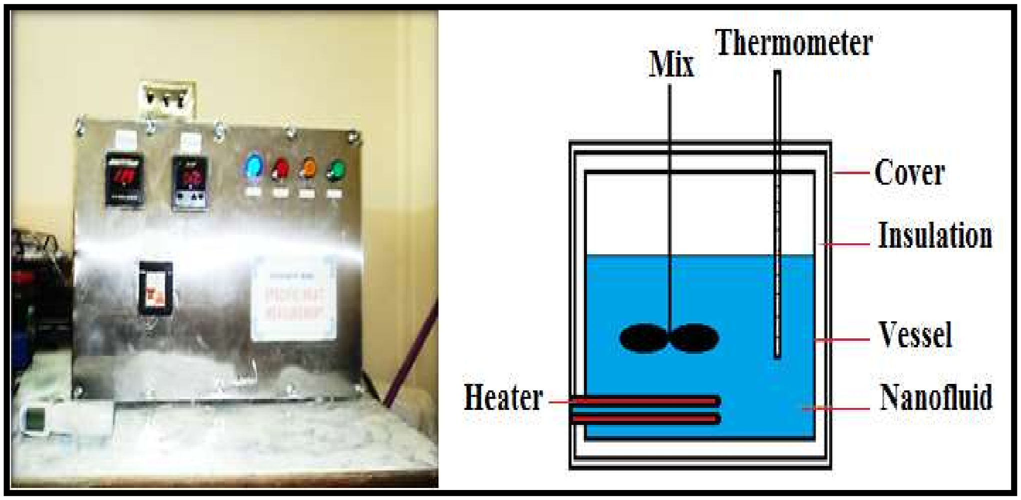

Figure. (3-27): Specific Heat Apparatus (ESD – 201)

3.4.2.3 Measurement of viscosity

In the present work, using a viscometer type [Brookfield digital viscometer model DV – E], (The board of industrial R & D - Petrochemical Research Center-Ministry of Science and Technology) is used as shown in figure (3-28). The principle of operation of the viscometer is to rotate a spindle immersed in the nanofluid sample and connected to a calibrated spring. The experimental measurements of viscosity presented in **appendix D**. There is a little difference in viscosity measurements with the empirical relation (3-9) used by **Zan Wu et al. [95],** and the differences are given in table (3-16).

$$\mu_{nf} = \mu_{bf}(1 + 2.5\varphi_p) \qquad (3\text{-}9)$$

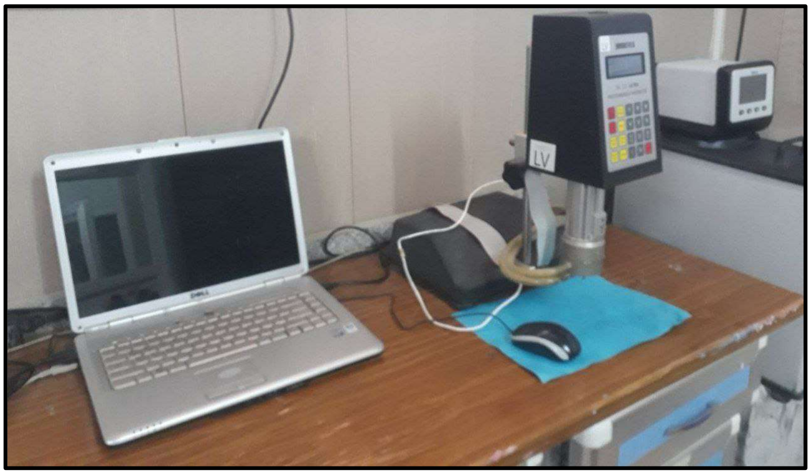

Figure (3-28): Brookfield DV-I prime viscometer

3.4.2.4. Measurement of Thermal Conductivity

The thermal conductivity of water-MgO fluid experimentally measured by using transient hot-wire technique as demonstrated in Figure (3-29). The results of measurements of thermal conductivity are given in table (3-17). There is a little difference of the thermal conductivity measurements with the empirical relation (3-10) used by **Zan Wu et al. [95],** and the differences are shown in **appendix D**.

$$k_{nf} = k_{bf}\,\frac{k_p + (n-1)k_{bf} + (n-1)\varphi\,(k_p - k_{bf})}{k_p + (n-1)k_{bf} - \varphi\,(k_p - k_{bf})} \qquad (3\text{-}10)$$

Figure. (3-29): Hot Disk Thermal Conductivity Apparatus

3.5. Preparations of Water–CMC Fluid

There are several techniques that employed to prepare CMC-water fluid. The technique that is presented in this work depending on the use of a swirling device. Preparing this fluid must take into account several notes. This fluid resulted from mixing CMC powder with distilled water together. The mixing operation done normally by adding CMC at concentrations range between (0.2 – 0.5) % by weight. The CMC-water fluid that resulted is non-Newtonian fluid. The CMC-water fluid is better selected in the thermal storge system than distilled water because it heats up quickly and saves heat for a period of time. This fluid used mainly in a thermal storge system in several application like building and industrial process. The properties of a carboxymethyl cellulose (CMC) are presented in **appendix D**. Figure (3-30) presents label on the preservative box containing carboxymethyl cellulose (CMC) powder.

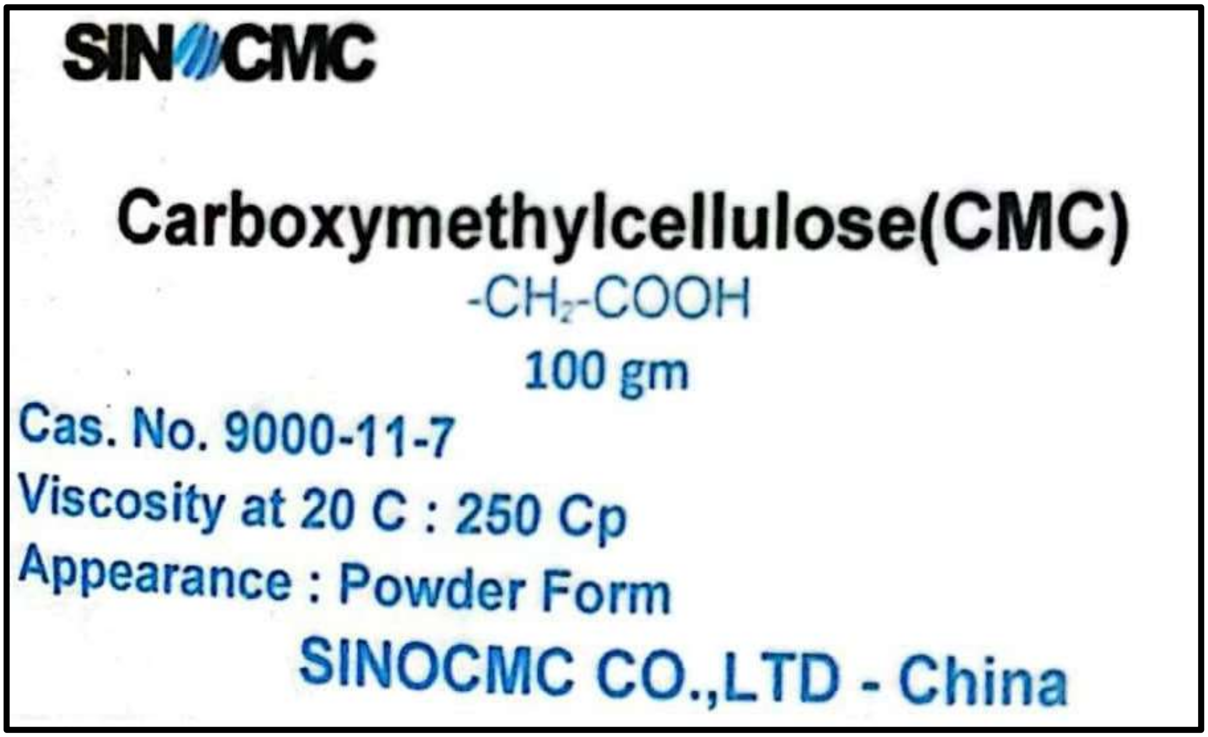

SINOCMC

Carboxymethylcellulose(CMC)

$-CH_2-COOH$

100 gm

Cas. No. 9000-11-7

Viscosity at 20 C : 250 Cp

Appearance : Powder Form

SINOCMC CO.,LTD - China

Figure (3-30): CMC properties

3.5.1. Steps of Preparation Water–CMC Fluid

1. The CMC powder concentrations that are added to pure water normally at range (0.2 – 0.5) by weight.
2. The amount of CMC powder that is added to pure water being measured by mixture law of weight concentration.

$$\varphi = \frac{mass\ of\ CMC}{mass\ of\ CMC + mass\ of\ Water} \quad (3\text{-}11)$$

$$\varphi = \frac{m_{Cmc}}{m_{Cmc} + m_w} \quad (3\text{-}12)$$

3. The mass CMC powder for each concentration is presented in **appendix D**.
4. electronic weighting machine used to measure mass of CMC powder at each concentration.
5. Before adding CMC powder to distilled water, this water must heat approximately to 40 ºC.
6. The hot pure water is put in mixture container and run swirl device on it without stopping, just during adding CMC.
7. The amount of CMC that is specified according to concentration range must be added to distilled water in very small quantities.
8. Swirl device stopped until finish adding the specified amount of CMC powder.
9. Continuing mixing operation using the swirl device for the purpose of ensuring no agglomeration and accumulation CMC powder in distilled water.
10. At the end of mixing operation all amount of the CMC-water fluid put in ultrasonic to complete mixing process and to ensure complete dissolution of CMC powder in distilled water.

3.5.2. The Water-CMC Fluid Property Measurements

The thermo-physical properties of CMC-water fluid must be measured experimentally by laboratory devices. When CMC powder mixed with distilled water produce new fluid normally this process is done by adding concentration by weight. The new fluid considered as non-Newtonian fluid. CMC-water fluid is a new fluid and thermo-physical properties of it must measure experimentally because these properties not documented in any references. After input CMC-water fluid in any laboratory device must be heated to 50 ºC and then measured the required property. The measurement is carried out in the Laboratories of Babylon University.

3.5.2.1. Measurement of Density

Sample weight with different concentrations of CMC powder is weighted and this weight mixed equivalent amount of distilled water. Measurements are repeated three times and then the average is taken to get an accurate measurement, as presented in section (3.4.2.1). The results of experimental measurements of density are shown in **appendix D**.

3.5.2.2. Measurement of Specific Heat

Specific heat is measured by using (ESD–201) type, as presented in section (3.4.2.2). The results of experimental measurements of specific heat are shown in **appendix D**.

3.5.2.3. Measurement of the Viscosity

The procedure of measured CMC-water fluid viscosity is the same procedure that is done in section (3.4.2.3). The experimental measurements of CMC-water fluid viscosity presented in **appendix D**.

3.5.2.4. Measurement of Thermal Conductivity

The thermal conductivity is measured as presented in section (3.4.2.4). The results of measurements of thermal conductivity are shown in **appendix D**.

3.6. Preparations of Water–MgO - CMC Fluid

The working fluid (CMC-MgO-Water fluid) that presents in this work depended on method of preparation. This method based on the principle of non-agglomeration of polymer and nanoparticles. Therefore, the process of preparing this fluid requires time in addition to some complications. This working fluid is prepared in two stages, and each of these stages requires time and mastery of preparation. The process of preparing and measuring the properties of this fluid will be explained as follows:

3.6.1. Steps of Preparation Water–MgO-CMC Fluid

As it is clear that the preparation of this fluid is accomplished in two stages:

1. The first stage includes preparing the CMC-water fluid by adding CMC powder concentrations to distilled water normally at range (0.2 – 0.5) % by weight as presented in the section (3.6.1). At this stage, the thermal properties must be measured in experimentally.
2. The second stage includes adding MgO nanoparticles to the CMC-water fluid. The resulting solution from this addition is prepared in the same manner as shown in the section (3.5.1). The concentration of MgO nanoparticles added normally at (0.125 %, 0.25 %, 0. 5 % and 1 %) by volume.

3.6.2. The Water-MgO-CMC Fluid Property Measurements

The thermal properties of the working fluid (Water-MgO-CMC fluid) could measure experimentally and empirically. The CMC-water fluid was base fluid and it is thermal properties measured experimentally. When added MgO nanoparticles the new fluid (CMC-MgO-Water fluid) thermal properties measured experimentally by using laboratory devices, and measured empirically by using empirical equation that is presented in section (3.4.2). After input CMC-water fluid in any laboratory device must be heated to 50 ºC and then measured the required property. The measurement is carried out in the fluid laboratories of the Laboratories of Babylon University.

3.6.2.1. Measurement of Density

The results of experimental and empirical measurements of density are shown in **appendix D**.

3.6.2.2. Measurement of Specific Heat

The results of experimental and empirical measurements of specific heat are shown in **appendix D**.

3.6.2.3. Measurement of the Viscosity

The experimental and empirical measurements of the working fluid viscosity presented in **appendix D**.

3.6.2.4. Measurement of Thermal Conductivity

The thermal conductivity is measured experimentally and empirically as presented in **appendix D**.

3.7. Experimental Procedure

Experiments are repeated with varying the following parameter (working fluid flow rate, cold fluid flow rate, air flow rate, and concentration of MgO and CMC) to study their effect on the temperature, pressure, Nusselt number, heat transfer and effectiveness. The following procedure steps are conducted for each experimental session:

1. The hot fluid flows through inner pipe and this called the inner hot cycle.
2. Cold fluid flows through the annular section and this called the outer cold cycle.
3. The cold fluid presented in this work either pure water or two-phase (pure water and air).
4. The pure water placed in an outer cold cycle tank.
5. The air will be supplied by using a compressor.
6. The hot fluid that used in this work are either pure water, a pure water – CMC fluid, a pure water – MgO fluid and pure water – CMC – MgO fluid.
7. Prepare each type of fluids and then place it in the inner hot cycle tank, after that the experimental starts with using a pure water.
8. The fluid in the inner hot cycle tank could be replaced and another working fluid is used.
9. Connect the main electrical power to the control power switch.
10. Switch on an imbedded electric heater of 12 kW fixed at the bottom of the hot water tank (boiler) and adjust a thermostat for a desirable temperature (50 °C).
11. Switch on the two pumps.
12. Open the valves to circulate the hot water or nanofluid in the inner tube and cold water in the annulus.
13. Adjust the control valves and the bypass valves in order to select the desired flow rate in the inner tube and in the annulus.
14. Wait until the system reach to steady state then take the readings as follows:

Hot working fluid temperature for inlet and outlet pass the inner tube, cold water temperature for inlet and outlet passes the annulus and pressure drop for inlet and outlet pass in the inner tube.

15. The readings will be taken for each single flow rate in the annulus (pure water) 24 l/min for the flow rate in the inner tube (pure water) (8, 10, 12 and 14) l/min.
16. Repeat step 15 for each type of hot working fluid which flows in inner cycle.
17. Take the readings at effect of two phases (air – water) flow as follows:
    Hot working fluid temperature for inlet and outlet pass the inner tube, cold water temperature for inlet and outlet passes the annulus and pressure drop for inlet and outlet pass in the inner tube.
18. The readings will be taken for each single and two phases flow. The flow rate in the inner pipe (8, 10, 12 and 14) L/min. The two phases (air-water) flow investigated from constant water flow rate 24 L/min and mixing with various air flow rate (360, 420 and 480) L/hr.
19. Repeat step 18 for each type of hot working fluid which flows in inner cycle.
20. The experimental layout is shown in figure (3-31) and photo for each working fluid that is presented in figure (3-32).

3.8 Uncertainty Analysis

21. An experiment in a laboratory always involves the determination of various inter linked parameters. The results expected from this experiment have to reach certain level of accuracy depending on the problem and hence repeated measured is required but this may not yield the same result every time mainly due to the involvement of errors.
22. The error analysis in experimental measurements is important. So, the measured data by the temperature sensors for 10 experiments is presented in **Appendix E**.

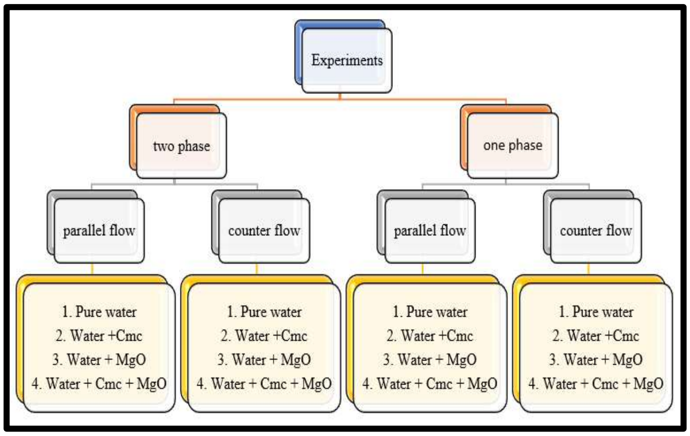

Figure (3-31): Experiments layout.

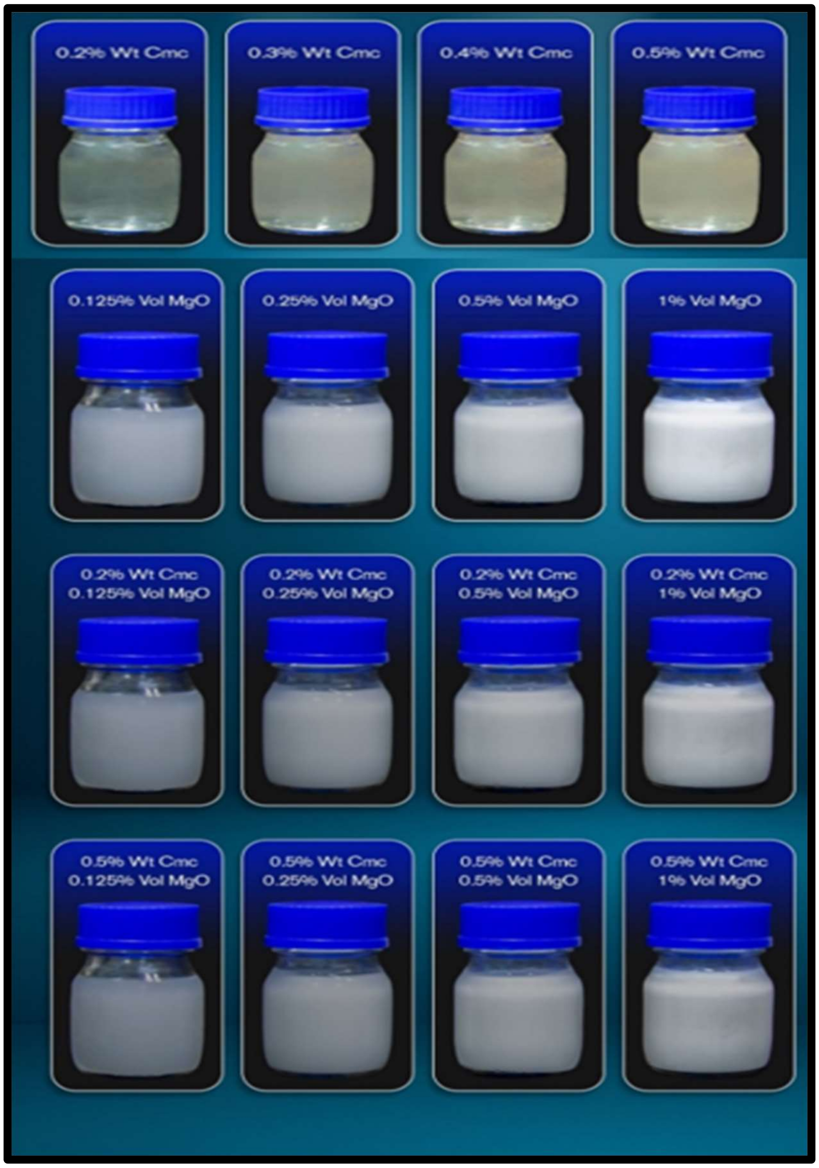

Figure (3-32): photo of hot working fluid.

4

CHAPTER FOUR

NUMERICAL ANALYSES

CHAPTER FOUR
NUMERICAL ANALYSES

4.1. Background

Computational Fluid Dynamics (CFD) code is used for prediction the behaviors of the water-MgO-CMC flow as well as pressure, velocity, and temperature fields in a double pipe heat exchanger. This chapter deals with the CFD simulation using the commercial code ANSYS Fluent 2020 R1. The impact of geometric parameters and flow conditions effect on the temperature field and pressure drop in the single-phase and two-phase flow during the test section with and without nanofluid is investigated. The necessary dimensions of the test section for double pipe heat exchanger are specified in this chapter. Several steps were taken to accomplish the CFD simulation, which will be explained deeply in this chapter. These steps are:

1. Creating the geometry of the system (computational domain).
2. Meshing the computational domain.
3. Choosing the solution models i.e., viscous, energy, multiphase.
4. Setting the materials properties.
5. Setting the boundary conditions.
6. Choosing the solution methods.
7. Specifying the convergence criteria.

4.2. Investigated Cases

Four cases for the double-pipe heat exchanger are investigated using a CFD simulation. Two directions for the fluid flow are taken, parallel flow and counter flow. The flow directions along with the dimensions of the double-pipe heat exchanger are shown in figure (4-1).

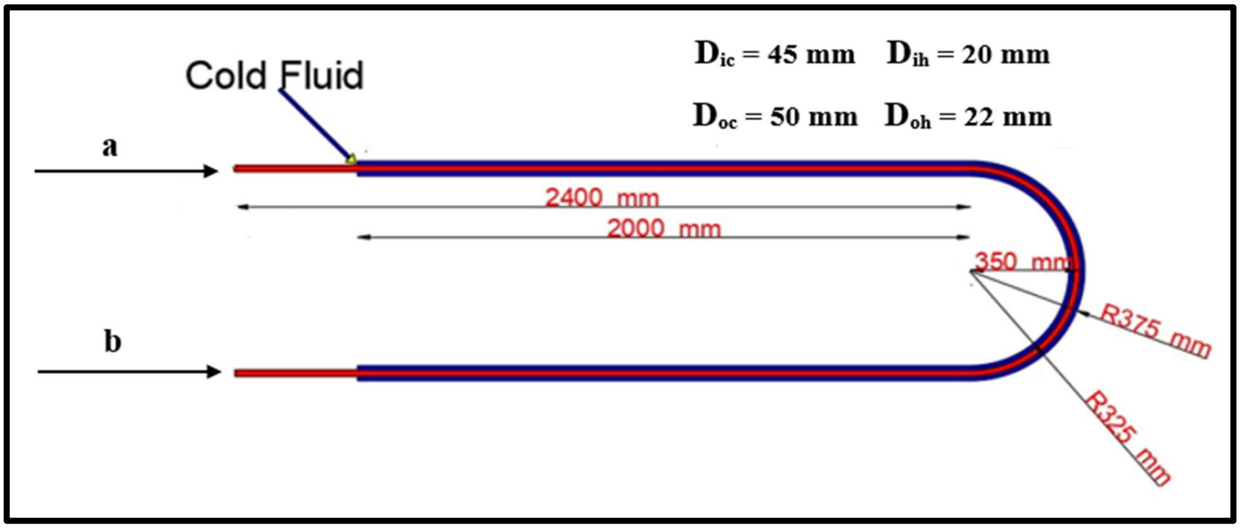

Figure (4-1): Investigated flow directions. (a) the inlet of hot working fluid in case of parallel flow and (b) the inlet of hot working fluid in case of counter flow.

For each of the four flow cases, four different particles concentration are considered. The produces are eight simulation cases, and each case is investigated for different mass flow rates for the cold and hot fluids. The volumetric flow rate of hot fluid is variable from 8 to 14 L/min. The density of working fluid changes depending on concentration of CMC and MgO. Therefore, the mass flow rate changes depending on these concentrations. Table (4-1) summarizes the considered cases for the double-pipe heat exchanger.

4.3. Computational Domain and Meshing Method

The geometry of the system is created by ANSYS Design Modeler. The system comprises with multiple parts that represent both the solid and fluid regions of the computational domain. The computational domain is shown in figure (4-2). Four regions are created and connected by interfaces. These regions in sequence are: the outer pipe, cold fluid, inner pipe and hot fluid. The pipes are specified as solid regions, while the hot and cold fluid are specified as fluid regions.

Table (4-1): A summary for the investigated cases of the double-pipe heat exchanger

Flow arrangement	No. of phases	Mass flowrate of water (kg/s)	Mass flowrate of air (kg/s) (10^{-3})	Concentrations CMC % wt.	Concentrations MgO % vol.	Mass flowrate of Water-MgO-CMC fluid kg/s
Parallel flow	Single phase	0.39524	0	0.5	0.125	$\dot{m}_{nf} = 0.133$ to 0.237
	Two phases	0.39524	0.1184		0.25	
			0.1381		0.5	
			0.1578		1	
Counter flow	Single phase	0.39524	0	0.5	0.125	$\dot{m}_{nf} = 0.133$ to 0.237
	Two phases	0.39524	0.1184		0.25	
			0.1381		0.5	
			0.1578		1	

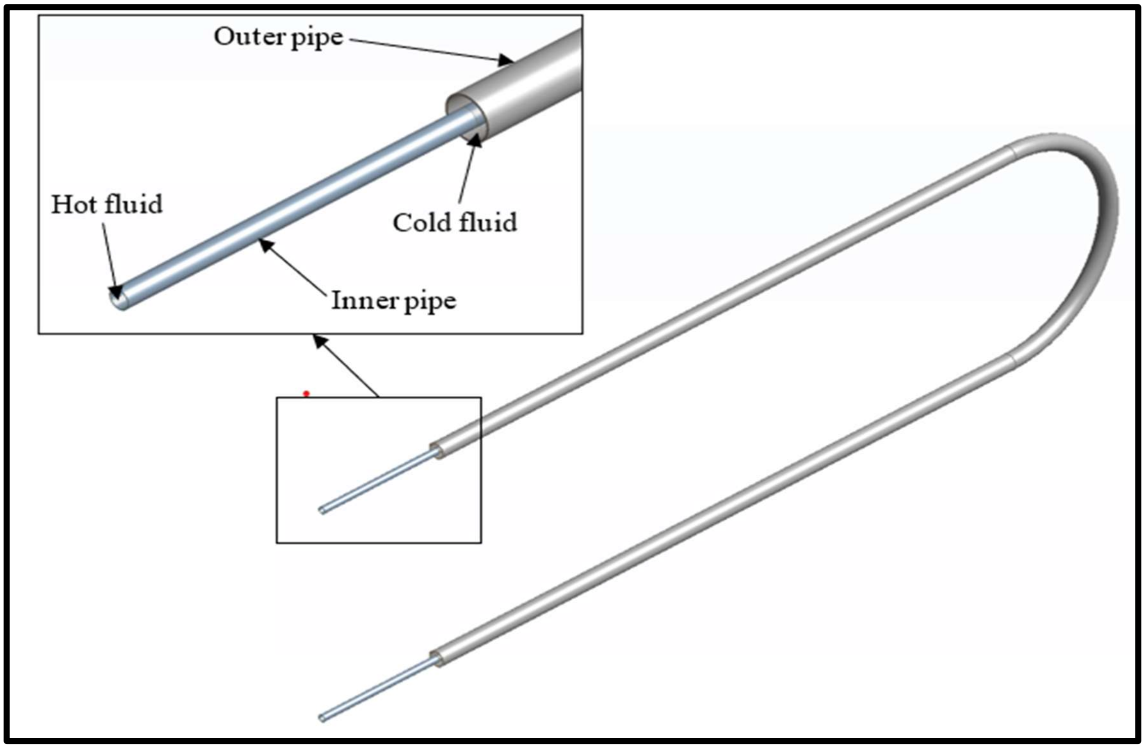

Figure (4-2): Computational domain of the double-pipe heat exchanger.

The computational domain is meshed by ANSYS ICEM. Figure (4-3) shows the meshed geometry. Structured hexahedral cells are used for creating the mesh. Few prism cells are considered to account for some regions that could not be meshed with hexahedral cells. The multizone method is used to create the structured mesh. The mesh interfaces between the solid and fluid regions are assigned as coupled walls in the Fluent solver.

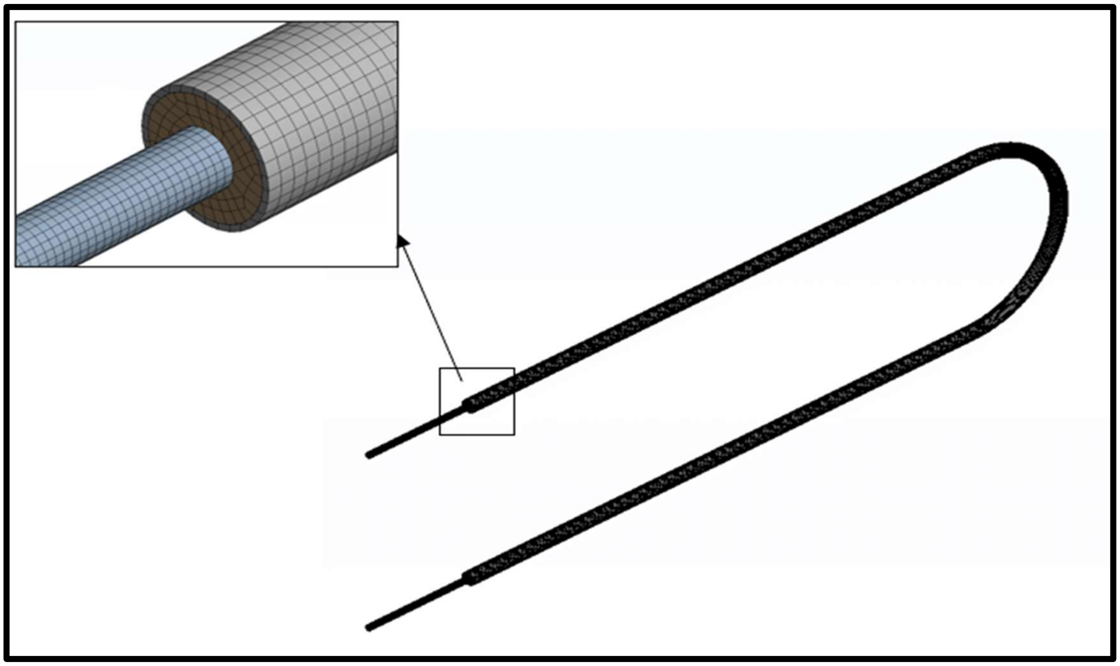

Figure (4-3): Meshing criteria.

A mesh independency study is conducted to acquire a mesh independent solution from the simulation. Six different cell sizes are compared with each other producing a different number of cells. The outlet temperature and velocity of both hot and cold fluid are compared for the different cases. The outcome is independent of the mesh size when the percentage change in these variables is insignificant. The independent results of the mesh are presented in table (4-2). The solution is found independent of the mesh size even with the largest size, therefore the cell size considered as the one that produced 257275 cells.

The quality of the mesh is determined through many parameters, the most important being the skewness and orthogonal quality. A low skewness value close to zero represents a high-quality mesh. In contrast, a high orthogonal quality close to one indicates a high-quality mesh. The minimum, maximum, orthogonal quality, and average skewness values are depicted in table (4-3).

Inflation layers are not considered as the chosen turbulence model provides an alternative for solving the boundary layer regions, as will be further discussed in section 4.6.

Table (4-2): Mesh independency study.

No. of cells	T_{c_o} (K)	Error	T_{h_o} (°C)	Error	V_{c_o} (m/s)	Error	V_{h_o} (m/s)	Error
257275	303.971		317.012		0.446		0.818	
288390	303.94	1.02 X10^{-4}	317.041	0.91X10^{-4}	0.445	2.24 X10^{-3}	0.818	0
475631	303.856	2.76 X10^{-4}	317.11	2.17X10^{-4}	0.444	2.24 X10^{-3}	0.814	4.89 X10^{-3}
720531	303.717	4.57 X10^{-4}	317.264	4.85X10^{-4}	0.444	0	0.811	3.68 X10^{-3}
1370520	303.677	1.31 X10^{-4}	317.315	1.6 X10^{-4}	0.444	0	0.81	1.23 X10^{-3}
3191387	303.734	1.87 X10^{-4}	317.25	2.05X10^{-4}	0.444	0	0.807	3.7 X10^{-3}

Table (4-3): Mesh quality parameters.

Value	Skewness	Orthogonal quality
Maximum	0.76	0.99
Minimum	1.98×10-2	0.35
Average	0.28	0.88

4.4. Boundary Conditions

Table (4-4) shows the boundary conditions that are taken into account for the CFD simulation cases. The values of the inlet mass flowrates and temperatures are taken from the experimental measurements. The outlet of the pipes is given a pressure outlet with an atmospheric pressure value. The outer surface of the outer pipe is insulated, while the other walls of both pipes are given coupled thermal boundary condition to account for the interaction between the solid and fluid regions.

Table (4-4): Boundary conditions.

Part	Boundary condition	Values
Outer pipe inlet	Inlet mass flowrate	$\dot{m}_c$ = section 4.2. $\dot{m}_a$ = section 4.2. $T_{c_{in}} = 298$ K
Inner pipe inlet	Inlet mass flowrate	$\dot{m}_{nf}$: section 4.2. $T_{h_{in}} = 323$ K
Outer pipe outlet	Pressure outlet	0 Pa
Inner pipe outlet	Pressure outlet	0 Pa
Outer pipe outer surface	Insulated	$\frac{dT}{dx} = 0, \frac{dT}{dy} = 0, \frac{dT}{dz} = 0$
Other surfaces	Via system coupling	-

4.5. Assumptions

To accomplish the CFD simulation, several assumptions are considered as follows:

1. Steady state conditions.
2. No heat generation.

3. Incompressible fluid.
4. Constant physical properties for all fluid flow.
5. No phase change for all the flowing fluids.
6. Radiation effects are negligible.
7. Newtonian fluid.
8. Three dimensional.
9. Turbulent flow.

4.6. Governing Equations

ANSYS Fluent employs the FV approach to tackle the governing equations, which comprise momentum, mass, turbulence model, and energy equations. Specifically, for steady-state conditions, the software resolves the conservation equations given below:

Continuity equation:

$$\nabla.(\rho\vec{v}) = 0 \tag{4.1}$$

Momentum equation:

$$\nabla.(\rho\vec{v}\vec{v}) = -\nabla P + \nabla.(\bar{\bar{\tau}}) + \rho\vec{g} \tag{4.2}$$

Energy equation:

$$\nabla.\left(\vec{v}(\rho E + P)\right) = -\nabla.\left(\sum_j h_j J_j\right) \tag{4.3}$$

The realizable (k-ε) turbulence model is considered. This model resolves a pair of equations to obtain both the kinetic energy and its dissipation rate, which are expressed as follows:

$$\frac{\partial}{\partial x_j}\left(\rho k u_j\right) = \frac{\partial}{\partial x_j}\left[\left(\mu + \frac{\mu_t}{\sigma_k}\right)\frac{\partial k}{\partial x_j}\right] + G_k + G_b - \rho\varepsilon - Y_M \tag{4.4}$$

$$\frac{\partial}{\partial x_j}\left(\rho \varepsilon u_j\right) = \frac{\partial}{\partial x_j}\left[\left(\mu + \frac{\mu_t}{\sigma_\varepsilon}\right)\frac{\partial \varepsilon}{\partial x_j}\right] + \rho C_1 S \varepsilon - \rho C_2 \frac{\varepsilon^2}{k+\sqrt{\nu\varepsilon}} C_{1\varepsilon}\frac{\varepsilon}{k} C_{3\varepsilon} G_b \tag{4.5}$$

The symbol μ_t is determined by (ε) and (k) in the following manner:

$$\mu_t = \rho C_\mu \frac{k^2}{\varepsilon} \tag{4.6}$$

In order to handle boundary layer regions and avoid the need for highly resolved inflation layers near walls, the realizable (k-ε) turbulence model features near-wall treatment functions. This study employed the Menter-Lechner near-wall treatment, which is insensitive to y+ function. Finally, the volume of fluid (VOF) multiphase model is considered to enable different fluids to be considered at the inlet, as explained earlier in section 4.2.

4.7. Materials Properties

The properties of the solid and fluid materials are presented in this section. The outer pipe of the heat exchanger is made from Perspex, while the inner pipe is made from copper. The properties of both materials are shown in Table (4-5).

The thermal and physical properties of air and water at different temperatures are available in numerous references. The water-MgO-CMC fluids properties are unavailable and are measured experimentally as explained in chapter three. The values acquired from the experimental procedure are used in the numerical simulation.

Table (4-5): Materials properties of the pipes.

Material	Density (kg/m^3)	Specific heat (J/kg·K)	Thermal conductivity (W/m·K)
Perspex	1200	1170	0.19
Copper	8978	381	387.6

4.8. Solution Methods

The governing equations are solved using the pressure-based coupled algorithm. Equation of the pressure is obtained by equations of momentum and continuity so that the velocity vector (field), adjusted by the pressure, achieves the equation of continuity. Due to the coupled and nonlinear feature of the governing equations, the solving process entails iterative steps, whereby the governing equations are solved continually till convergence is reached. The momentum and the pressure-based continuity equations form a coupled (interacted) equations system that the algorithm solves. Due to the closely coupled nature of these equations, the solution convergence rate is notably enhanced when compared to segregated algorithms. The flowchart presented in Figure (4-4) outlines the solution procedure utilized in the coupled algorithm.

The gradient spatial discretization is set to (Least Squares Cell Based) and (PRESTO!) for the pressure. The (Second-Order-Upwind) spatial discretization is adopted for both momentum and the dissipation rate and kinetic energy of the turbulent. The volume fraction is set to the default option of (Compressive).

4.9. Convergence Criteria

The solution convergence is judged by multiple criteria. First, the governing equations residuals reached an accuracy of 10^{-5}. Figure (4-5) shows the residuals for one of the considered simulation cases. The second method is by checking the energy imbalances and mass, which are found to be close to zero for all the simulation cases. Finally, monitors are set to check that the important physical properties reached steady state. In this case, these properties are the outlet temperature and velocity of the hot and cold fluids. The above-mentioned criteria for convergence are satisfied for all of the conducted CFD simulation cases.

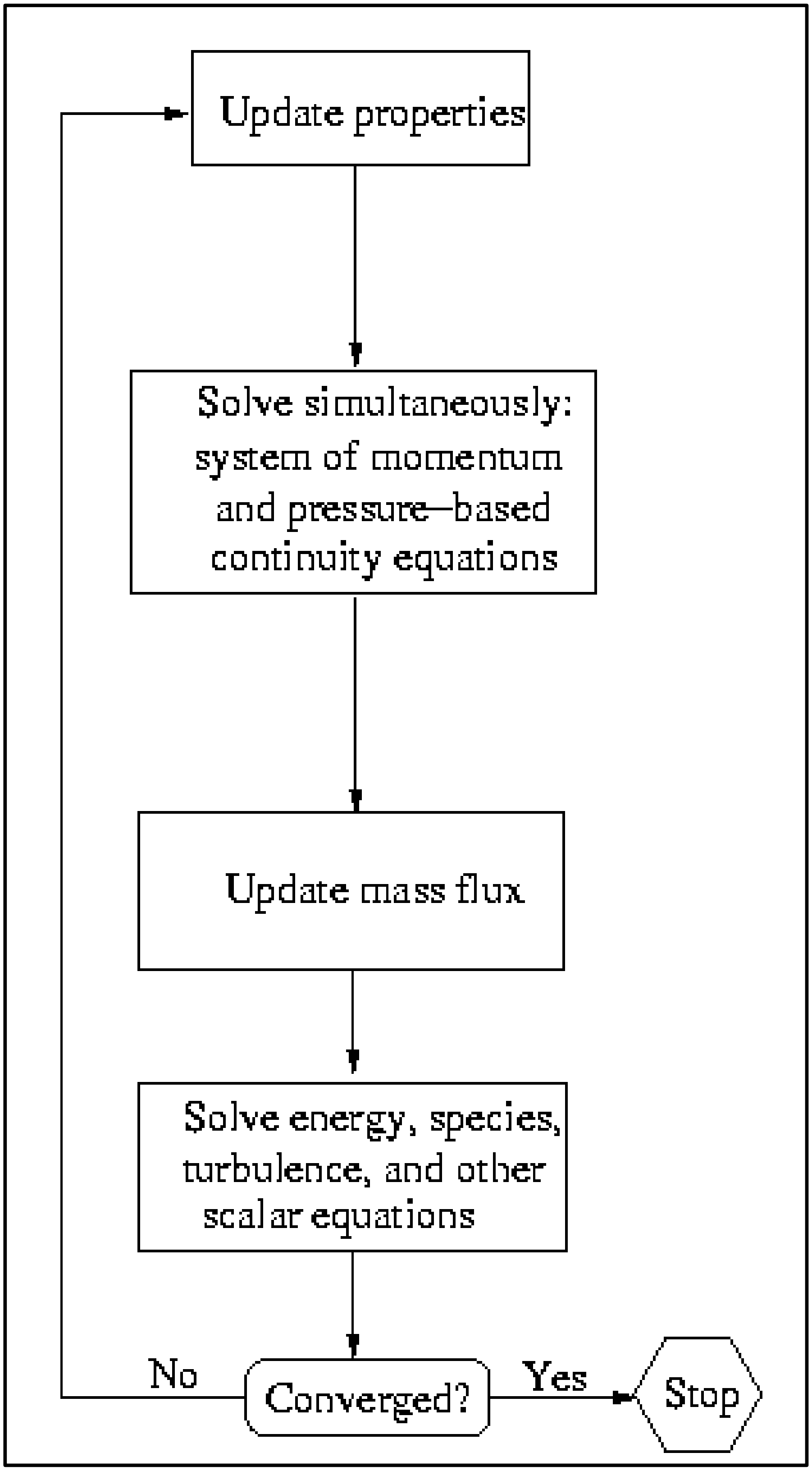

Figure (4-4): Flowchart showing the pressure-based coupled algorithm solution procedure.

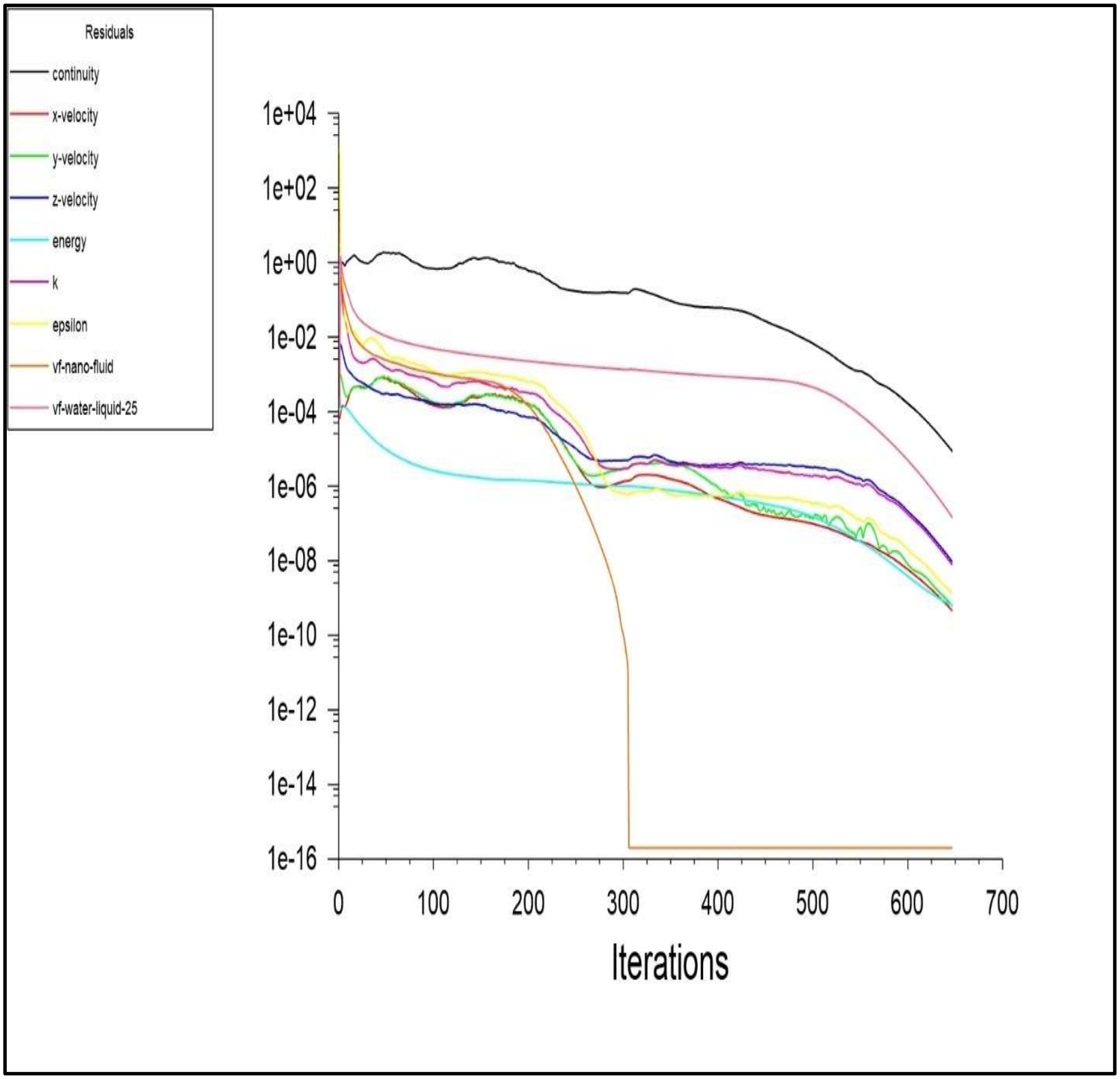

Figure (4-5): Residual convergence.

4.10 Thermo-Physical Properties of Air–Water Two Phases Flow

To calculate the effective properties for mixture of two-phase air-water mixtures are often expressed with the help of certain mixing rules and definitions **ANSYS 15 guides**. Assume the water is the primary phase and the air is the secondary phases.

4.10.1 The Velocity of Air-Water Two Phases Mixture

The velocity of the air-water two phases flow can be evaluated as follows [97]:

$$V = \frac{\dot{V}_a + \dot{V}_f}{\frac{\pi}{4} D_i^2} \tag{4- 7}$$

4.10.2 The Density of Air-Water Two Phases Mixture

The density of the air-water two phases flow is illustrated by [97]. They present equation for calculating density as follows:

$$\rho = \frac{\rho_a \dot{V}_a + \rho_f \dot{V}_f}{\dot{V}_a + \dot{V}_f} \tag{4- 8}$$

4.10.3 The Viscosity of Air-Water Two Phases Mixture

The viscosity of the air-water two phases flow can be evaluated by the below equation, which has been demonstrated by [97] as follows:

$$\mu = \frac{\mu_a \dot{V}_a + \mu_f \dot{V}_f}{\dot{V}_a + \dot{V}_f} \tag{4- 9}$$

4.10.4 The Air Void Fraction

The air void fraction is ratio of air flow rate to the total flow rate of mixture. It can be calculated by the below equation, which has been introduced by [97].

$$\mathrm{Vf} = \frac{\dot{V}_a}{\dot{V}_a + \dot{V}_f} \tag{4- 10}$$

5

CHAPTER FIVE

RESULTS AND DISSCUSION

Chapter Five

Results and Discussion

5.1 Motivation

There are several experimental parameters that must be investigated and measured such as temperature at different positions, pressure at the inlet and outlet and fluid flow rates control. These parameters authorized calculating convection coefficient, inner pipe friction coefficient, heat exchanger effectiveness and required pumping power for hot fluid.

The cold fluid flow in annular side either single phase or two phases. The single phase is a pure water which flows in the annular side and the two phases flow forms from a compensation of air and water that flow in the annular side as well. The effect of the two phases flow takes into account various air flow rates ranging from (360 to 480) L/hr mixed with a constant water flow rate (24 L/min) to get a different flow regime. The various flow regimes appear in annular side. The hot fluid flows in inner pipe at flow rate ranging from (8 to 14) L/min. The data has been systematically controlled so that the heat transfer behavior could be better understood. Then relations implemented lead to given full description of thermal performance for various hot fluid types. The hot fluid types implement in this work are:

1. Pure water.
2. Water – CMC fluid.
3. Water – MgO fluid.
4. Water – MgO – CMC fluid.

The water flow rate, the air flow rate, the concentration of MgO nanoparticles, and CMC polymer nanoparticles have been studied to see their effect on the heat transfer behavior. Experimental steps repeat for each fluid types. The concentrations of CMC polymer nanoparticles are 0.2% and 0.5% by weight. The concentration of nanoparticles 0.125, 0.25, 0.5 and 1% by volume. The results obtained experimentally and numerically are presented and discussed in this chapter for various hot fluid types under a different condition. The inlet temperatures for the hot fluid are chosen as 50 °C, while for cold water and for air are 25 °C.

5.2. Experimental Work

In this chapter experimental results for various hot fluid types flow in inner pipe under different flow conditions and particles concentrations are presented and discussed. The results described in this chapter are under the influence of single and two-phase flow at parallel and counter flow.

5.2.1 Convection Heat Transfer Coefficient

Convection coefficient of heat exchange presents the relation between amount of heat rate as driving force of the heat flow (temperature difference). The convective heat transfer coefficient obtained for various hot fluid flow as presented in section (5.1). It has been obtained according to equation (F-10) for inner side. The differential of convection heat exchange coefficient value along hot fluid flow rate at inner pipe range (8-14) L/min, under influence of single and two phases flow. The cold water flow as single phase 24 L/min and mixed with air at flow rate (360, 420 and 480 L/hr) in mixing chamber to get two phases flow.

5.2.1.1 Convection Heat Transfer Coefficient of Pure Water

Pure water presents as basic working fluid that used in double pipe heat exchanger. Also, it is a tradition fluid that is implemented in different application of heat exchanger. The pure water in this case used as cold and hot fluid in annular and inner pipe respectively. Figures (5-1) and (5-2) demonstrate that the convection heat transfer coefficient value dependent of hot fluid flow rate, air flow rate and flow direction. The flow conditions for parallel and counter cases are shown in the above each mentioned figures. The hot fluid that used in these cases is pure water. These figures present the effect of single phase and two phases air-water flow on value of convective heat transfer coefficient. The convection coefficient increases at increase in volume flow rate of hot fluid. The effect of two phases flow on the pure water convection heat transfer coefficient for parallel and counter flow increase when air flow rate increases in the annular side. The air flow rate increases due to the increase of turbulence and velocity for the air-water two phase flow. This leads to enhance heat exchange rate between cold and hot fluids. The convective heat transfer coefficient for this case at different flow conditions present in table (5-1).

Table (5-1): Experimental value of convective heat transfer coefficient for pure water

Number of phases	Flow direction	Level	Cold fluid flow rate (L/min)	Hot fluid flow rate (L/min)	Air flow rate (L/min)	h (W/m^2. K)
Single phase	Parallel flow	Maximum	24	14	0	2771.71
		Minimum	24	8	0	2532.4
	Counter flow	Maximum	24	14	0	2861.54
		Minimum	24	8	0	2622.4
Two phases	Parallel flow	Maximum	24	14	480	2998.39
		Minimum	24	8	360	2618.08
	Counter flow	Maximum	24	14	480	3085.53
		Minimum	24	8	360	2708.21

5.2.1.2 Convection Heat Transfer Coefficient of The Water – CMC Fluid

There are two concentrations 0.2% and 0.5% wt. impalement in this case. The CMC partials has a good agreement of physical properties and that leads to improve pure water properties as presented in chapter three. The fluid resulting from the addition of the CMC particles has a higher viscosity than pure water. The viscosity of the water-CMC fluid increase with increasing CMC concentration. An increase in the viscosity of the fluid leads to an increase in the heat gain rate and enhancement of heat exchange between hot and cold fluids. Figures (5-3) to (5-6) illustrate the convection coefficient of heat transfer for the water-CMC fluid dependent on various parameter as pointed over each figure. These figures present the effect of single phase and two phases on hot fluid convection coefficient in annular side. For single phase flow, the convection coefficient increases when the water -CMC hot fluid flow increases. On the other hand, the convection heat transfer coefficient is affected by two phases flow in annular side and hot fluid flow rate. So, the convection coefficient under influence of two phases flow increases when air flow rate and the water-CMC hot fluid flow rate increases. The increase in CMC particles lead to increase the convection heat transfer coefficient and 0.5% wt. is a better CMC concentration. The convection heat transfer coefficient under various flow condition and 0.5% wt. CMC is shown in table (5-2).

Table (5-2): Experimental value of convective heat transfer coefficient for the water + 0.5% CMC wt.

Number of phases	Flow direction	Level	Cold fluid flow rate (L/min)	Hot fluid flow rate (L/min)	Air flow rate (L/min)	h (W/m^2. K)
Single phase	Parallel flow	Maximum	24	14	0	3142.32
		Minimum	24	8	0	2879.15
	Counter flow	Maximum	24	14	0	3232.15
		Minimum	24	8	0	2969.95
Two phases	Parallel flow	Maximum	24	14	480	3373.72
		Minimum	24	8	360	2968.22
	Counter flow	Maximum	24	14	480	3460.86
		Minimum	24	8	360	3058.22

5.2.1.3 Convection Heat Transfer Coefficient Water – MgO Fluid

Generally, the nanoparticles present a better absorb and carrier for thermal energy specially when these particles near to exchange thermal energy walls. The MgO particles added to a pure water at different concentrations (0.125%, 0.25%, 0.5% and 1% by volume) to enhance physical properties of the Water-MgO fluid. The increase in concentration of MgO particles lead to increase the Water-MgO fluid (nanofluids) thermophysical properties than pure water. The Water-MgO fluid as hot fluid flow in inner pipe of heat exchanger to enhance heat transfer rate. Figures (5-7) to (5-14) demonstrate the relationship between convection heat transfer coefficient in the inner pipe and hot fluid flow for different flow conditions that achieve over each figure. It has been shown that there is some deviation in the convection coefficient between the parallel flow and counter flow. The variation of the convection coefficient with the Water-MgO fluid volume flow rate range (8-14 L/min), and at influence single phase fixed cold fluid flow rate 24 L/min, for two - phase flow cold water mixed with air flow rate at 360-480 L/hr under turbulent condition that is investigated in the annular side. Moreover, convection coefficient increases under the influence of increasing the Water-MgO volume flow rate. Also, under the effect of two phases flow the convection heat transfer coefficient increases under the effect of the turbulence which is shown in the annular region as a result from mixing air and water. It is found that the better concentration of MgO 1% by volume is added to pure water. Table (5-3) shows the convection heat transfer coefficient values under different flow conditions and MgO concentration 1% by volume.

Table (5-3): Experimental value of convective heat transfer coefficient for the water + 1% MgO vol.

Number of phases	Flow direction	Level	Cold fluid flow rate (L/min)	Hot fluid flow rate (L/min)	Air flow rate (L/min)	h (W/m^2. K)
Single phase	Parallel flow	Maximum	24	14	0	3753.16
		Minimum	24	8	0	3401.25
	Counter flow	Maximum	24	14	0	3842.99
		Minimum	24	8	0	3491.25
Two phases	Parallel flow	Maximum	24	14	480	4004.6
		Minimum	24	8	360	3496.05
	Counter flow	Maximum	24	14	480	4091.74
		Minimum	24	8	360	3586.05

5.2.1.4 Convection Heat Transfer Coefficient Water–MgO–CMC Fluid

Nanofluid is used in heat exchanger to enhance the heat transfer rate better than pure water. Nanoparticles that dissolve in water suffer from agglomeration and deposition problems Thus, a good circulation of the nanofluid does not occur. This problem is due to the reduce in heat exchange rate. The agglomeration and deposition problems could be solved by using CMC as surfactant and also, to enhance thermophysical process. The convection heat transfer coefficient value for the Water-MgO-CMC fluid increases more than that of the value of pure water because of two reasons; First reason increasing thermal conductivity when the concentrations of MgO particles and CMC powder and other physical properties (density and viscosity) increase. Second reason is in turbulence of MgO particles result from the Brownian motion.

The Water-MgO-CMC fluid is used as hot fluid flow in inner pipe value at flow rate range (8-14 L/min). Figures (5-15) to (5-30) present a relation between the convection heat transfer coefficient of the Water-MgO-CMC fluid and flow rate under various flow conditions as shown in the above mentioned figures. In this case four different concentrations of the MgO nanoparticles (0.125%, 0.25%, 0.5% and 1% by volume) mixed with two CMC concentrations, namely, 0.2 and 0.5% by weight are used. The flow conditions for all eight cases are shown above each figure and all are the same except for the concentrations of the MgO nanoparticles and CMC mixture. From these figures, it is pointed that the convection heat transfer coefficient of the Water-MgO-CMC fluid increase as concentration of MgO and CMC increase. Also, it is affected by single phase and two phases flow that flow in annular side. For single-phase cold-water flow at 24 L/min in annular side but for two phases added air volume flow rate range (360, 420 and 480 L/hr) that mixed with cold water in mixing chamber to get two phases flow. The convection coefficient of the Water-MgO-CMC fluid increases with the increase of volume flow rate and air flow rate. Increasing the air flow rate that mixes with water in annular region due to increasing the level of water layer turbulence. This turbulence in water layer influence on the thermal boundary layer, that is formed on inner pipe outer surface area region. The highest convection heat transfer coefficient is observed with the highest CMC and MgO nanoparticles concentration as shown in table (5-4) under different flow conditions.

Table (5-4): Experimental value of convective heat transfer coefficient for the water + 1% MgO vol. + 0.5% CMC wt.

Number of phases	Flow direction	Level	Cold fluid flow rate (L/min)	Hot fluid flow rate (L/min)	Air flow rate (L/min)	h (W/m^2. K)
Single phase	Parallel flow	Maximum	24	14	0	5545.24
		Minimum	24	8	0	5062.57
	Counter flow	Maximum	24	14	0	5635.07
		Minimum	24	8	0	5153.57
Two phases	Parallel flow	Maximum	24	14	480	5826.23
		Minimum	24	8	360	5172.85
	Counter flow	Maximum	24	14	480	5913.37
		Minimum	24	8	360	5262.85

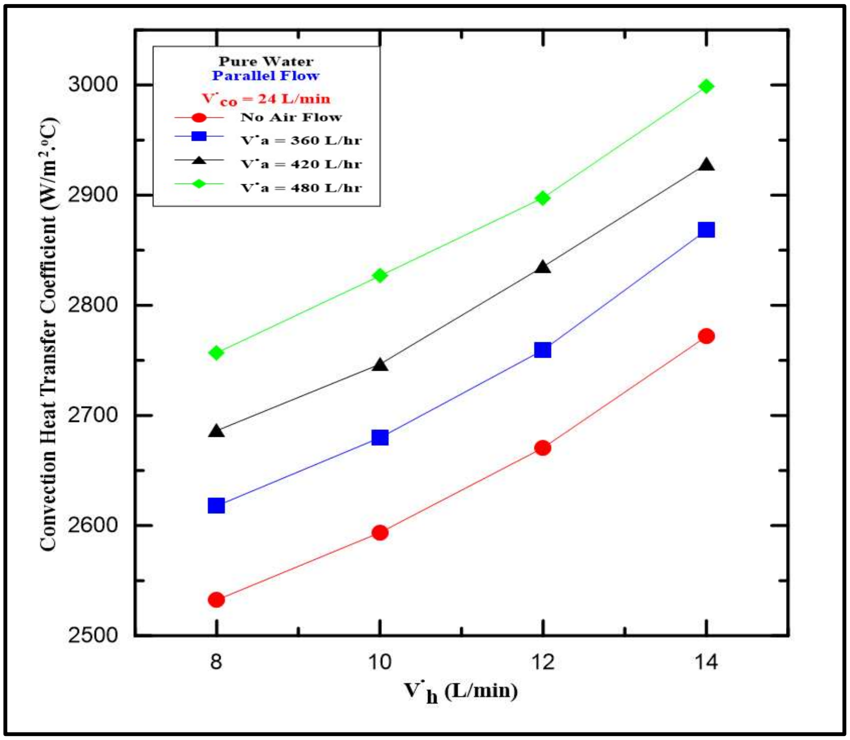

Figure (5-1): Variation of convective heat transfer coefficient with hot fluid (pure water) flow rate for parallel flow.

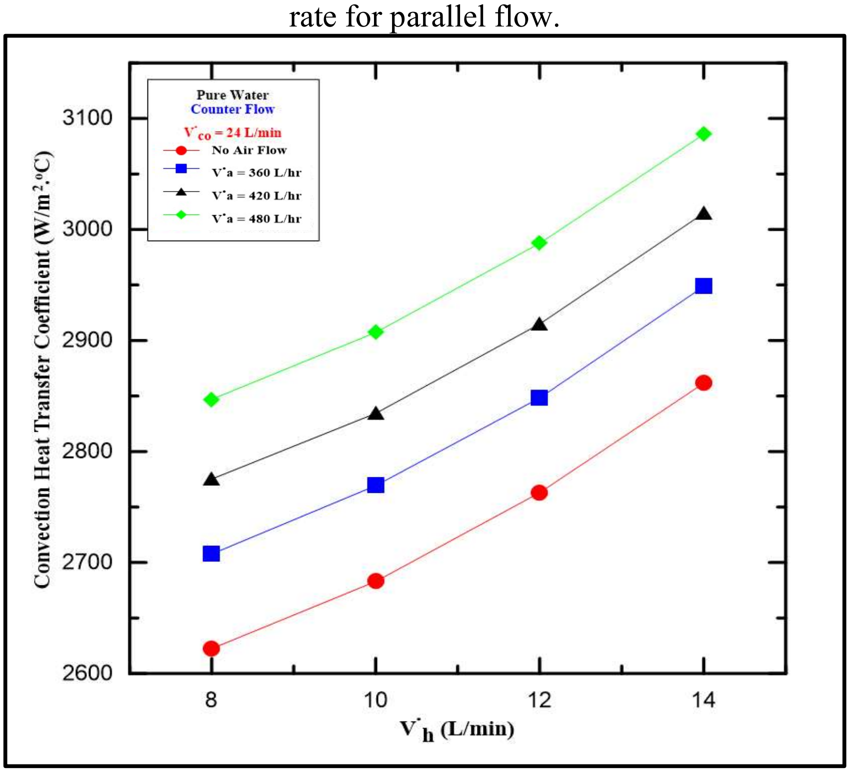

Figure (5-2): Variation of convective heat transfer coefficient with hot fluid (pure water) flow rate for counter flow.

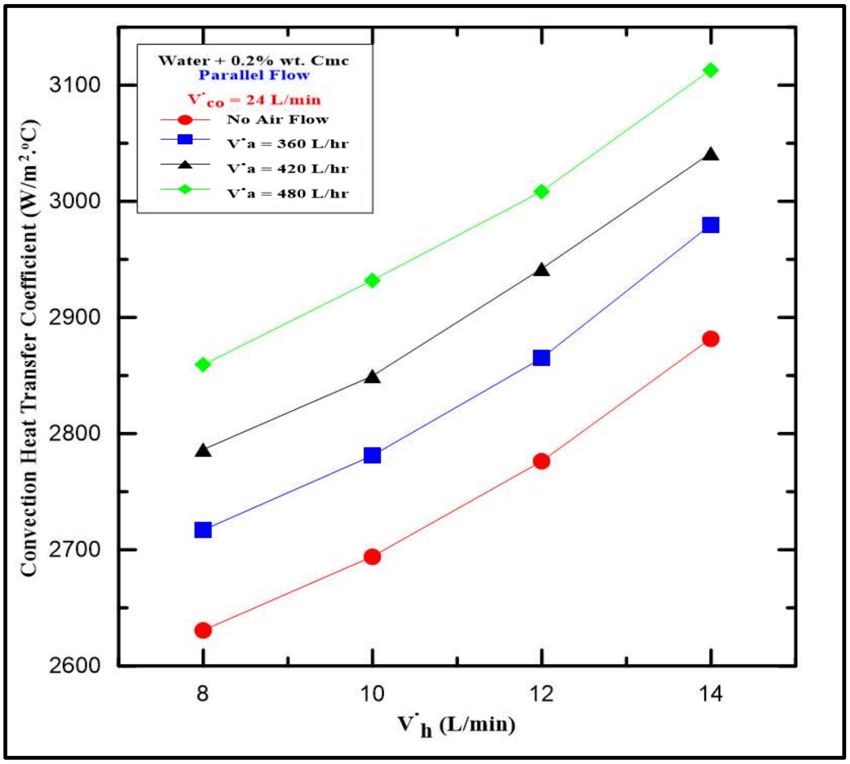

Figure (5-3): Variation of convective heat transfer coefficient with hot fluid (water – 0.2% CMC wt.) flow rate for parallel flow.

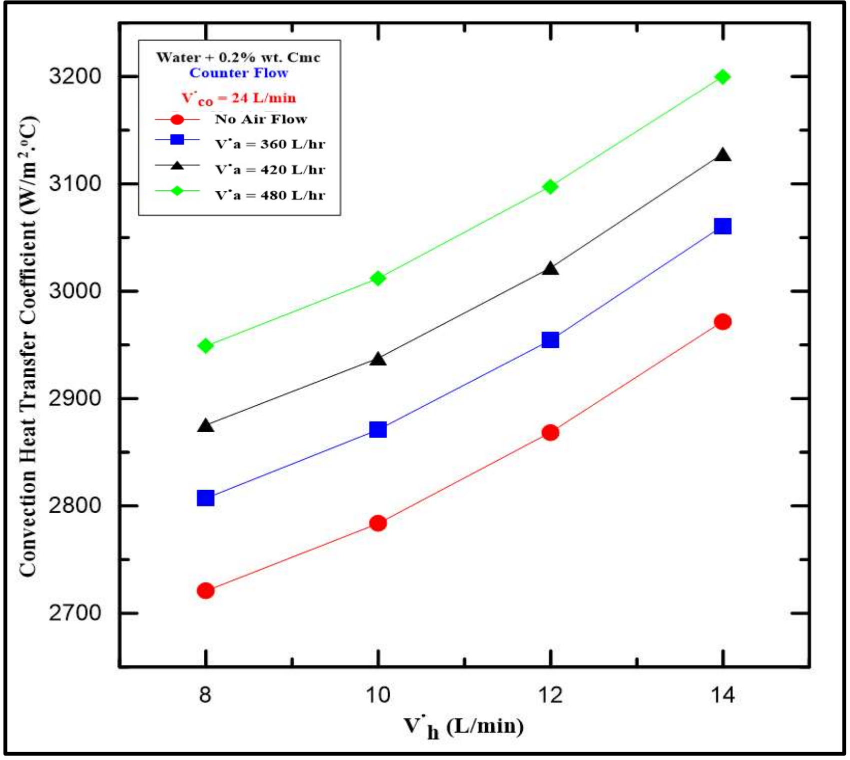

Figure (5-4): Variation of convective heat transfer coefficient with hot fluid (water – 0.2% CMC wt.) flow rate for counter flow.

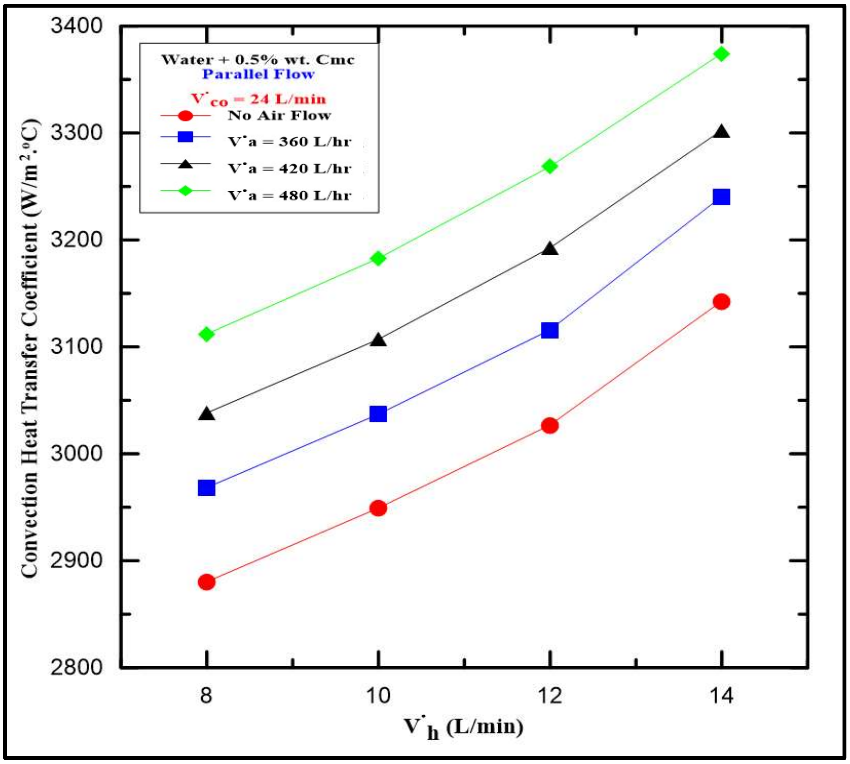

Figure (5-5): Variation of convective heat transfer coefficient with hot fluid (water – 0.5% CMC wt.) flow rate for parallel flow.

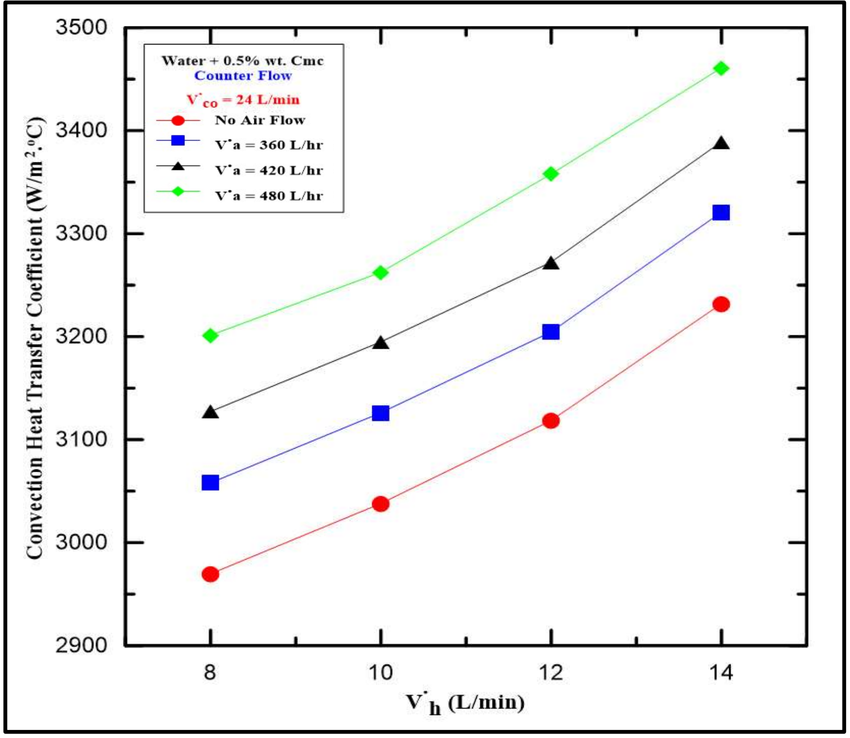

. **Figure (5-6)**: Variation of convective heat transfer coefficient with hot fluid (water – 0.5% CMC wt.) flow rate for counter flow.

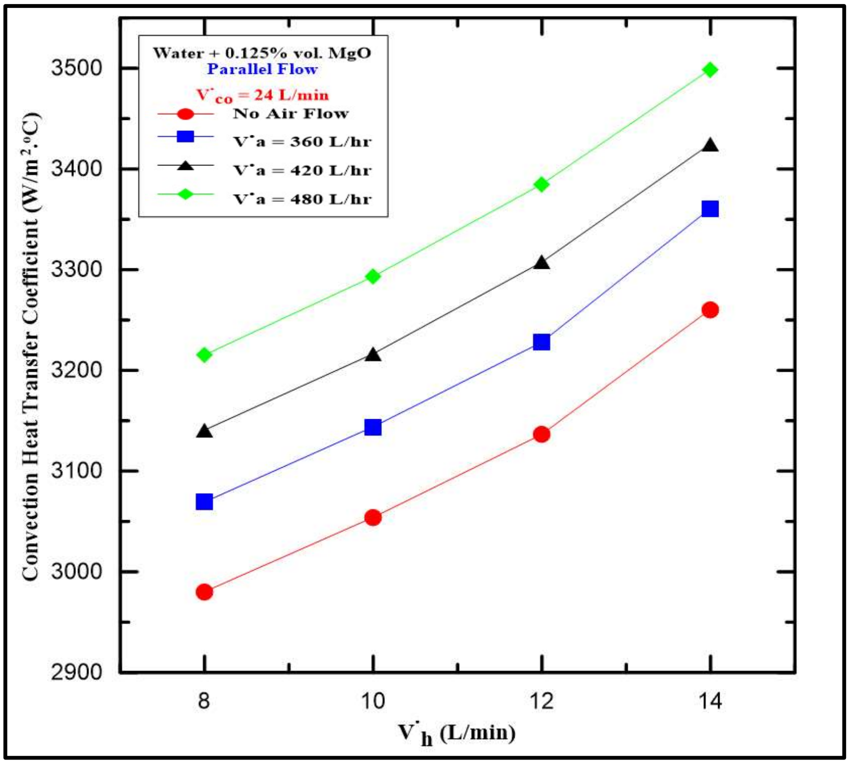

Figure (5-7): Variation of convective heat transfer coefficient with hot fluid (water – 0.125% MgO vol.) flow rate for parallel flow.

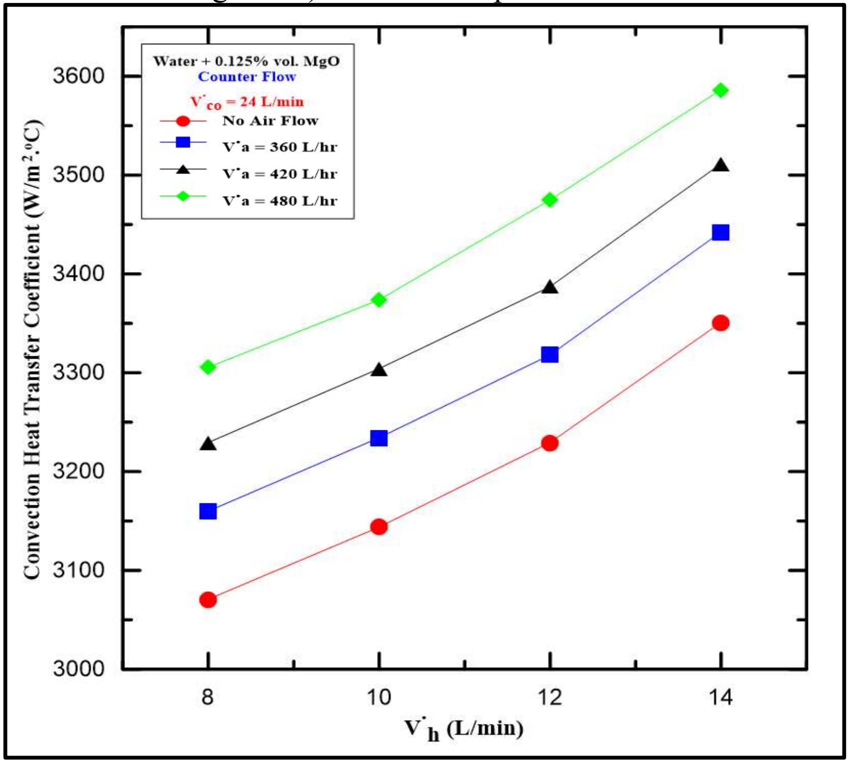

Figure (5-8): Variation of convective heat transfer coefficient with hot fluid (water – 0.125% MgO vol.) flow rate for counter flow.

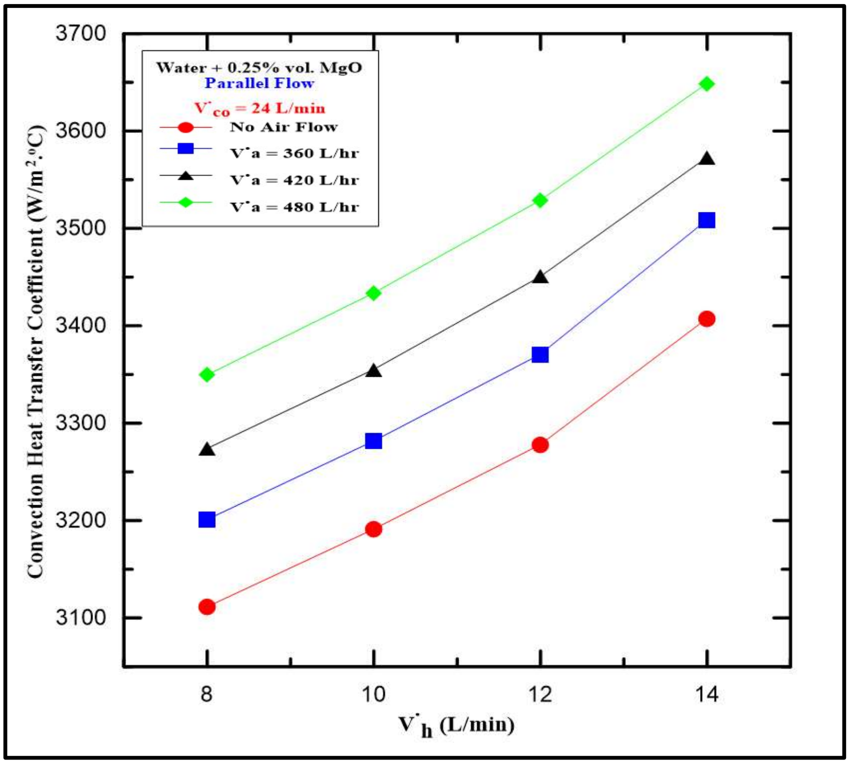

Figure (5-9): Variation of convective heat transfer coefficient with hot fluid (water – 0.25% MgO vol.) flow rate for parallel flow.

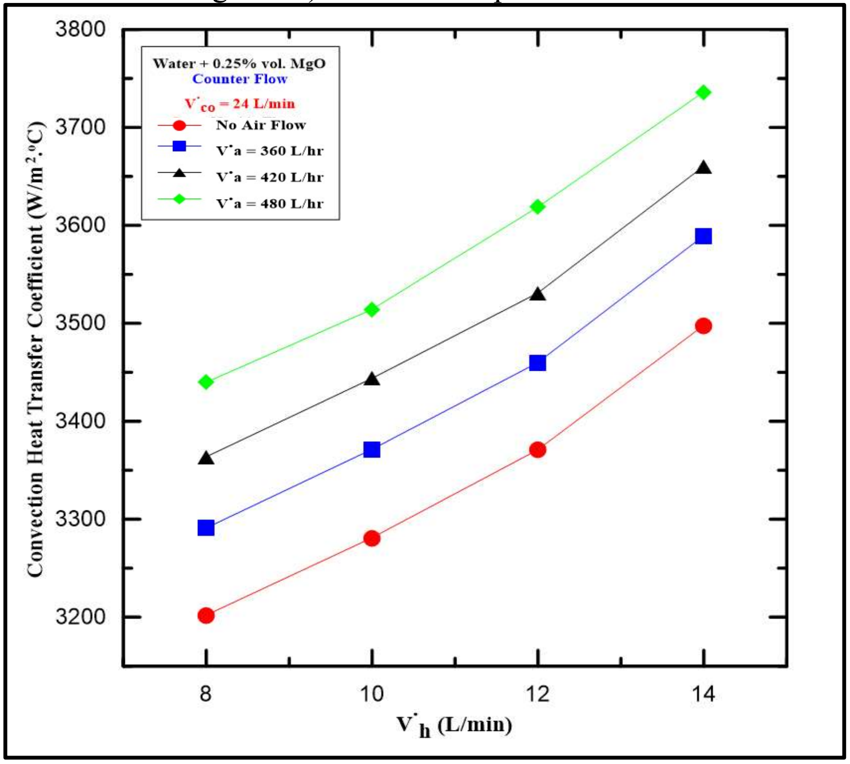

Figure (5-10): Variation of convective heat transfer coefficient with hot fluid (water – 0.25% MgO vol.) flow rate for counter flow.

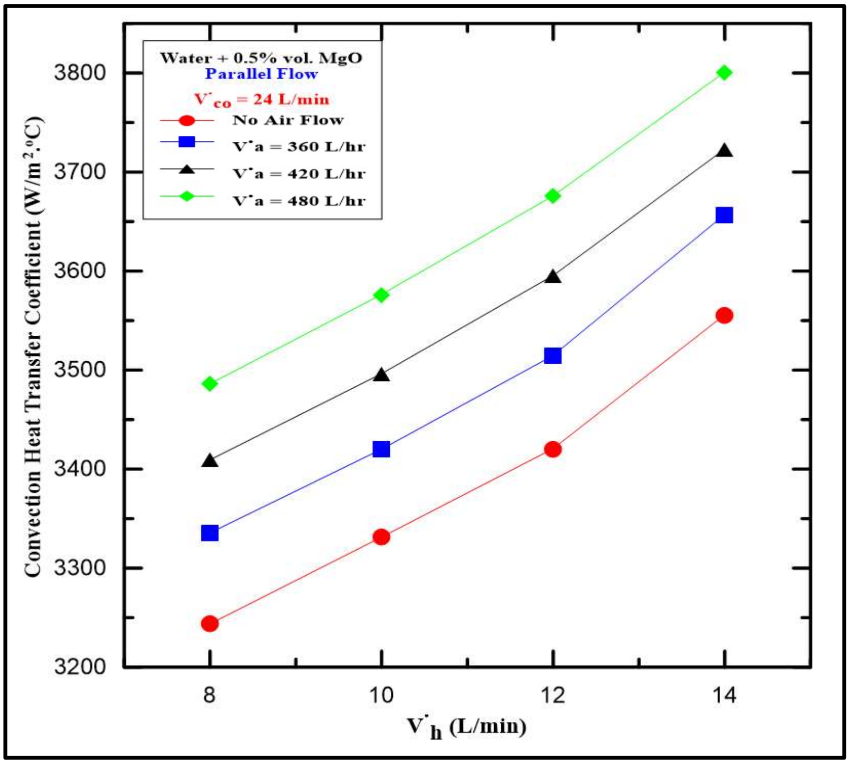

Figure (5-11): Variation of convective heat transfer coefficient with hot fluid (water – 0.5% MgO vol.) flow rate for parallel flow.

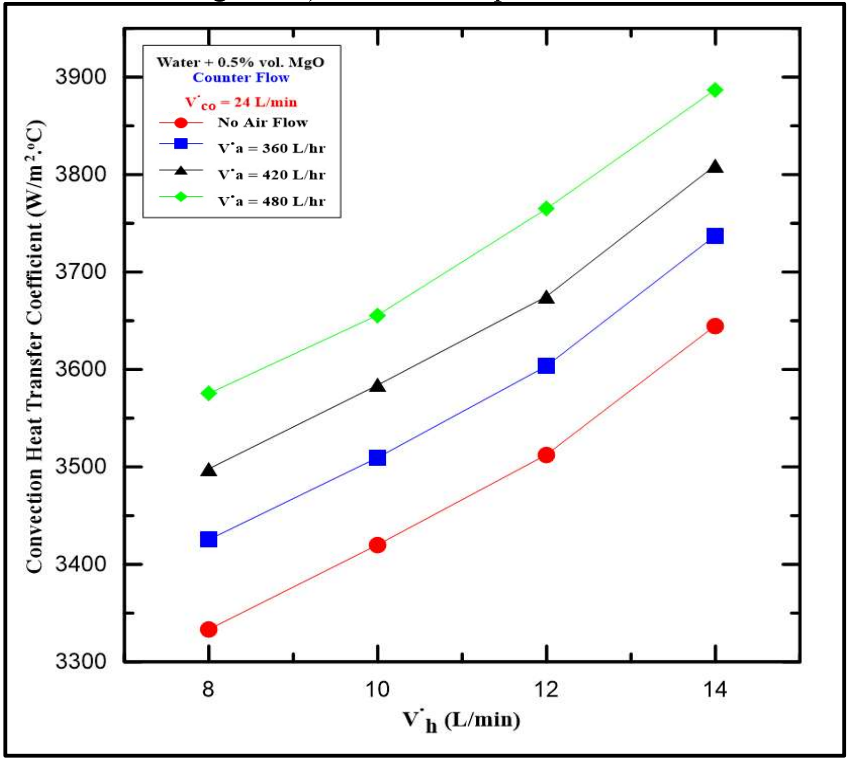

Figure (5-12): Variation of convective heat transfer coefficient with hot fluid (water – 0.5% MgO vol.) flow rate for counter flow.

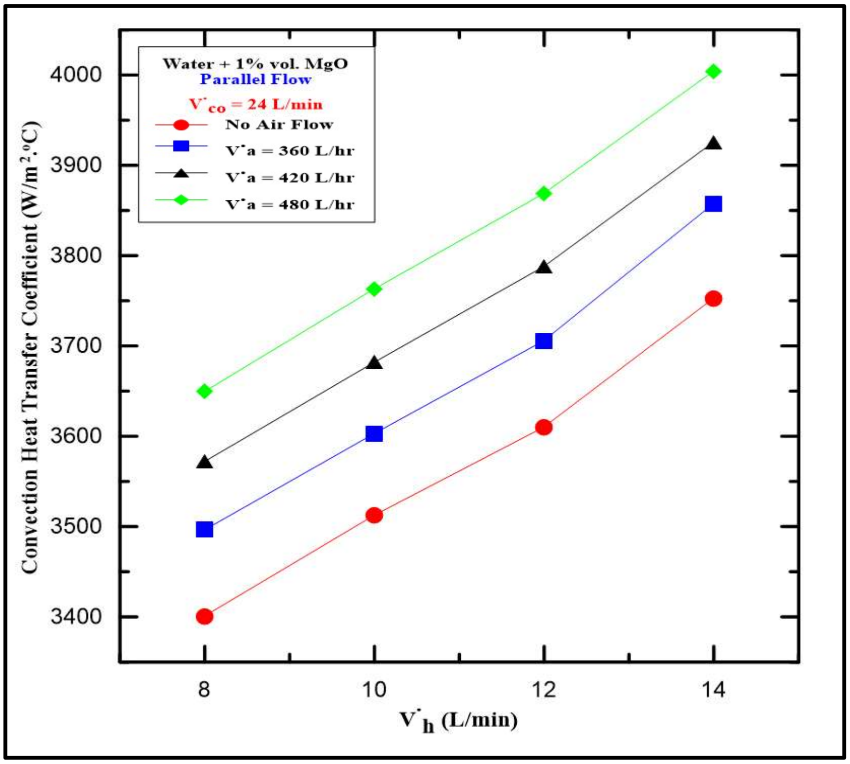

Figure (5-13): Variation of convective heat transfer coefficient with hot fluid (water – 1% MgO vol.) flow rate for parallel flow.

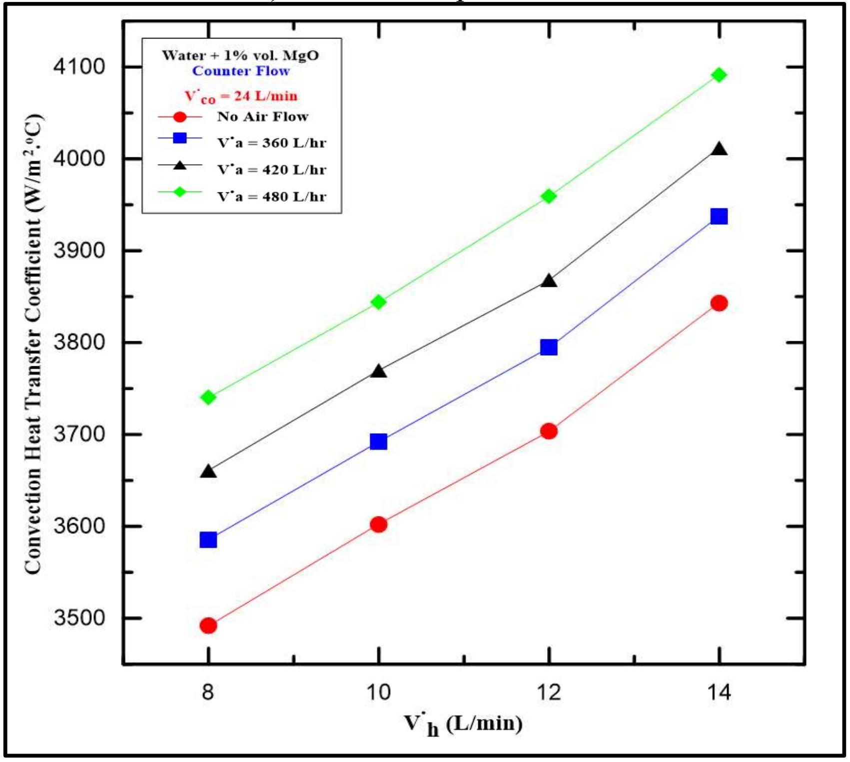

Figure (5-14): Variation of convective heat transfer coefficient with hot fluid (water – 1% MgO vol.) flow rate for counter flow.

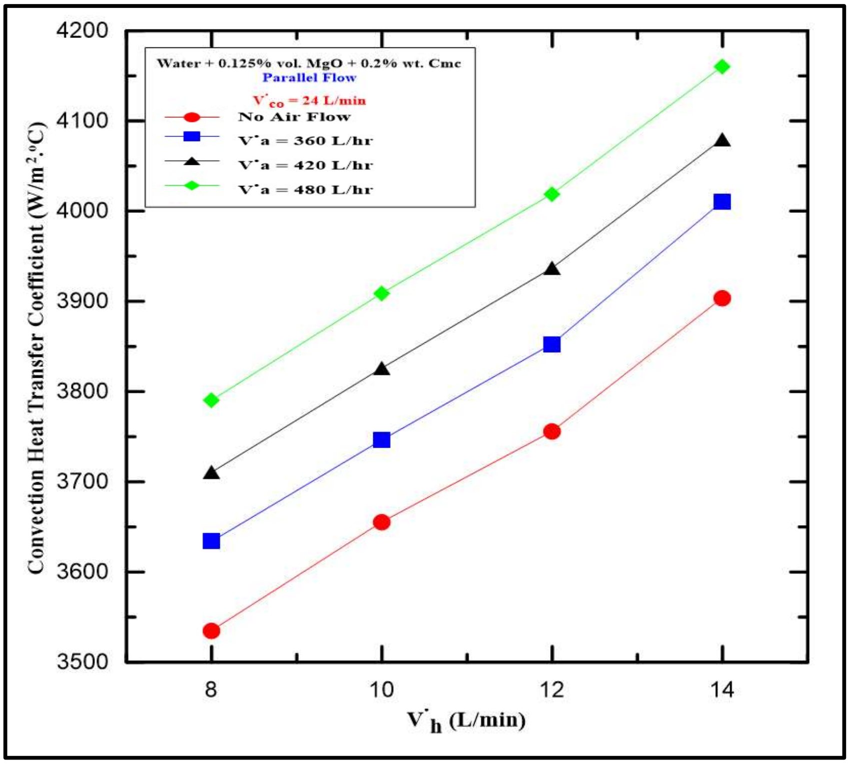

Figure (5-15): Variation of convective heat transfer coefficient with hot fluid (water + 0.125% MgO vol. + 0.2% CMC wt.) flow rate for parallel flow.

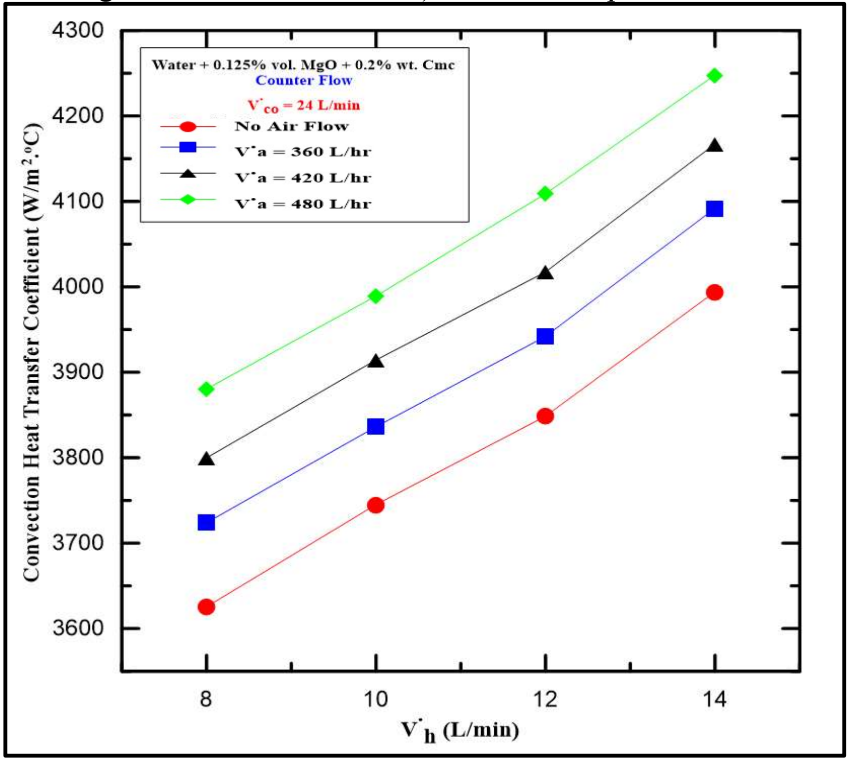

Figure (5-16): Variation of convective heat transfer coefficient with hot fluid (water + 0.125% MgO vol. + 0.2% CMC wt.) flow rate for counter flow.

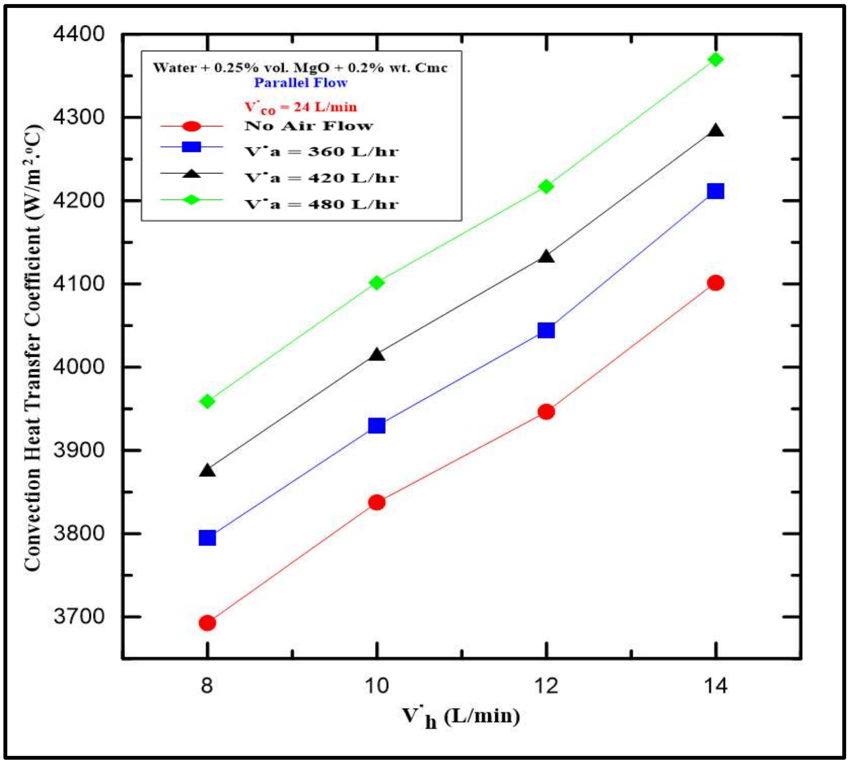

Figure (5-17): Variation of convective heat transfer coefficient with hot fluid (water + 0.25% MgO vol. + 0.2% CMC wt.) flow rate for parallel flow.

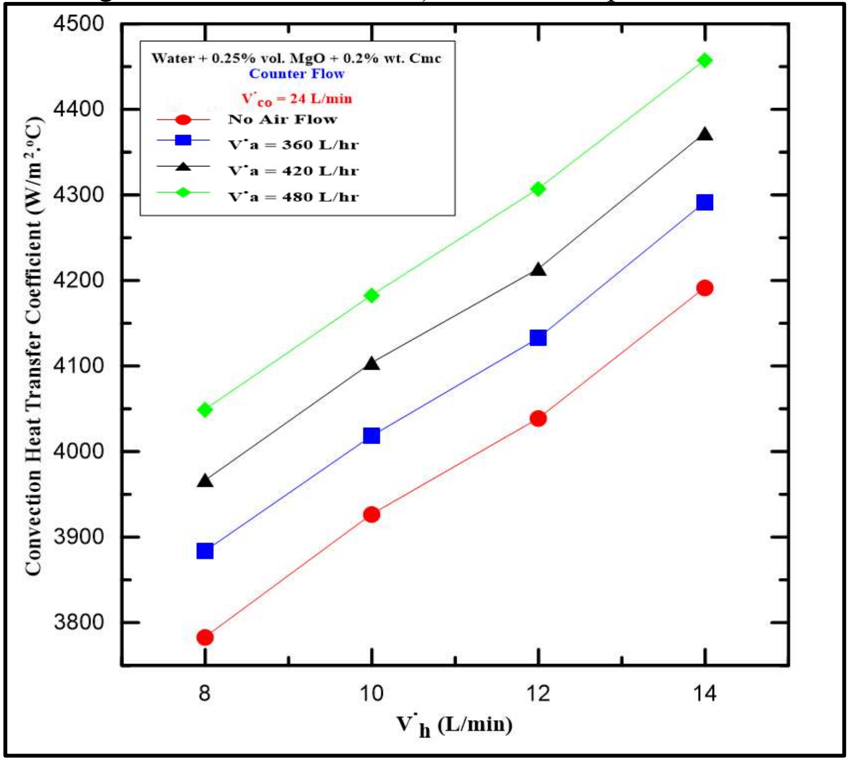

Figure (5-18): Variation of convective heat transfer coefficient with hot fluid (water + 0.25% MgO vol. + 0.2% CMC wt.) flow rate for counter flow.

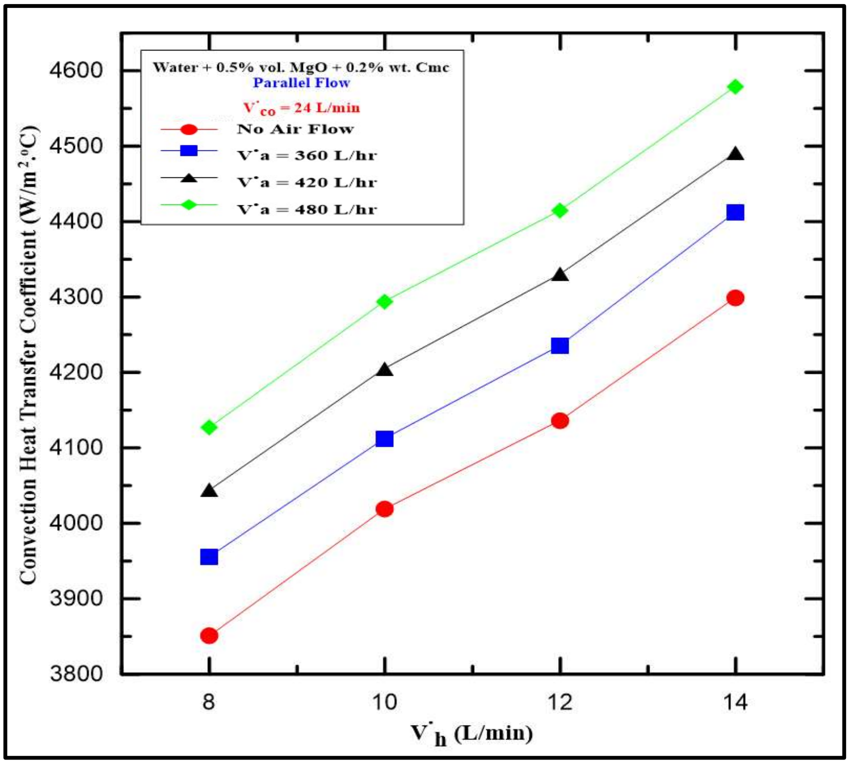

Figure (5-19): Variation of convective heat transfer coefficient with hot fluid (water + 0.5% MgO vol. + 0.2% CMC wt.) flow rate for parallel flow.

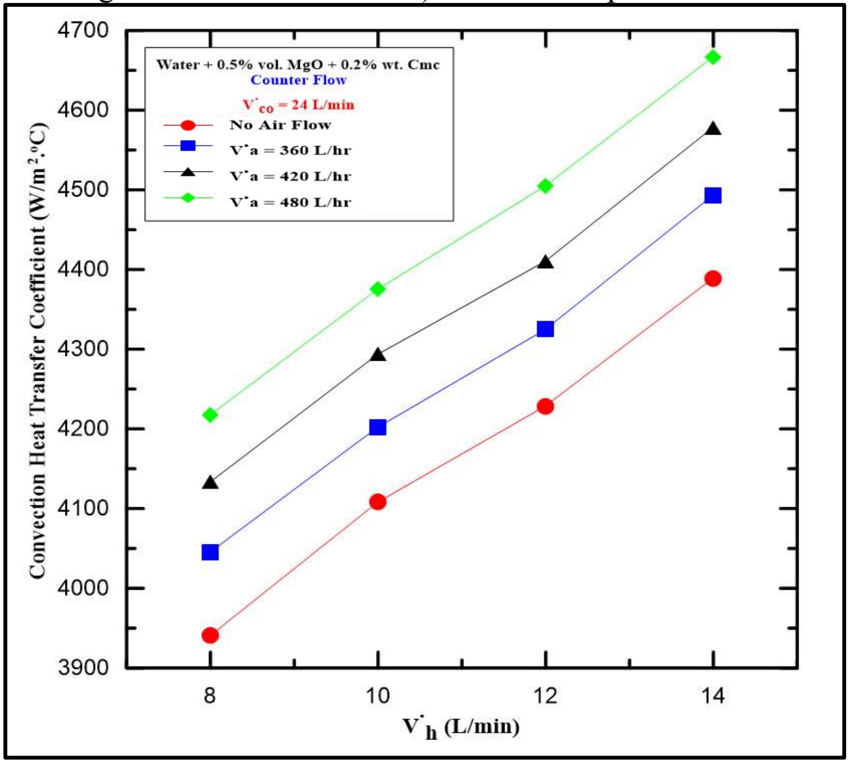

Figure (5-20): Variation of convective heat transfer coefficient with hot fluid (water + 0.5% MgO vol. + 0.2% CMC wt.) flow rate for counter flow.

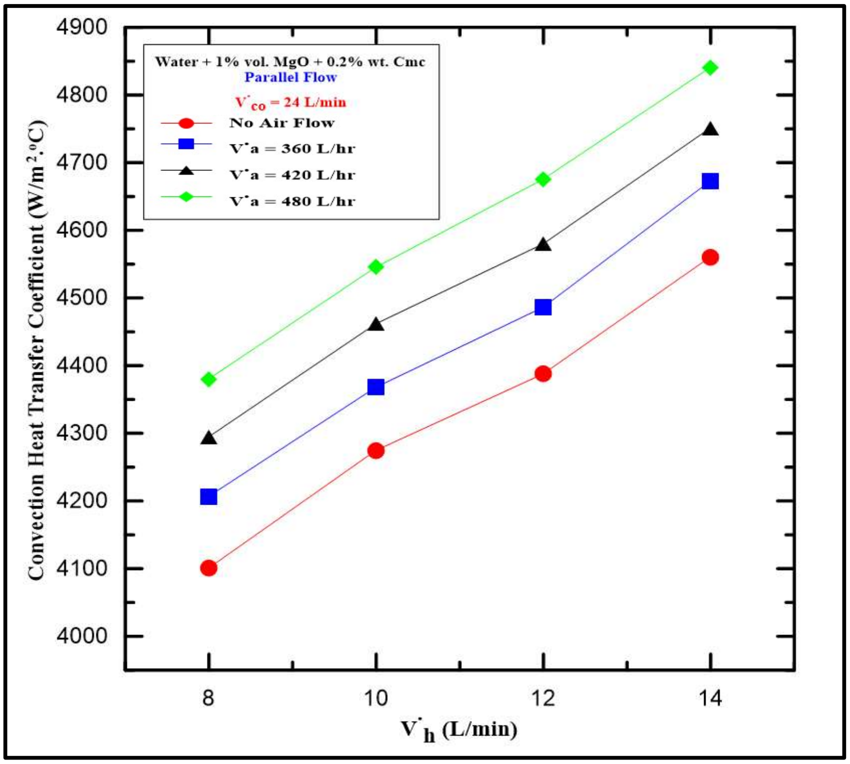

Figure (5-21): Variation of convective heat transfer coefficient with hot fluid (water + 1% MgO vol. + 0.2% CMC wt.) flow rate for parallel flow.

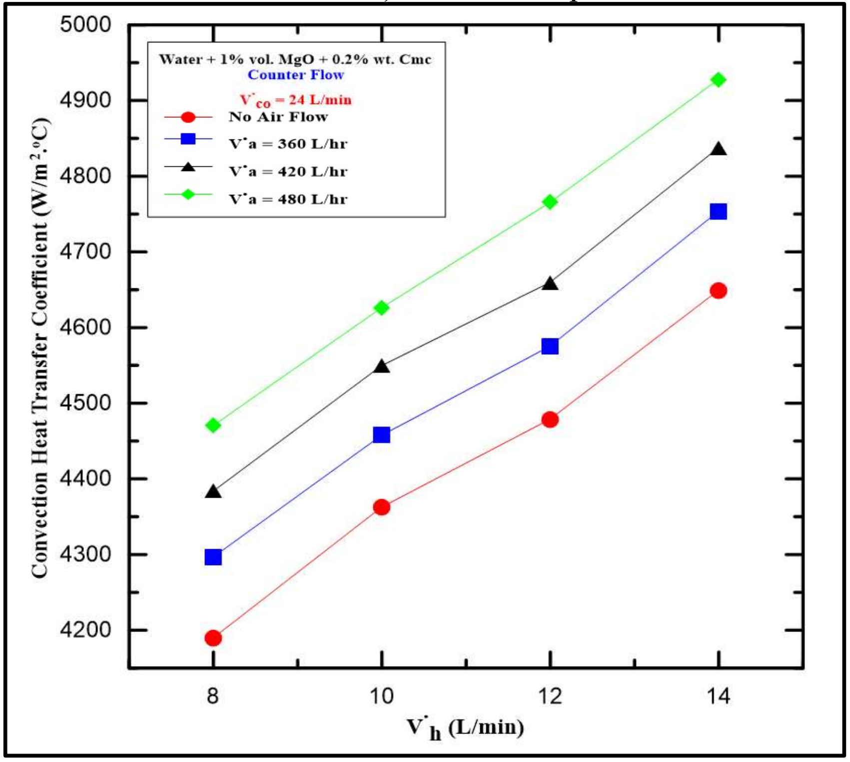

Figure (5-22): Variation of convective heat transfer coefficient with hot fluid (water + 1% MgO vol. + 0.2% CMC wt.) flow rate for counter flow.

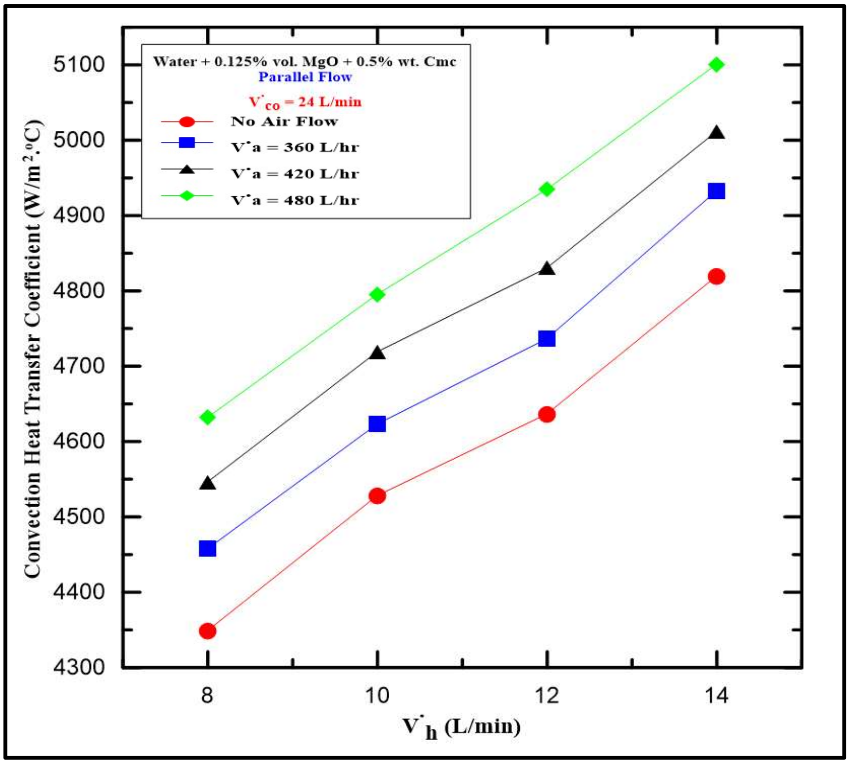

Figure (5-23): Variation of convective heat transfer coefficient with hot fluid (water + 0.125% MgO vol. + 0.5% CMC wt.) flow rate for parallel flow.

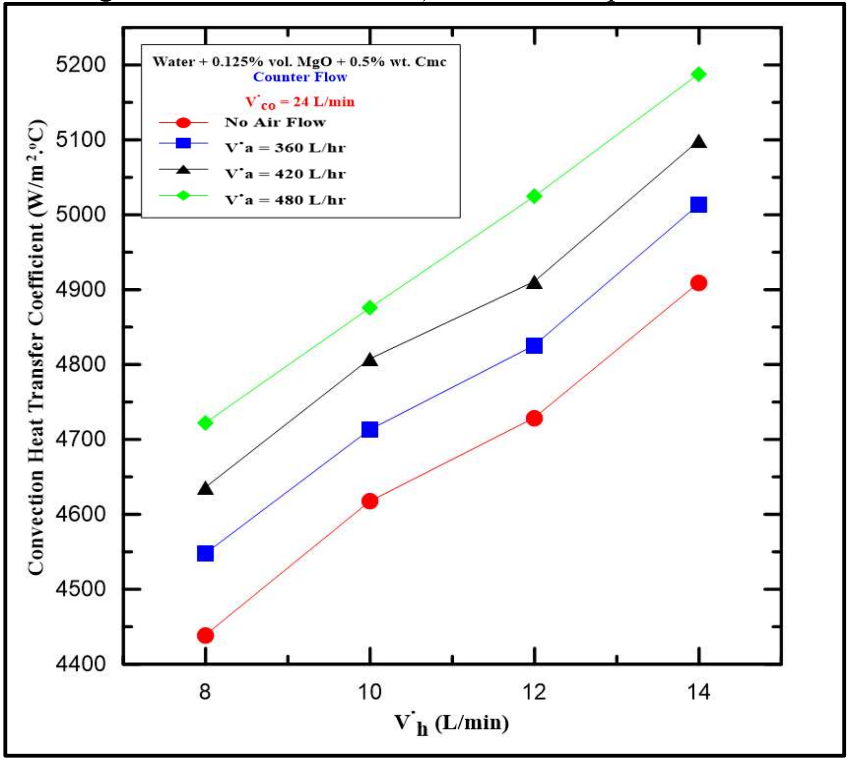

Figure (5-24): Variation of convective heat transfer coefficient with hot fluid (water + 0.125% MgO vol. + 0.5% CMC wt.) flow rate for counter flow.

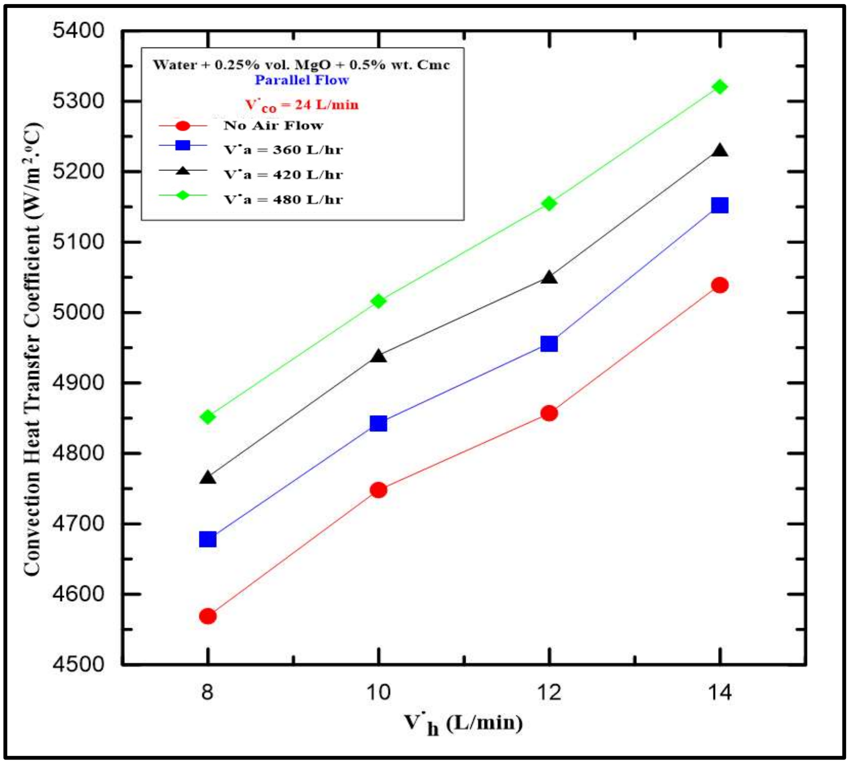

Figure (5-25): Variation of convective heat transfer coefficient with hot fluid (water + 0.25% MgO vol. + 0.5% CMC wt.) flow rate for parallel flow.

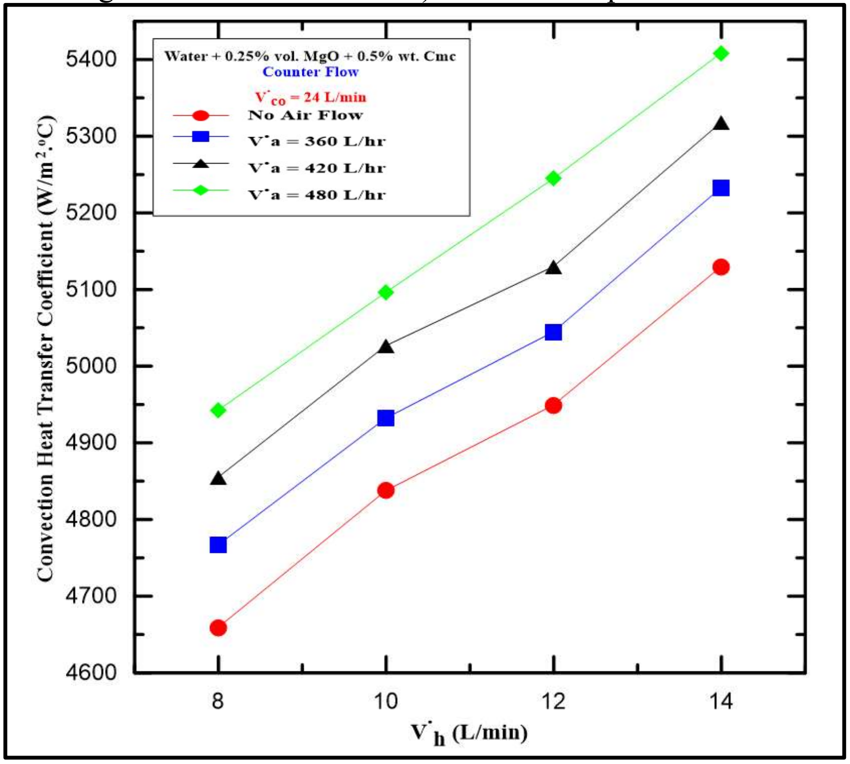

Figure (5-26): Variation of convective heat transfer coefficient with hot fluid (water + 0.25% MgO vol. + 0.5% CMC wt.) flow rate for counter flow.

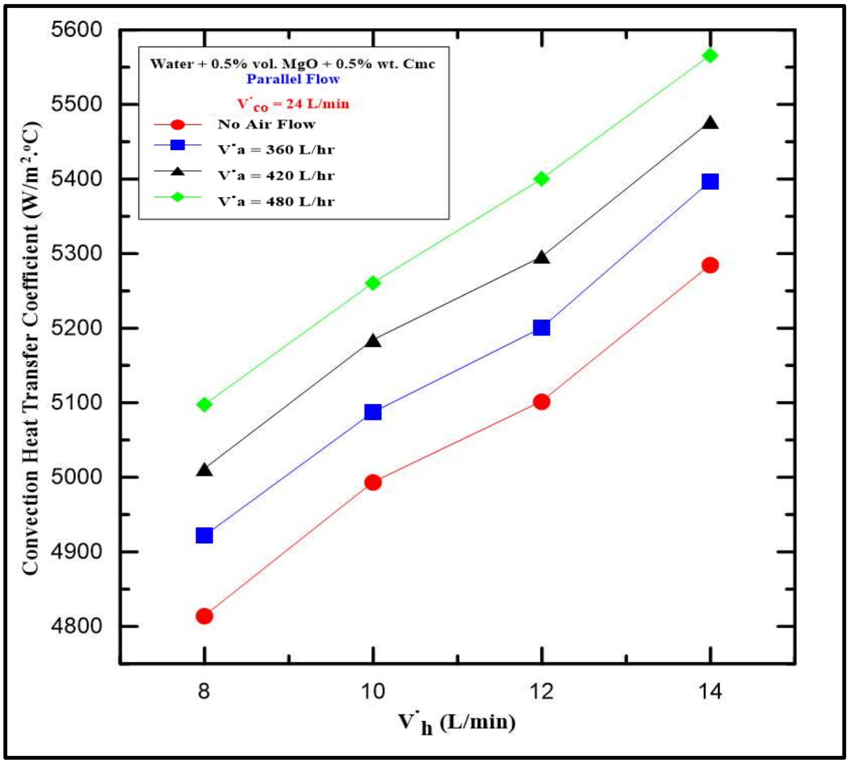

Figure (5-27): Variation of convective heat transfer coefficient with hot fluid (water + 0.5% MgO vol. + 0.5% CMC wt.) flow rate for parallel flow.

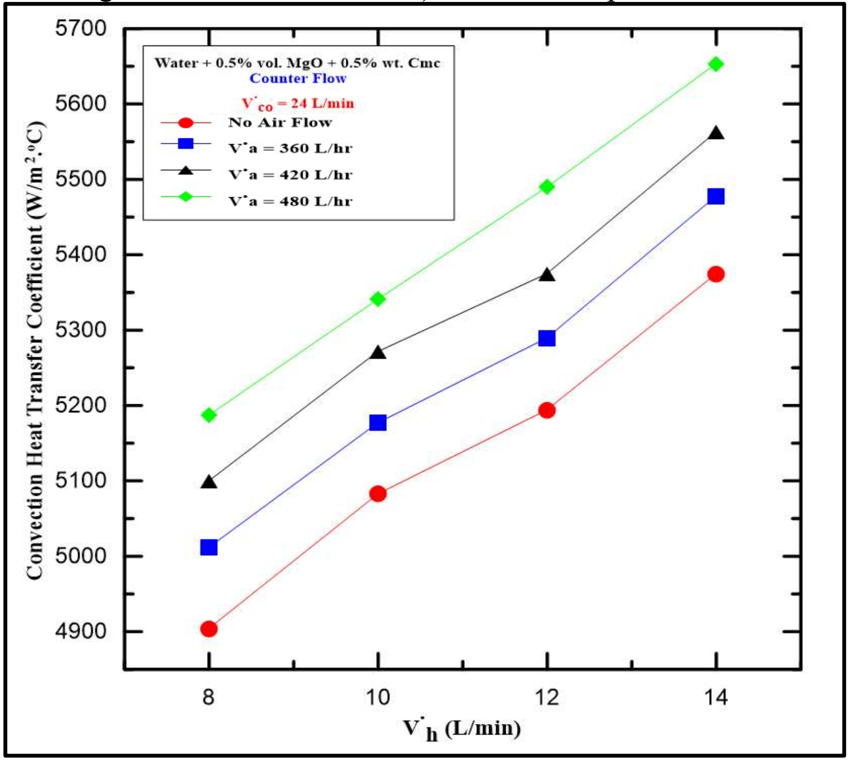

Figure (5-28): Variation of convective heat transfer coefficient with hot fluid (water + 0.5% MgO vol. + 0.5% CMC wt.) flow rate for counter flow.

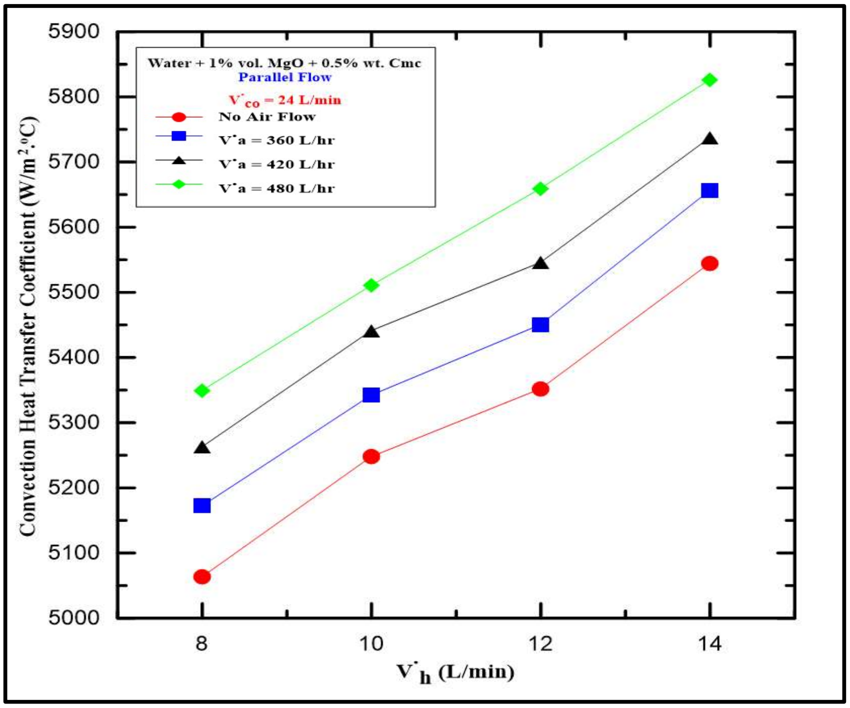

Figure (5-29): Variation of convective heat transfer coefficient with hot fluid (water + 1% MgO vol. + 0.5% CMC wt.) flow rate for parallel flow.

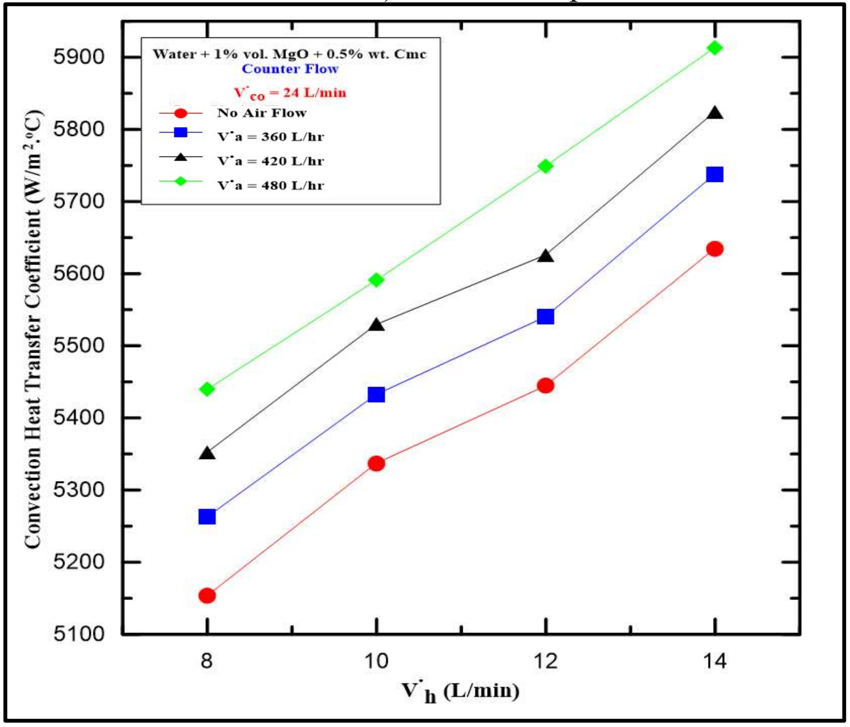

Figure (5-30): Variation of convective heat transfer coefficient with hot fluid (water + 1% MgO vol. + 0.5% CMC wt.) flow rate for counter flow.

5.2.2 Heat Transfer Effectiveness of Double Pipe Heat exchanger

The heat transfer effectiveness means heat exchanger effectiveness. The heat exchanger effectiveness presents a heat exchanger's performance. It is defined as the ratio of the actual heat transfer rate to the maximum heat transfer rate. Also, it is calculated according to equation (F-20) or by computing NTU and using equations (F-21). In this case, calculating the effectiveness of heat exchanger effected by cold fluid flow type in annular side either single phase or two-phase flow. The single-phase flow means cold water flow only in annular side at volume flow rate 24 L/min. On the other hand, the two phases flow means cold water flow at volume flow rate 24 L/min and mixing with air flow rate range (360, 420 and 480 L/hr). Also, the heat transfer effectiveness depends on hot fluid type and range of its flow rate. The hot fluid flow rate ranges (8, 10, 12 and 14 L/min).

5.2.2.1 Heat Transfer Effectiveness of DPHE using Pure Water

Figures (5-31) and (5-32) show the relation between the heat transfer effectiveness with pure water flow as hot fluid in inner pipe under different flow condition which pointed out in each figure. In addition, these figures demonstrate the effect of single and two phases flow in annular side on the heat transfer effectiveness. It can be noticed that the heat transfer effectiveness increases with increasing flow rate of hot fluid in inner pipe when cold fluid in annular side is (24 L/min). It has been shown that increasing air flow rate will increase the effectiveness according to equations (F-21) and the hot fluid has a minimum thermal capacity at (8-14) L/min. So, that the increase of cold flow rate, will increase the average heat transfer which increases the heat transfer effectiveness. The behavior of air bubbles also increases leading to air mixing with water in annular region due to the increase of the level of water layer turbulence. This turbulence in water layer influences the thermal boundary layer, that is formed on the inner pipe outer surface area region.

The heat transfer effectiveness for this case at different flow conditions is present in table (5-5).

Table (5-5): Experimental value of the heat transfer effectiveness at using pure water.

Number of phases	Flow direction	Level	Cold fluid flow rate (L/min)	Hot fluid flow rate (L/min)	Air flow rate (L/min)	e
Single phase	Parallel flow	Maximum	24	14	0	0.287
		Minimum	24	8	0	0.242
	Counter flow	Maximum	24	14	0	0.312
		Minimum	24	8	0	0.264
Two phases	Parallel flow	Maximum	24	14	480	0.334
		Minimum	24	8	360	0.301
	Counter flow	Maximum	24	14	480	0.359
		Minimum	24	8	360	0.322

5.2.2.2 Heat Transfer Effectiveness of DPHE using Water-CMC Fluid

Figures from (5-33) to (5-36) describe the variation of the heat transfer effectiveness of heat exchanger with hot fluid (Water-CMC fluid) volume flow rate in inner pipe under effect of single and two phases flow in annular region. The CMC partials which are added to pure water lead to improve pure water properties as presented in chapter three. The Water-CMC fluid has higher physical properties than that of pure water. The important result from this addition gets higher viscosity fluid than that of pure water. The viscosity of the water-CMC fluid increases with increasing CMC concentration. The CMC particles are added at two different concentration 0.2% and 0.5% by weight. An increase in the viscosity of the fluid leads to an increase in heat exchange gain and rate between fluids in the contact regions. As well, the better concentration is 0.5% by weight. The air injection in mixing chamber at (360, 420 and 480 L/hr) flow rate in the different conditions as shown over each figure. It has been observed that the heat transfer effectiveness under the influence of single phase flow has the same response in parallel and counter flow increase with increasing flow rate in inner pipe. For two phases flow, increasing air flow rate lead to increase the heat transfer effectiveness according to equations (F-21) and the hot fluid has minimum thermal capacity in this equation, and to be varied from 8 to 14 L/min. So, that the increase of hot flow rate, will increase the average heat transfer which increases the heat transfer effectiveness. Increasing the air flow rate that is mixed with water in annular region the level of water layer turbulence also increases. This turbulence in water layer influence on the thermal boundary layer, is formed on the inner pipe outer surface area region. Table (5-6) shows the heat transfer effectiveness values under different flow conditions and CMC concentration by weight.

Table (5-6): Experimental value of the heat transfer effectiveness at using hot fluid water + 0.5% CMC by weight.

Number of phases	Flow direction	Level	Cold fluid flow rate (L/min)	Hot fluid flow rate (L/min)	Air flow rate (L/min)	e
Single phase	Parallel flow	Maximum	24	14	0	0.310
		Minimum	24	8	0	0.270
	Counter flow	Maximum	24	14	0	0.334
		Minimum	24	8	0	0.293
Two phases	Parallel flow	Maximum	24	14	480	0.353
		Minimum	24	8	360	0.325
	Counter flow	Maximum	24	14	480	0.380
		Minimum	24	8	360	0.347

5.2.2.2 Heat Transfer Effectiveness of DPHE using Water-MgO Fluid

Figures from (5-37) to (5-44) illustrate the heat transfer effectiveness variation with hot fluid (Water-MgO Fluid) flow rate in the inner pipe for different MgO nanoparticles concentration (0.125%, 0.25%, 0.5% and 1% by volume) in different flow conditions which are pointed out in each figure. It can be noticed that the nanoparticle enhances the heat transfer effectiveness of heat exchanger at increasing hot fluid volume flow rates. The two phases flow in annular side and air flow rate increase due to the heat transfer effectiveness. The effectiveness increases with increasing nanoparticle concentration because the nanoparticle reduces the temperature difference between the wall and bulk nanofluid causing an increase in heat transfer coefficient then effectiveness increases. The best MgO nanoparticles concentration in this case is 1% by volume, and the result for this case is shown in table (5-7).

Table (5-7): Experimental value of the heat transfer effectiveness at using hot fluid water + 1% MgO by volume.

Number of phases	Flow direction	Level	Cold fluid flow rate (L/min)	Hot fluid flow rate (L/min)	Air flow rate (L/min)	e
Single phase	Parallel flow	Maximum	24	14	0	0.326
		Minimum	24	8	0	0.29
	Counter flow	Maximum	24	14	0	0.351
		Minimum	24	8	0	0.312
Two phases	Parallel flow	Maximum	24	14	480	0.367
		Minimum	24	8	360	0.342
	Counter flow	Maximum	24	14	480	0.395
		Minimum	24	8	360	0.365

5.2.2.2 Heat Transfer Effectiveness of DPHE using Water-MgO-CMC Fluid

In the previous section, the Water-MgO fluid is used as hot fluid to enhance the heat exchange rate. In this fluid, MgO particles suffer from agglomeration, because of the effect on stability of nanofluid and where it become weaker and nanoparticles deposit on the bottom of vessel. This leads to accounting the use of nanoparticles in various application. Therefore, a solution must be found to this problem and prevent nanoparticles from agglomeration and deposit on the bottom of vessel. In this case, MgO particles dispersed in Water-CMC as working fluid to prevent agglomeration and deposit of MgO particles and to enhance physical properties of base fluid.

Figures from (5-45) to (5-58) illustrate the relationship of the heat transfer effectiveness with hot fluid (Water-MgO-CMC Fluid) volume flow rate in inner pipe for different flow conditions. The cold fluid is pure water flow in annulus side and remains constant at 24 L/min for single phase. The air is injecting in mixing chamber to mix with water that flow in annulus side to generate two phases flow at air volumetric flow rate range (360, 420 and 480 L/hr) to get different flow pattern. This relation is an upward relationship. As the heat transfer effectiveness has the same response in previous figures at various flow conditions. It has been shown that the increase in flow rate of air, will increase effectiveness according to equation (F-21) the maximum thermal capacity in this equation is for cold fluid and it constant at 24 L/min so that the increase of hot flow rate from 8 to 14 L/min will increase the average heat transfer which increases the heat transfer effectiveness. The air flow rate that mixing with water in annular region increases, due to increase the level of water layer turbulence. This turbulence in water layer influences the thermal boundary layer, that is formed on the inner pipe outer surface area region. For single phases flow, the heat transfer effectiveness slightly increases dependent on type of hot fluid. The heat transfer effectiveness for two phases flow do not depend on hot fluid type only, but also, dependent on-air volumetric flow rate. There are two concentrations of CMC particles used 0.2% and 0.5% by weight, and each concentrations makes a change in the MgO concentrations by volume at range (0.125%, 0.25%, 0.5% and 1% by volume). It has been shown no significant change in the effectiveness under different flow conditions as pointed out in each figure. The highest values of effectiveness marks with 1% MgO by volume and 0.5% CMC by weight as shown in table (5-8).

Table (5-8): Experimental value of the heat transfer effectiveness at using hot fluid water + 1% MgO vol.+ 0.5% CMC by weight.

Number of phases	Flow direction	Level	Cold fluid flow rate (L/min)	Hot fluid flow rate (L/min)	Air flow rate (L/min)	e
Single phase	Parallel flow	Maximum	24	14	0	0.347
		Minimum	24	8	0	0.317
	Counter flow	Maximum	24	14	0	0.374
		Minimum	24	8	0	0.340
Two phases	Parallel flow	Maximum	24	14	480	0.385
		Minimum	24	8	360	0.366
	Counter flow	Maximum	24	14	480	0.416
		Minimum	24	8	360	0.390

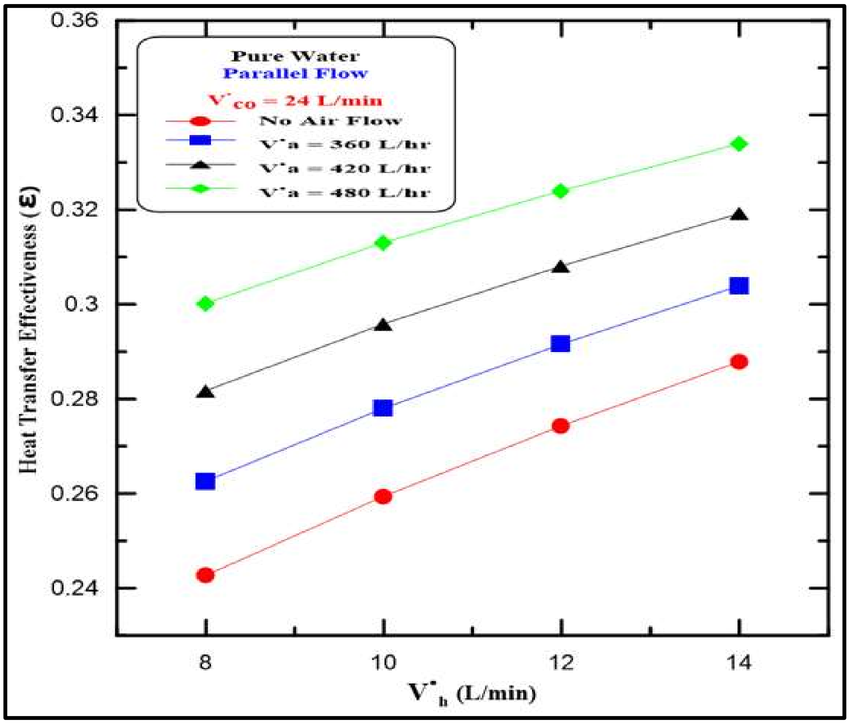

Figure (5-31): Variation of heat transfer effectiveness with hot fluid (pure water) flow rate for parallel flow.

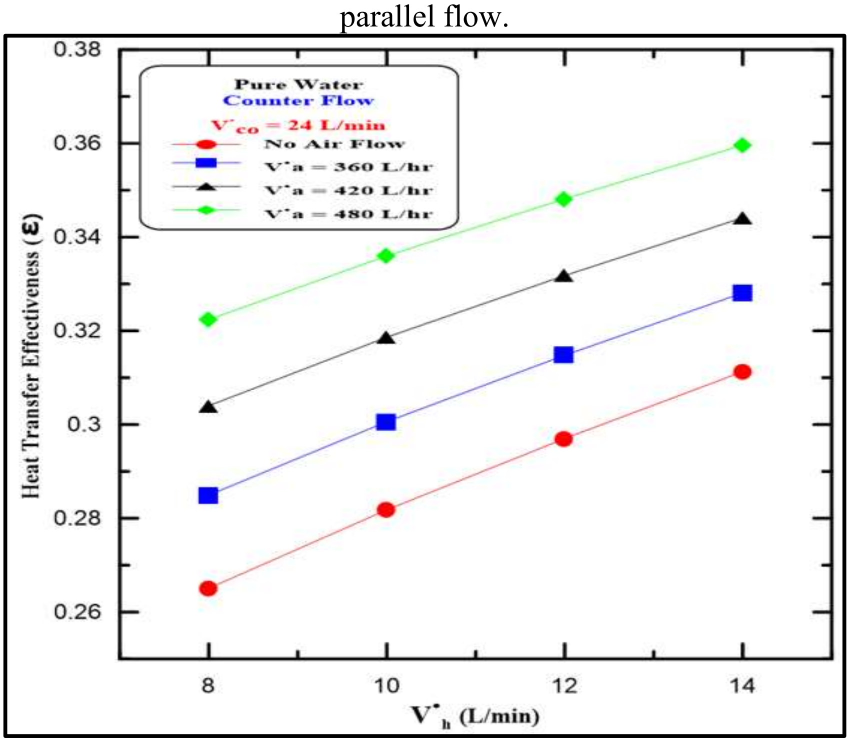

Figure (5-32): Variation of heat transfer effectiveness with hot fluid (pure water) flow rate for counter flow.

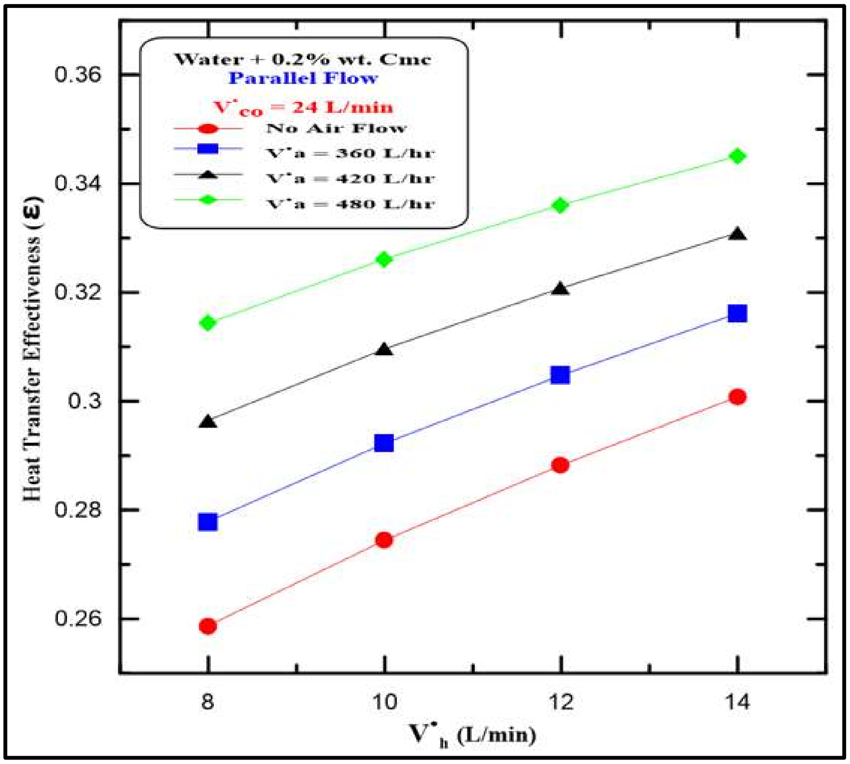

Figure (5-33): Variation of heat transfer effectiveness with hot fluid (water+0.2% CMC wt.) flow rate for parallel flow.

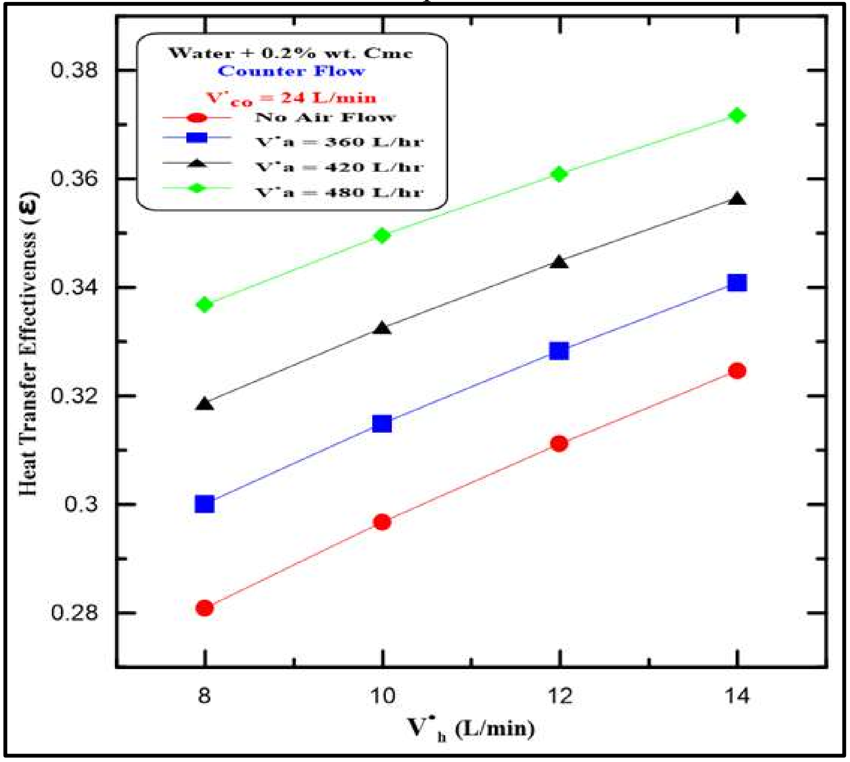

Figure (5-34): Variation of heat transfer effectiveness with hot fluid (water+0.2% CMC wt.) flow rate for counter flow.

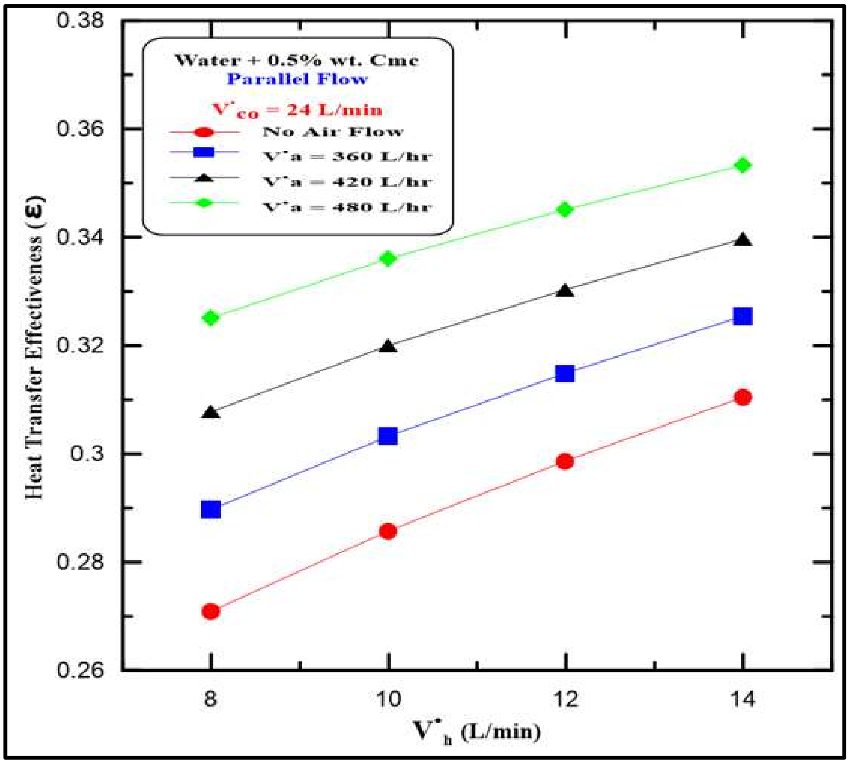

Figure (5-35): Variation of heat transfer effectiveness with hot fluid (water+0.5% CMC wt.) flow rate for parallel flow.

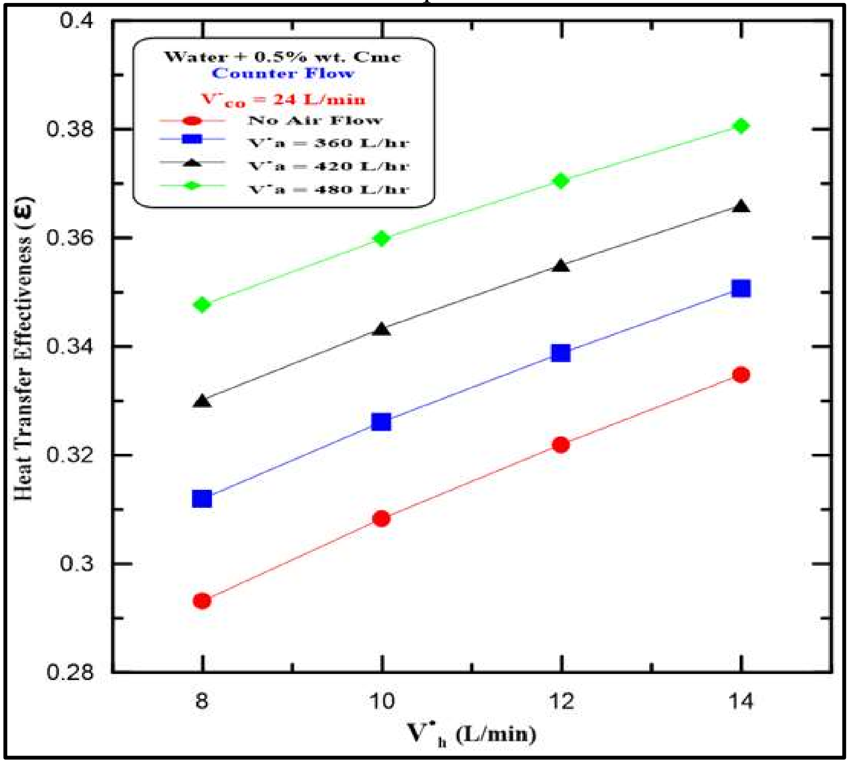

Figure (5-36): Variation of heat transfer effectiveness with hot fluid (water+0.5% CMC wt.) flow rate for counter flow.

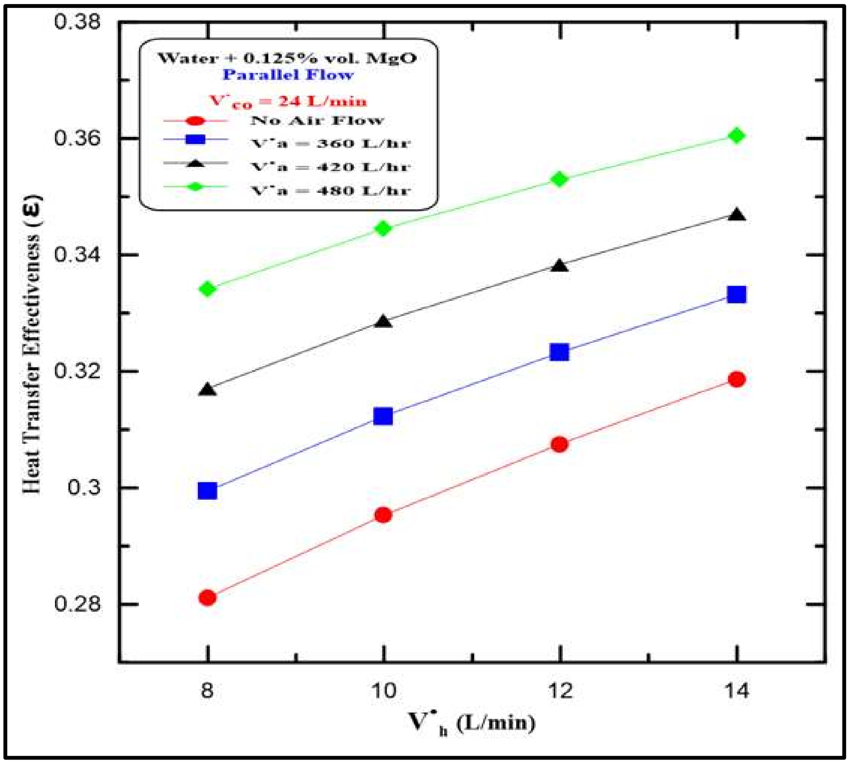

Figure (5-37): Variation of heat transfer effectiveness with hot fluid (water+0.125% MgO vol.) flow rate for parallel flow.

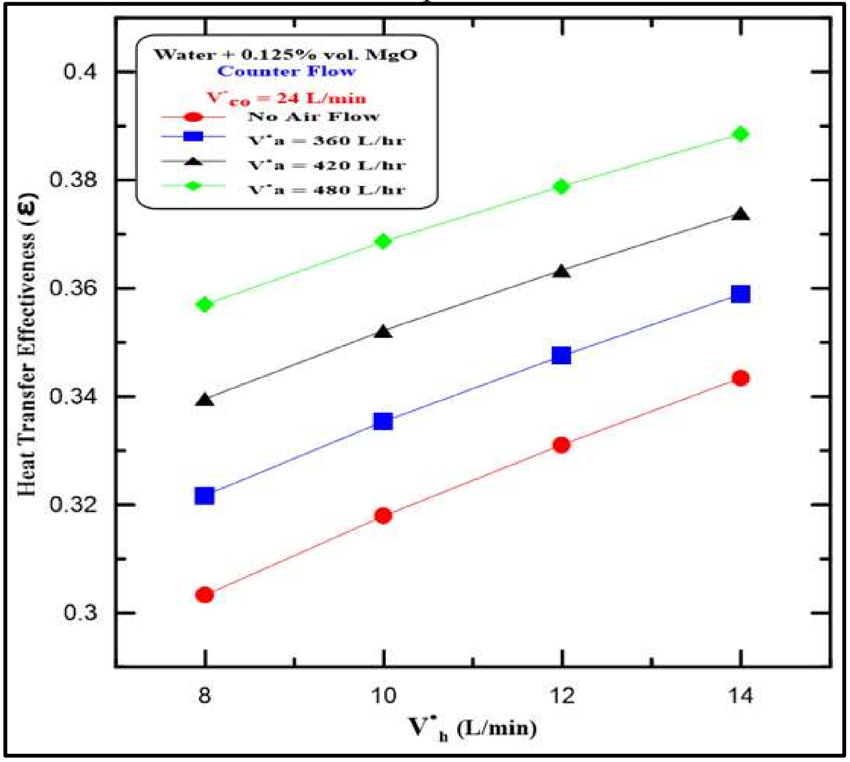

Figure (5-38): Variation of heat transfer effectiveness with hot fluid (water+0.125% MgO vol.) flow rate for counter flow.

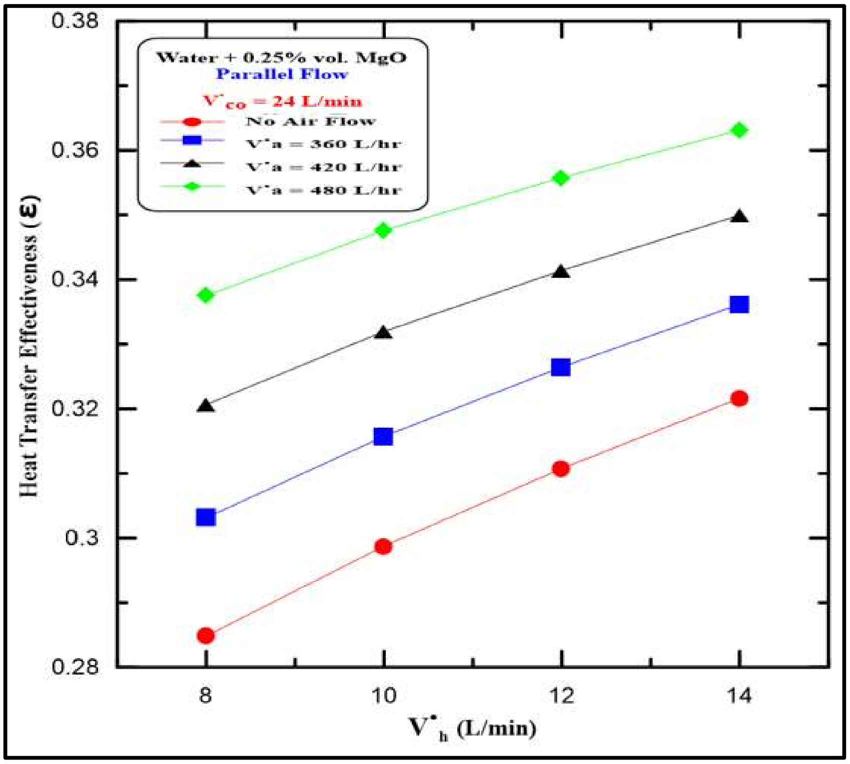

Figure (5-39): Variation of heat transfer effectiveness with hot fluid (water+0.25% MgO vol.) flow rate for parallel flow.

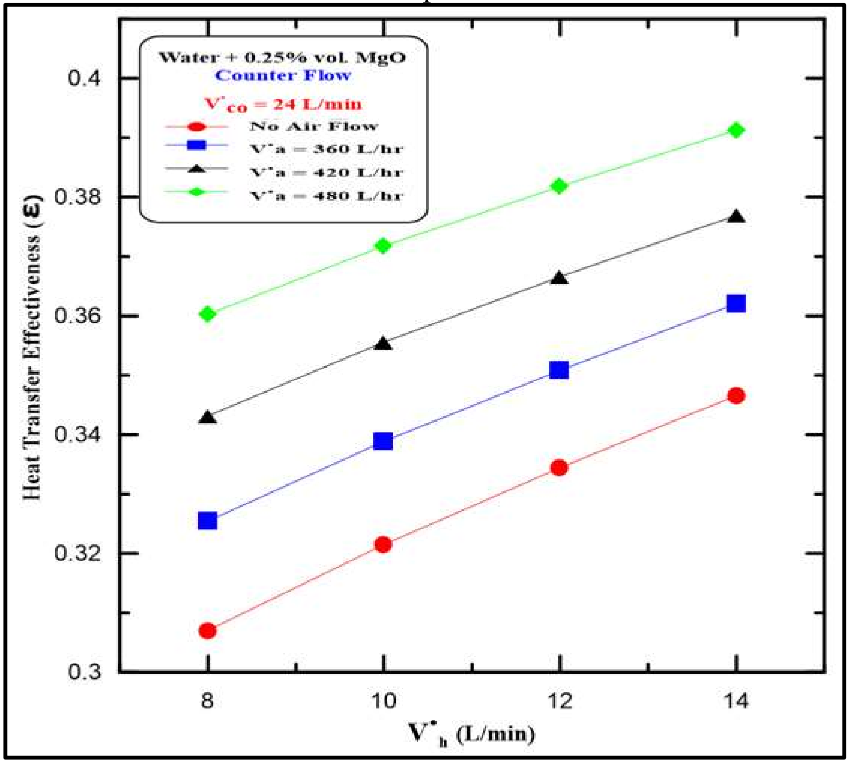

Figure (5-40): Variation of heat transfer effectiveness with hot fluid (water+0.25% MgO vol.) flow rate for counter flow.

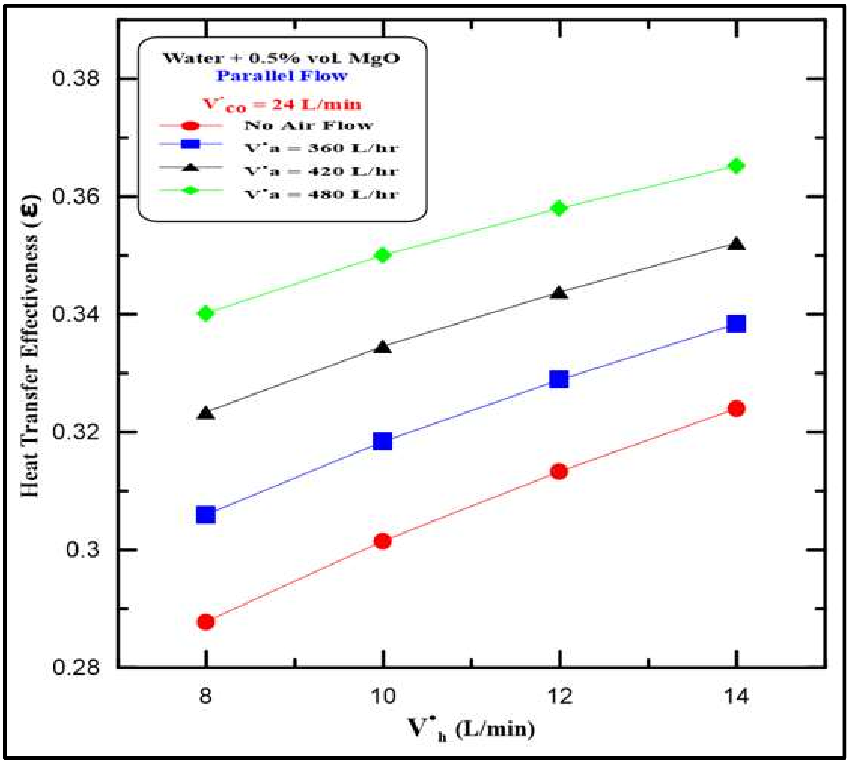

Figure (5-41): Variation of heat transfer effectiveness with hot fluid (water+0.5% MgO vol.) flow rate for parallel flow.

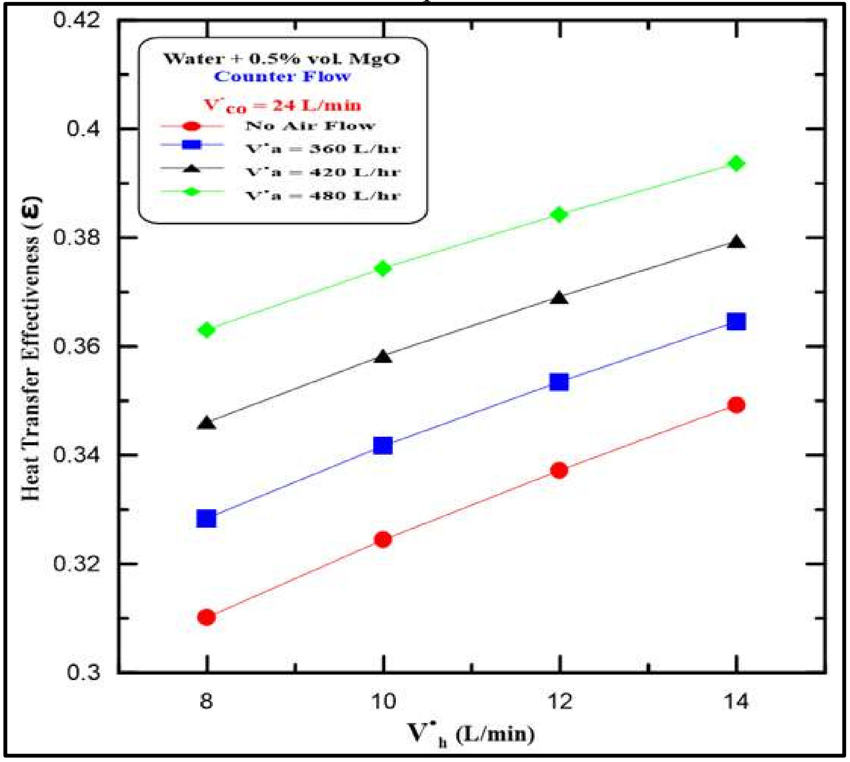

Figure (5-42): Variation of heat transfer effectiveness with hot fluid (water+0.5% MgO vol.) flow rate for counter flow.

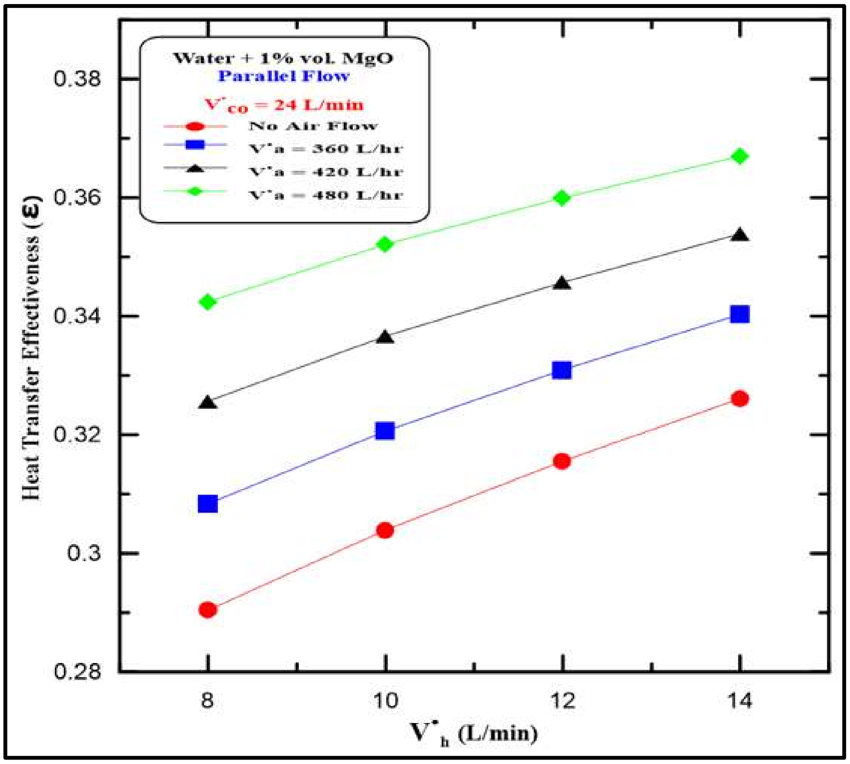

Figure (5-43): Variation of heat transfer effectiveness with hot fluid (water+1% MgO vol.) flow rate for parallel flow.

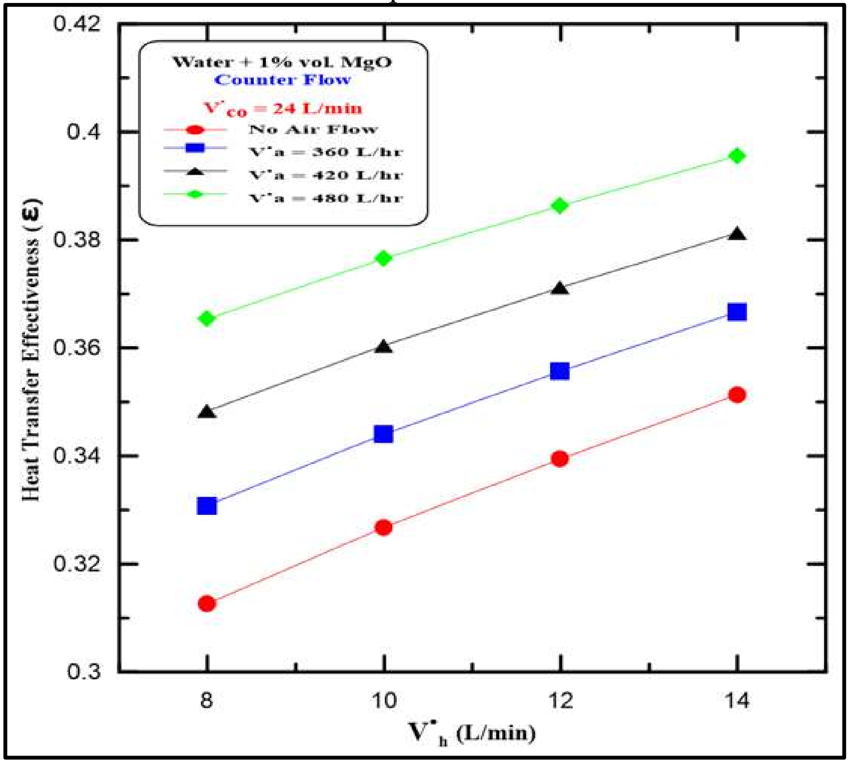

Figure (5-44): Variation of heat transfer effectiveness with hot fluid (water+1% MgO vol.) flow rate for counter flow.

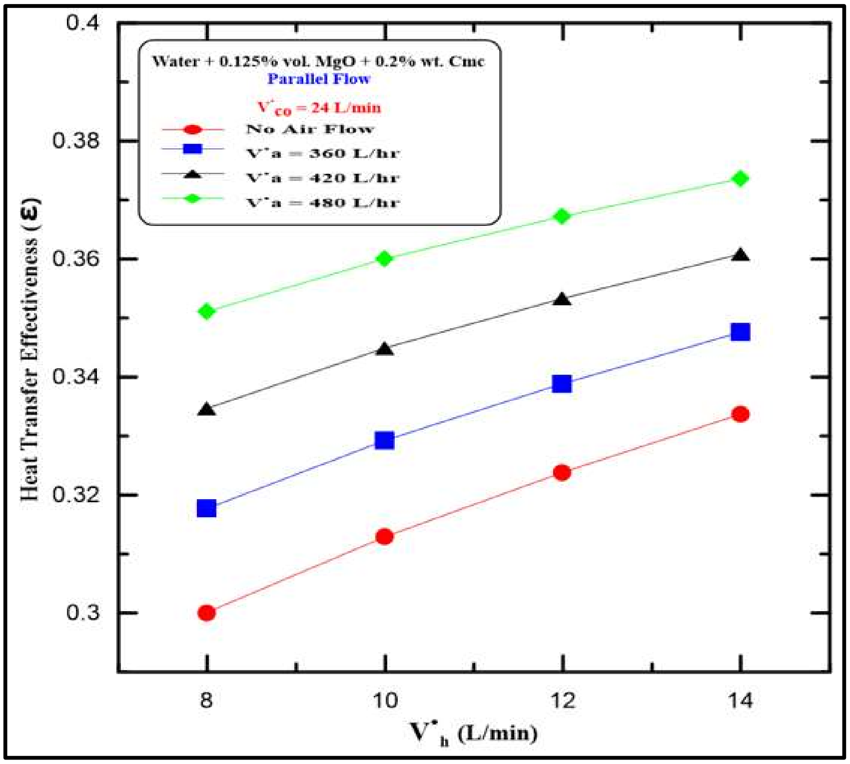

Figure (5-45): Variation of heat transfer effectiveness with hot fluid (water+0.125% MgO vol.+0.2% CMC) flow rate for parallel flow.

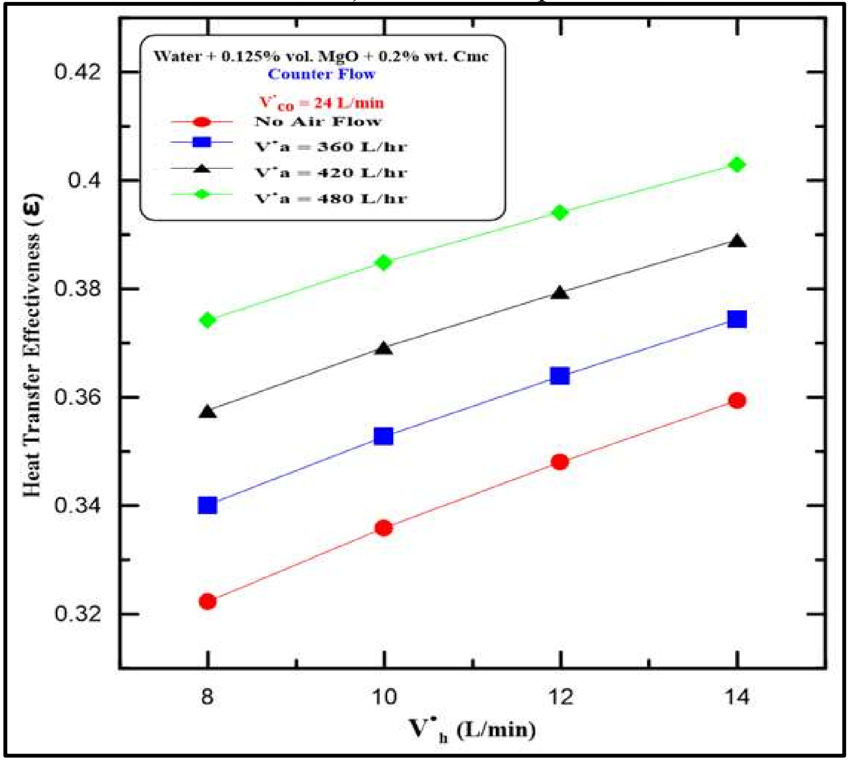

Figure (5-46): Variation of heat transfer effectiveness with hot fluid (water+0.125% MgO vol.+0.2% CMC) flow rate for counter flow.

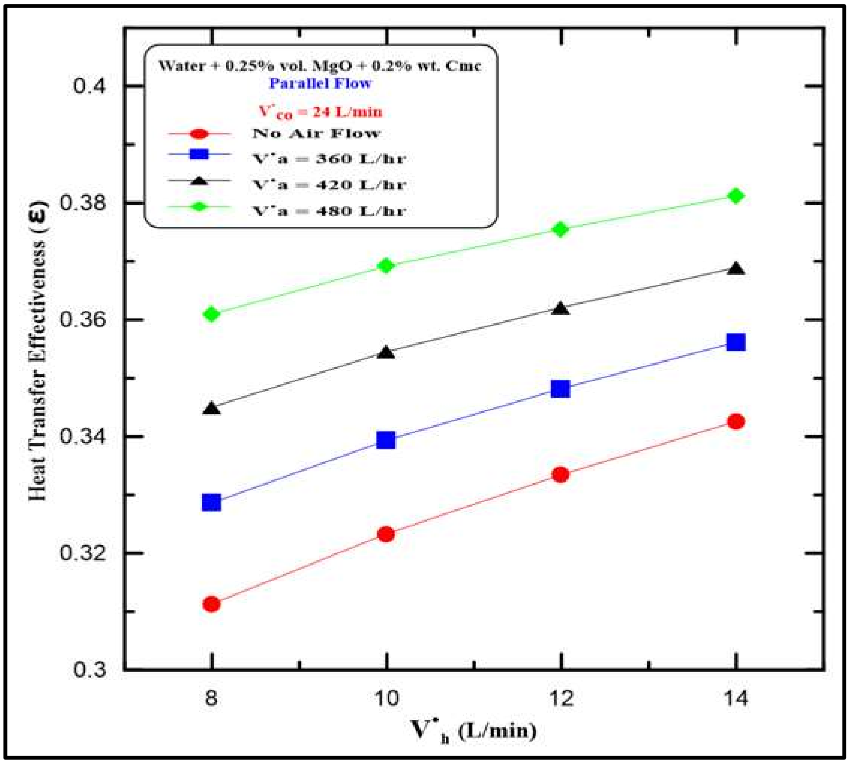

Figure (5-47): Variation of heat transfer effectiveness with hot fluid (water+0.25% MgO vol.+0.2% CMC) flow rate for parallel flow.

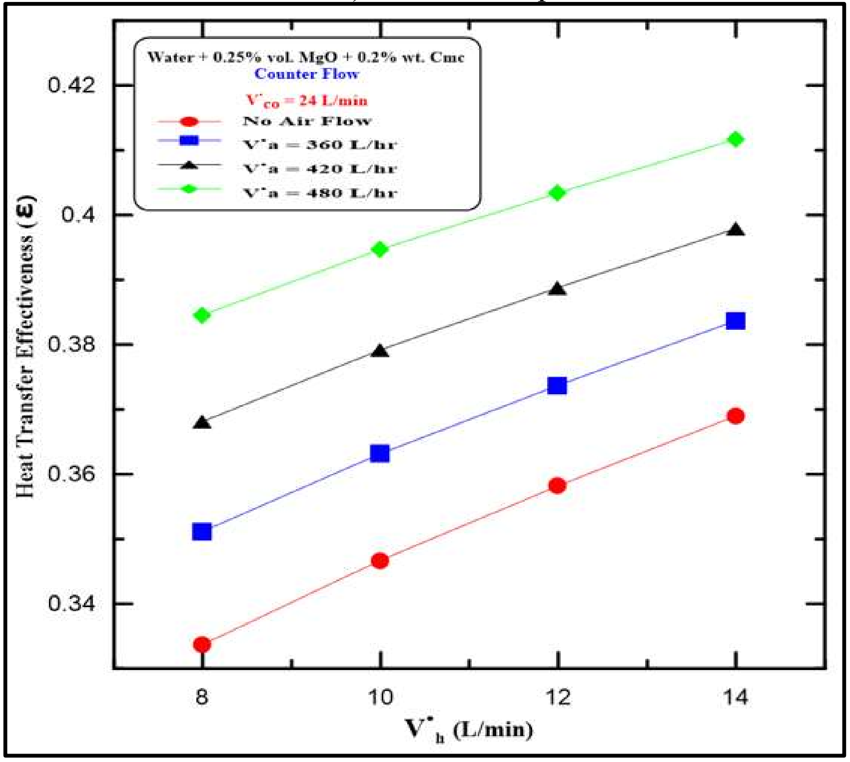

Figure (5-48): Variation of heat transfer effectiveness with hot fluid (water+0.25% MgO vol.+0.2% CMC) flow rate for counter flow.

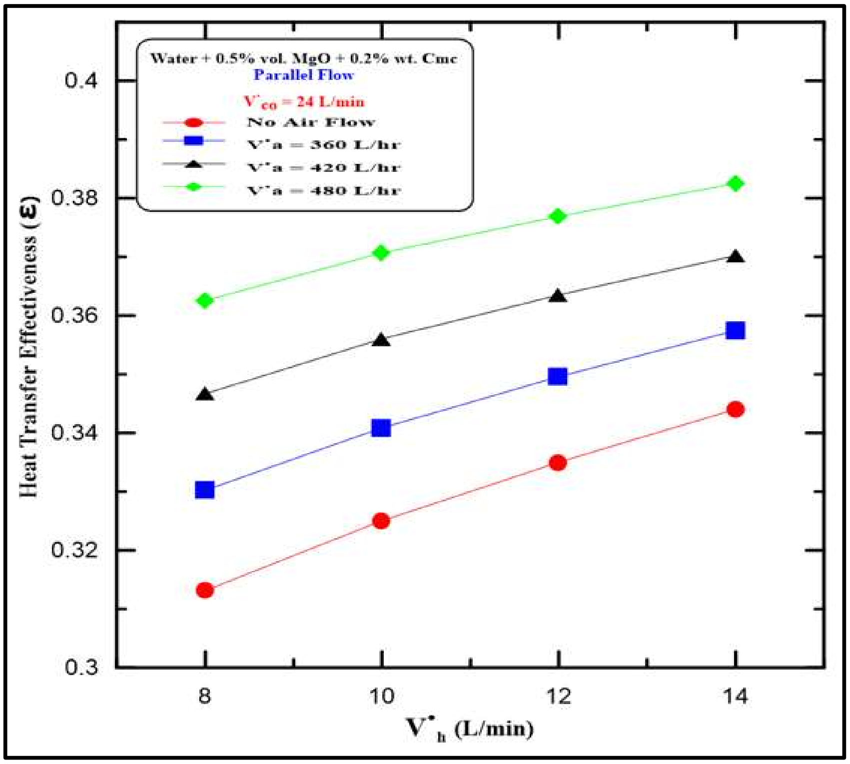

Figure (5-49): Variation of heat transfer effectiveness with hot fluid (water+0.5% MgO vol.+0.2% CMC) flow rate for parallel flow.

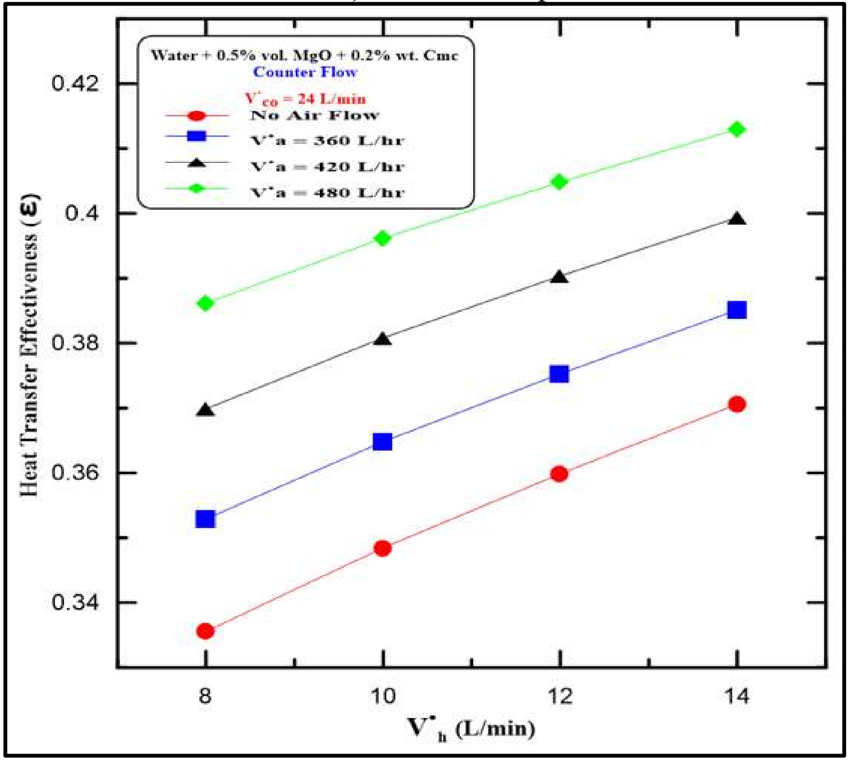

Figure (5-50): Variation of heat transfer effectiveness with hot fluid (water+0.5% MgO vol.+0.2% CMC) flow rate for counter flow.

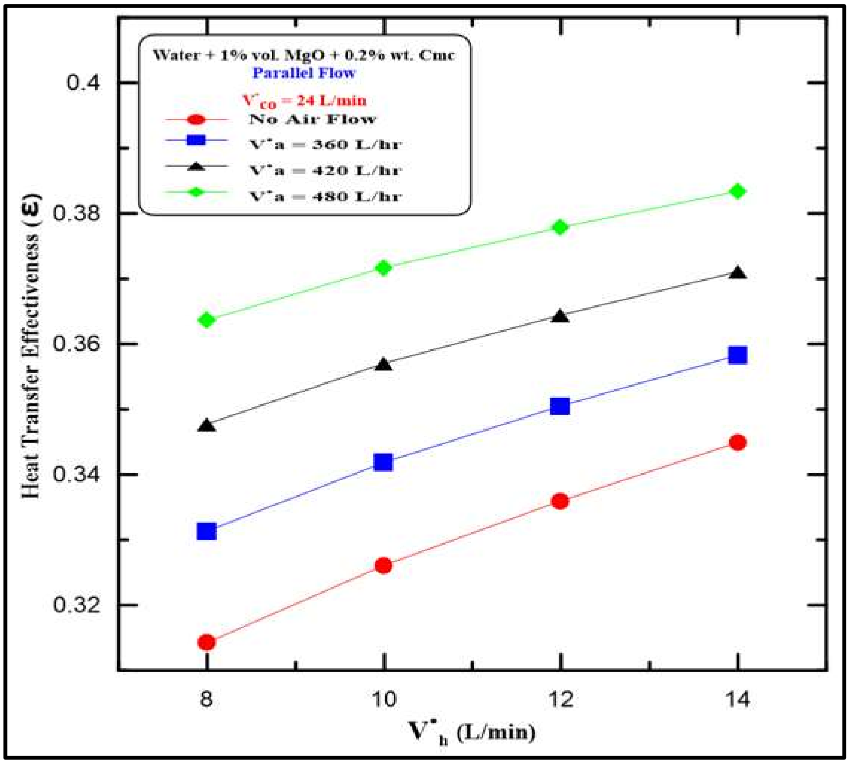

Figure (5-51): Variation of heat transfer effectiveness with hot fluid (water+1% MgO vol.+0.2% CMC) flow rate for parallel flow.

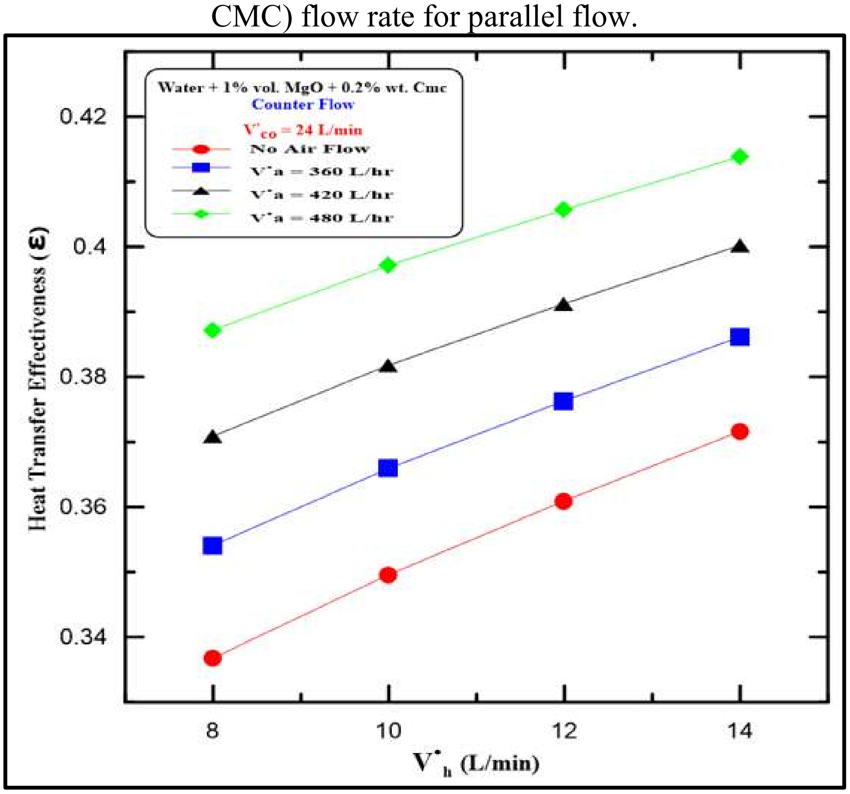

Figure (5-50): Variation of heat transfer effectiveness with hot fluid (water+1% MgO vol.+0.2% CMC) flow rate for counter flow.

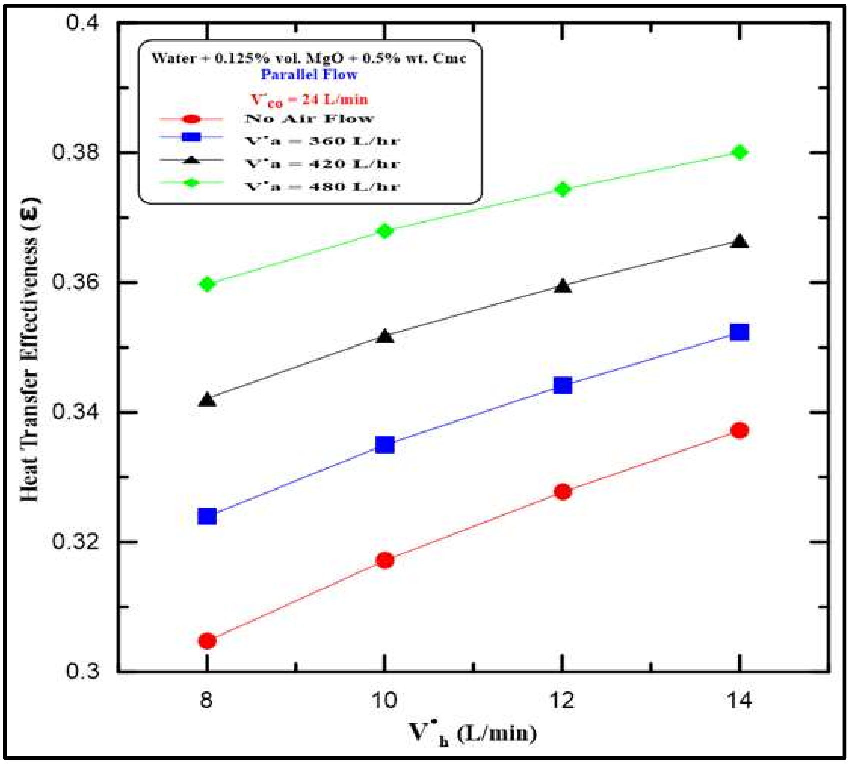

Figure (5-53): Variation of heat transfer effectiveness with hot fluid (water+0.125% MgO vol.+0.5% CMC) flow rate for parallel flow.

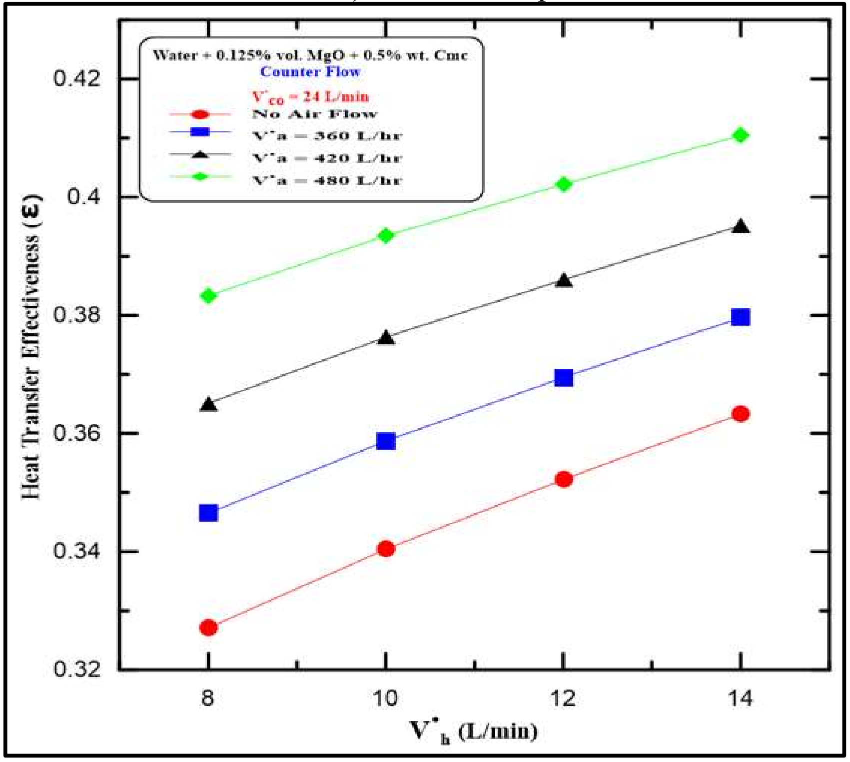

Figure (5-54): Variation of heat transfer effectiveness with hot fluid (water+0.125% MgO vol.+0.5% CMC) flow rate for counter flow.

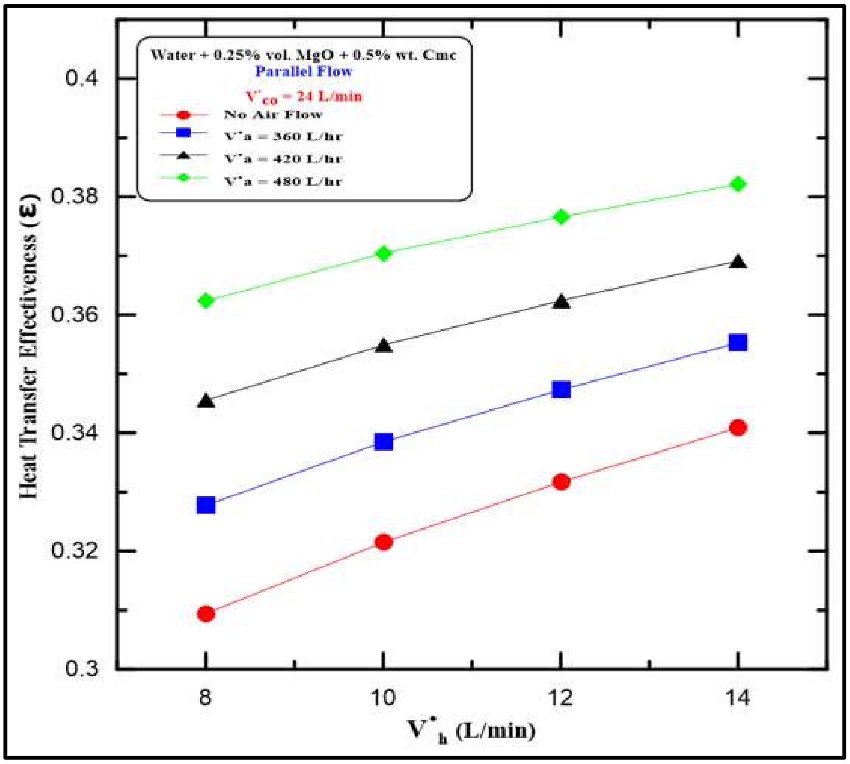

Figure (5-55): Variation of heat transfer effectiveness with hot fluid (water+0.25% MgO vol.+0.5% CMC) flow rate for parallel flow.

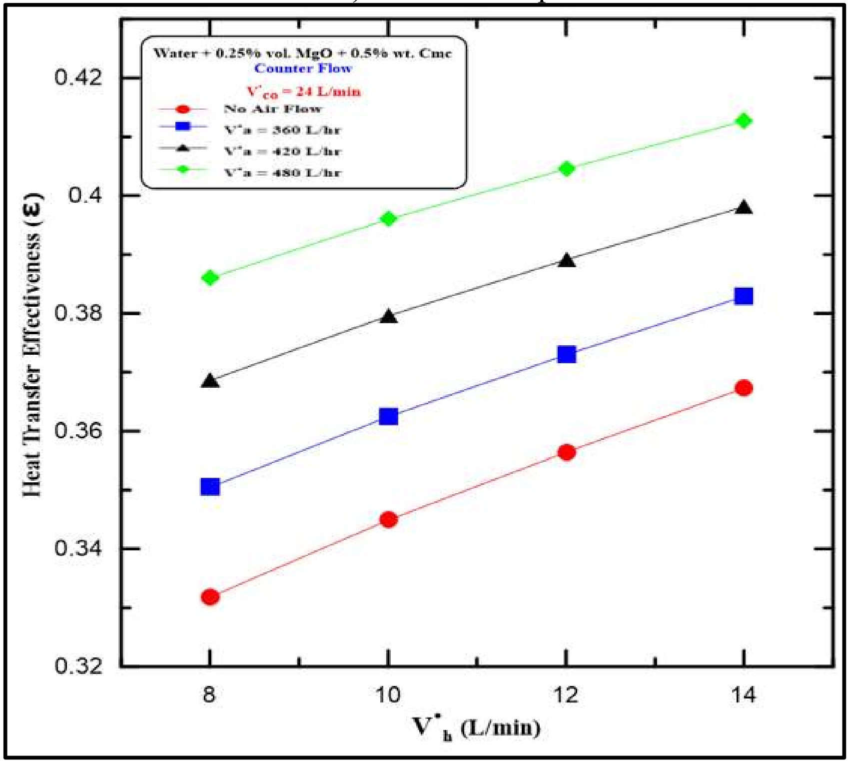

Figure (5-56) Variation of heat transfer effectiveness with hot fluid (water+0.25% MgO vol.+0.5% CMC) flow rate for counter flow.

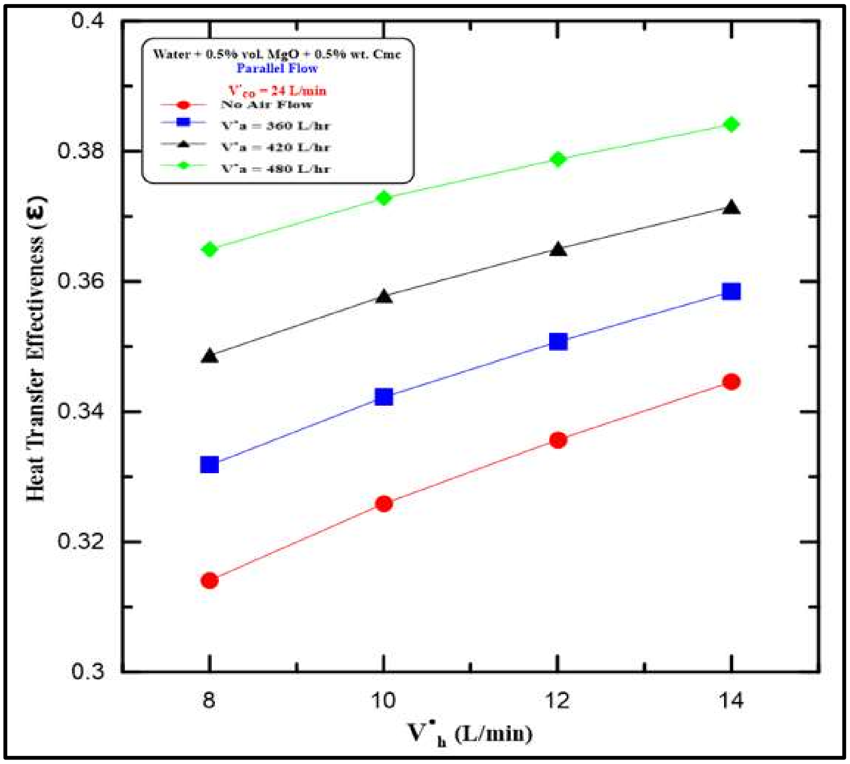

Figure (5-57): Variation of heat transfer effectiveness with hot fluid (water+0.5% MgO vol.+0.5% CMC) flow rate for parallel flow.

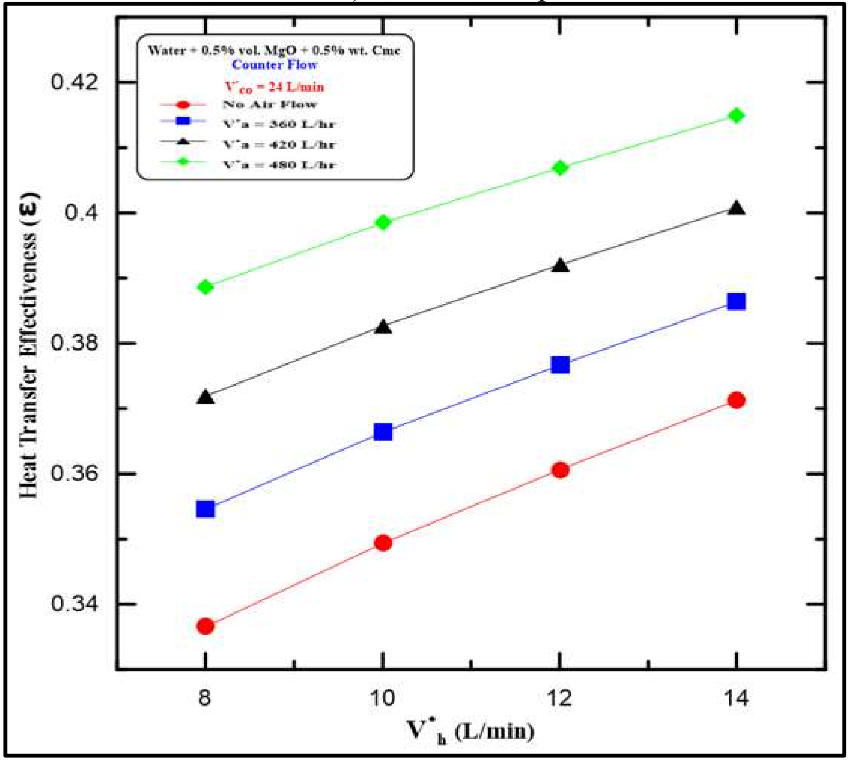

Figure (5-58): Variation of heat transfer effectiveness with hot fluid (water+0.5% MgO vol.+0.5% CMC) flow rate for counter flow.

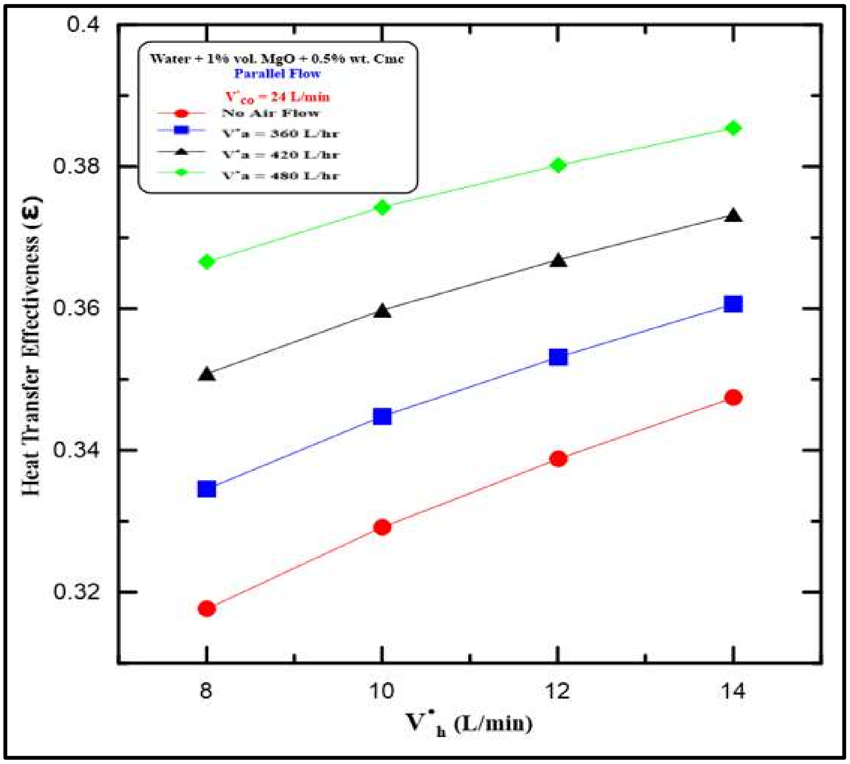

Figure (5-59): Variation of heat transfer effectiveness with hot fluid (water+1% MgO vol.+0.5% CMC) flow rate for parallel flow.

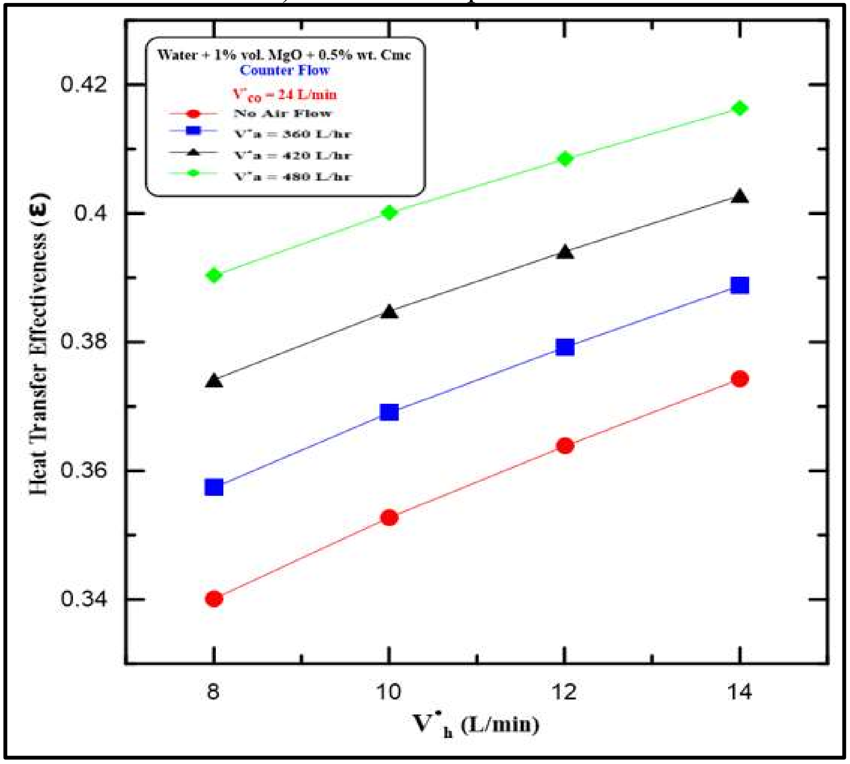

Figure (5-58): Variation of heat transfer effectiveness with hot fluid (water+1% MgO vol.+0.5% CMC) flow rate for counter flow.

5.2.3 Overall Heat Transfer Coefficient (Ui)

The implementations device contains two fluid streams separated by solid wall. The heat transfer process in heat exchanger involves both convection and conduction. The heat is transferred from hot fluid to cold fluid, for this reason overall heat transfer calculate for each stream. The overall heat transfer coefficient in heat exchanger depend one:

1. Position of working fluid.
2. State of working fluid cold or hot.
3. Fluid type and property.
4. Flow type.
5. Property of separated wall.
6. The transmission surfaces.

This section presents the overall coefficient of inner pipe for implementation device. It is often convenient to work with an overall heat transfer coefficient, known as a (Ui) with this systems. The overall heat transfer coefficient of inner pipe for double pipe heat exchanger calculated according to equation (F-9) for various flow conditions. It is dependent on hot fluid type and range of its flow rate, and the hot fluid flow rate range (8-14 L/min). Also, it is affected by cold fluid flow type in annular side either single phase or two-phase flow. The single-phase flow means cold water flow only in annular side at volume flow rate 24 L/min. On the other hand, the two phases flow means cold water flow at volume flow rate 24 L/min and mixing with air flow rate range (360-480 L/hr).

5.2.3.1 Overall Heat Transfer Coefficient Using Pure Water

Figures (5-59) and (5-60) introduce the relation between overall heat transfers and pure water flow rate at inner pipe under different flow conditions which are demonstrated in each figure. For this case pure water is used as hot fluid flow rate range (8, 10, 12 and 14 L/min), and take into account the effect of a single phase and two-phase flow in annular side. The cold-water flow in annular side 24 L/min, and to generate two phases flow air must be mixed in mixing chamber at (360, 420 and 480 L/hr) under turbulent condition. It has been shown that the increase of volume flow rate of hot fluid increases the overall coefficient that influences the increase of thermal capacity. This effect is noticed by the equation (F-9), where the average heat transfer rate will increase the overall heat transfer according to equation (F-9). The effect of two phases flow in heat exchanger helps to mix and increase turbulent and then increase thermal conductivity and reduce logarithmic mean temperature difference (LMTD) for various flow conditions, that increases the overall coefficient. The increment in overall coefficient presented in table (5-9).

Table (5-9): Experimental value for overall heat transfer coefficient of inner pipe using pure water as working fluid

Number of phases	Flow direction	Level	Cold fluid flow rate (L/min)	Hot fluid flow rate (L/min)	Air flow rate (L/min)	Ui (W/m^2. K)
Single phase	Parallel flow	Maximum	24	14	0	1158.98
		Minimum	24	8	0	512.7
	Counter flow	Maximum	24	14	0	1249.76
		Minimum	24	8	0	565.2
Two phases	Parallel flow	Maximum	24	14	480	1431.33
		Minimum	24	8	360	670.196
	Counter flow	Maximum	24	14	480	1522.11
		Minimum	24	8	360	722.7

5.2.3.2 Overall Heat Transfer Coefficient Using Water-CMC Fluid

The pure water is a tradition fluid that is used in different thermal application, and need to different additives to improve its physical properties. In this case CMC polymer particles are used at two concentrations 0.2% and 0.5% by weight. The resulted Water-CMC fluid has higher physical properties than pure water leading to increase overall heat transfer coefficient. Also, the overall heat transfer coefficient is affected by single and two phases flow which flow in annular pipe. Figures from (5-61) to (5-64) illustrate the relationship between the overall heat transfer coefficient and the hot fluid volume flow rate (water-CMC fluid) and take into account the effect of single and two phases flow. The flow conditions pointed over each figure that affect the overall heat transfer values. For single phase flow, overall coefficient increases as the Water-CMC hot fluid flow increases. On the other hand, the overall heat transfer coefficient is affected by two phases flow in annular side and hot fluid (Water-CMC fluid) flow rate. So, the overall heat transfer coefficient increases with the increase of air flow rate and the water-CMC hot fluid flow rate. The CMC particles increase lead to increase the overall heat transfer coefficient and 0.5% wt. is better CMC concentrations. The overall heat transfer coefficient under various flow condition and 0.5% wt. CMC is shown in table (5-10).

Table (5-10): Experimental value for overall heat transfer coefficient of inner pipe using water+ 0.5% CMC wt. as working fluid.

Number of phases	Flow direction	Level	Cold fluid flow rate (L/min)	Hot fluid flow rate (L/min)	Air flow rate (L/min)	Ui ($W/m^2. K$)
Single phase	Parallel flow	Maximum	24	14	0	1298.3
		Minimum	24	8	0	592.14
	Counter flow	Maximum	24	14	0	1389.736
		Minimum	24	8	0	654.02
Two phases	Parallel flow	Maximum	24	14	480	1572.59
		Minimum	24	8	360	750.76
	Counter flow	Maximum	24	14	480	1664.026
		Minimum	24	8	360	803.63

5.2.3.3 Overall Heat Transfer Coefficient Using Water-MgO Fluid

The increase in heat transfer rate is due to the increase in the overall heat transfer coefficient, and this is needed to enhance physical properties of pure water. In this case MgO nanoparticles are used with various range (0.125%, 0.25%, 0.5% and 1% by volume) to do this enhancement. This process lead to increase almost physical properties and reduce specific heat as shown in chapter three. The heat transfer rate doesn’t depend only on specific heat, but also to the thermal conductivity of MgO particles play a major rule in increasing heat transfer rate. Figures from (5-65) to (5-72) demonstrate the increase in overall coefficient as the increase in flow rate of hot fluid (Water-MgO Fluid) in inner pipe with different MgO nanoparticles concentration (0.125%, 0.25%, 0.5% and 1% by volume) in different flow conditions as they are pointed over each figure. It can be noticed that the nanoparticle enhances the inner pipe overall coefficient at increasing hot fluid volume flow rates. The two phases flow in annular side and air flow rate increase due to increase in the overall coefficient. Nanoparticle reduces the temperature difference of wall and bulk nanofluid which increases convection coefficient, then increase heat exchange rate leading increase the inner pipe overall coefficient. This due to that the overall heat transfer coefficient increases with increasing nanoparticle concentration coming out with finding that the best MgO nanoparticles concentration in this case is 1% by volume, and the result for this case is shown in table (5-11).

Table (5-11): Experimental value for overall heat transfer coefficient of inner pipe using water+ 1% MgO vol. as working fluid.

Number of phases	Flow direction	Level	Cold fluid flow rate (L/min)	Hot fluid flow rate (L/min)	Air flow rate (L/min)	Ui (W/m^2. K)
Single phase	Parallel flow	Maximum	24	14	0	1386.522
		Minimum	24	8	0	643.8732
	Counter flow	Maximum	24	14	0	1477.541
		Minimum	24	8	0	696.5
Two phases	Parallel flow	Maximum	24	14	480	1659.58
		Minimum	24	8	360	801.7713
	Counter flow	Maximum	24	14	480	1740.062
		Minimum	24	8	360	848.166

5.2.3.4 Overall Heat Transfer Coefficient Water-MgO-CMC Fluid

The addition of nanoparticles to pure water has a side effect that the nanoparticles suffer from deposition and agglomeration. This effect leads to the nanoparticles not being properly distributed during the flow, while remaining deposition, and this affects on the heat transfer rate. This leads to accounting the use of nanoparticles in various application. Therefore, a solution must be found to this problem and prevent nanoparticles from agglomeration and deposition on the bottom of tank. In this case, MgO particles dispersed in Water-CMC as working fluid to prevent agglomeration and deposition of MgO particles and to enhance physical properties of base fluid. Figures (5-73) to (5-86) introduce the relation between overall heat transfers of inner pipe as hot fluid volume flow through inner pipe at various flow conditions and influence of single and two phases flow. In this case, these flow conditions present at two CMC concentrations (0.2% and 0.5% by weight) and four MgO particles concentrations (0.125%, 0.25%. 0.5% and 1% by weight). It has been shown that the increase of volume flow rate of hot fluid increases overall coefficient because of thermal capacity increase. It can be noticed this effect by equation (F-9), where increasing the average heat transfer rate increases the overall heat transfer according to equation (F-9). The effect of air with cold water in the annulus of heat exchanger helps to mix and increase turbulent and then increase thermal conductivity and reduce (LMTD) for counter flow, that increases the overall heat transfer coefficient. It's found that is significant impact by comparing the parallel flow and counter flow configuration on overall heat transfer coefficient. It is found that the best result at using 0.5% CMC wt. and 1% MgO vol. as shown in table (5-12).

Table (5-12): Experimental value for overall heat transfer coefficient of inner pipe using water+ 1% MgO vol.+ 0.5% CMC wt.as working fluid.

Number of phases	Flow direction	Level	Cold fluid flow rate (L/min)	Hot fluid flow rate (L/min)	Air flow rate (L/min)	Ui (W/m^2. K)
Single phase	Parallel flow	Maximum	24	14	0	1536.94
		Minimum	24	8	0	729.73
	Counter flow	Maximum	24	14	0	1628.607
		Minimum	24	8	0	782.74
Two phases	Parallel flow	Maximum	24	14	480	1811.94
		Minimum	24	8	360	888.75
	Counter flow	Maximum	24	14	480	1903.6
		Minimum	24	8	360	941.756

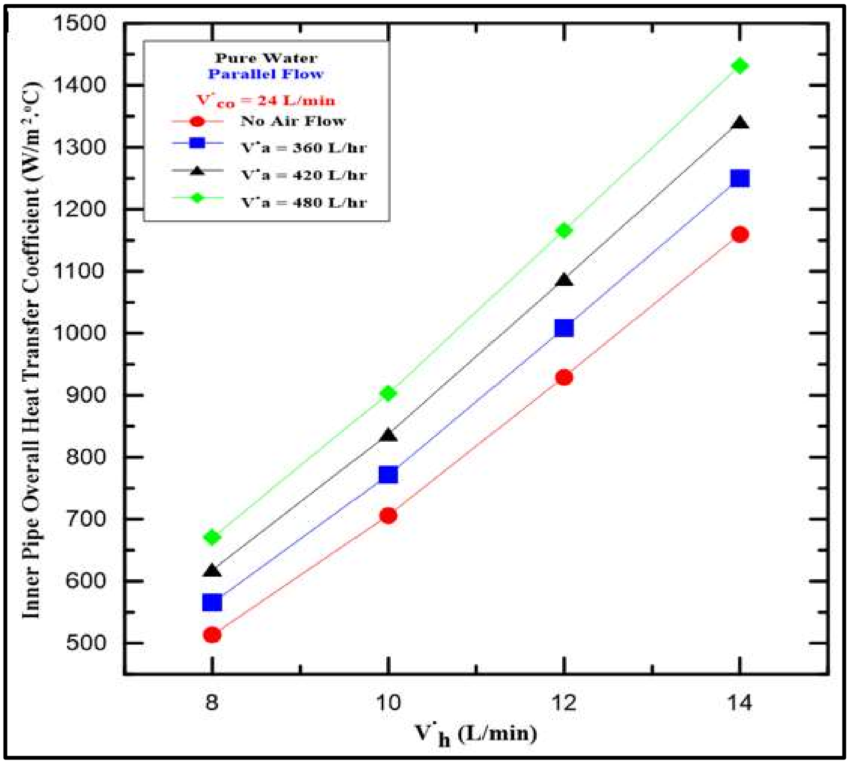

Figure (5-59): Variation of inner pipe overall heat transfer coefficient with hot fluid (pure water) flow rate for parallel flow.

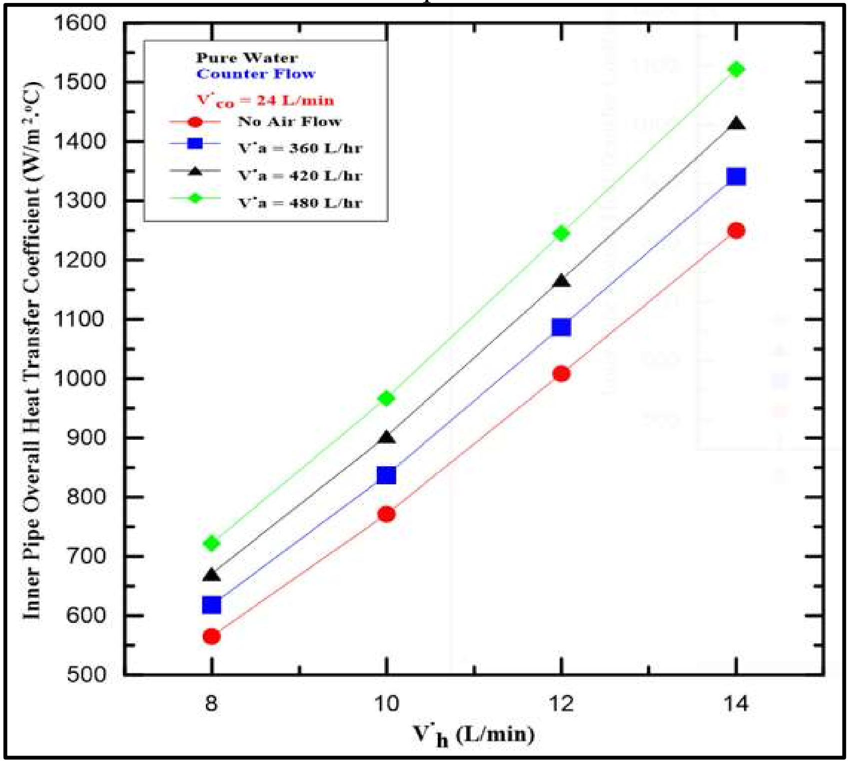

Figure (5-60): Variation of inner pipe overall heat transfer coefficient with hot fluid (pure water) flow rate for counter flow.

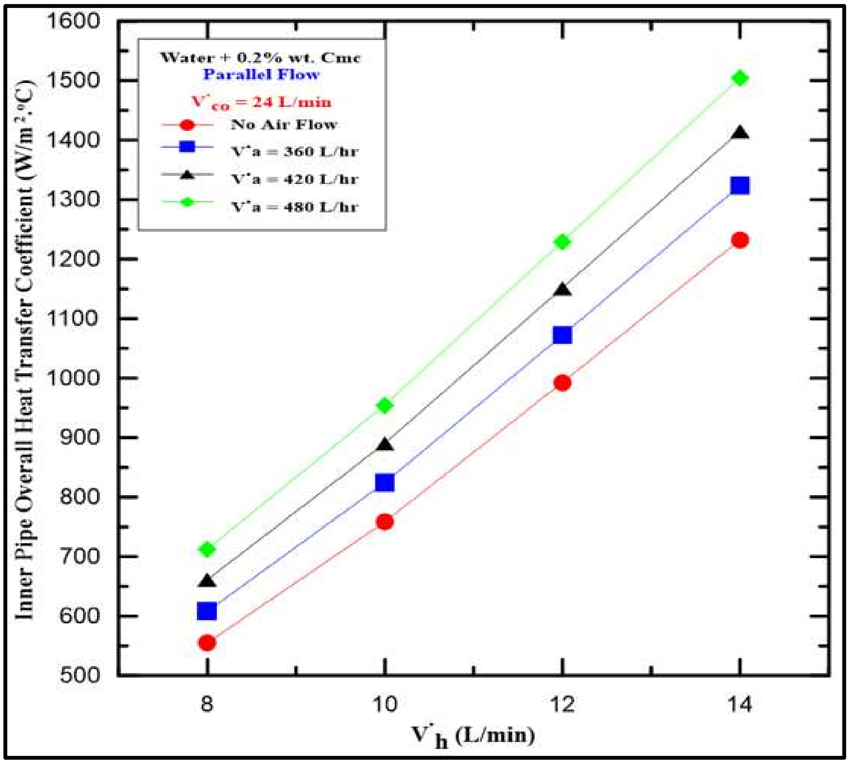

Figure (5-61): Variation of inner pipe overall heat transfer coefficient with hot fluid (water + 0.2% CMC wt.) flow rate for parallel flow.

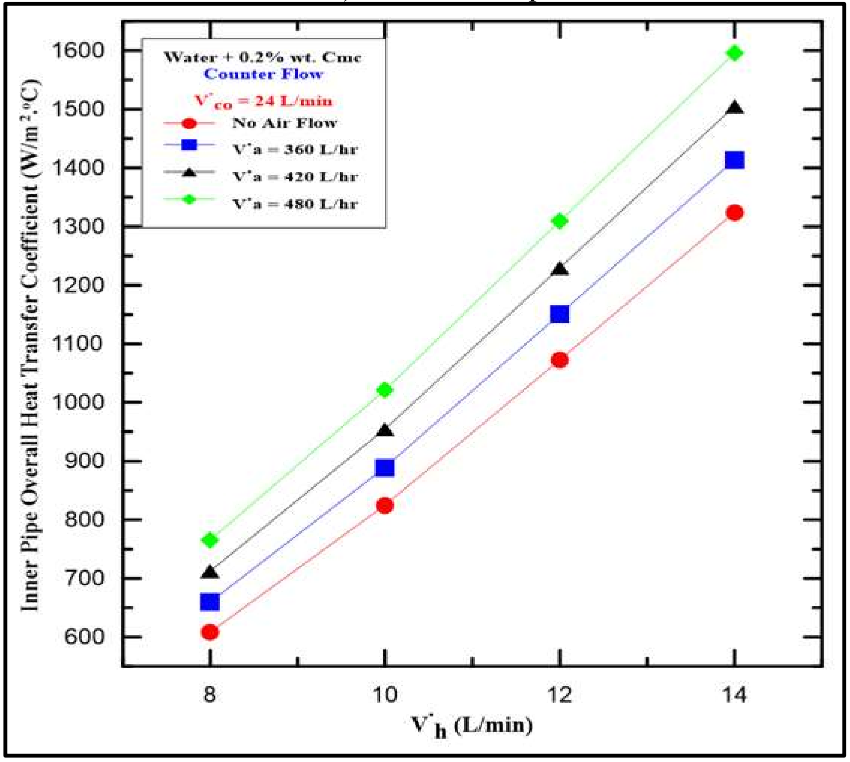

Figure (5-62): Variation of inner pipe overall heat transfer coefficient with hot fluid (water + 0.2% CMC wt.) flow rate for counter flow.

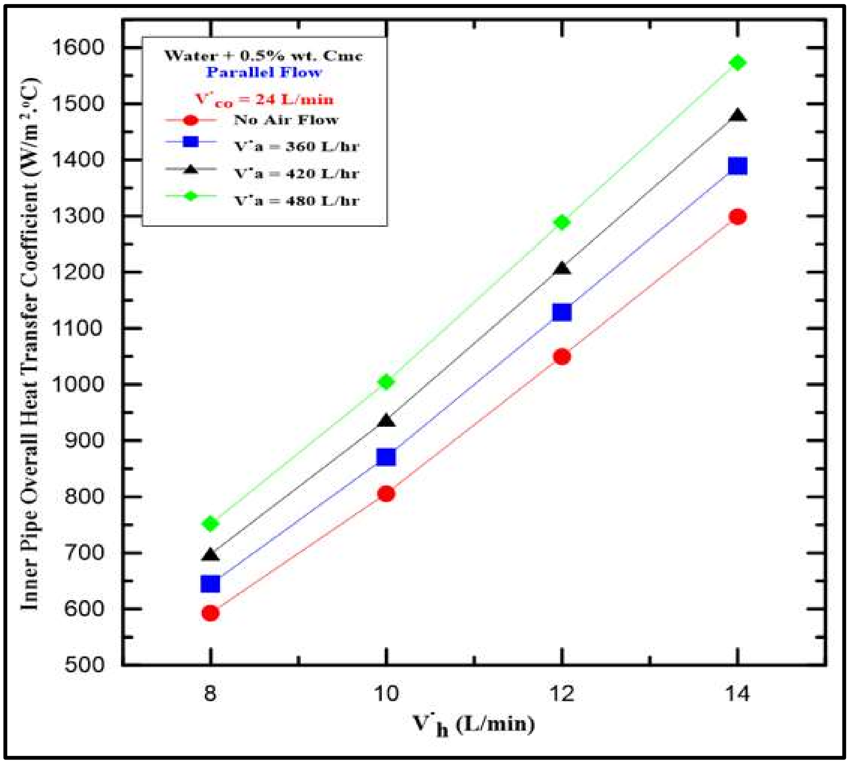

Figure (5-63): Variation of inner pipe overall heat transfer coefficient with hot fluid (water + 0.5% CMC wt.) flow rate for parallel flow.

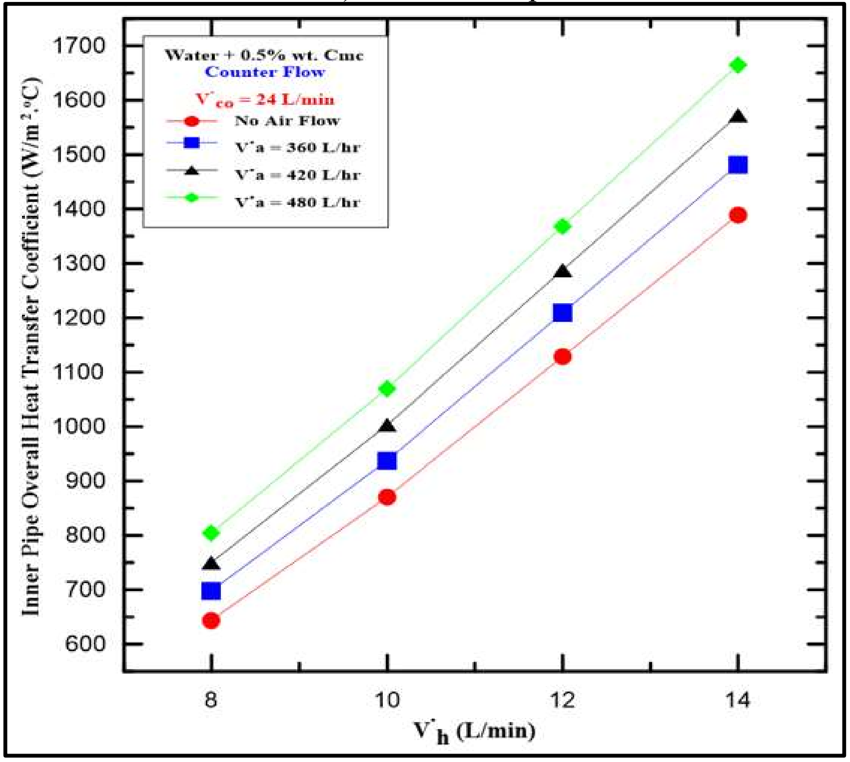

Figure (5-64): Variation of inner pipe overall heat transfer coefficient with hot fluid (water + 0.5% CMC wt.) flow rate for counter flow.

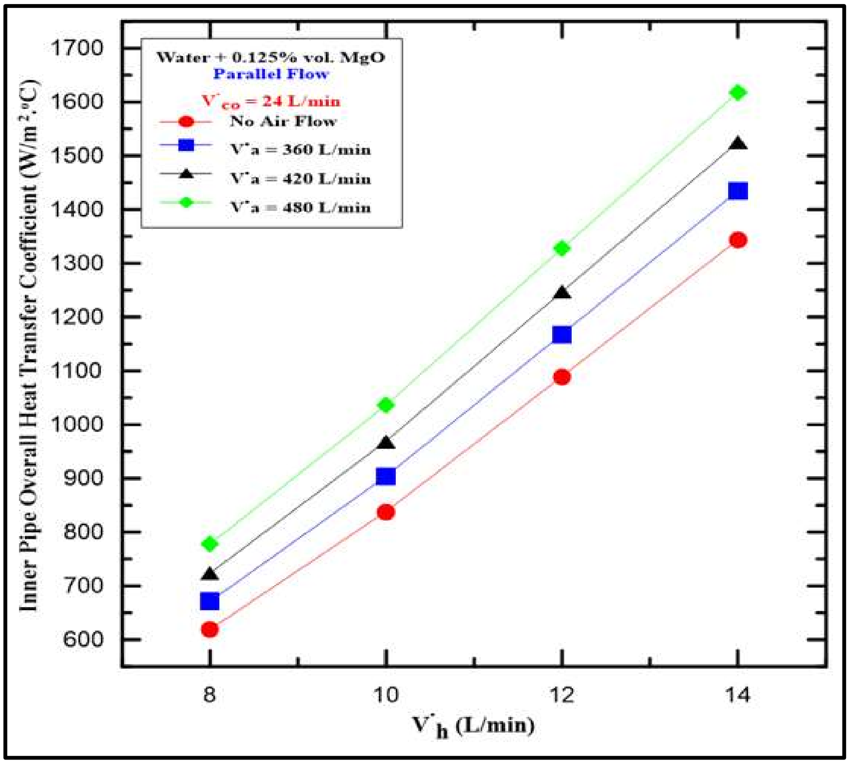

Figure (5-65): Variation of inner pipe overall heat transfer coefficient with hot fluid (water + 0.125% MgO vol.) flow rate for parallel flow.

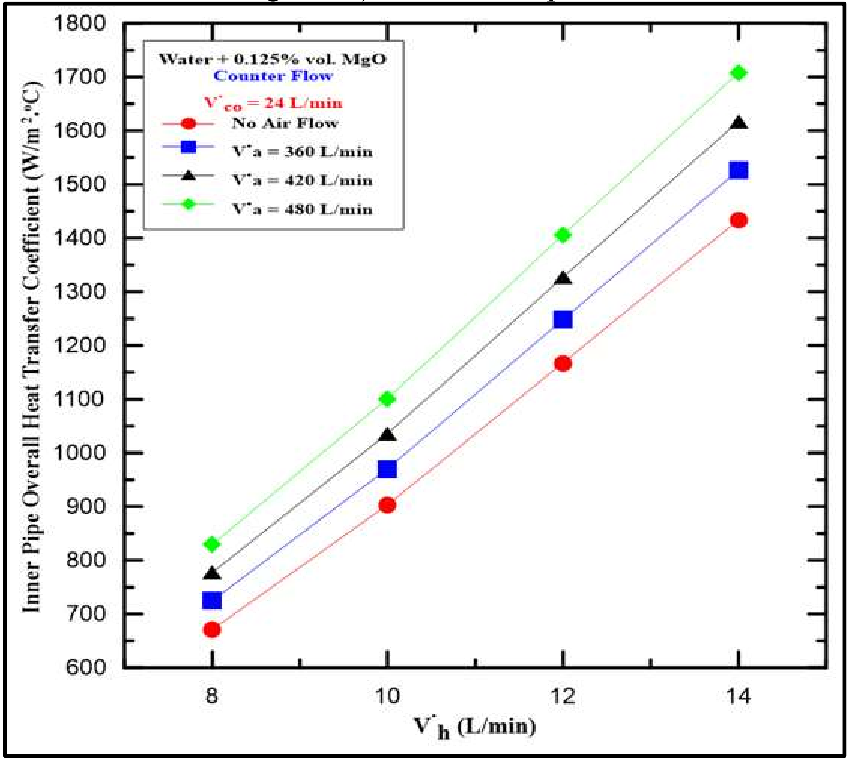

Figure (5-66): Variation of inner pipe overall heat transfer coefficient with hot fluid (water + 0.125% MgO vol.) flow rate for counter flow.

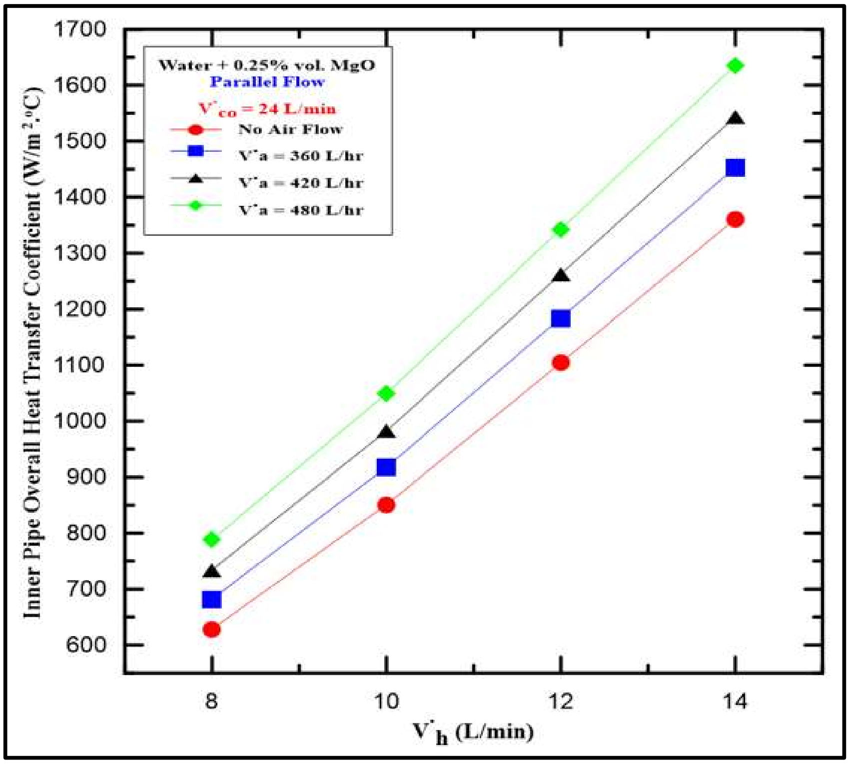

Figure (5-67): Variation of inner pipe overall heat transfer coefficient with hot fluid (water + 0.25% MgO vol.) flow rate for parallel flow.

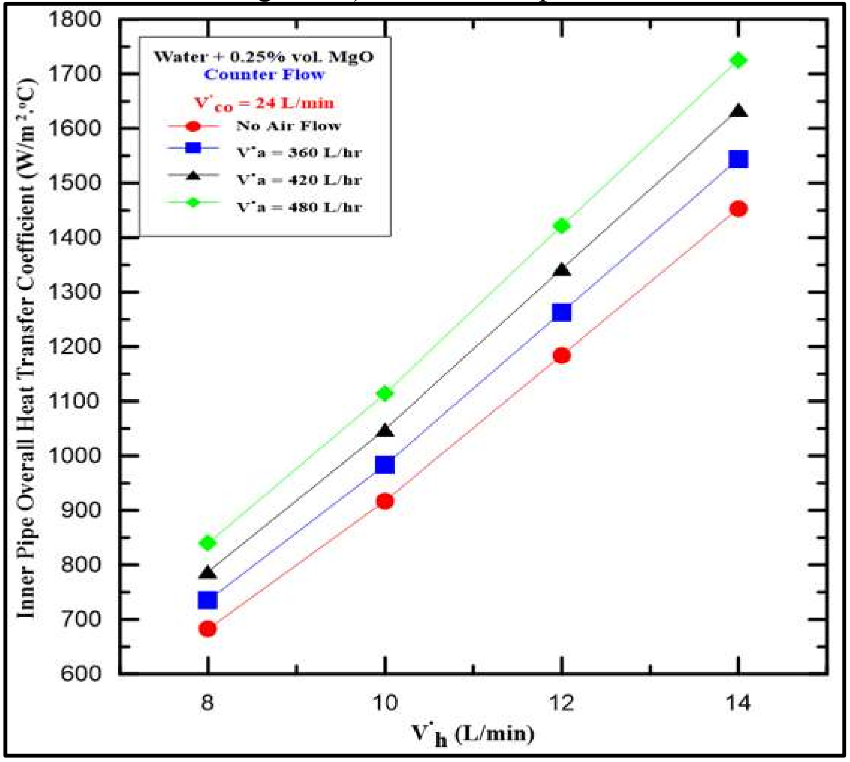

Figure (5-68): Variation of inner pipe overall heat transfer coefficient with hot fluid (water + 0.25% MgO vol.) flow rate for counter flow.

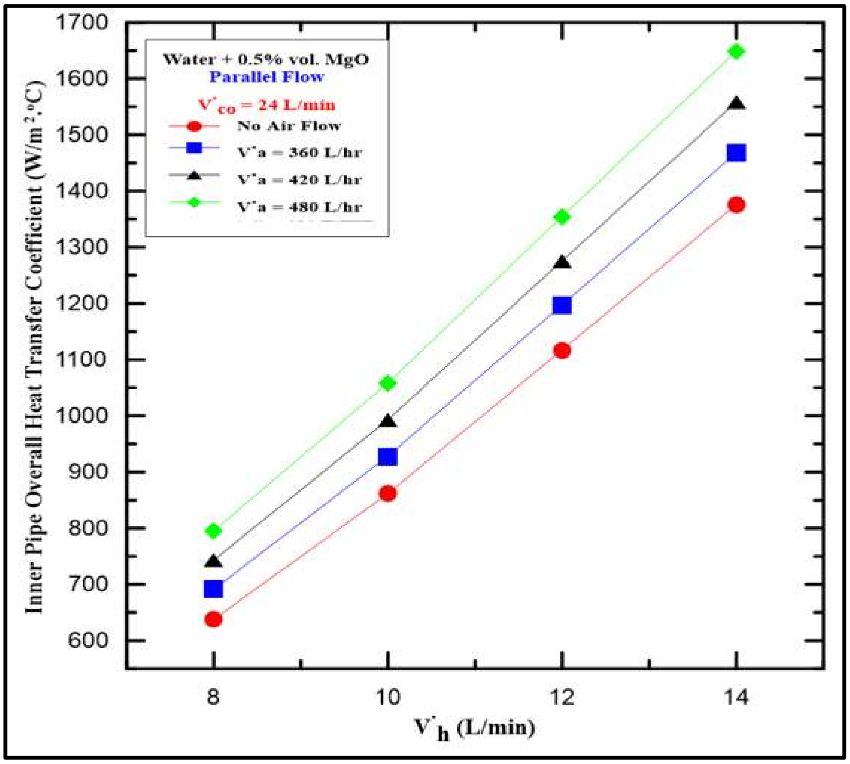

Figure (5-69): Variation of inner pipe overall heat transfer coefficient with hot fluid (water + 0.5% MgO vol.) flow rate for parallel flow.

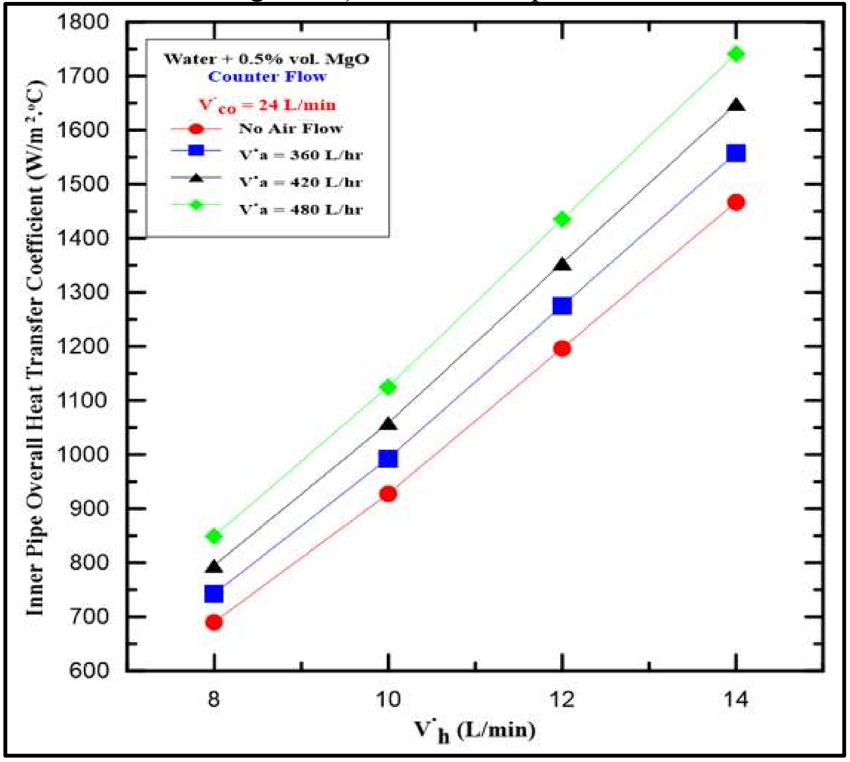

Figure (5-70): Variation of inner pipe overall heat transfer coefficient with hot fluid (water + 0.5% MgO vol.) flow rate for counter flow.

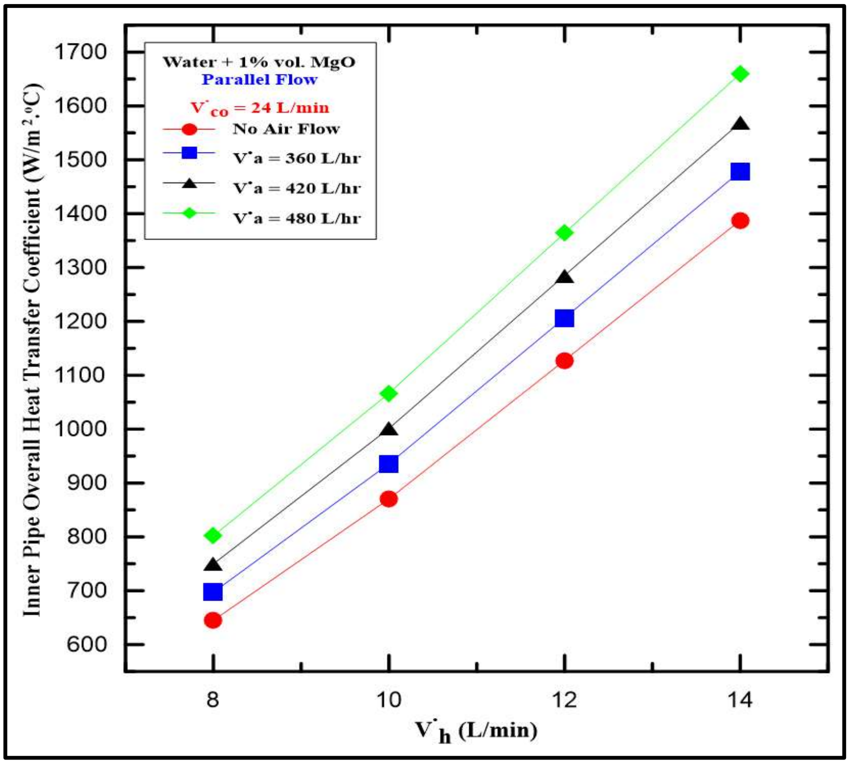

Figure (5-71): Variation of inner pipe overall heat transfer coefficient with hot fluid (water + 1% MgO vol.) flow rate for parallel flow.

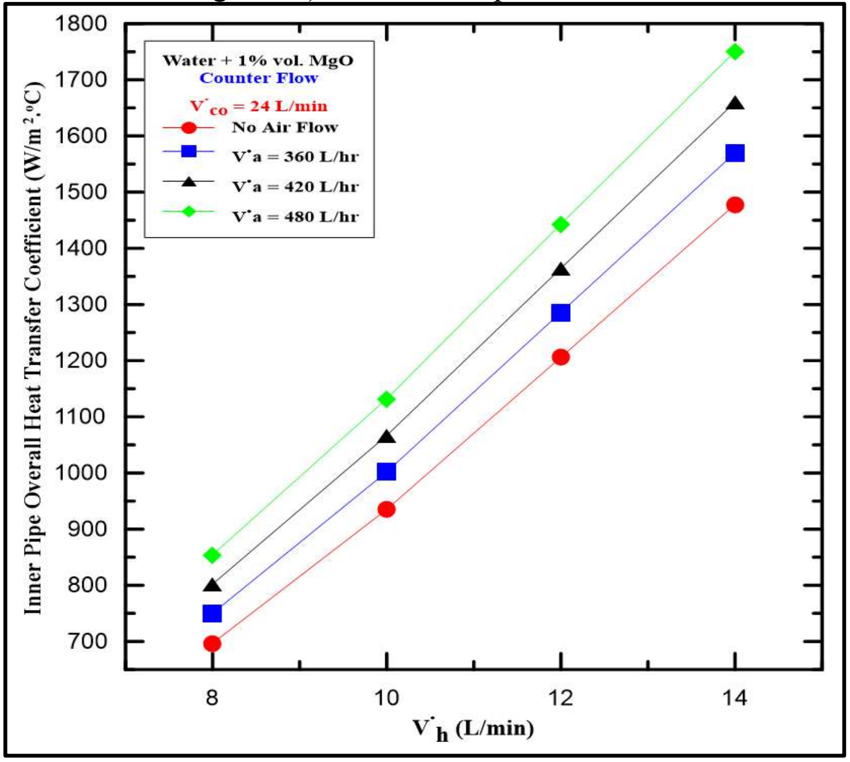

Figure (5-72): Variation of inner pipe overall heat transfer coefficient with hot fluid (water + 1% MgO vol.) flow rate for counter flow.

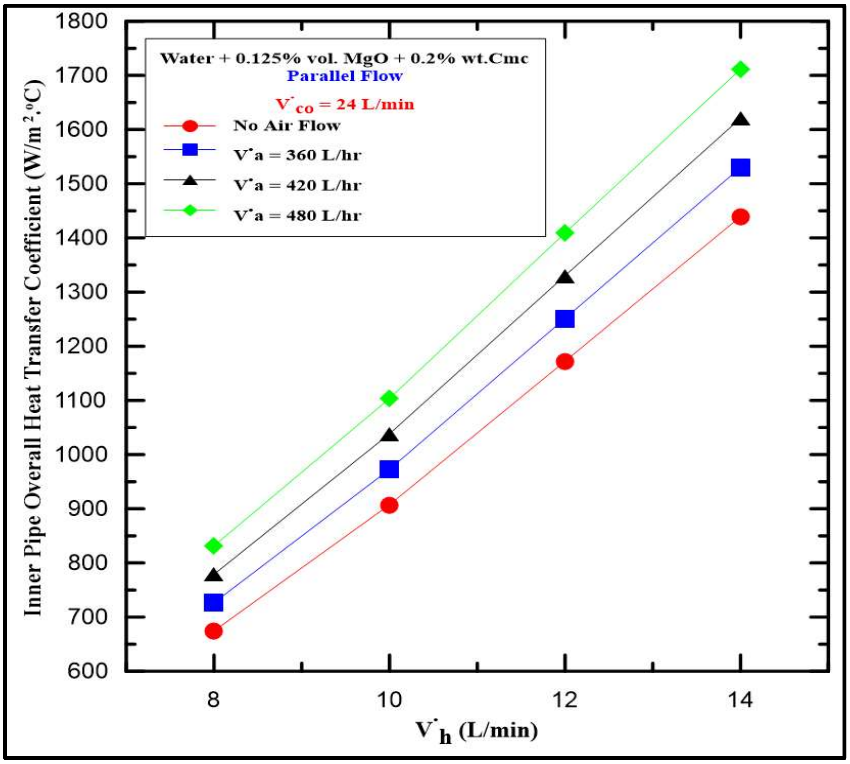

Figure (5-73): Variation of inner pipe overall heat transfer coefficient with hot fluid (water + 0.125% MgO vol.+0.2% CMC wt.) flow rate for parallel flow.

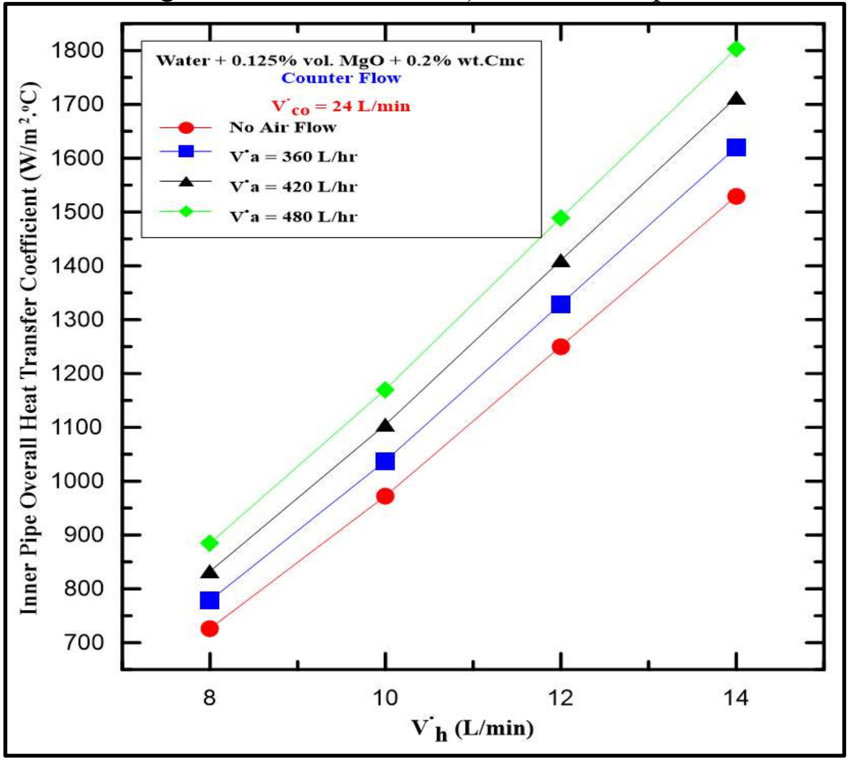

Figure (5-74): Variation of inner pipe overall heat transfer coefficient with hot fluid (water + 0.125% MgO vol.+0.2% CMC wt.) flow rate for counter flow.

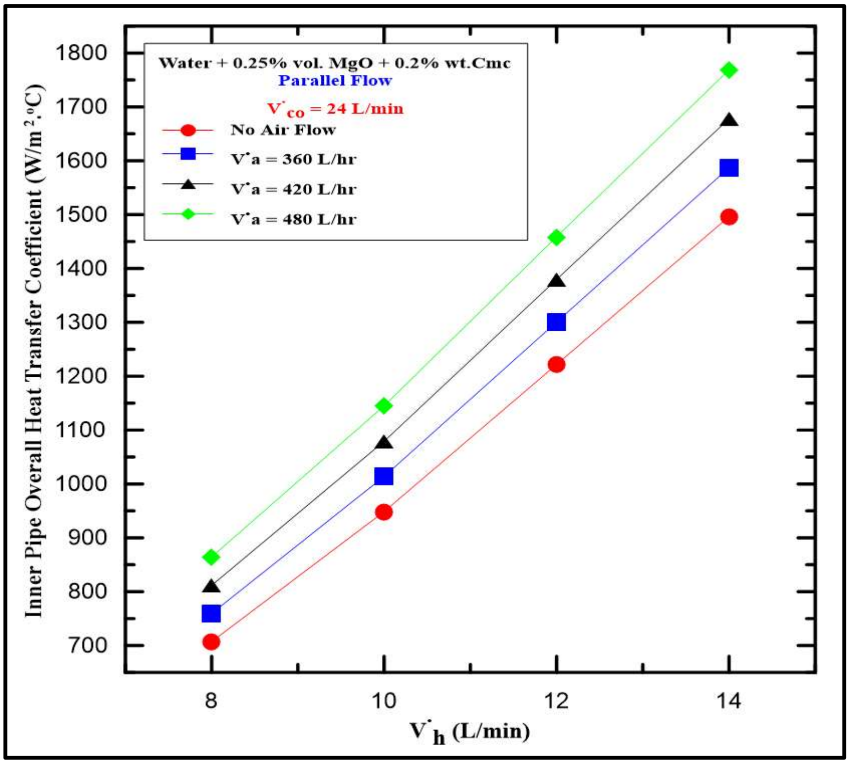

Figure (5-75): Variation of inner pipe overall heat transfer coefficient with hot fluid (water + 0.25% MgO vol.+0.2% CMC wt.) flow rate for parallel flow.

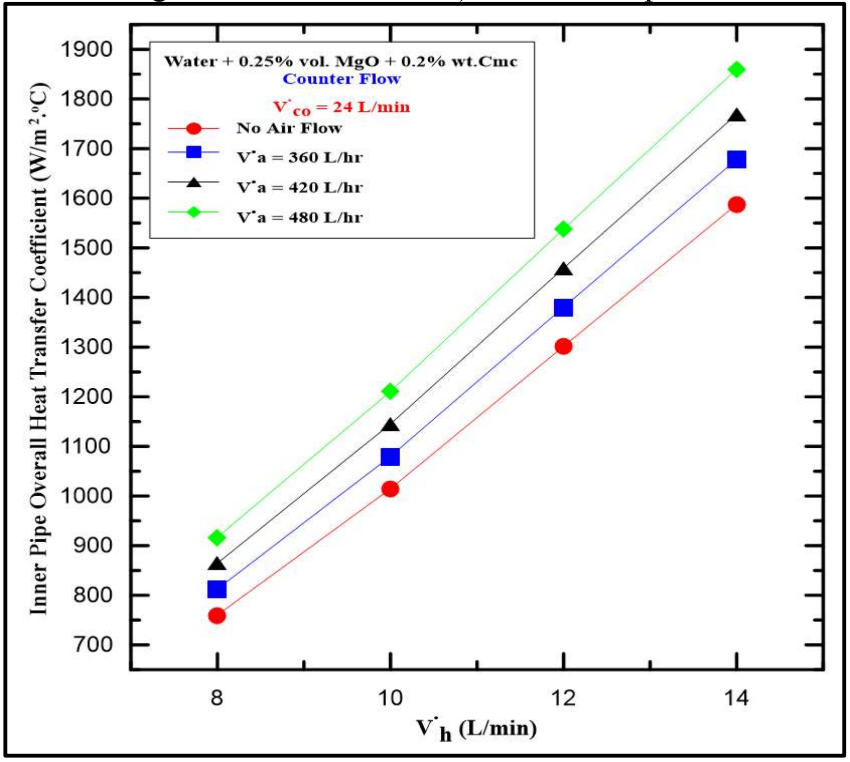

Figure (5-76): Variation of inner pipe overall heat transfer coefficient with hot fluid (water + 0.25% MgO vol.+0.2% CMC wt.) flow rate for counter flow.

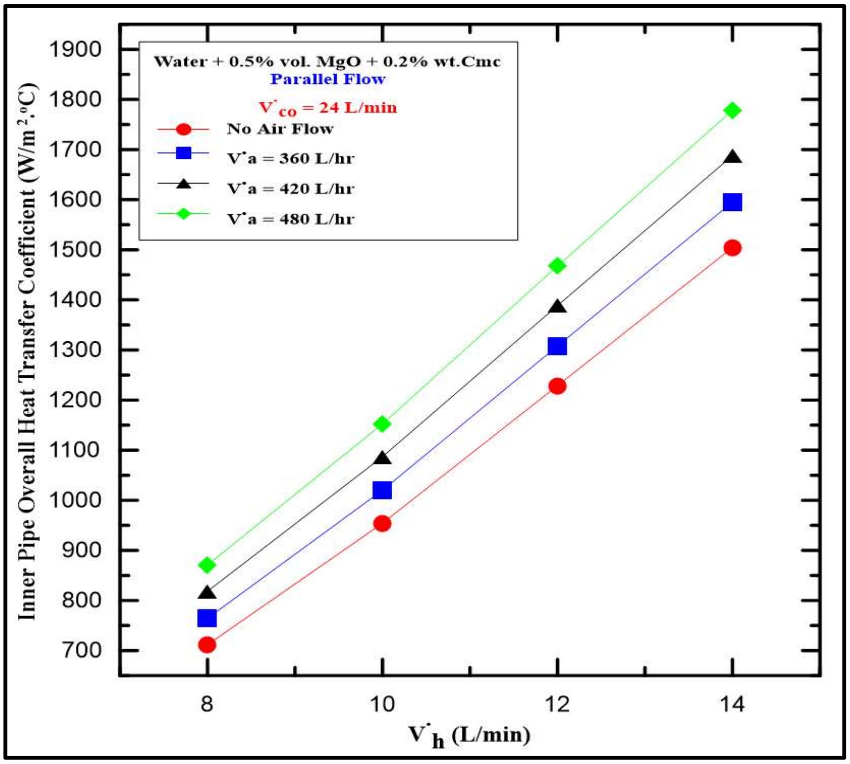

Figure (5-77): Variation of inner pipe overall heat transfer coefficient with hot fluid (water + 0.5% MgO vol.+0.2% CMC wt.) flow rate for parallel flow.

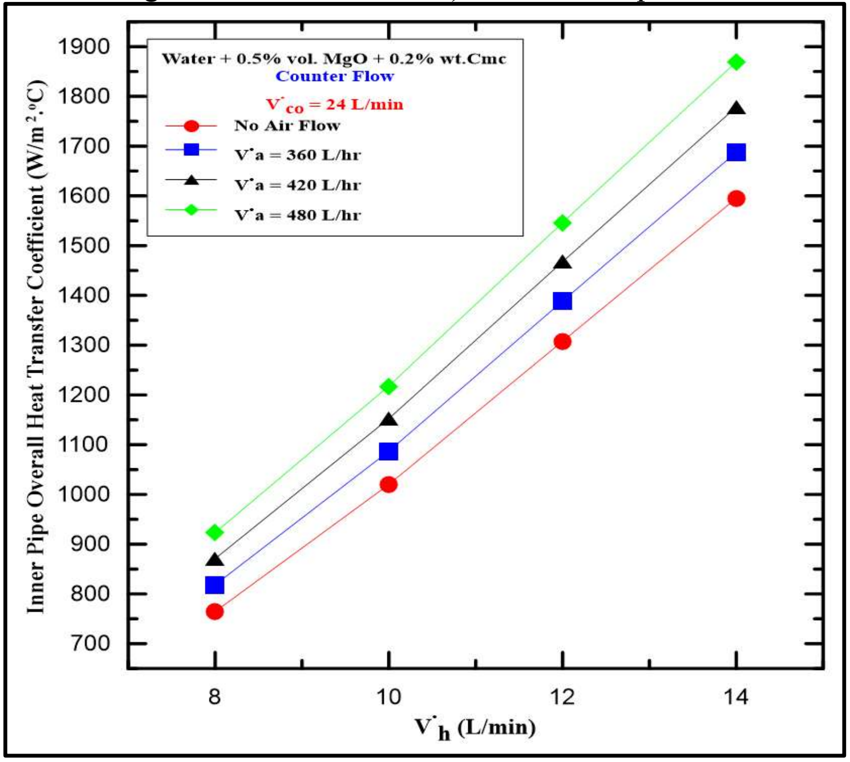

Figure (5-78): Variation of inner pipe overall heat transfer coefficient with hot fluid (water + 0.5% MgO vol.+0.2% CMC wt.) flow rate for counter flow.

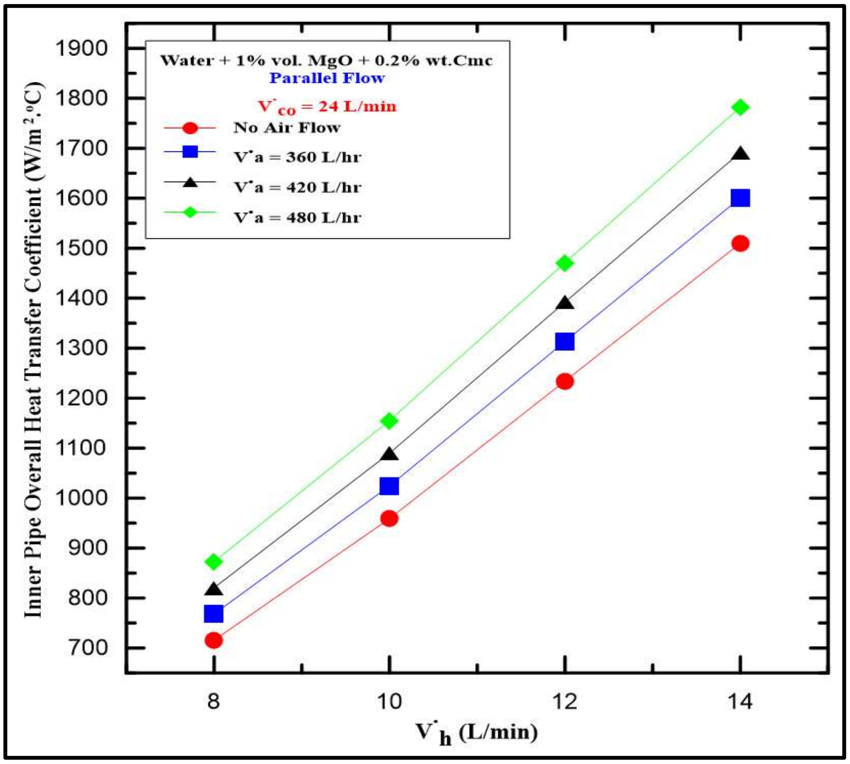

Figure (5-79): Variation of inner pipe overall heat transfer coefficient with hot fluid (water + 1% MgO vol.+0.2% CMC wt.) flow rate for parallel flow.

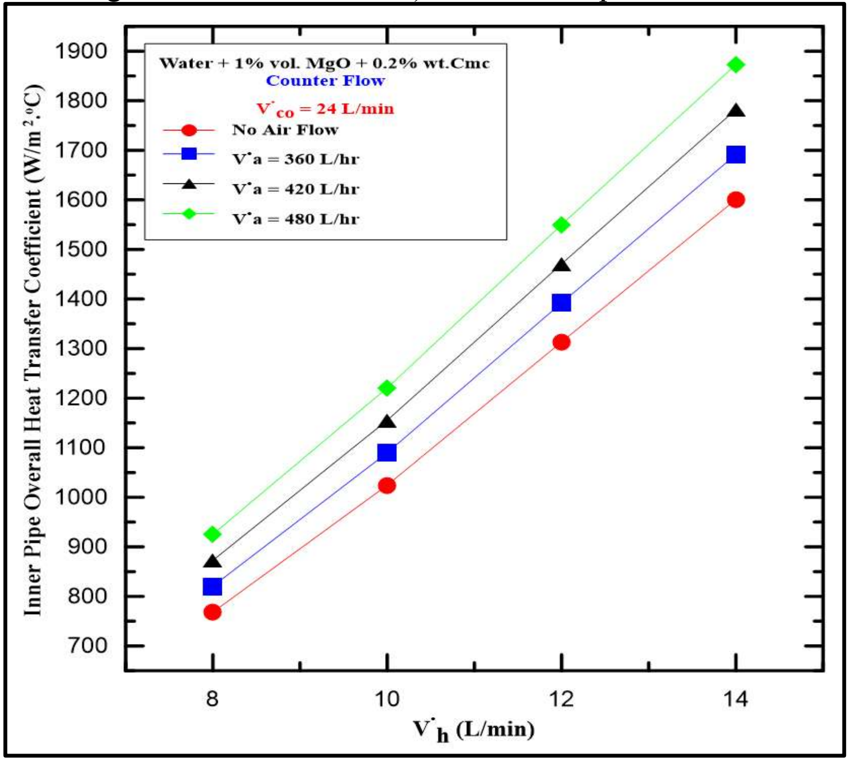

Figure (5-80): Variation of inner pipe overall heat transfer coefficient with hot fluid (water + 1% MgO vol.+0.2% CMC wt.) flow rate for counter flow.

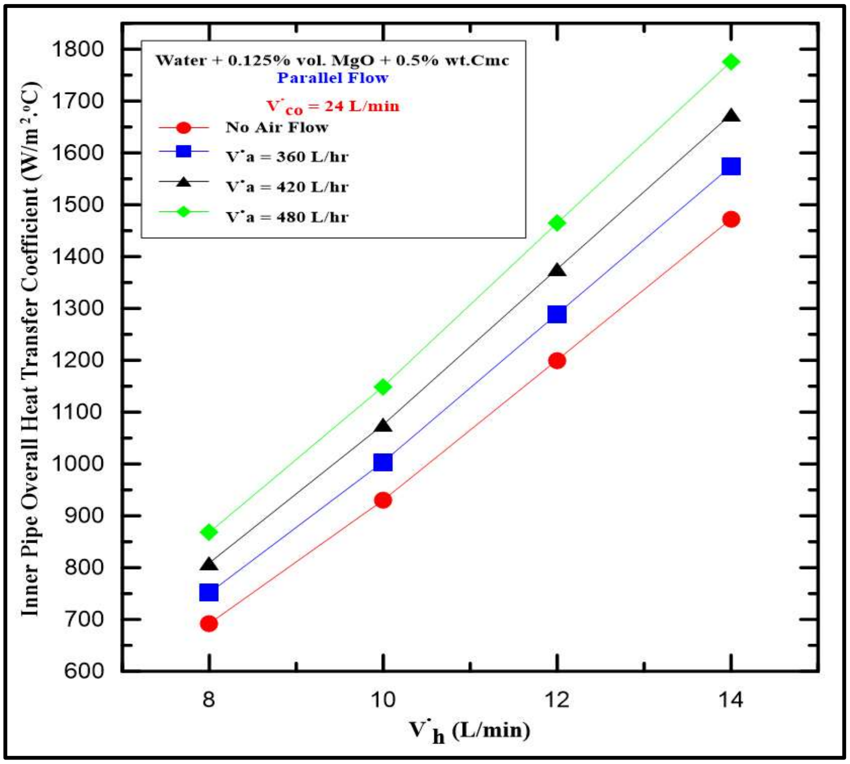

Figure (5-81): Variation of inner pipe overall heat transfer coefficient with hot fluid (water + 0.125% MgO vol.+0.5% CMC wt.) flow rate for parallel flow.

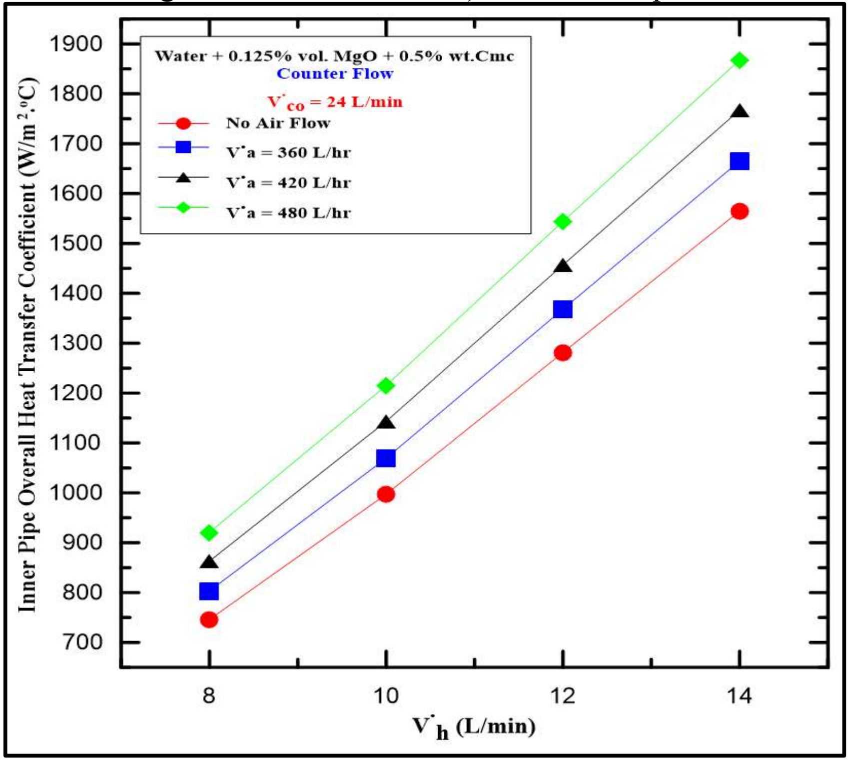

Figure (5-82): Variation of inner pipe overall heat transfer coefficient with hot fluid (water + 0.125% MgO vol.+0.5% CMC wt.) flow rate for counter flow.

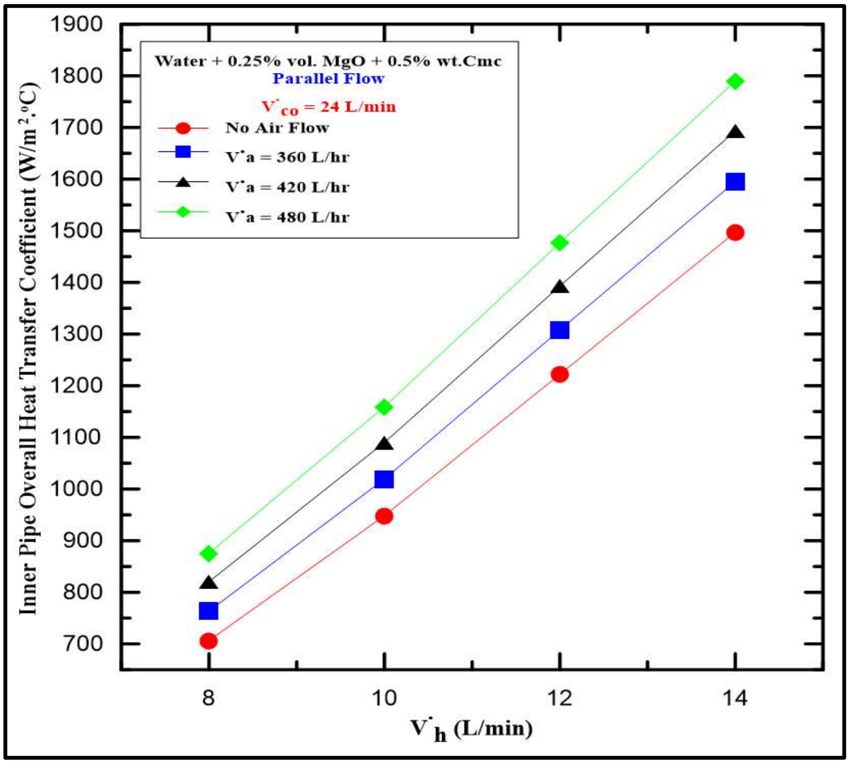

Figure (5-83): Variation of inner pipe overall heat transfer coefficient with hot fluid (water + 0.25% MgO vol.+0.5% CMC wt.) flow rate for parallel flow.

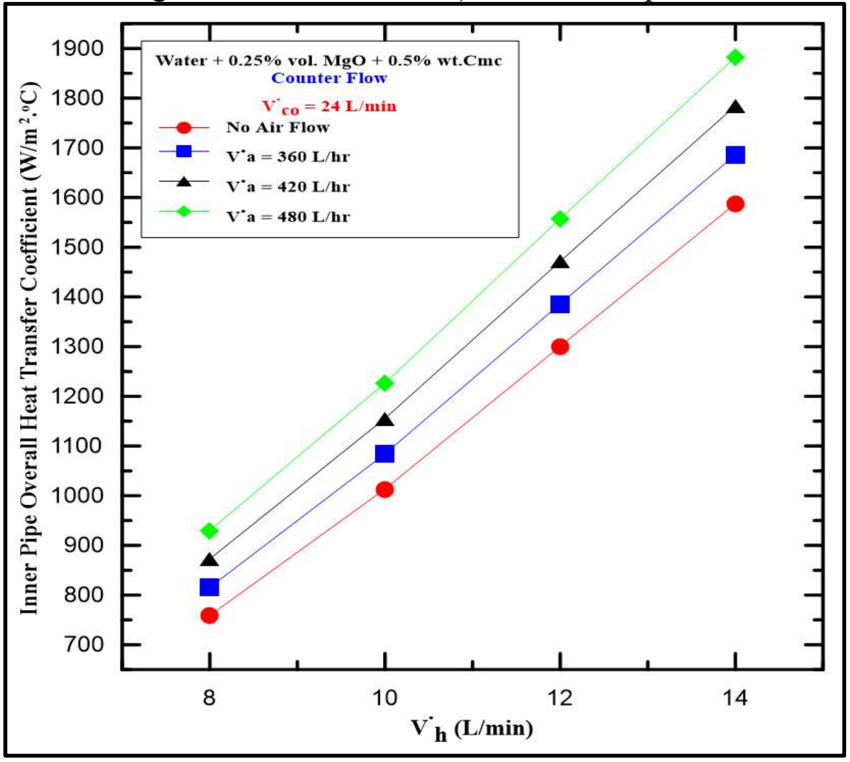

Figure (5-84): Variation of inner pipe overall heat transfer coefficient with hot fluid (water + 0.25% MgO vol.+0.5% CMC wt.) flow rate for counter flow.

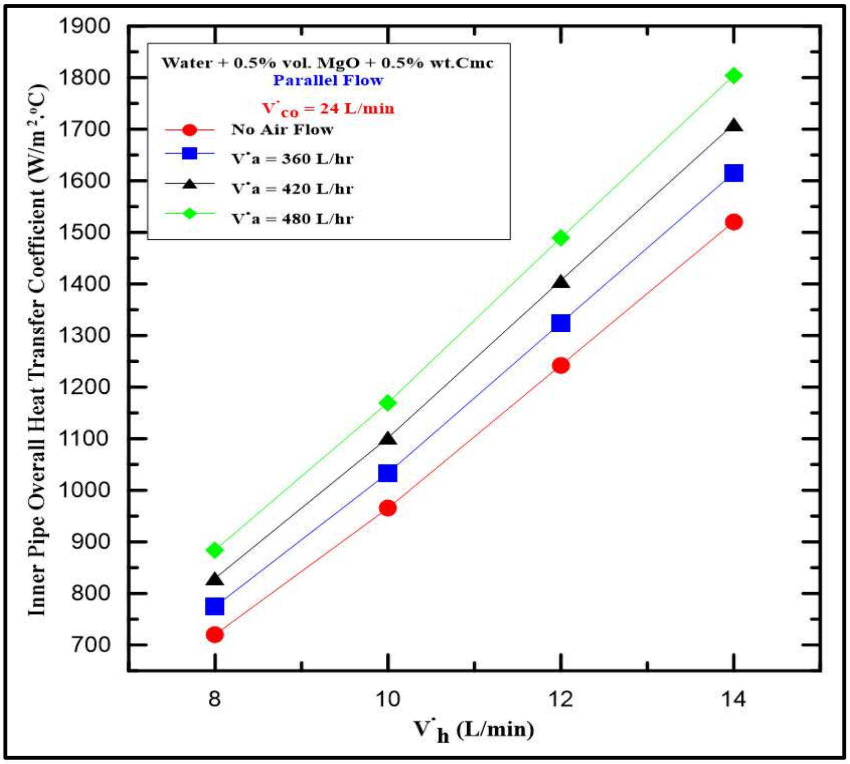

Figure (5-85): Variation of inner pipe overall heat transfer coefficient with hot fluid (water + 0.5% MgO vol.+0.5% CMC wt.) flow rate for parallel flow.

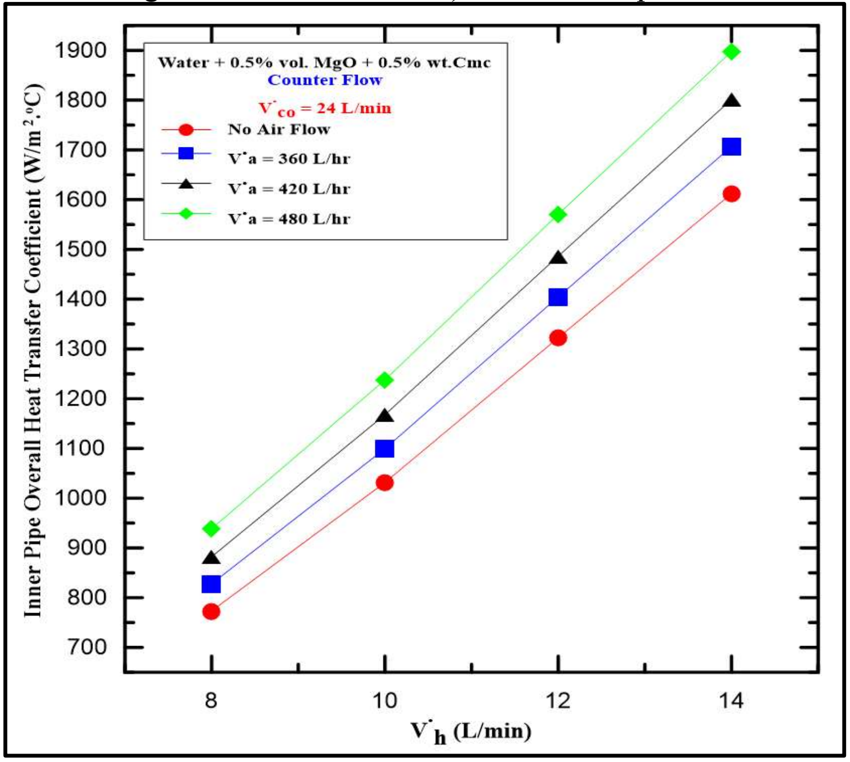

Figure (5-86): Variation of inner pipe overall heat transfer coefficient with hot fluid (water + 0.5% MgO vol.+0.5% CMC wt.) flow rate for counter flow.

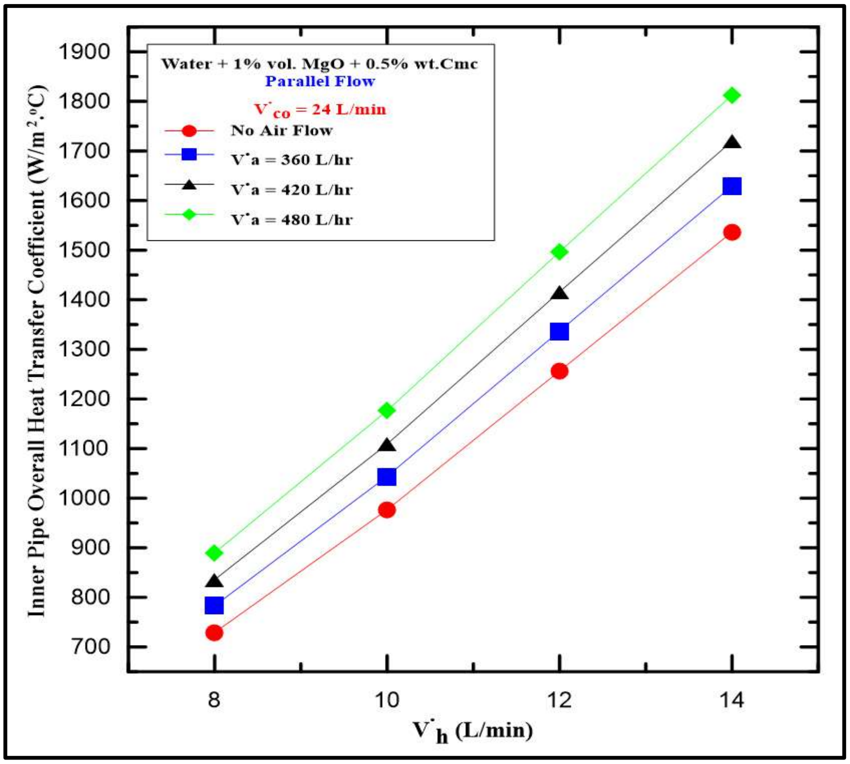

Figure (5-87) Variation of inner pipe overall heat transfer coefficient with hot fluid (water + 1% MgO vol.+0.5% CMC wt.) flow rate for parallel flow.

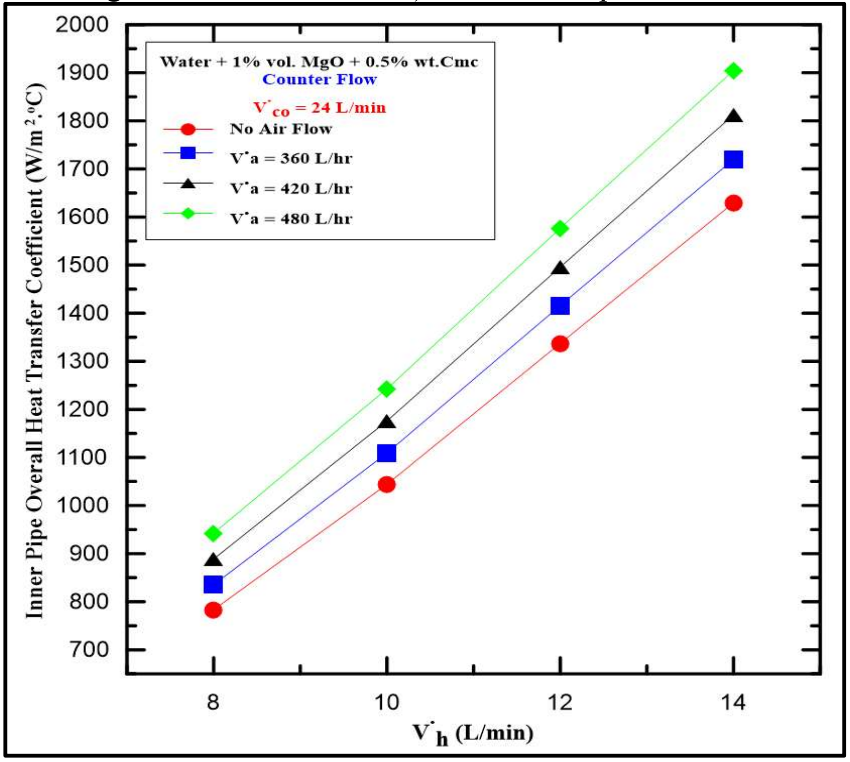

Figure (5-88): Variation of inner pipe overall heat transfer coefficient with hot fluid (water + 1% MgO vol.+0.5% CMC wt.) flow rate for counter flow.

5.2.4 Pressure Drop in Double Pipe Heat Exchanger

Figure (5-89) access the relation between pressure drop and the volumetric flow rate for different hot fluid types. This figure marks pressure drop comparison between pure water and the water-CMC fluid with different CMC concentrations 0.2% and 0.5% by weight. The values of this case measured experimentally under different flow conditions which are shown in this figure. It can be noticed that the increase in the pressure drop value is due to an increase in the flow rate, pressure drop of the water-CMC fluid higher than pressure drop of pure water to be increased with CMC concentration increase. The water-CMC fluid is suitable for system which need to higher pressure because of it has high viscosity and density. The increase in pressure and physical properties improve heat exchange rate because the water-CMC fluid has the ability to gain and transfer heat quickly when flow in inner pipe. The highest pressure drops values for this case is shown in table (5-13) at hot fluid flow rate 14 L/min.

Table (5-13): Maximum experimental value of pressure drop in inner pipe using pure water and water-CMC fluid

Hot fluid types	Hot fluid flow rate (L/min)	Pressure drop (Kpa)
Pure water	14	1.21
Water + 0.2% CMC wt.	14	1.37
Water + 0.5% CMC wt.	14	1.6

Figure (5-90) presents pressure drop variation with the volumetric flow rate of nanofluid (water-MgO fluid) and pure water. The flow conditions for this case pointed over this figure. It has been shown that the pressure drops of nanofluid higher than pressure drop of pure water and this increases the increasing of volume flow rate. The increase MgO nanoparticles concentration lead to increased pressure drop values because of increasing viscosity and density. The collisions between the nanofluid particles and the wall of inner pipe, cause an impediment to the fluid flow.

Also, these reasons improve heat transfer rate because increasing physical properties of the water-MgO fluid. Table (5-14) presents maximum values of pressure drop for this case under a volume flow rate 14 L/min.

Table (5-14): Maximum experimental value of pressure drop in inner pipe using pure water and water-MgO fluid

Hot fluid types	Hot fluid flow rate (L/min)	Pressure drop (Kpa)
Pure water	14	1.21
Water + 0.125% MgO vol.	14	1.63
Water + 0.25% MgO vol.	14	1.67
Water + 0.5% MgO vol.	14	1.74
Water + 1% MgO vol.	14	1.82

Figures (5-91) and (5-92) illustrate the relation between pressure drop with the volumetric flow rate of hot fluid in inner pipe. These figures present pressure drop of pure water and the water-MgO-CMC fluid and made comparison between them. There are two CMC concentrations 0.2% and 0.5 by weight implement with MgO concentration range (0.125%, 0.25%, 0.5% and 1% by volume) under different flow conditions which are shown in each figure. It has been observed that the volume flow rate increases due to the increase pressure drop. It is found that for the same volume flow rate the value of pressure drop increase with an increase in concentration of nanofluid or CMC. This is due to three reasons, firstly, when the volume flow rate increases the pressure values increase; Secondly, when the concentrations of nanofluid increases, the pressure values increase because of the increase in viscosity and density of nanofluid; Third reason, the collisions between the nanofluid particles and the CMC particles and wall of pipe, cause an obstruction to the fluid flow. It is also found that pressure drop at (water + 1% vol. MgO + 0.5% wt. CMC) that maximum volume flow rate is the highest. The MgO particles disperse in the water- CMC fluid and this gives stability to MgO particles leading to an increase in pressure and enhancing heat exchange rate. The maximum values of this case are presented in table (5-15).

Table (5-15): Maximum experimental value of pressure drop in inner pipe using pure water and water-MgO-CMC fluid

Hot fluid types	Hot fluid flow rate (L/min)	Pressure drop (Kpa)
Pure water	14	1.21
Water + 0.125% MgO vol.+0.2% CMC wt.	14	1.8
Water + 0.25% MgO vol. +0.2% CMC wt.	14	1.86
Water + 0.5% MgO vol. +0.2% CMC wt.	14	1.92
Water + 1% MgO vol. +0.2% CMC wt.	14	2
Water + 0.125% MgO vol.+0.5% CMC wt.	14	1.85
Water + 0.25% MgO vol. +0.5% CMC wt.	14	1.92
Water + 0.5% MgO vol. +0.5% CMC wt.	14	1.97
Water + 1% MgO vol. +0.5% CMC wt.	14	2.05

5.2.5 Friction Factor in Double Pipe Heat Exchanger

Figures from (5-93) to (5-96) induces a comparison between friction factors for different hot fluid types with their volume flow rate. These figures present a comparison between pure water pressure drop and pressure drop for different types of hot fluid under different flow conditions that are shown in each figure. It can be seen from the figures that the friction factors tend to decrease as volume flow rate increases according to the equation (F-16). Figure (5-93) presents friction factor values when CMC is added at two concentrations 0.2% and 0.5% wt. This leads to increase pressure drop and heat exchange rate because the enhancement in physical properties for the water-CMC fluid. The effect of adding MgO nanoparticles at different concentrations present in figure (5-94) under various flow conditions and concentrations range (0.125%, 0.25%, 0.5% and 1% by volume). Figures (5-95) and (5-96) show friction factor coefficient at two CMC concentration 0.2% and 0.5 by weight implement with MgO concentration range (0.125%, 0.25%, 0.5% and 1% by volume) under different flow conditions which are shown in each figure. Generally, the fraction factor increases with the increasing of concentration of MgO nanoparticle and CMC that is due to increase of density of nanofluid. Table (5-16) demonstrates the friction factor values for different hot fluids types.

Table (5-16): Maximum experimental value of friction factor in inner pipe for different hot fluids types.

Hot fluid types	Hot fluid flow rate (L/min)	Friction factor
Pure water	14	0.015
Water + 0.5% CMC wt.	14	0.0198
Water + 1% MgO vol.	14	0.022
Water + 1% MgO vol. +0.5% CMC wt.	14	0.0248

5.2.6 Pumping Power of Double Pipe Heat Exchanger

This section demonstrates pumping power that is required to push various hot fluid types in inner pipe. The estimate of the pumping power is necessary to calculate the cost of pushing hot fluid for specific heat exchanger design. The pumping power is directly proportional to pressure drop according to equation (F-22), and pressure drop is directly affected by the square of fluid velocity according to equation (F-16). So, pumping power directly affected by the square of fluid velocity. So, when hot fluid is used with high viscosity a density, increase pumping power and required cost.

Figures (5-97) from (5-100) demonstrate the relation between pumping power and the value of volume flow rate of pure water, water-CMC fluid, water-MgO fluid, water-MgO-CMC fluid respectively under different flow conditions which are pointed in each figure. The values of pumping power at each figure present base case which compare other cases with it. Figure (5-97) shows the pumping power of water-CMC fluid at two CMC concentration 0.2% and 0.5 by weight. Figure (5-98) presents the pumping power of water-MgO fluid with its flow rate at different concentrations range (0.125%, 0.25%, 0.5% and 1% by volume). Figures (5-99) and (5-100) illustrate the pumping power of water-MgO-CMC fluid at two CMC concentration 0.2% and 0.5 by weight implement with MgO concentration range (0.125%, 0.25%, 0.5% and 1% by volume) under different flow conditions that are shown in each figure. From the previous figures of the pumping power, it is found that the pumping power of different hot fluid types increases for two reasons. Firstly, when volume flow rate of hot fluid increases inside the inner pipe. Secondly, when concentration of MgO nanoparticle and CMC increases. The response of pumping power has taken same behavior of pressure drop with flow rate. The maximum values for pumping power of better additives in each case are demonstrate in table (5-17) when hot fluid flow rate 14 L/min.

Table (5-17): Maximum experimental value of pumping power in inner pipe for different hot fluids types.

Hot fluid types	Hot fluid flow rate (L/min)	Pumping power (W/m)
Pure water	14	0.282
Water + 0.5% CMC wt.	14	0.374
Water + 1% MgO vol.	14	0.425
Water + 1% MgO vol. +0.5% CMC wt.	14	0.479

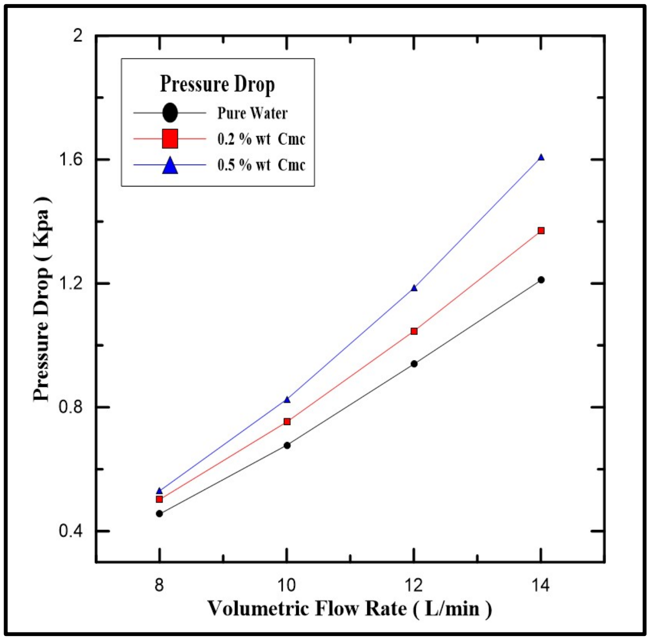

Figure (5-89): Variation of pure water pressure drop with volume flow rate

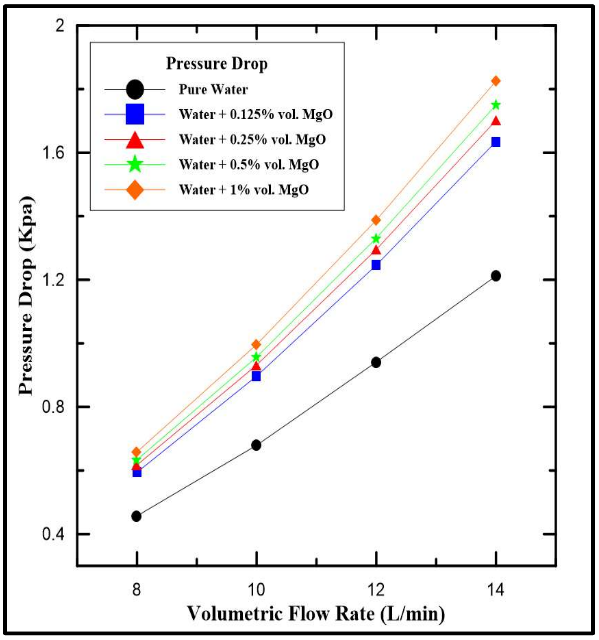

Figure (5-90): Variation of water-CMC fluid pressure drop with volume flow rate

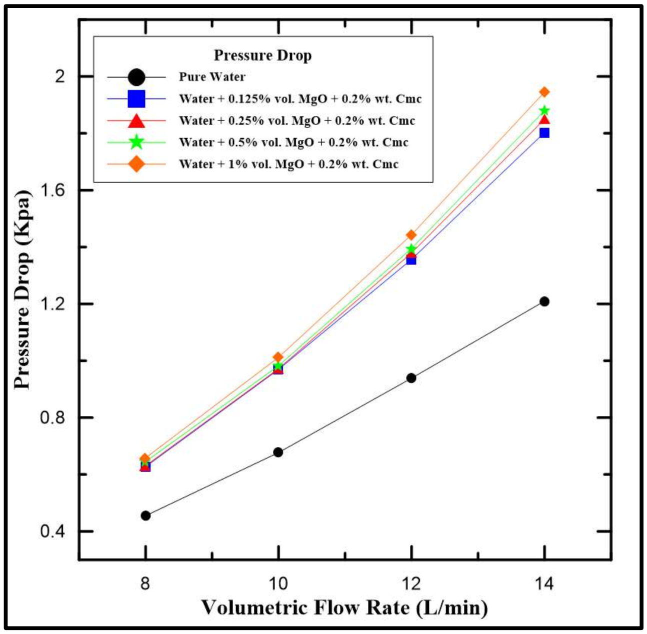

Figure (5-91): Variation of water-MgO fluid pressure drop with volume flow rate

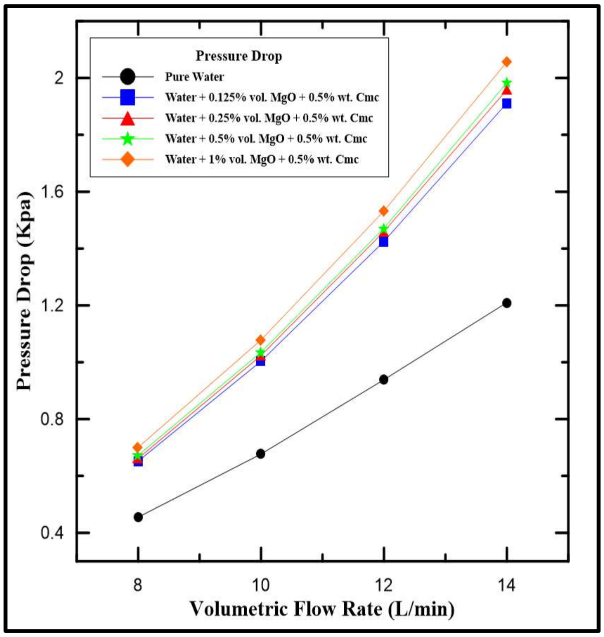

Figure (5-92): Variation of water-MgO-CMC fluid pressure drop with volume flow rate

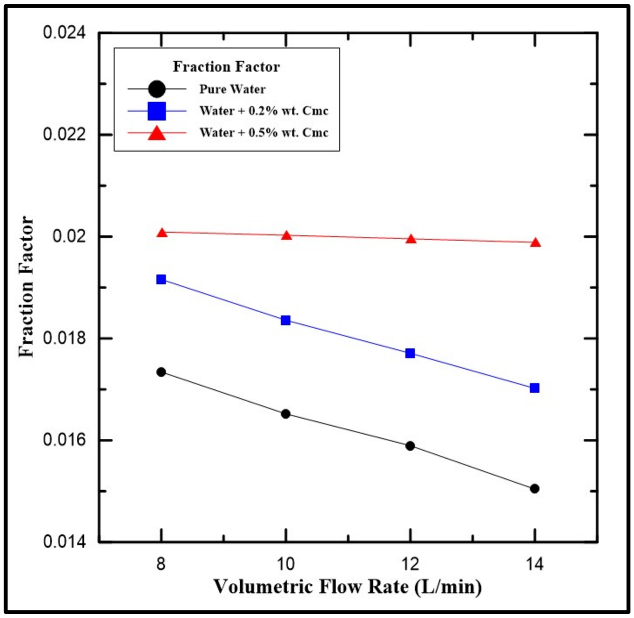

Figure (5-93): Variation of pure water friction factor with volume flow rate

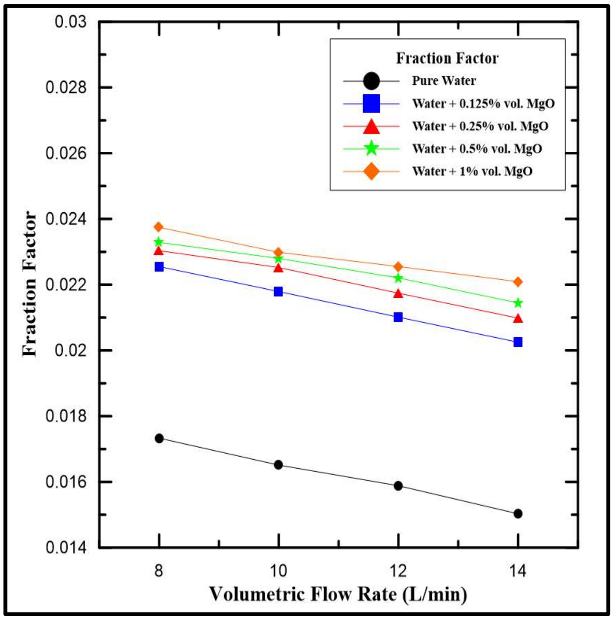

Figure (5-94): Variation of water-CMC fluid friction factor with volume flow rate

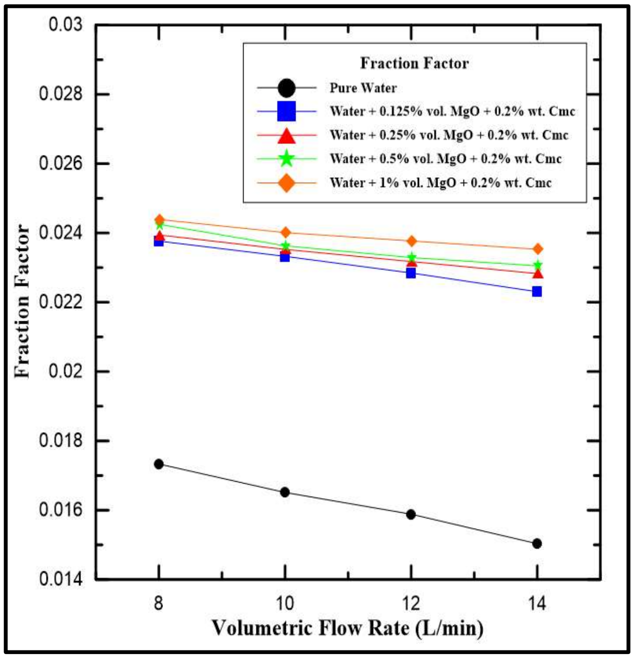

Figure (5-95): Variation of water-MgO fluid friction factor with volume flow rate

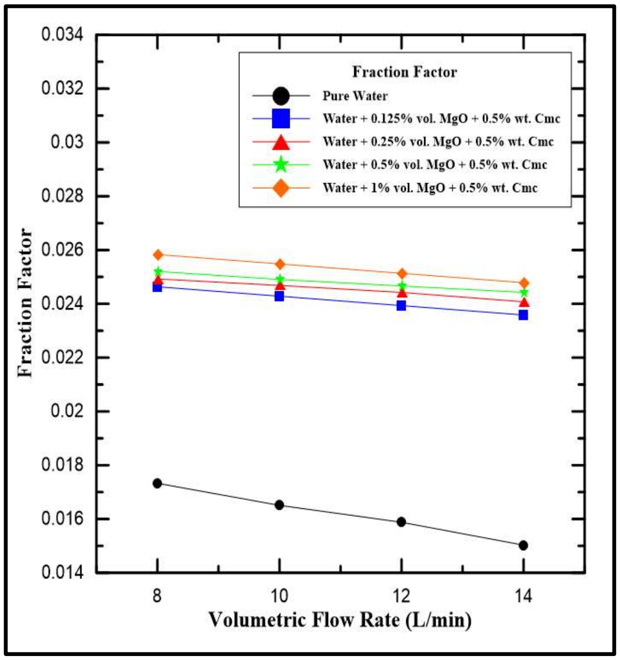

Figure (5-96): Variation of water-MgO-CMC fluid friction factor with volume flow rate

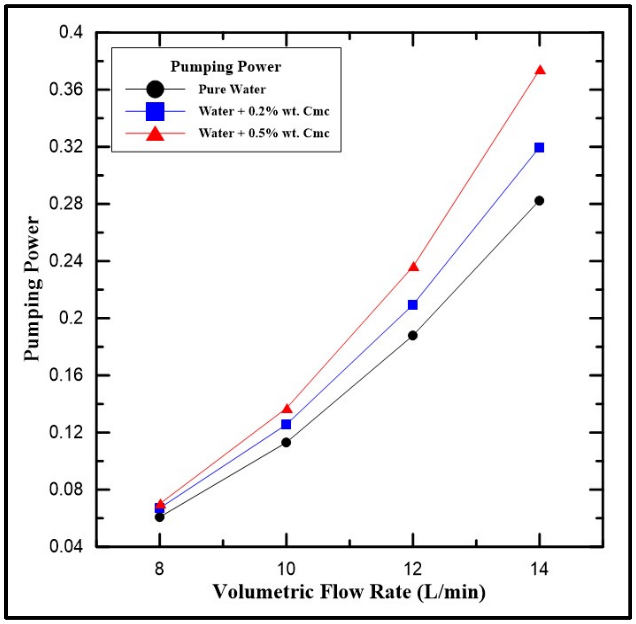

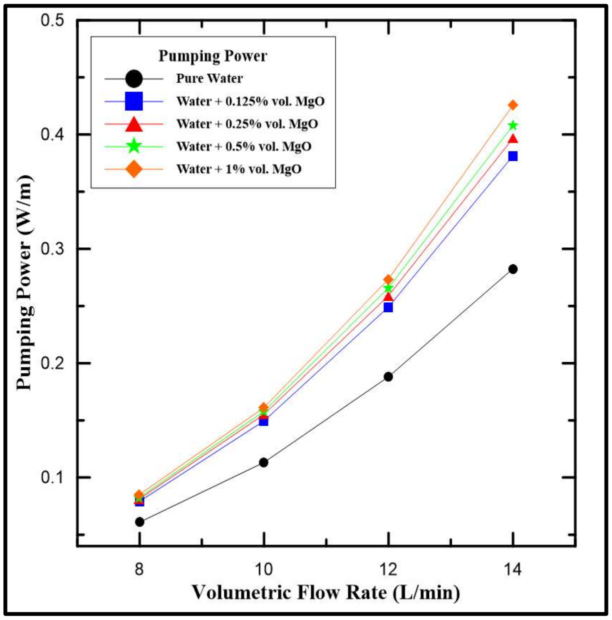

Figure (5-97): Variation of pure water Pumping Power with volume flow rate

Figure (5-98): Variation of water-CMC fluid Pumping Power with volume flow rate

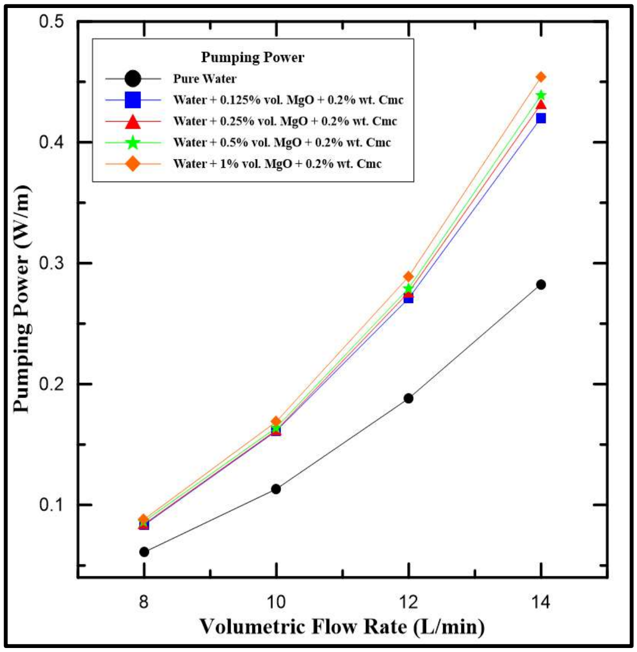

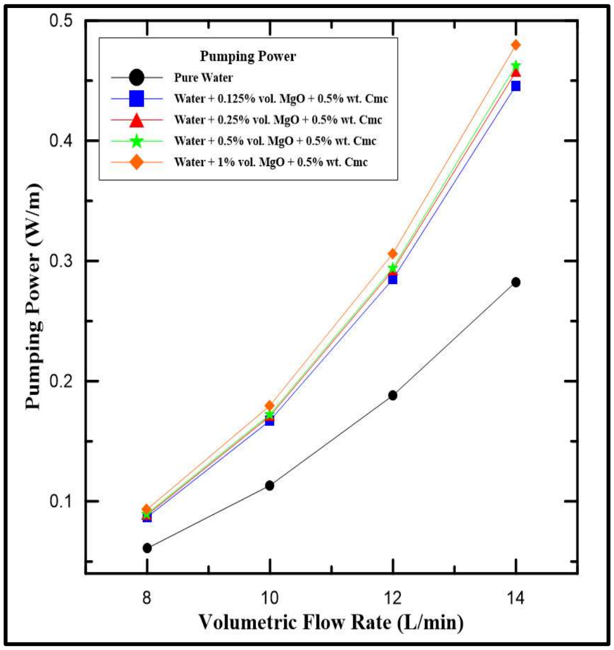

Figure (5-99): Variation of water-MgO fluid Pumping Power with volume flow rate

Figure (5-100): Variation of water-MgO-CMC fluid Pumping Power with volume flow rate

5.3. Flow Patterns

The flow patterns of air-water two-phase flow in a vertical, horizontal and inclined pipe with define pipe diameter are measured experimentally and demonstrate in different flow patterns maps. These maps present according to pipe diameter and pipe inclination. The flow patterns that result from present work not subject to any previously mentioned map. Images of flow patterns recorded by ordinary camera. These images give description of the flow pattern at length of 1.7 m from the beginning of the cold fluid flow.

In the present experimental work, the measurements in two-phase flow are performed for different air-water flow regimes. Most flow regimes in the pipe are closed or most closed in bubbly, slug and stratified flow. In order to present various flow regimes of two phases air-water flow by variation air and water flow rate are recommended. The suggested water flow rates are 24, 26, 28 and 30 L/min, and the air flow rates are in range of 360, 420 and 480 L/hr.

Figures from (5-101) to (5-103) characterize different flow regimes, two phases flow at water flow rate is 24 L/min, and the air flow rate varies from 360 to 480 L/hr.

Figure (5-101) characterizes flow regime at water flow rate 24 L/min and air flow rate 360/hr. Figure (5-50) shows bubbly flow pattern that recognize by the video camera zone. The bubbles that appearance and move in this figure as cloud.

Figures (5-102) and (5-103) demonstrate various flow regimes at fixed water flow rate 24 L/min with different air flow rate 420 and 480 L/hr. The air bubble shape appears by using video camera giving the named flow regime. Figure (5-102) shows slug flow pattern and Figure (5-103) shows stratified flow pattern.

Figures (5-104) to (5-106) give the stages of observation and growing of air bubbles in water flow. These figures demonstrate flow regime at fixed water flow rate 26 L/min and various air flow rate. Figures (5-104) and (5-105) present bubbly flow pattern at air flow rate 360 and 420 L/hr. Figure (5-106) shows stratified flow pattern at air flow rate 460 L/hr.

Figures from (5-107) to (5-109) characterize flow patterns at various flow conditions, these flow patterns are recognized by the video camera. This case done under conditions of constant water flow rates 28 L/min. Figure (5-107) presents bubbly flow regime at air flow rate 360 L/hr. Figures (5-108) and (5-109) illustrate various flow regimes, slug flow pattern with air flow rate 420 L/hr and stratified flow pattern at air flow rate 480 L/hr respectively.

Figures (5-110) to (5-111) show the air-water flow pattern under the condition of constant water flow rate and various air flow rate. The air bubbles that move in these figures moves faster than bubbles in previous conditions. Figure (5-110) presents bubbly flow regime at water flow rate 30 L/min, and air flow rate 360 L/hr with spherical bubbles shape and moves in line. Figure (5-111) shows bubbly flow regime at water flow rate 30 L/min air flow rate 420 L/hr with irregular bubbles shape, large and moves in line. Figures (5-112) shows a stratified flow regime under conditions at water flow rate 30 L/min air flow rate 480 L/h.

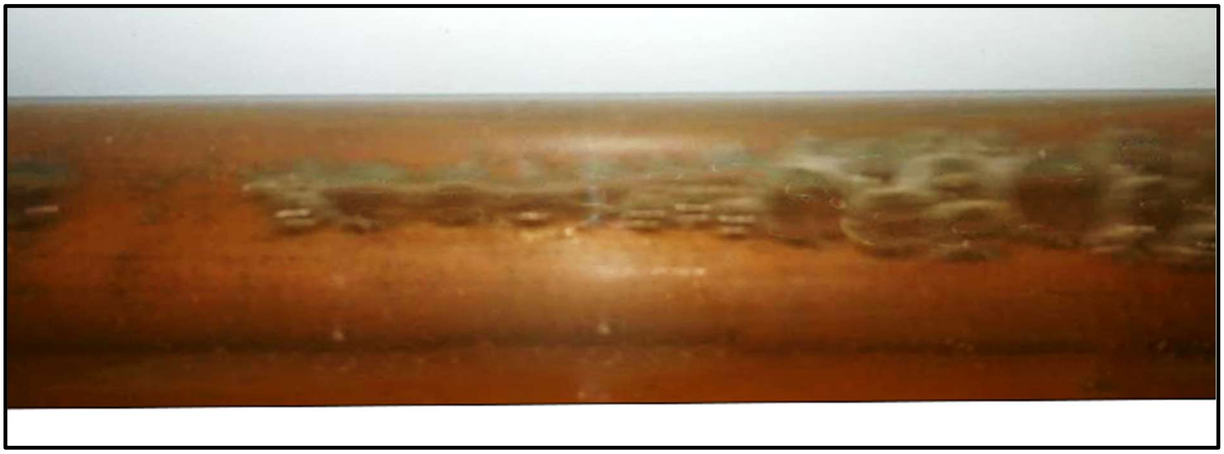

Figure (5-101): Flow regime at V$^\bullet$w = 24 L/min and V$^\bullet$a = 360

Figure (5-102): Flow regime at V$^\bullet$w = 24 L/min and V$^\bullet$a = 420

Figure (5-103): Flow regime at V$^\bullet$w = 24 L/min and V$^\bullet$a = 480

Figure (5-104): Flow regime at V•w = 26 L/min and V•a = 360 L/hr.

Figure (5-105): Flow regime at V•w = 26 L/min and V•a = 420 L/hr.

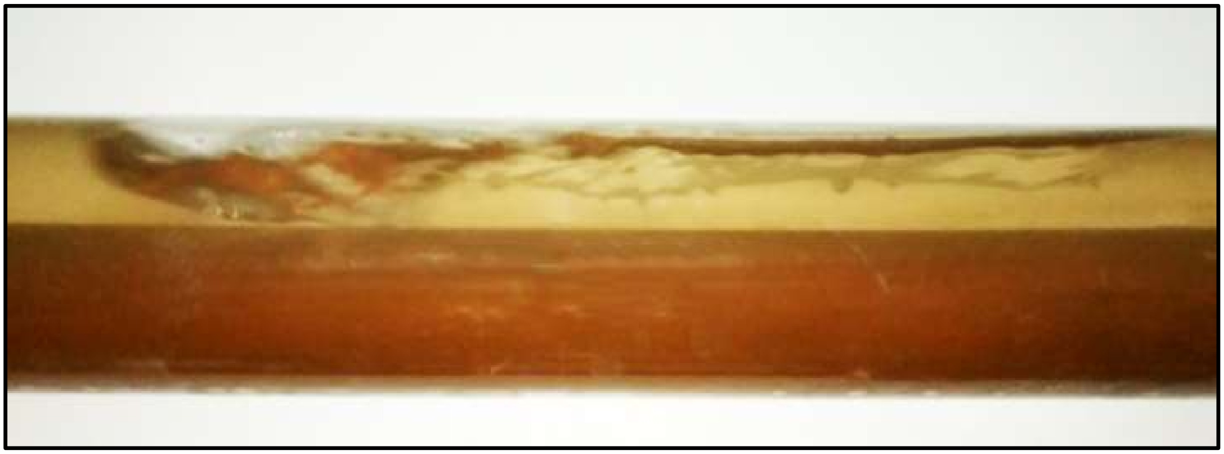

Figure (5-106): Flow regime at V•w = 26 L/min and V•a = 480 L/hr.

Figure (5-107): Flow regime at V·w = 28 L/min and V·a = 360 L/hr.

Figure (5-108): Flow regime at V·w = 28 L/min and V·a = 420 L/hr.

Figure (5-109): Flow regime at V·w = 28 L/min and V·a = 460 L/hr.

Figure (5-110): Flow regime at V·w = 30 L/min and V·a = 360 L/hr.

Figure (5-111): Flow regime at V·w = 30 L/min and V·a = 420 L/hr.

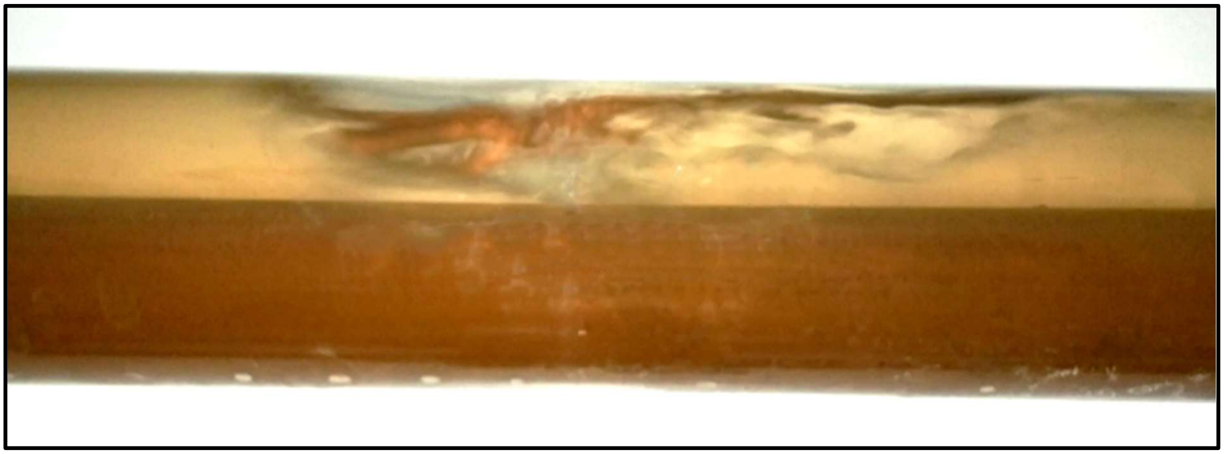

Figure (5-112): Flow regime at V·w = 30 L/min and V·a = 460 L/hr.

5.4. Numerical Result

In the numerical study, 3D simulation for the system is accomplished by employing the computational fluid dynamics (CFD) analysis software (ANSYS 2020 R1, FLUENT package). The parameters investigated in the CFD simulation are:

- Different concentrations are studied for the considered additives to the hot fluid.
- Different materials are used as additives to improve the performance of the system.
- Various values for the volumetric flowrate of both the hot fluids are investigated.
- The flow direction is investigated considering two cases, namely, parallel flow in which both fluids flow in the same direction and counter flow in which the fluids flow in the opposite directions.
- The effect of two-phase flow is investigated through the CFD simulation.

5.4.1 Effect of The Concentration of Additives

Two different materials are used as additives to improve the properties of the flow field. However, four different cases are considered as explained in section 5.1. In this section, different concentrations for additive are considered. For the CMC, max concentration is used 0.5% wt. While for the MgO nano particles, four concentrations were considered which are (0.125%, 0.25%, 0.5% and 1% vol.). Finally, a mixture of CMC and MgO nano particles are considered as additives to the water. In this case, four concentrations are taken in which one concentration of CMC is selected with the four concentrations of MgO nano particles. Table (5-18) shows the numerical results for this case.

5.4.1.1 Pressure Contours

Figure (5-113) presents the pressure contours for the 4 different concentrations of the MgO nanoparticles mixed with 0.5% wt. CMC concentrations. The flow conditions for the four cases are shown in the figure above, and all are the same except for the concentrations of the MgO nanoparticles and CMC mixture. The highest pressure is observed with the highest CMC and MgO nanoparticles concentration. The value is the highest among all cases including the previous cases presented in the previous experimental work figures. Also, the pressure in tube side is higher than that in the annulus side, due to the small cross section area of tube comparable with cross section area of annulus. The pressure value at the outlet of tube side and annular side will be zero as simulate with the experimental setup.

5.4.1.2 Temperature Contours

In the current study, different additives are considered as mentioned in the previous section. In this section, temperature contours for four cases are compared. Figures (5-114) and (5-115) demonstrate temperature contours for hot fluid flow and cold fluid flow respectively. The flow conditions for all cases are shown in the mentioned figure and all are the same except for the concentrations of the MgO nanoparticles and CMC mixture.

5.3.1.3 Velocity Contours

The velocity contours of the previous cases are presented in figure (5-116). The change in the MgO concentrations shows no significant change in the velocity of the working fluid, thus it can be neglected. However, when the CMC concentration was changed, the change in the hot fluid velocity becomes clearer compared to that when the MgO concentration is changed. So, the CMC addition to the hot fluid has an important effect on the fluid velocity.

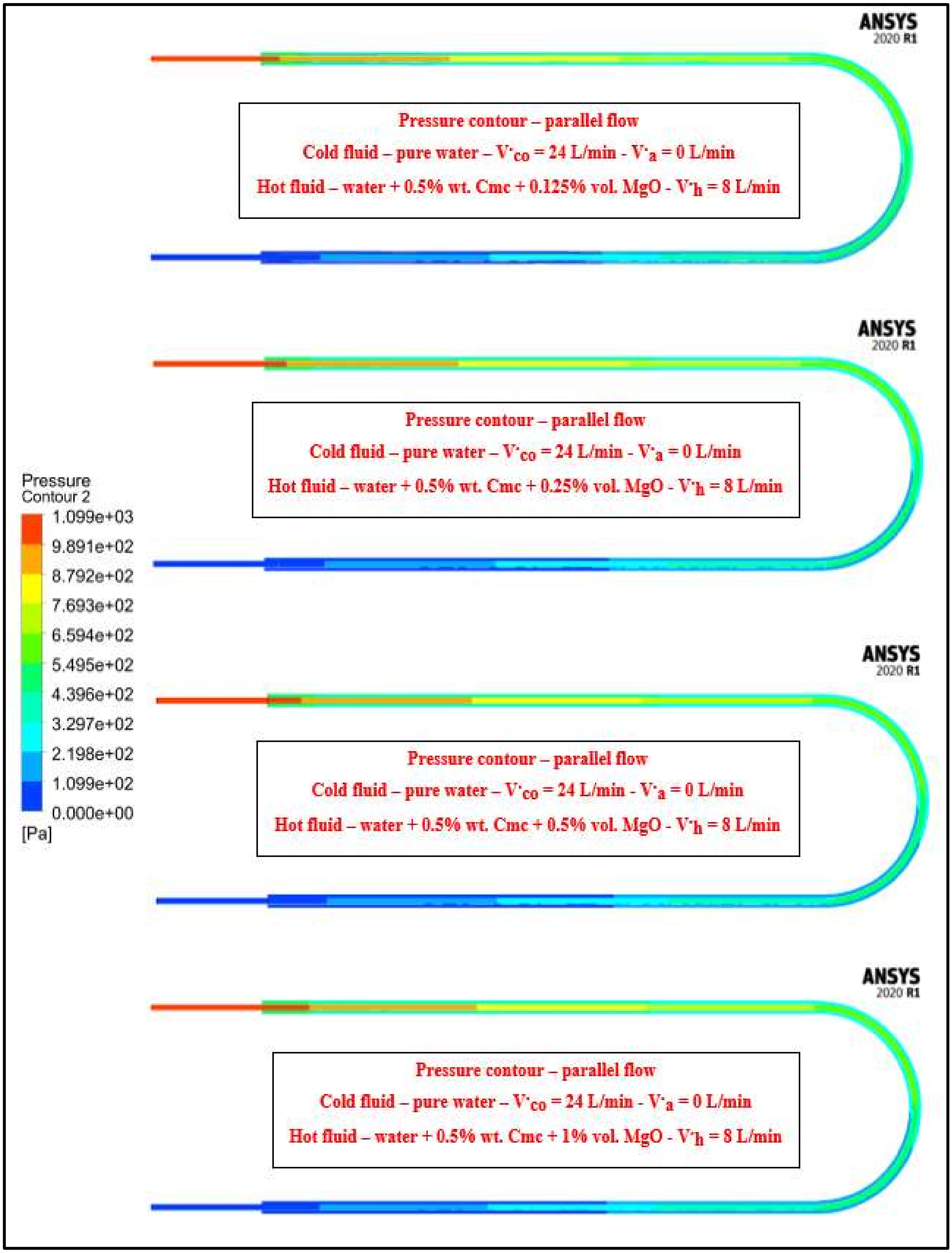

Figure (5-113): Pressure contour along heat exchanger.

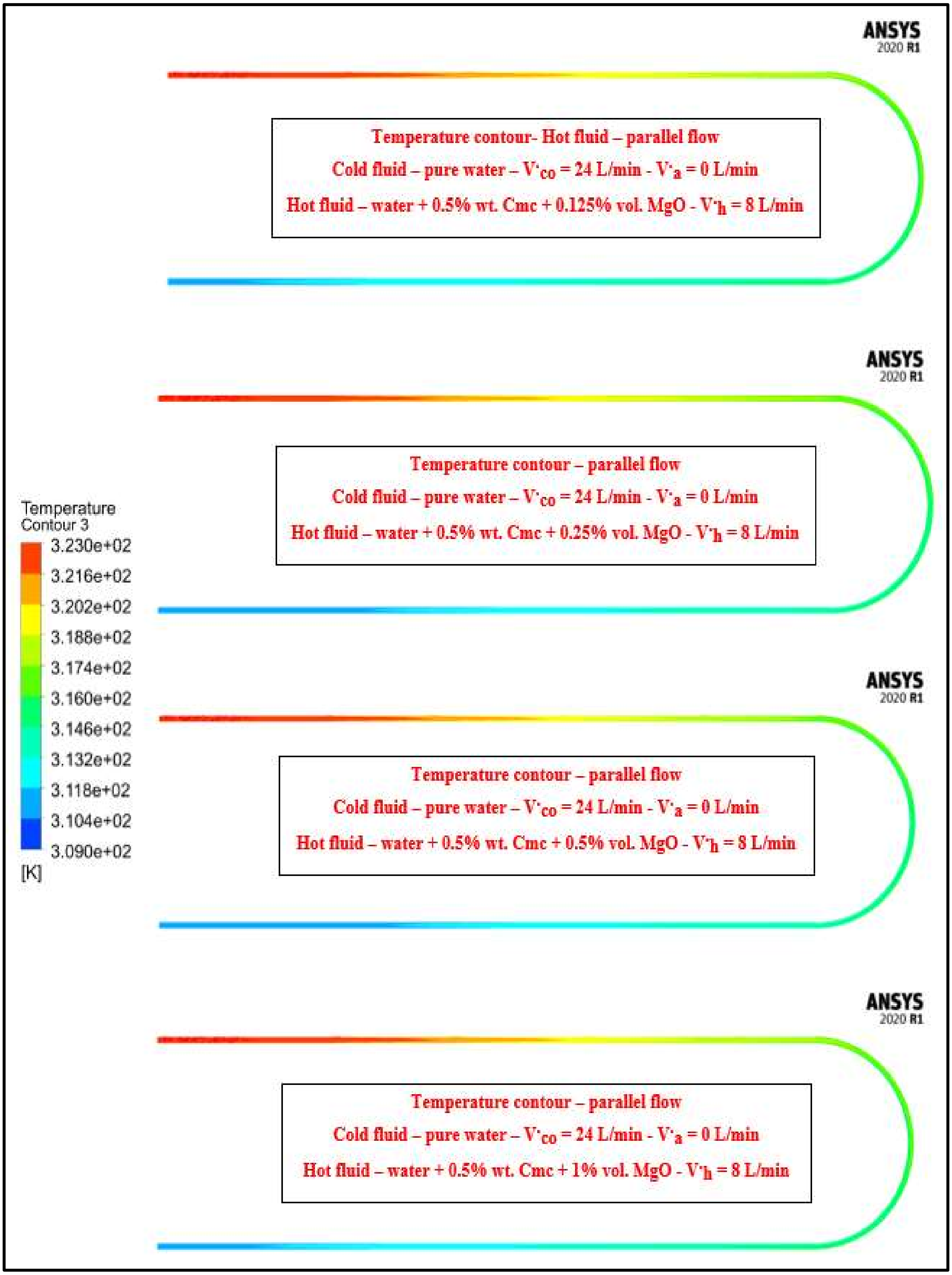

Figure (5-114): Temperature contour along inner pipe of heat exchanger.

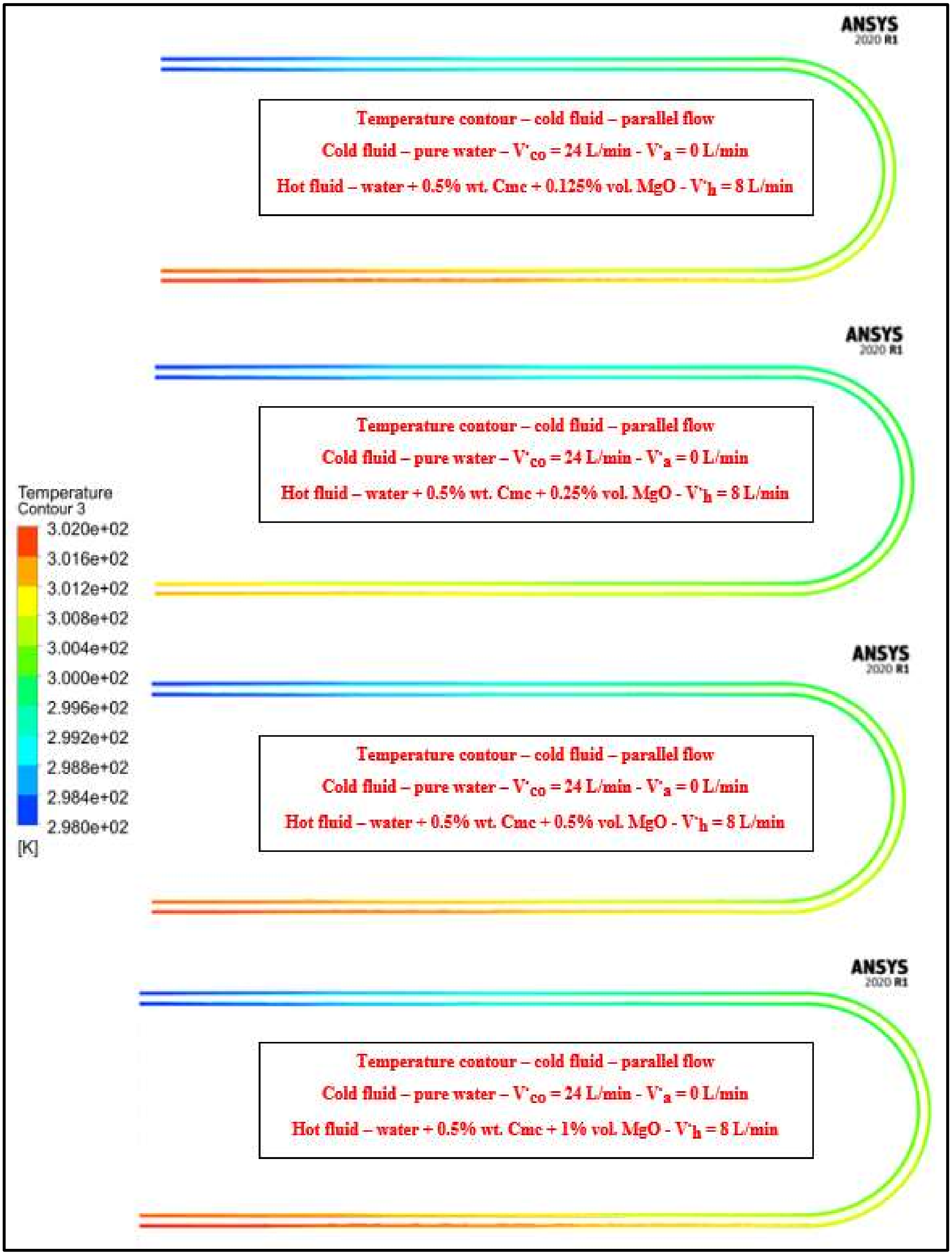

Figure (5-115): Temperature contour along annular pipe of heat exchanger.

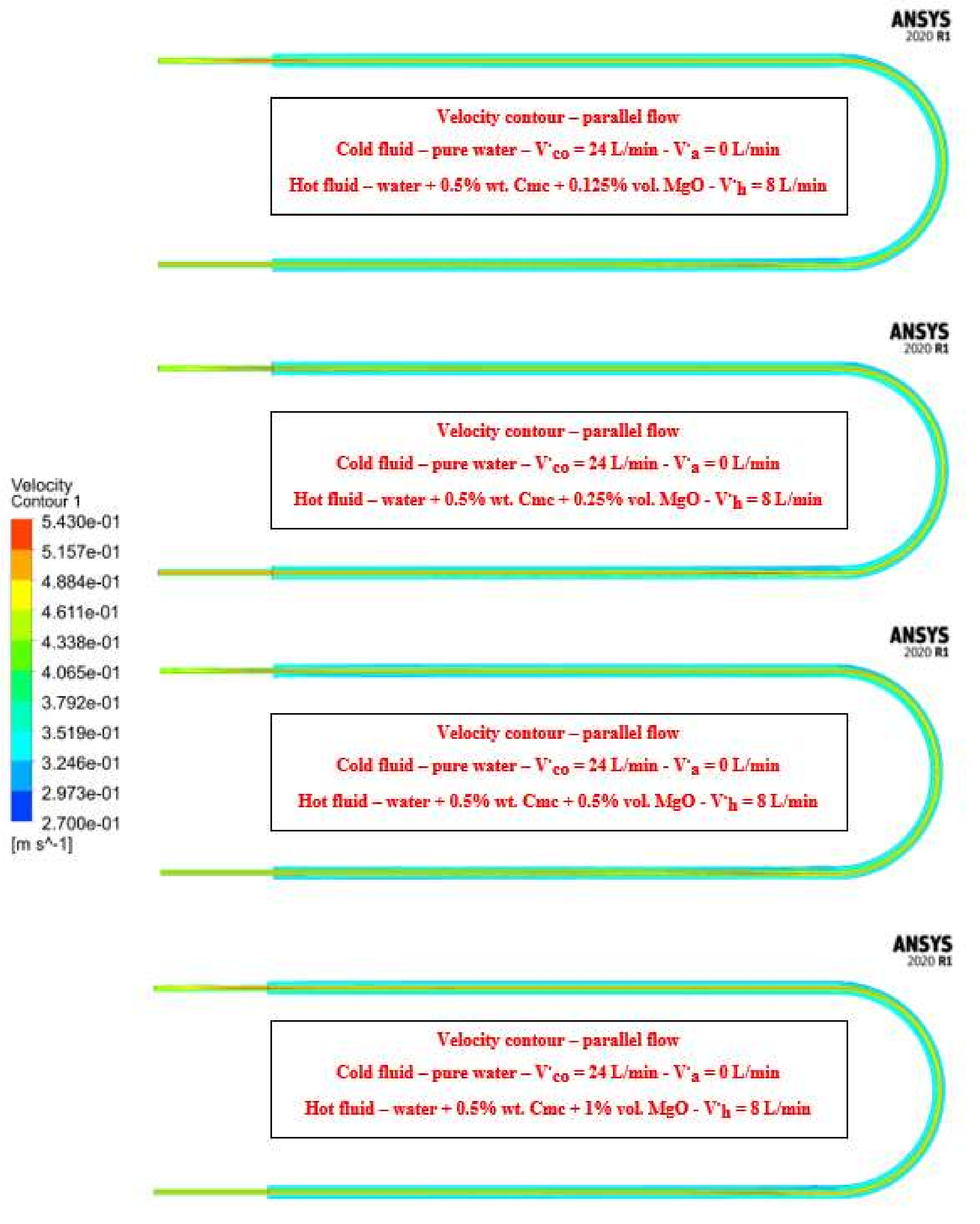

Figure (5-116): Velocity contour along heat exchanger.

5.4.2 Effect of Hot Fluid Flow Rate

One of the most important parameters that affect the enhancement of heat transfer rate is flow rate. The flow rate is directly proportion with amount of heat transfer rate. The hot fluid is a mixture between pure water, MgO and CMC. The mixture contains max amount of CMC concentration 0.5% wt. with four concentrations of MgO nano particles (0.125%, 0.25%, 0.5% and 1% vol.). The range of hot fluid volumetric flow rates are (8, 10, 12 and 14 L/min). Table (5-19) shows numerical results for boundary condition that is considered in this case.

5.4.2.1 Pressure Contours

The pressure contours for different flowrates of the hot fluid are shown in figure (5-117). the operational conditions are identical for the different cases except the value of the volumetric flowrate of the hot fluid. The pressure increases significantly as the volumetric flow rate is increase. The flow conditions for all four cases are shown in the above mentioned figure and all are the same except for the concentrations of the MgO nanoparticles and CMC mixture. The highest pressure is observed with the highest flow rate. the pressure value at outlet of tube side and annular side will be zero as a simulate with experimental setup.

5.4.2.1 Temperature Contours

Figure (5-118) represents the temperature contour for hot fluid in inner pipe of heat exchanger. It has been observed that the temperature of hot fluid in inner pipe at outlet is inversely proportionally with hot flow rate. The flow condition that dependent in this case is demonstrated in the above mentioned each figure. The lowest temperature is observed with the highest flow rate.

5.4.2.1 Velocity Contours

The velocity contours are shown in figure (5.119) for various hot fluid flow rates and constant cold fluid flow rate. All condition information is implemented in the above mentioned figure. The velocity of a hot fluid is directly proportional to its flow rate. This will enhance the heat transfer.

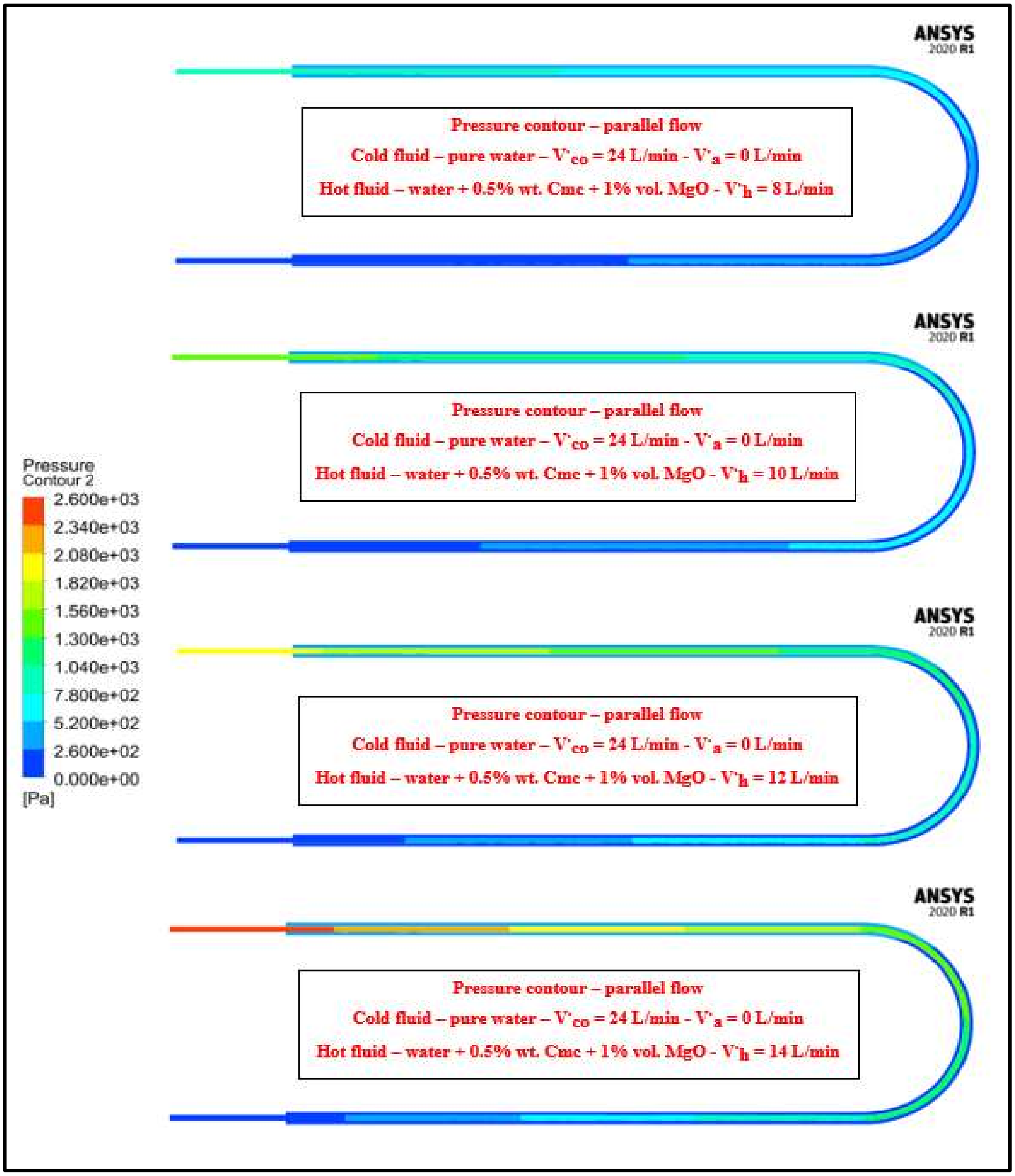

Figure (5-117): Pressure contour along heat exchanger at different hot fluid flow rates.

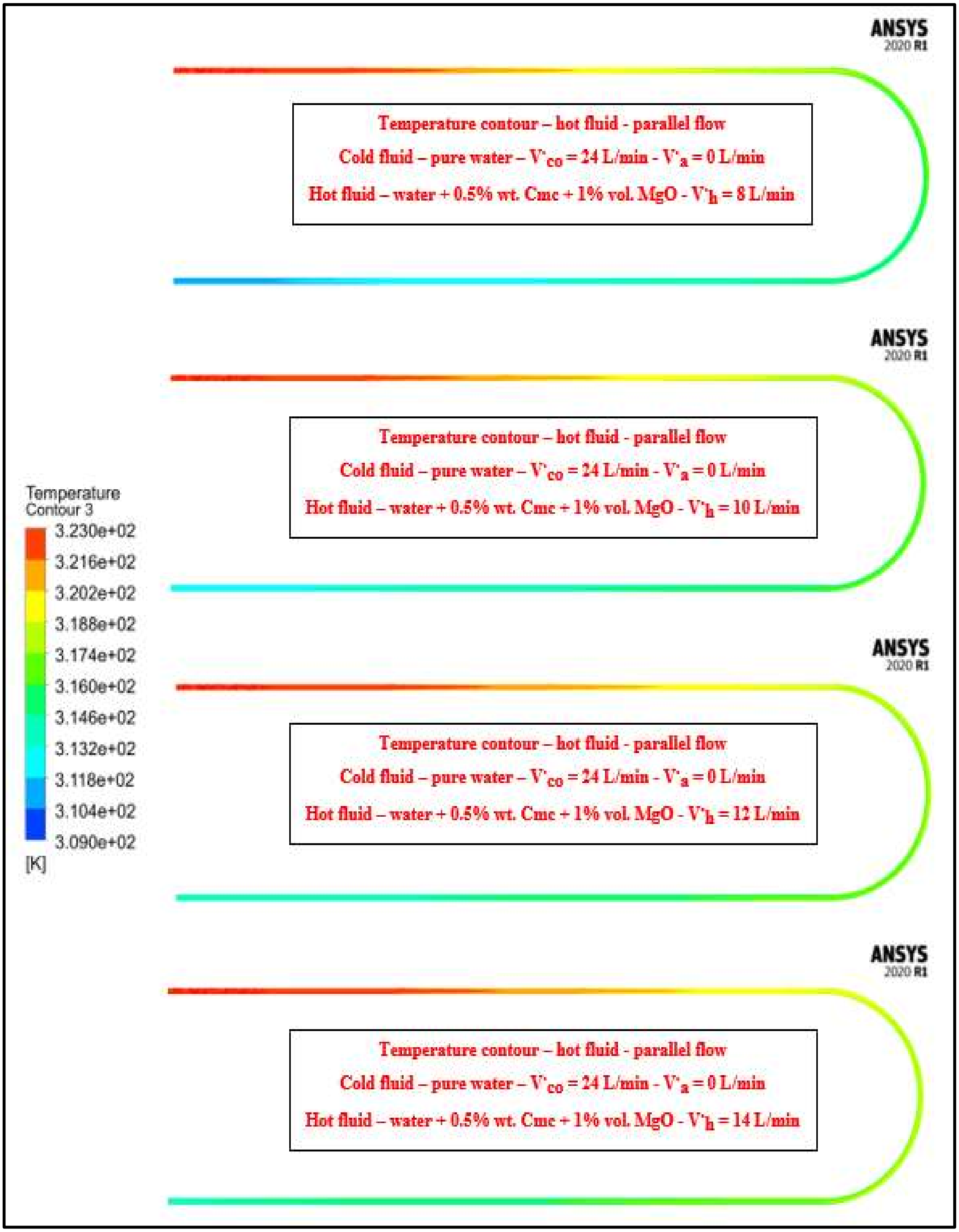

Figure (5-118): Temperature contour along inner pipe of heat exchanger at different hot fluid flow rates.

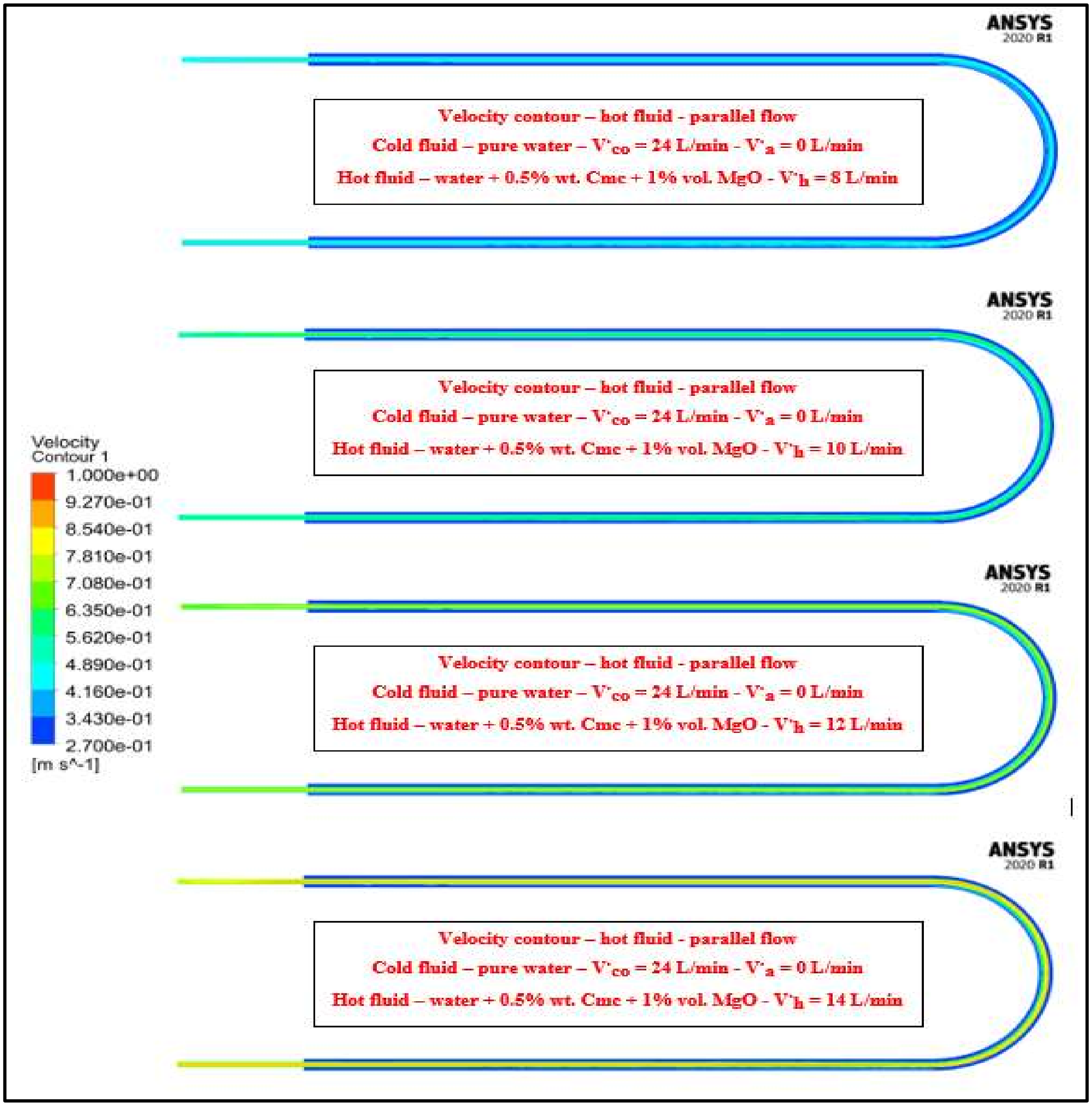

Figure (5-119): Velocity contour along heat exchanger at different hot fluid flow rates.

5.4.3 Direction of Flow

The flow direction of the flowing fluids is investigated in this section. Two cases are considered which are parallel and counter flow, as characterized in figure (5-120) through the velocity vectors. Table (5-20) shows numerical results for boundary condition that is implemented in this case.

5.4.3.1 Pressure Contours

The effect of the direction of flow on the inlet pressure is presented in figure (5-121) through the pressure contours. The counter flow system results in a higher inlet pressure for the hot fluid which improves the characteristics of the system making it more suitable for higher pressure systems. the pressure value at outlet of tube side and annular side will be zero as a simulate with experimental setup.

5.4.3.2 Temperature Contours

Figure (5-122) represents the temperature contour for parallel and counter flow. This figure shows temperature contour on surface of annulus side and tube side at different locations for plane of heat exchanger. It has been observed that the temperature in tube side is higher than annulus side because of the hot fluid in this study flows inside tube. The supply flow condition, the concentrations of MgO nanoparticles and CMC are pointed over each figure.

5.4.3.3 Velocity Contours

Figure (5-123) shows the velocity contours along the system. The counter flow case presents a higher value for the fluid velocity which improves the heat transfer along the system as well as the effectiveness of the heat exchanger. The change in the direction of the flow shows no significant change in the velocity of the hot working fluid, thus it can be neglected. However, the cold fluid direction keep constant, and this lead to no change in its velocity. The flow conditions for parallel and counter flow are shown in figure (5-123).

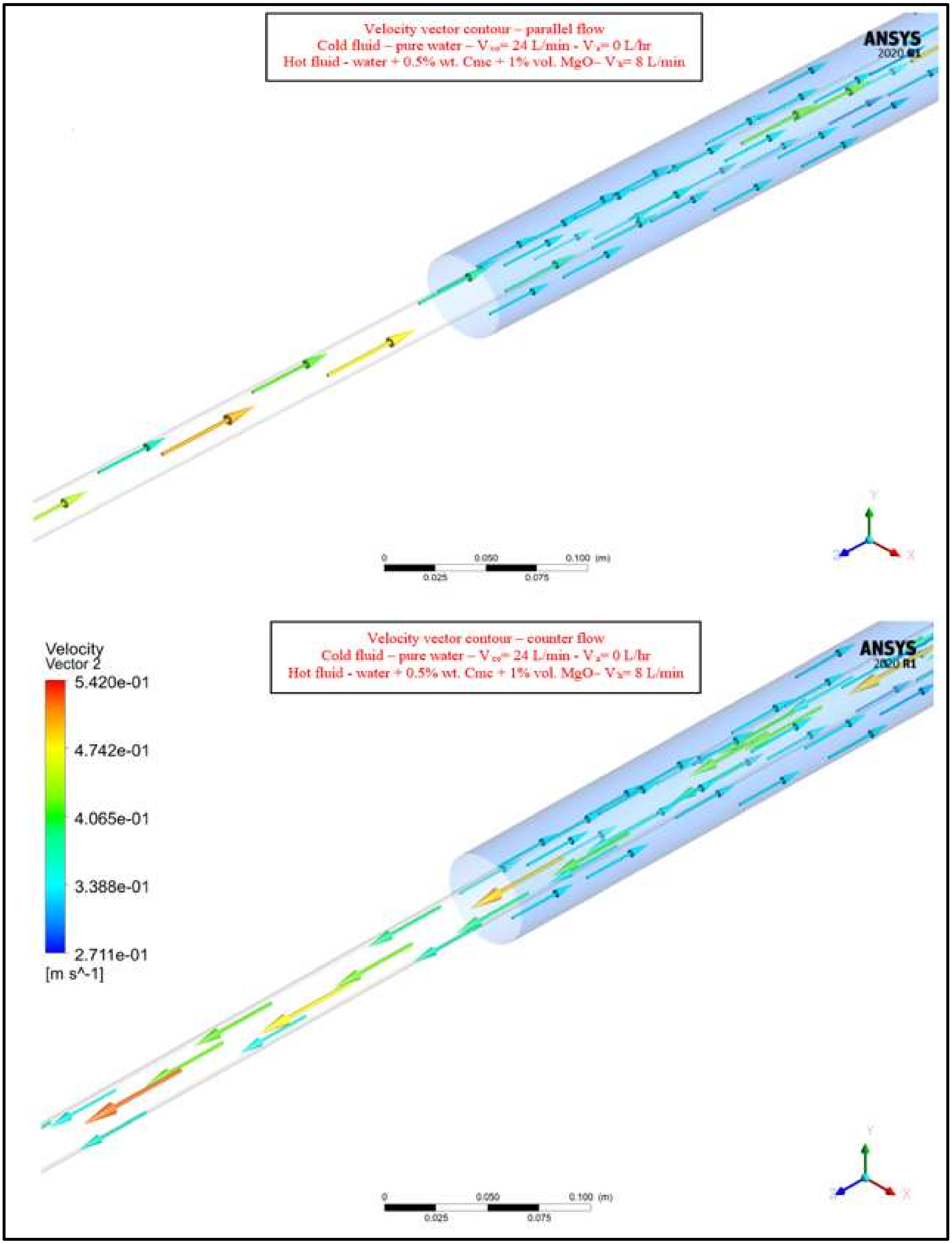

Figure (5-120): Velocity vector contour for direction fluid flow.

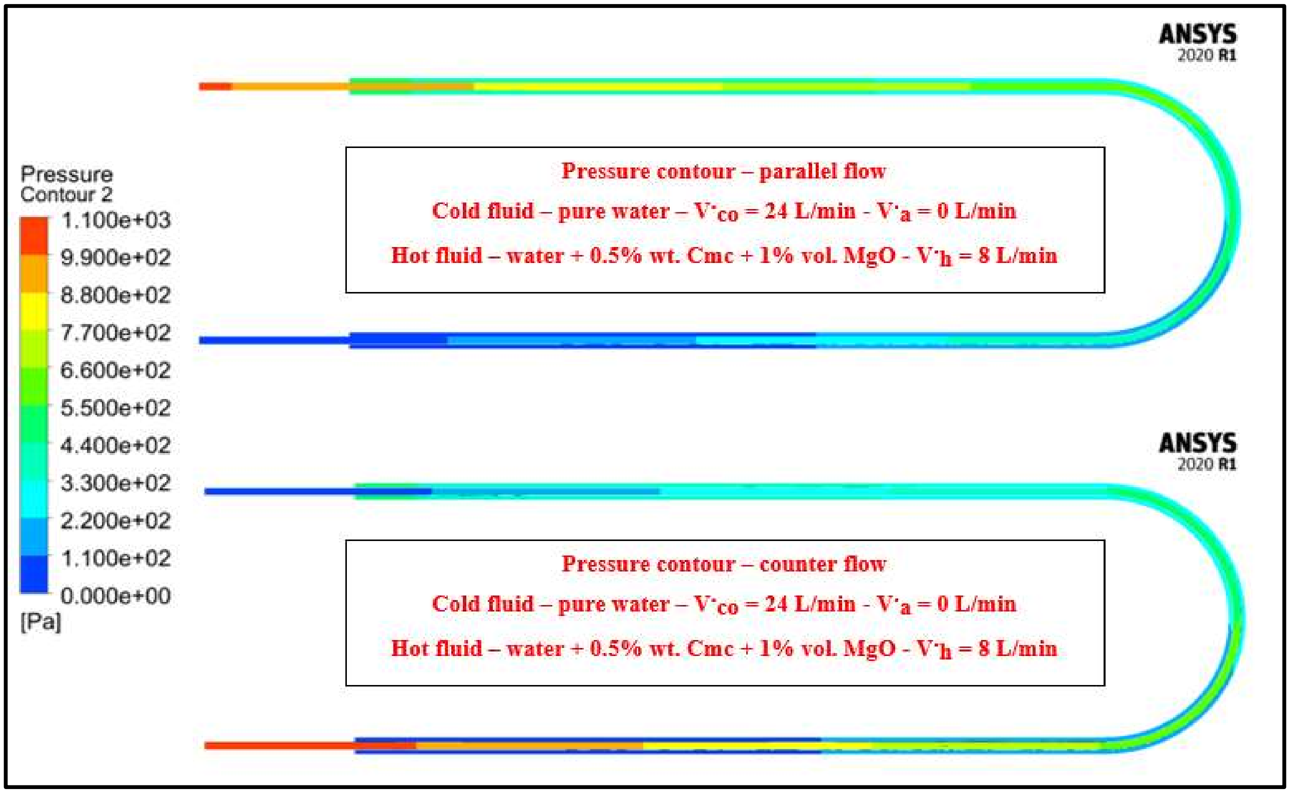

Figure (5-121): Pressure contour for different configuration flow of heat exchanger.

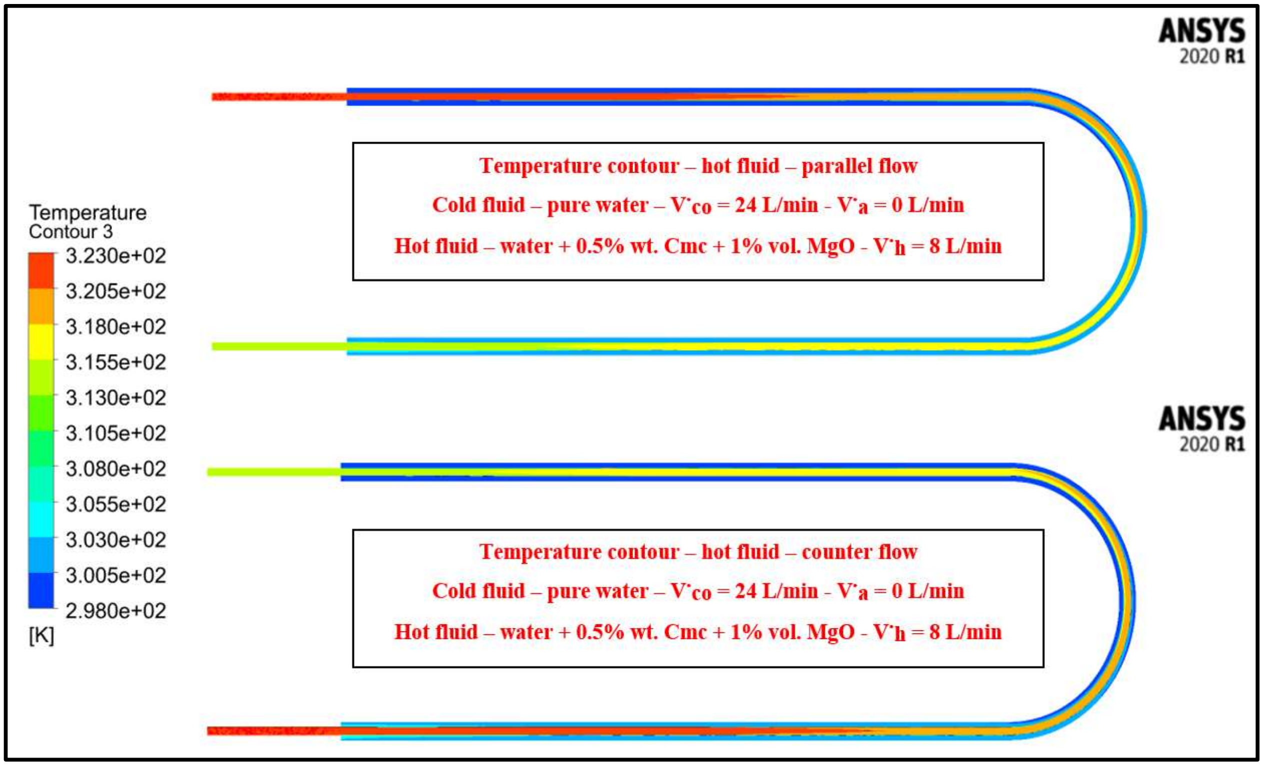

Figure (5-122): Temperature contour for different configuration flow of heat exchanger.

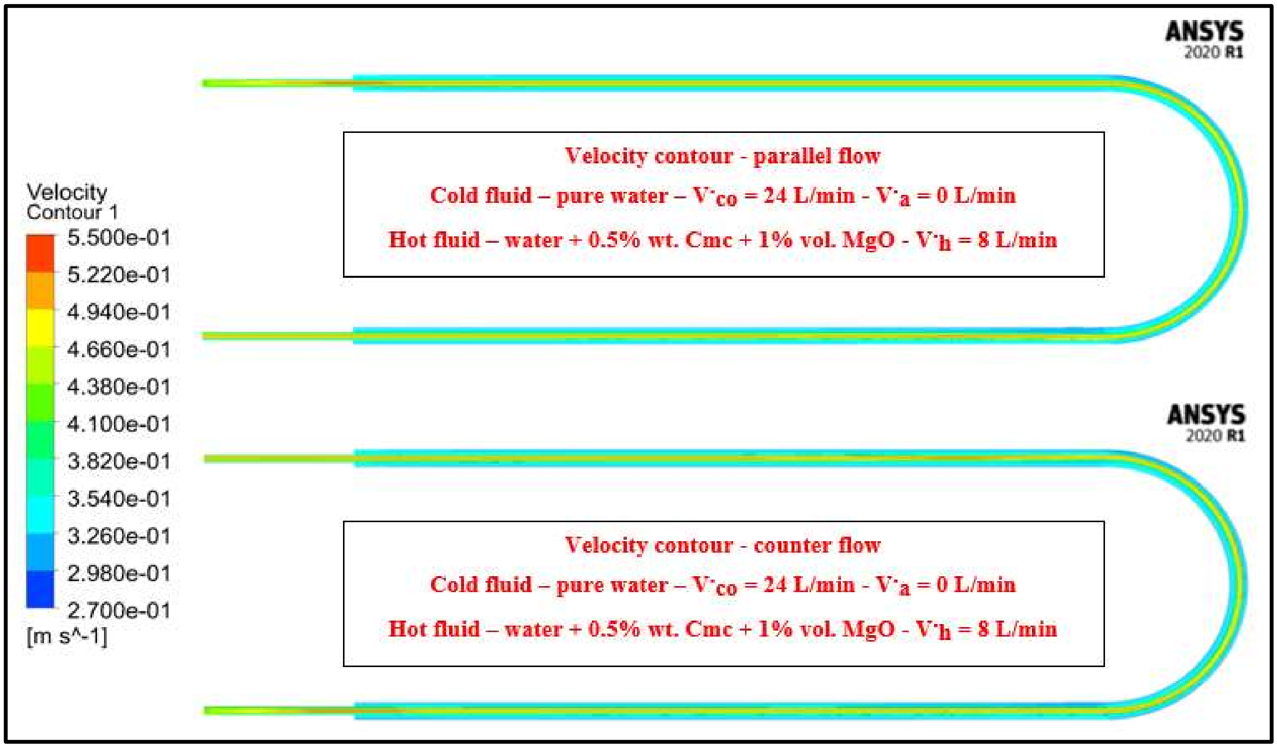

Figure (5-123): Velocity contour for different configuration flow of heat exchanger.

5.4.4 Effect of two-phase flow

Two different fluids were injected as two phases in annular side. The air-water two phases flow use to enhance heat exchange rate. However, three different air flow rates are considered as explained in section (5.1.). For the water flow rate 24 L/min is used while for the air flow rate, three flow rates are considered which are (360, 420 and 480 L/hr). Finally, in this section, a comparison between single-phase and two-phase flow is presented. Table (5-21) shows numerical results for boundary condition to be considered in this case.

5.4.4.1 Pressure Contours

Figure (5-124) details the map of pressure contour at cold fluid in annular side, pressure value is characterized through annular side in table (5-2). The pressure at the begging in the annulus side has largest value, this value decreases as the cold fluid continues in flow. The pressure of the cold fluid increases significantly as the air volumetric flow rate increases. the pressure value at outlet of annular side will be zero as a simulate with the experimental setup.

5.3.4.2 Temperature Contours

Figures (5-125) and (5-126) represent the temperature contour on surface of annulus side and tube side at different locations for plane of heat exchanger respectively. The supply flow conditions are pointed over each figure. It has been observed that the temperature in tube side is higher than annulus side because of the hot fluid in this study flows inside tube. Table (5-21) presents the effect of increase air flow rate in out let temperature of cold and hot fluid.

5.3.4.3 Velocity Contours

The velocity contours of air-water two phases flow at annular side are shown in figure (5-127). The air flow rate varies with constant cold fluid flow rate as present over each figure. The velocity of the air-water two phases flow increases with the increase in the air flowrate. This will enhance the heat transfer characteristics along the system.

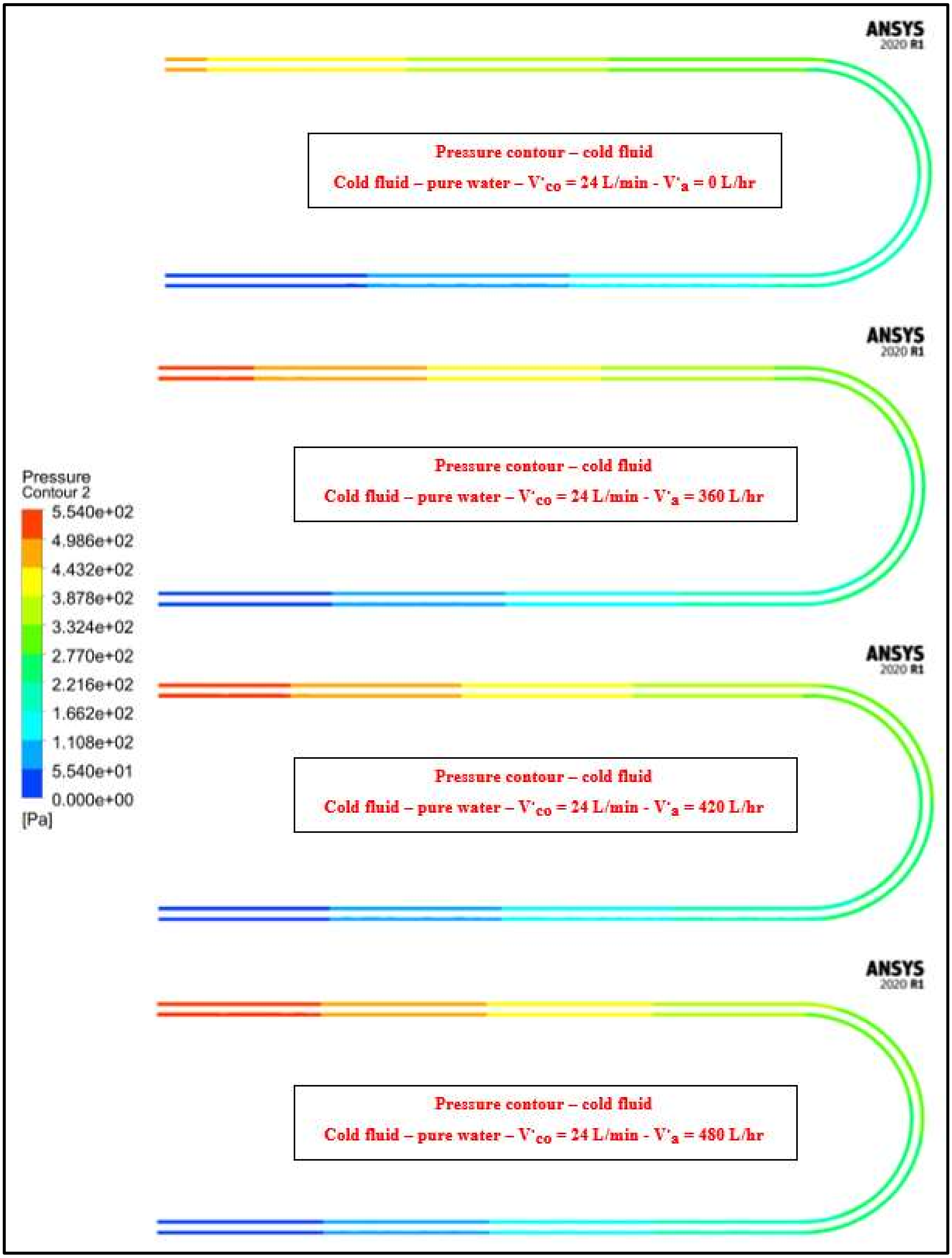

Figure (5-124): Pressure contour for air-water flow in annular pipe of heat exchanger.

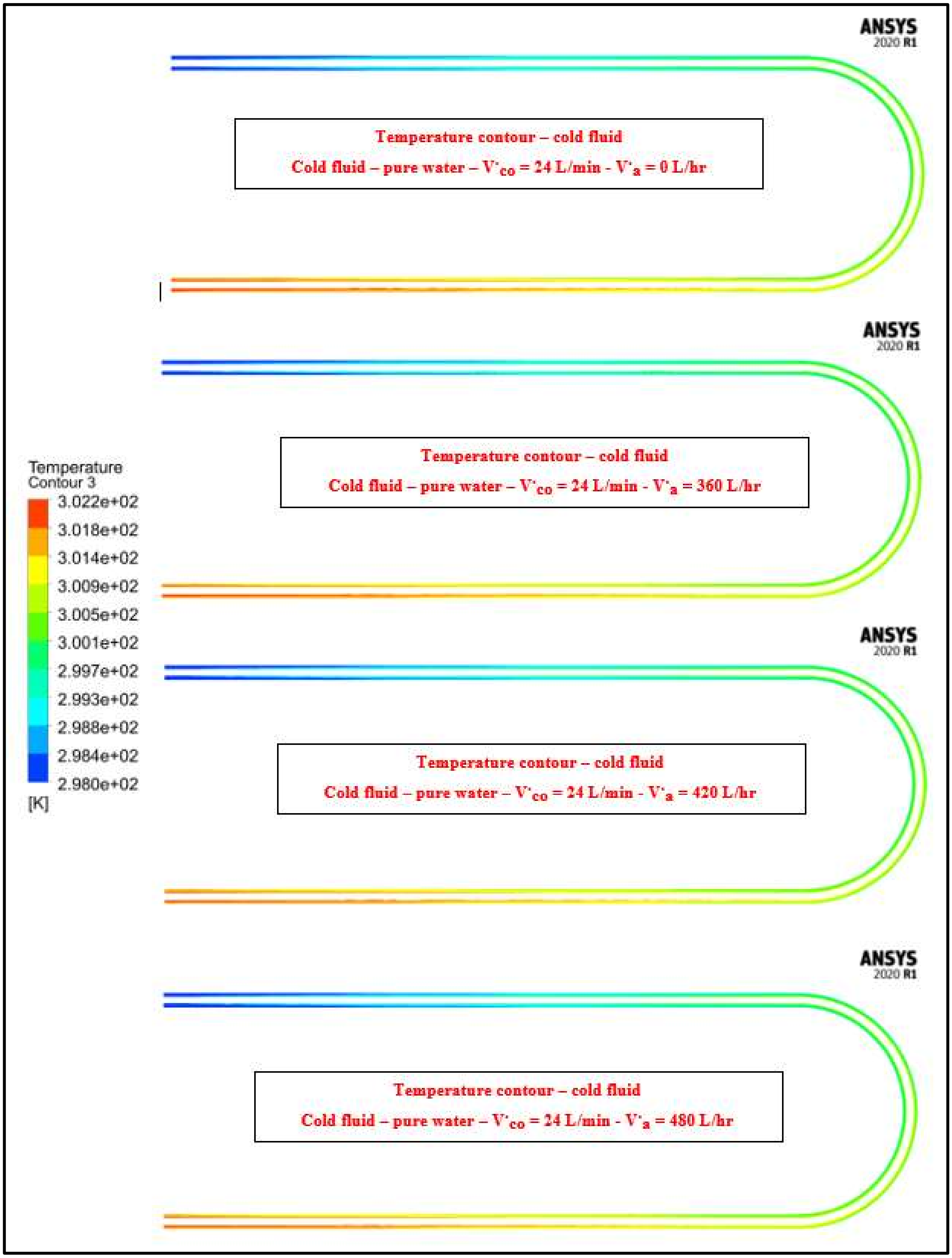

Figure (5-125): Temperature contour for air-water flow in annular pipe of heat exchanger.

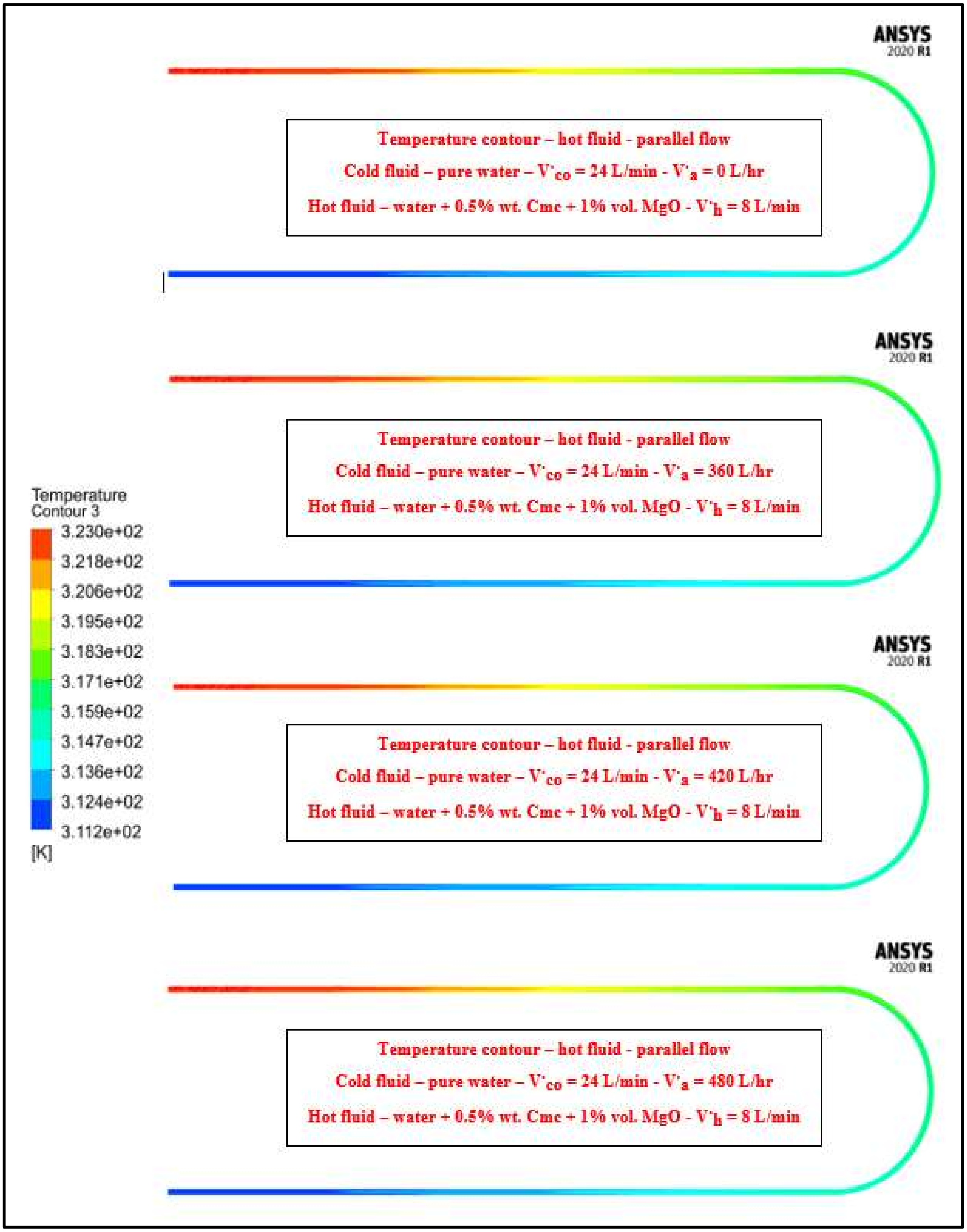

Figure (5-126): Temperature contour of hot fluid flow in inner pipe because air-water flow in annular pipe of heat exchanger.

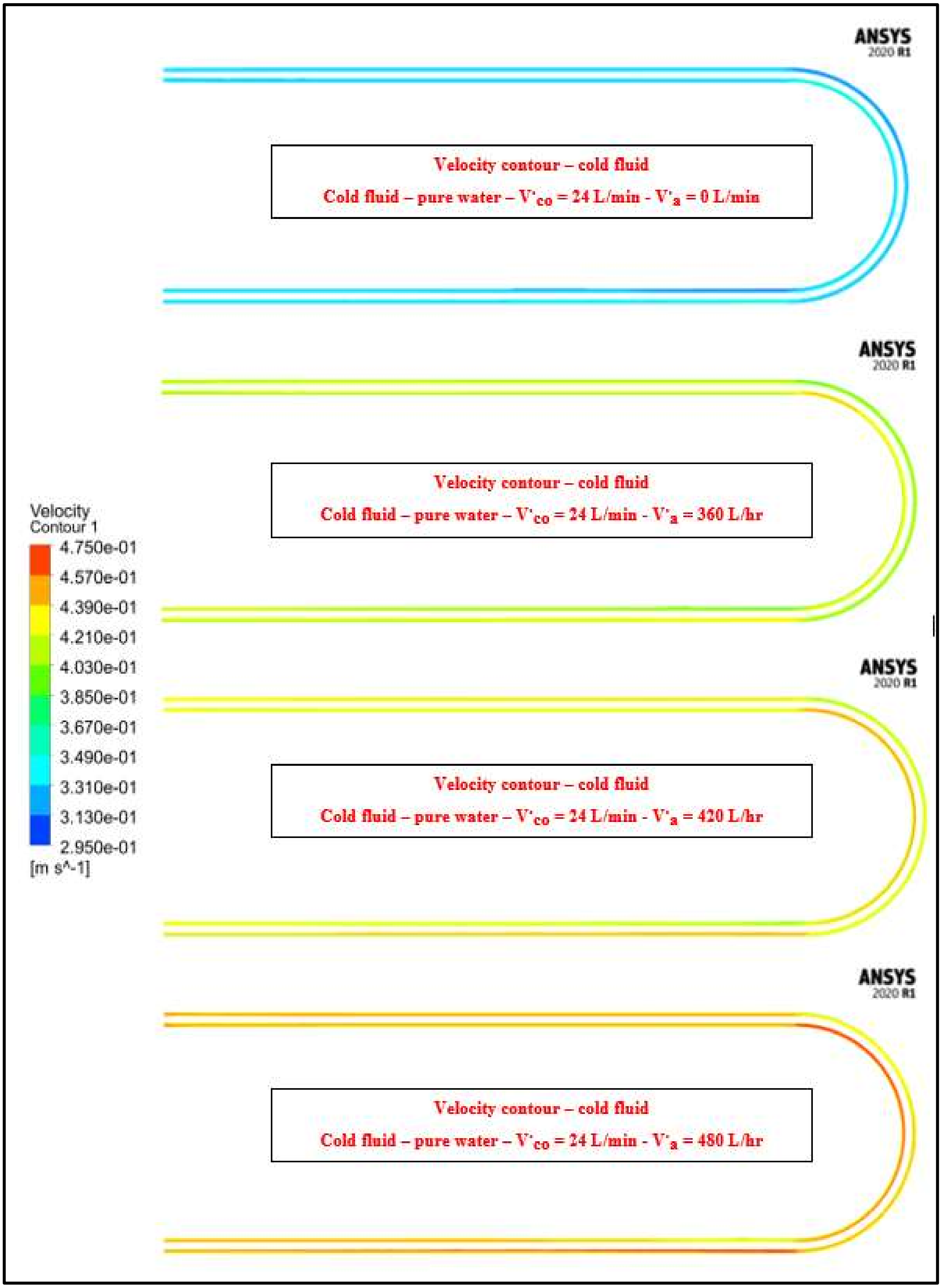

Figure (5-127): Velocity contour for air-water flow in annular pipe of heat exchanger.

Table (5-18): The numerical values at different additive concentration.

MgO % vol.	CMC % wt.	$P_{h, max}$ (pa)	$P_{C, max}$ (pa)	$T_{C, in}$ (K)	$T_{C, out}$ (K)	$T_{h, in}$ (K)	$T_{h, out}$ (K)	$V_{C, min}$ (m/s)	$V_{C, max}$ (m/s)	$V_{h, min}$ (m/s)	$V_{h, max}$ (m/s)
0.5	0.125	1079.84	454.322	298	301.67	323	311.94	0.295	0.355	0.299	0.542
0.5	0.25	1082.28	454.322	298	301.69	323	311.88	0.295	0.355	0.299	0.542
0.5	0.5	1089.56	454.322	298	301.7	323	311.86	0.295	0.355	0.299	0.542
0.5	1	1099.02	454.322	298	301.71	323	311.81	0.295	0.355	0.299	0.542

Table (5-19): The numerical values at various hot fluid flow rates.

$\dot{V}_h$ L/min	$P_{h, max}$ (pa)	$P_{C, max}$ (pa)	$T_{C, in}$ (K)	$T_{C, out}$ (K)	$T_{h, in}$ (K)	$T_{h, out}$ (K)	$V_{C, min}$ (m/s)	$V_{C, max}$ (m/s)	$V_{h, min}$ (m/s)	$V_{h, max}$ (m/s)
8	1099.02	454.322	298	301.71	323	311.81	0.295	0.355	0.299	0.542
10	1480.81	454.322	298	302.2	323	313.17	0.295	0.355	0.39	0.666
12	1997.51	454.322	298	302.49	323	313.96	0.295	0.355	0.471	0.79
14	2597.43	454.322	298	302.8	323	314.73	0.295	0.355	0.917	0.554

Table (5-20): The numerical values at depend on the flow direction

Flow direction	$P_{h, max}$ (pa)	$P_{C, max}$ (pa)	$T_{C, in}$ (K)	$T_{C, out}$ (K)	$T_{h, in}$ (K)	$T_{h, out}$ (K)	$V_{C, min}$ (m/s)	$V_{C, max}$ (m/s)	$V_{h, min}$ (m/s)	$V_{h, max}$ (m/s)
Parallel flow	1099.02	454.322	298	301.71	323	311.81	0.295	0.355	0.305	0.535
Counter flow	1099.02	454.322	298	301.94	323	311.52	0.295	0.355	0.306	0.535

Table (5-21): The numerical values that result from effect of two-phase flow.

$\dot{V}_C$ L/min	$\dot{V}_a$ L/hr	$P_{C, max}$ (pa)	$T_{C, in}$ (K)	$T_{C, out}$ (K)	$T_{h, in}$ (K)	$T_{h, out}$ (K)	$V_{C, min}$ (m/s)	$V_{C, max}$ (m/s)	Air volume fraction
24	0	454.322	298	301.71	323	311.81	0.295	0.355	0
24	360	529.512	298	301.64	323	312.01	0.37	0.443	0.2
24	420	541.625	298	301.63	323	312.04	0.382	0.458	0.225
24	480	553.65	298	301.62	323	312.06	0.395	0.475	0.25

5.5 Code Validation

In order to present the validity CFD model of present work, it must be compared with a previous work. Firstly with V.Nageswara Rao and B.Ravi Sankar [62], and secondly with Hadi H. Sh [99], which investigates the analysis heat of exchange of U-bend double pipe heat exchanger and being accomplished by employing the computational fluid dynamics (CFD) analysis software (ANSYS, FLUENT package). It has to take a constant cold fluid mass flow rates in annulus side (0.134 kg/sec) and mass flow rate of hot fluid (pure water) varies from (0.134 to 0.267kg/sec) with nanofluid 0 % concentration by volume. The flow boundary condition is shown in table (5-22). The average percentage error for all the cases was about (7% to 8%) with first researcher and about (2% to 3%) with second researcher as shown in figure (5-129).

Table (5- 22): Boundary condition.

No.	Boundary type	Annulus Pipe	Inside Pipe
1	Mass flow rate at Inlets	0.134 kg/sec	0.134 to 0.267 kg/sec
2	Temperatures	333 K	300 K
3	heat flux at pipe wall (Insulation)	0 W/m^2	------

5.6 Comparison between the Experimental Work and Its Numerical Work

Figure (5-130) illustrates a Comparison between the numerical and experimental convection heat transfer coefficient of the better case with volume flow rate. It shows that the experimental Nusselt number curve is less than the numerical one. This could be related to the losses associated with the experimental part, which are not taken into account numerically. However, the comparison gives a good agreement between experimental and numerical result about 7%. It should take constant cold pure water mass flow rates in annulus side (0.3979 kg/sec) and mass flow rate of hot fluid (Water+1% MgO vol.+0.5% CMC wt.) varies from (0.1326 to 0.2321kg/sec). The flow boundary condition is shown in table (5-23).

Table (5- 23): Boundary condition.

No.	Boundary type	Annulus Pipe	Inside Pipe
1	Mass flow rate at Inlets	0.134 kg/sec	0.1326 to 0.2321 kg/sec
2	Temperatures	298 K	323 K
3	heat flux at pipe wall (Insulation)	0 W/m^2	------

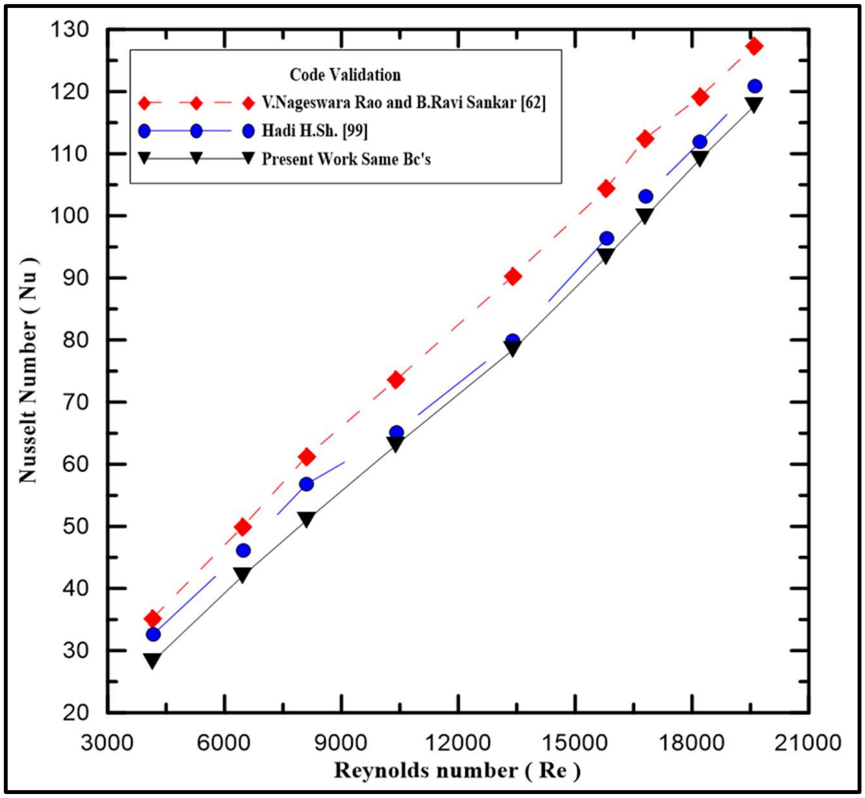

Figure (5-129): Code validation of present work with another researcher.

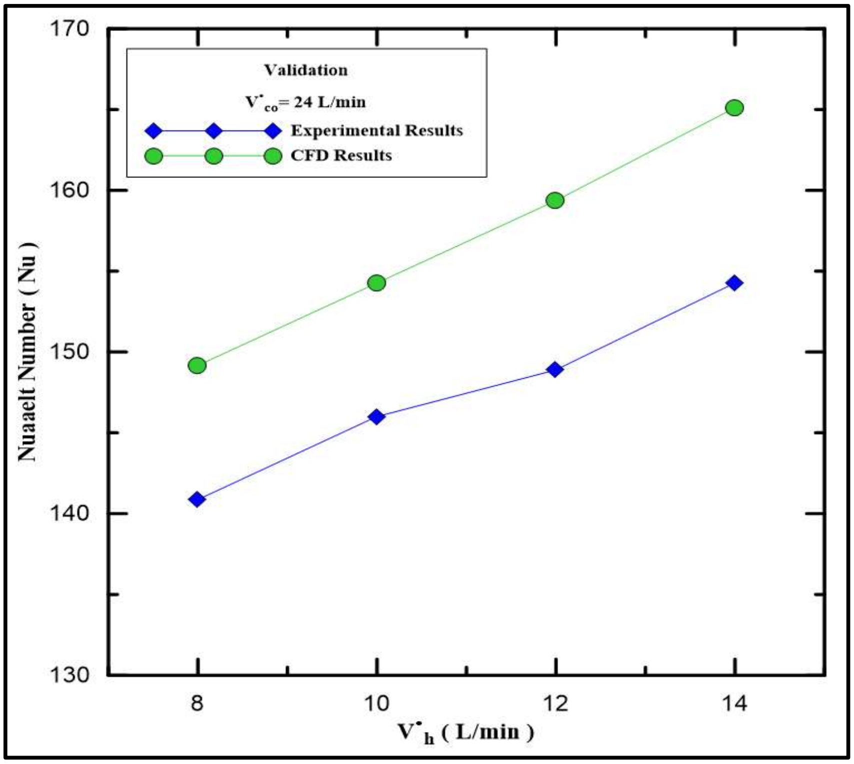

Figure (5-130): Comparison between experimental and numerical Nusselt number.

CHAPTER SIX

CONCLOUSION AND SUGGES TION FOR FUTURE WORKS

CHPTER SIX

CONCLUSIONS AND SUGGESTIONS FOR FUTURE WORK

6.1 Conclusions

In this work the U-bend double pipe heat exchanger rig is built relying on the calculating of the convective coefficient of heat transfer and pressure drop for different hot fluid types. A steady state CFD simulation implemented by using the commercial code ANSYS Fluent 2020 R1. The following main conclusions can be drawn:

1. The acceptable CMC concentration range (0.2% - 0.5%) by weight, and 0.5% present best concentration.
2. The best MgO particles concentration is 1% by volume which is pointed in the experimental work.
3. The type of additives (CMC and MgO) to pure water has a huge impact on the improvement of water-MgO-CMC fluid thermal conductivity and leads to the enhancement of heat exchange rate.
    - The thermal conductivity improves with adding CMC of concentrations 0.5% by weight about (2%).
    - The thermal conductivity improves at added MgO particles concentrations 1% by volume about (4%).
    - The thermal conductivity improves at the addition of concentrations MgO 1% by volume and CMC concentrations 0.5% by weight about (11%), and this presents a better case.
4. The increase in concentrations of additives (CMC and MgO) enhances viscosity of new fluid, and this leads to an increase in pressure drop and

friction coefficient. The MgO nanofluid and the CMC particles may not lead to high attendance drop in pressure but a very little raise in pressure drop compared to pure water and for this case an additional pumping power is no required.

- The raising of pressure drops for the water- 0.5% CMC wt. about (25%).
- The raising of pressure drops for the water- 1% MgO vol. about (54%).
- The raising of pressure drops for the water- 1% MgO vol. - 0.5% CMC wt. about (41%).

5. The nanofluid (water-MgO) suffers from conglomeration and deposition in a nanofluid tank. So, to prevent this problem CMC as surfactant for MgO particles in nanofluid is used.
6. The MgO particles has high stability in the water-CMC fluid which gives a better heat exchange rate, and therefore it shows shows more enhancement of heat transfer compared to the other fluids.
7. The experimental results mention that the convective coefficient of heat transfer (h) is increased by raising the mass of the additives concentrations and the hot fluid volume flow rate. The heat transfer coefficient increases from (2532.4) at 8 L/min to (2771.71) 14 L/min for pure water for parallel flow under single phase flow effect.
    - The heat transfer coefficient enhances from (2879.15) at 8 L/min to (3142.32) 14 L/min after the addition of 0.5% CMC wt., the percentage of enhancement about (15%)
    - The heat transfer coefficient enhances from (3401.25) at 8 L/min to (3753.16) 14 L/min after the addition of 1% MgO vol., the percentage of enhancement about (28%).

  - The heat transfer coefficient enhances from (5062.57) at 8 L/min to (5545.24) 14 L/min after adding a 1% vol. of MgO and 0.5% CMC wt., the percentage of enhancement about (51%)

8. The case of counter direction investigates the overall coefficient is higher than the case of parallel direction for various hot fluid under single phase flow effect.
   - The pure water heat transfer coefficient ameliorates is about (4.2%).
   - The water-CMC fluid heat transfer coefficient ameliorates is about (3%).
   - The water-MgO fluid heat transfer coefficient ameliorates is about (2%).
   - The water-MgO-CMC fluid heat transfer coefficient ameliorates is about (2%).
9. The experimental results recommend that the convection heat transfer coefficient (h) is increased under two phases flow effect at air flow rate range (360 L/hr, 420 L/hr and 480 L/hr) and various flow conditions for different hot fluid types.
   - The pure water heat transfer coefficient (h) increases about (7%) for parallel flow and (3%) for counter flow.
   - The water-CMC fluid heat transfer coefficient (h) increases about (7%) for parallel flow and (6%) for counter flow.
   - The water-MgO fluid heat transfer coefficient (h) increases about (6%) for parallel flow and (6%) for counter flow.
   - The water-MgO-CMC fluid heat transfer coefficient (h) increases about (5%) for parallel flow and (5%) for counter flow.

10. The experimental results recommend that the effectiveness of heat exchanger (ε) was increased under effect of single and two phases flow at various flow condition. The effectiveness of better case presents according to the following:
    - The better case increases the effectiveness of parallel flow about (8%), and for counter flow about (9%) under single phase flow effect.
    - The better case increases the effectiveness of parallel flow about (5%), and for counter flow about (6%) under two phases flow effect.
11. The experimental results recommend that the inner pipe overall heat transfer coefficient (Ui) is increased under two phases flow effect and various flow conditions for better case.
    - The better case increases the overall heat transfer coefficient of parallel flow about (52%), and for counter flow about (52%) under single phase flow effect.
    - The better case increases the overall heat transfer coefficient of parallel flow about (51%), and for counter flow about (51%) under two phases flow effect.
12. The numerical results show the variation of pressure, temperature and velocity under various flow conditions.
13. The simulated model has given results similar to the experimental results with a maximum deviation of 7 %.

6.2 Suggestions for Future Work

Several suggestions could be considered for future works as follows:

1. Clarify the thermal performance of U-bend heat exchanger with hybrid nanofluids and surfactant, and presenting their effect on pumping power.
2. Developing heat transfer correlations.

3. Studying the different pipe shapes (elliptical, eggs shape, square, various pin fins on pipe surface).
4. Entropy generation can be studied experimentally.
5. Using pure metallic nanoparticles with its suitable surfactant because it has high thermal conductivity, which is about 50 times larger than that of oxides nanoparticles.
6. Using the water-CMC fluid in the shell side of heat exchanger.

REFERENCES

References

1. Ghani, S., et al., ***Experimental investigation of double-pipe heat exchangers in air conditioning applications. Energy and Buildings,*** 2018. 158: p. 801-811.
2. Louis, S.P., et al., ***Application of Nanofluids in Improving the Performance of Double-Pipe Heat Exchangers—A Critical Review.*** Materials, 2022. 15(19): p. 6879.
3. Gabir, M.M. and D. Alkhafaji. ***Comprehensive Review on Double Pipe Heat Exchanger Techniques.*** in Journal of Physics: Conference Series. 2021. IOP Publishing.
4. Zhang, Z., et al., ***Heat transfer enhancement in double-pipe heat exchanger by means of rotor-assembled strands.*** Chemical Engineering and Processing: Process Intensification, 2012. 60: p. 26-33.
5. Yadav, A.S., ***Effect of half length twisted-tape turbulators on heat transfer and pressure drop characteristics inside a double pipe U-bend heat exchanger.*** JJMIE, 2009. 3(1): p. 17-22.
6. Duangthongsuk, W. and S. Wongwises, ***An experimental investigation of the heat transfer and pressure drop characteristics of a circular tube fitted with rotating turbine-type swirl generators.*** Experimental thermal and fluid science, 2013. 45: p. 8-15.
7. El-Maghlany, W., et al., ***Experimental study for double pipe heat exchanger with rotating inner pipe.*** Int J Adv Sci Tech Res, 2012. 4(2): p. 507-524.
8. Bharadwaj, P., A. Khondge, and A. Date, ***Heat transfer and pressure drop in a spirally grooved tube with twisted tape insert.***

International Journal of Heat and Mass Transfer, 2009. 52(7-8): p. 1938-1944.

9. Shewale Omkar, M., et al., ***Experimental investigation of double-pipe heat exchanger with helical fins on the inner rotating tube.*** International Journal of Research in Engineering and Technology, ISSN, 2015: p. 2321-7308.
10. Kitagawa, A., et al., ***Heat transfer enhancement for laminar natural convection along a vertical plate due to sub-millimeter-bubble injection.*** Experiments in fluids, 2008. 45: p. 473-484.
11. Ghajar, A.J., ***Non-boiling heat transfer in gas-liquid flow in pipes: a tutorial.*** Journal of the Brazilian Society of Mechanical Sciences and Engineering, 2005. 27: p. 46-73.
12. Honkanen, M., ***Turbulent multiphase flow measurements with particle image velocimetry:*** application to bubbly flows. 2002: Tampereen teknillinen korkeakoulu.
13. Azzopardi, B., Multiphase flow. ***Chemical Engineering and Chemical Process Technology-Volume I:*** Fundamentals of Chemical Engineering, 2010: p. 97.
14. Awad, M. and S. Kazi, Two-phase flow. ***An overview of heat transfer phenomena,*** 2012. 783.
15. Holland, F. and R. Bragg, ***Fluid flow for chemical engineers.*** 1995: Elsevier.
16. Xuan, Y. and Q. Li, ***Heat transfer enhancement of nanofluids. International Journal of heat and fluid flow,*** 2000. 21(1): p. 58-64.
17. Mukherjee, S. and S. Paria, ***Preparation and stability of nanofluids-a review. IOSR Journal of Mechanical and civil engineering,*** 2013. 9(2): p. 63-69.

18. Yu, W. and H. Xie, ***A review on nanofluids: preparation, stability mechanisms, and applications.*** Journal of nanomaterials, 2012. 2012: p. 1-17.
19. Qiu, L., et al., ***A review of recent advances in thermophysical properties at the nanoscale: From solid state to colloids.*** Physics Reports, 2020. 843: p. 1-81.
20. Xuan, Y., Q. Li, and W. Hu, ***Aggregation structure and thermal conductivity of nanofluids.*** AIChE Journal, 2003. 49(4): p. 1038-1043.
21. Wole-Osho, I., et al., ***An experimental investigation into the effect of particle mixture ratio on specific heat capacity and dynamic viscosity of Al_2O_3-ZnO hybrid nanofluids. Powder Technology,*** 2020. 363: p. 699-716.
22. Yang, L., et al., ***An updated review on the influential parameters on thermal conductivity of nano-fluids.*** Journal of Molecular Liquids, 2019. 296: p. 111780.
23. Simpson, S., et al., ***Nanofluid thermal conductivity and effective parameters.*** Applied Sciences, 2018. 9(1): p. 87.
24. Mahian, O., et al., ***Recent advances in modeling and simulation of nanofluid flows-Part I: Fundamentals and theory.*** Physics reports, 2019. 790: p. 1-48.
25. Pil Jang, S. and S.U. Choi, ***Effects of various parameters on nanofluid thermal conductivity.*** 2007.
26. Keblinski, P., et al., ***Mechanisms of heat flow in suspensions of nano-sized particles (nanofluids).*** International journal of heat and mass transfer, 2002. 45(4): p. 855-863.
27. Xie, H., M. Fujii, and X. Zhang, ***Effect of interfacial nanolayer on the effective thermal conductivity of nanoparticle-fluid mixture.***

International Journal of Heat and Mass Transfer, 2005. 48(14): p. 2926-2932.

28. I Roumaissa, D., ***Transfert de chaleur d'un nanofluide dans un récipient conique.*** 2022, university center of abdalhafid boussouf-MILA.
29. Sheikholeslami, M., M. Gorji-Bandpy, and D.D. Ganji, ***Review of heat transfer enhancement methods: Focus on passive methods using swirl flow devices.*** Renewable and Sustainable Energy Reviews, 2015. 49: p. 444-469.
30. Abusafa, A., ***Effect of Pressure on the Performance of Passive Two-Phase Closed Thermosyphon System Using R-134a.*** Journal of Engineering Research and Technology, 2020. 7(1).
31. Iyengar, S.V. and C. Rutland, ***Effect of physical properties on spray models.*** 2013, SAE Technical Paper.
32. Rao, V.N. and B.R. Sankar, ***CFD analysis of CuO/water nanofluid flow in a double pipe U-Bend heat exchanger.*** Int. J. Dyn. Fluid, 2017. 13(1): p. 137-152.
33. Al-Shamani, A.N., et al., ***Nanofluids for improved efficiency in cooling solar collectors–a review.*** Renewable and Sustainable Energy Reviews, 2014. 38: p. 348-367.
34. Bianco, V., et al., ***Heat transfer enhancement with nanofluids "in Heat Transfer Enhancement with Nanofluids.*** 2015.
35. Ahmed, A., et al., ***Use of nanofluids in solar PV/thermal systems. International Journal of Photoenergy,*** 2019.
36. Cioncolini, A. and J.R. Thome, ***Prediction of the entrained liquid fraction in vertical annular gas–liquid two-phase flow.*** International Journal of Multiphase Flow, 2010. 36(4): p. 293-302.

37. Kashinsky, O., V. Randin, and A. Chinak, ***Heat transfer and shear stress in a gas-liquid flow in an inclined flat channel.*** Journal of Engineering Thermophysics, 2014. 23: p. 39-46.
38. Dizaji, H.S. and S. Jafarmadar, ***Heat transfer enhancement due to air bubble injection into a horizontal double pipe heat exchanger.*** International Journal of Automotive Engineering, 2014. 4(4): p. 902-910.
39. Ortiz-Vidal, L.E., N. Mureithi, and O. Rodriguez, ***Two-phase friction factor in gas-liquid pipe flow.*** Revista de Engenharia Térmica, 2014. 13(2): p. 81-88.
40. de Paula Jr, C. and L. Lima, ***Comparison analysis of correlations for interfacial friction factor applied in gas-liquid annular flow in vertical pipes.*** Revista de Engenharia Térmica, 2017. 16(2): p. 54-61.
41. Aliyu, A.M., et al., ***Interfacial friction in upward annular gas–liquid two-phase flow in pipes.*** Experimental Thermal and Fluid Science, 2017. 84: p. 90-109.
42. Wang, Y. and L. Guo, ***Theoretical and experimental research on interfacial shear stress and interfacial friction factor of gas-liquid two-phase wavy stratified flow in horizontal pipe.*** Heat and Mass Transfer, 2019. 55: p. 2117-2135.
43. Ribeiro, J., et al., ***A Two-Fluid Model for High-Viscosity Upward Annular Flow in Vertical Pipes.*** Energies 2021, 14, 3485. 2021, Note: MDPI stays neutral with regard to jurisdictional claims in published ….
44. Gawandare, A., M. Dange, and D. Nalawade, ***Heat transfers enhancement with different square jagged twisted tapes.*** Int. J. Eng. Res. Appl, 2014. 4(3): p. 619-624.

45. Bianco, V., et al., ***Heat transfer enhancement with nanofluids.*** 2015.
46. Corcione, M., Rayleigh-Bénard, ***convection heat transfer in nanoparticle suspensions.*** International Journal of Heat and Fluid Flow, 2011. 32(1): p. 65-77.
47. Garnett, J.M., XII. ***Colours in metal glasses and in metallic films. Philosophical Transactions of the Royal Society of London.*** Series A, Containing Papers of a Mathematical or Physical Character, 1904. 203(359-371): p. 385-420.
48. Jang, S.P. and S.U. Choi, ***Role of Brownian motion in the enhanced thermal conductivity of nanofluids.*** Applied physics letters, 2004. 84 (21): p. 4316-4318.
49. Hamilton, R.L. and O. Crosser, ***Thermal conductivity of heterogeneous two-component systems.*** Industrial & Engineering chemistry fundamentals, 1962. 1(3): p. 187-191.
50. Xuan, Y. and Q. Li, ***Investigation on convective heat transfer and flow features of nanofluids.*** J. Heat transfer, 2003. 125(1): p. 151-155.
51. Maiga, S.E.B., et al., ***Heat transfer enhancement by using nanofluids in forced convection flows.*** International journal of heat and fluid flow, 2005. 26(4): p. 530-546.
52. Buongiorno, J., ***Convective transport in nanofluids.*** 2006.
53. Duangthongsuk, W. and S. Wongwises, ***Heat transfer enhancement and pressure drop characteristics of*** TiO_2***–water nanofluid in a double-tube counter flow heat exchanger.*** International Journal of Heat and Mass Transfer, 2009. 52(7-8): p. 2059-2067.
54. Zamzamian, A., et al., ***Experimental investigation of forced convective heat transfer coefficient in nanofluids of*** Al_2O_3***/EG***

and CuO/EG in a double pipe and plate heat exchangers under turbulent flow. Experimental Thermal and Fluid Science, 2011. 35(3): p. 495-502.

55. Darzi, A.R., M. Farhadi, and K. Sedighi, ***Heat transfer and flow characteristics of Al_2O_3–water nanofluid in a double tube heat exchanger.*** International Communications in Heat and Mass Transfer, 2013. 47: p. 105-112.
56. Aghayari, R., et al., ***Heat transfer of nanofluid in a double pipe heat exchanger.*** International Scholarly Research Notices, 2014.
57. Albadr, J., S. Tayal, and M. Alasadi, ***Heat transfer through heat exchanger using Al_2O_3 nanofluid at different concentrations.*** Case Studies in Thermal Engineering, 2013. 1(1): p. 38-44.
58. Maddah, H., et al., ***Effect of twisted-tape turbulators and nanofluid on heat transfer in a double pipe heat exchanger.*** Journal of Engineering, 2014. 2014.
59. Sahin, B., E. Manay, and E.F. Akyurek, ***An experimental study on heat transfer and pressure drop of CuO-water nanofluid.*** Journal of Nanomaterials, 2016. 16(1): p. 336-336.
60. Huang, D., Z. Wu, and B. Sunden, ***Pressure drop and convective heat transfer of Al2O3/water and MWCNT/water nanofluids in a chevron plate heat exchanger.*** International journal of heat and mass transfer, 2015. 89: p. 620-626.
61. Asadi, A. and F. Pourfattah, ***Heat transfer performance of two oil-based nanofluids containing ZnO and MgO nanoparticles; a comparative experimental investigation.*** Powder Technology, 2019. 343: p. 296-308.
62. Rao, V.N. and B.R. Sankar, ***Heat transfer and friction factor investigations of CuO nanofluid flow in a double pipe U-bend***

heat exchanger. Materials Today: Proceedings, 2019. 18: p. 207-218.

63. Pattanayak, B., et al., ***Estimation of Nusselt number and effectiveness of double-pipe heat exchanger with Al_2O_3, CuO, TiO2, and ZnO–water based nanofluids.*** Heat Transfer, 2020. 49(4): p. 2228-2247.
64. Shirazi, R., ***Experimental study of exergetic performance of Al2O3 nanofluid in a double-pipe heat exchanger fitted by a new modified twisted tape.*** Heat Transfer, 2020. 49(5): p. 2813-2830.
65. Jassim, E.I. and F. Ahmed, ***Experimental assessment of Al_2O_3 and Cu nanofluids on the performance and heat leak of double pipe heat exchanger.*** Heat and Mass Transfer, 2020. 56: p. 1845-1858.
66. Ali, M.H. and R.E. Jalal, ***Experimental investigation of heat transfer enhancement in a double pipe heat exchanger with a twisted inner pipe.*** Heat Transfer, 2021. 50(8): p. 8121-8133.
67. Ding, Z., et al., ***Numerical simulation of nanofluids forced convection in a corrugated double-pipe heat exchanger.*** The Canadian Journal of Chemical Engineering, 2022. 100(8): p. 1954-1964.
68. Akhtari, M., M. Haghshenasfard, and M. Talaie, ***Numerical and experimental investigation of heat transfer of α-Al_2O_3/water nanofluid in double pipe and shell and tube heat exchangers.*** Numerical Heat Transfer, Part A: Applications, 2013. 63(12): p. 941-958.
69. Khedkar, R.S., S.S. Sonawane, and K.L. Wasewar, ***Heat transfer study on concentric tube heat exchanger using TiO2–water based nanofluid.*** International communications in Heat and Mass transfer, 2014. 57: p. 163-169.

70. Davarnejad, R. and M. Jamshidzadeh, ***CFD modeling of heat transfer performance of MgO-water nanofluid under turbulent flow.*** Engineering Science and Technology, an International Journal, 2015. 18(4): p. 536-542.
71. Ali, F.H., H.K. Hamzah, and A. Abdulkadhim, ***Numerical study of mixed convection nanofluid in an annulus enclosure between outer rotating cylinder and inner corrugation cylinder.*** Heat Transfer—Asian Research, 2019. 48(1): p. 343-360.
72. Ramirez-Tijerina, R., et al., ***Numerical study of heat transfer enhancement for laminar nanofluids flow.*** Applied Sciences, 2018. 8(12): p. 2661.
73. Kaska, S.A., R.A. Khalefa, and A.M. Hussein, ***Hybrid nanofluid to enhance heat transfer under turbulent flow in a flat tube.*** Case Studies in Thermal Engineering, 2019. 13: p. 100398.
74. Naik, B., et al. ***Numerical Investigation of double pipe heat exchanger with different nanofluids.*** in IOP Conference Series: Earth and Environmental Science. 2020. IOP Publishing.
75. Bendaraa, A., M.M. Charafi, and A. Hasnaoui, ***Numerical and experimental investigation of alumina-based nanofluid effects on double-pipe heat exchanger thermal performances.*** SN Applied Sciences, 2021. 3: p. 1-10.
76. Semmar, N., J. Tanguier, and M. Rigo, ***Specific heat of carboxymethyl cellulose and Carbopol aqueous solutions.*** Thermochimica acta, 2003. 402(1-2): p. 225-235.
77. Semmar, N., J. Tanguier, and M. Rigo, ***Analytical expressions of specific heat capacities for aqueous solutions of CMC and CPE.*** Thermochimica acta, 2004. 419(1-2): p. 51-58.
78. Reddy, M.C.S. and V.V. Rao, ***Experimental investigation of heat transfer coefficient and friction factor of ethylene glycol water***

based TiO2 nanofluid in double pipe heat exchanger with and without helical coil inserts. International Communications in Heat and Mass Transfer, 2014. 50: p. 68-76.

79. Kholiya, K., J. Chandra, and S. Verma, ***Analysis of equation of states for the suitability at high pressure: MgO as an example.*** The Scientific World Journal, 2014. 2014.
80. Qiao, Z., et al., ***The Effect of Carboxymethyl Cellulose Addition on the Properties of Starch-based Wood Adhesive.*** Bio Resources, 2014. 9(4).
81. Akbari, O.A., et al., ***The effect of velocity and dimension of solid nanoparticles on heat transfer in non-Newtonian nanofluid.*** Physica E: Low-Dimensional Systems and Nanostructures, 2017. 86: p. 68-75.
82. Das, P.K., et al., ***Experimental investigation of thermophysical properties of Al_2O_3–water nanofluid: Role of surfactants.*** Journal of Molecular Liquids, 2017. 237: p. 304-312.
83. Arya, H., M. Sarafraz, and M. Arjomandi, ***Heat transfer and fluid flow of MgO/ethylene glycol in a corrugated heat exchanger.*** Journal of Mechanical Science and Technology, 2018. 32: p. 3975-3982.
84. Suppiah, K., et al., ***Thermal properties of carboxymethyl cellulose (CMC) filled halloysite nanotube (HNT) bio-nanocomposite films.*** Materials Today: Proceedings, 2019. 16: p. 1611-1616.
85. Gupta, S. and P.K. Varshney, ***Effect of plasticizer on the conductivity of carboxymethyl cellulose-based solid polymer electrolyte.*** Polymer Bulletin, 2019. 76(12): p. 6169-6178.
86. Arya, H., et al., ***Heat transfer and pressure drop characteristics of MgO nanofluid in a double pipe heat exchanger.*** Heat and Mass Transfer, 2019. 55: p. 1769-1781.

87. Svetlov, S., N. Levina, and A. Pivovarov, ***Determination of Thermal Conductivity Coefficient of Moist Sodium Carboxymethyl Cellulose.*** Chemical and Petroleum Engineering, 2019. 54(9-10): p. 723-727.
88. Arya, H., et al., ***Performance index improvement of a double-pipe cooler with MgO/water-ethylene glycol (50:50) nano-suspension.*** Propulsion and Power Research, 2020. 9(1): p. 75-86.
89. Ali, A.Y.M., et al. ***Effect of using MgO-oil nanofluid on the performance of a counter-flow double pipe heat exchanger.*** in Key Engineering Materials. 2019. Trans Tech Publ.
90. Akinpelu, F., R. Alabison, and O. Olaleye. ***Thermophysical properties of nanoparticles in carboxylmethyl cellulose water mixture for heat enhancement applications.*** in IOP Conference Series: Materials Science and Engineering. 2020. IOP Publishing.
91. Hasan, B.O., H.S. Majdi, and M.M. Hathal, ***Study on oil fouling in a double pipe heat exchanger with mitigation by a surfactant.*** Heat Transfer, 2020. 49(5): p. 2645-2658.
92. Li, Y., et al. ***Study on influence of dispersants on stability, thermal conductivity and viscosity of BN/EG nanofluids.*** in IOP Conference Series: Materials Science and Engineering. 2020. IOP Publishing.
93. Holman, J.P., ***Experimental Methods for Engineers EIGHTH EDITION.*** 2021.
94. Kadhim, Z.K., M.S. Kassim, and A.Y.A. Hassan, ***Effect of (MgO) nanofluid on heat transfer characteristics for integral finned tube heat exchanger.*** Int. J. Mech. Eng. Technol, 2016. 7: p. 11-24.
95. Wu, Z., L. Wang, and B. Sundén, ***Pressure drop and convective heat transfer of water and nanofluids in a double-pipe helical***

heat exchanger. Applied thermal engineering, 2013. 60(1-2): p. 266-274.

96. Maayah, E.S., H.M. Duwairi, and B. Maayah, ***Analytical model of solar energy storage using non—Newtonian Fluid in a saturated porous media in fully developed region: carboxymethyl cellulose (CMC) and graphite model.*** AIMS Energy, 2021: p. 213-237.
97. Al-Jibory, M., R. Al-Turaihi, and H. Al-Jibory. ***An experimental and numerical study for two phase flow (water-air) in rectangular ducts with compound turbulators.*** in IOP Conference Series: Materials Science and Engineering. 2018. IOP Publishing.
98. Cengel, Y.A., A.J. Ghajar, and M. Kanoglu, ***Heat and mass transfer: fundamentals and applications.*** 2011
99. Hadi H. Sh., ***Experimental and numerical study to the heat transfer enhancement of double pipe heat exchanger with bubbly flow and nanofluid,*** M.Sc. Thesis, Babylon University, 2020.

APPENDICES

Appendix A

Thermo-Physical Properties of Water and Air

Thermo-physical properties of water presented in table (A-1) for various temperature.

Table (A-1): Thermo-physical water properties [98].

Property / Temperature (°C)	Density (Kg/m^3)	Viscosity (kg/m.s) x 10^{-3}	Specific heat (j/kg.K)	Thermal conductivity (W/m.K)
25	997.1	0.8095	4183	0.5948
50	988	0.5042	4181	0.6305

Thermo-physical properties of air presented in table (A-2) at temperature 25°C.

Table (A-2): Physical properties of air at 25°C [98].

Density (Kg/m^3)	Viscosity (kg/m.s) x 10^{-5}	Specific heat (j/kg.K)	Thermal conductivity (W/m.K)
1.184	1.849	1007	0.02551

Appendix B

Calibrations

Pressure Regulators Calibration

All measuring instruments must be calibrated for determining their accuracy. The accuracy quantifies an instrument’s ability to measure a known value or standard. Standards define units of measurement and are essential in building measuring scales. The calibration operation for this device is done in Central Organization for Standardization and Quality Control.

Ministry of Higher Education
and Scientific Research
University of Babylon
Faculty of Graduate Studies

جمهورية العراق

زارة التعليم العالي والبحث العلمي
جامعة بابل
كلية الدراسات العليا
شعبة شؤون الطلبة

No:
Date:

العدد : ٨١٧
التاريخ : ٢٠١٩/٢/١٤

الى /الجهاز المركزي للتقييس والسيطرة النوعية / بغداد

م/تسهيل مهمة

تحية طيبة . . .

يرجى تفضلكم بتسهيل مهمة طالب الدراسات العليا (حيدر شاكر هادي صالح) المقبول في كلية الهندسة / الماجستير / قسم الهندسة الميكانيكية للعام الدراسي (٢٠١٧-٢٠١٨) لاجل معايرة منظم الضغط عدد(١) (Regulator pressure) ومعايرة مقياس تدفق الهواء عدد(١) (Rir flowmeter) ومعايرة مقياس تدفق السوائل عدد(٢) (Flowmeter)لغرض اكمال متطلبات بحثه راجين تقديم المساعدة الممكنة من قبلكم شاكرين ومقدرين حسن تواصلكم معنا .

تفضلوا بقبول وافر التحية والاحترام

الأستاذ الدكتور
محمد منصور كاظم
معاون عميد كلية الدراسات العليا
٢٠١٩/٢/١٣

نسخة منه الى//

- كلية الهندسة اشارة الى تأييدكم على استمارة الطالب اعلاه بتاريخ ٢٠١٩/٢/١٢ للتفضل بالعلم ومتابعة دوام الطالب من قبلكم . . . مع الاحترام .
- كلية الدراسات العليا /شعبة شؤون الطلبة مع الاوليات . . . مع الاحترام
- الصادرة"

زهراء

graduatefaculty@uobabylon.edu.iq
graduatefaculty@gmail.com

جمهورية العراق

وزارة التخطيط
الجهاز المركزي للتقييس والسيطرة النوعية

العدد : ٢١٥٩
التاريخ م : ٥/ ٣/ ٢٠١٩
هـ : / /

الدائره : التقييس
القسم : المقاييس

الى/ جامعة بابل / كلية الدراسات العليا

م/ معايرة مقاييس

يهدي الجهاز اطيب تحياته ...

إشارة الى كتابيكم المرقمين (٨١٦)و(٨١٧) في ١٤ /٢/ ٢٠١٩
نود اعلامكم انه قد تم معايرة مقياس ضغط عدد (٣) وكانت النتيجة كما مبين في شهادات المعايرة المرافقة للكتاب علما ان فترة المعايرة الدورية هي سنة من تاريخ المعايرة .
تم تسديد اجور المعايرة البالغه (٣٣٠٠٠) ثلاثة وثلاثون الف دينار فقط بموجب الوصل المرقم (١٥٤٧٧) في ٢٠ / ٢ /٢٠١٩.

مع التقدير........

الاجهزة :-
مقياس ضغط عدد (٣)

المرافقات:-
- شهادة معايرة عدد (٣) بالرقم (PRE/119/2019- PRE/117/2019)

م. مدير عام دائرة التقييس
كيلان هاشم مصطفى
٤/٣/٢٠١٩

نسخة منه الى /
دائرة التقييس / قسم المقاييس/ شعبة قياسات الكتلة والضغط / مختبر قياسات الضغط .

العراق ـ بغداد ـ الجادرية ـ ص . ب (١٣٠٣٢) ـ البريد الالكتروني : www.cosqc.gov.iq
هاتف ٨٤ / ٨٣ / ٨٢ / ٨١ / ٧٧٨٥١٨٠ تليفاكس ٧٧٦١٩٨١ cosqc@cosqc.gov.iq

جمهورية العراق

وزارة التخطيط
الجهاز المركزي للتقييس والسيطرة النوعية

العدد : ٢٠ ح ٧
التاريخ م : ٢٠١٩/٧/٢٤
هـ : / /

الدائره : التقييس
القسم : المقاييس

الى/ جامعة بابل / كلية الدراسات العليا

و ٣٦٨٤
٨/١

م/ معايرة مقاييس

يهدي الجهاز اطيب تحياته ...

الحاقاً بكتابنا المرقم(٢١٥٩)في ٢٠١٩/٣/٥
نود اعلامكم مايلي:-
١- انه قد تم معايرة مقياس ضغط عدد (١)المشار اليه في كتابكم المرقم(٨١٧)في(٢٠١٩/٢/١٤) والمبين ادناه.
تم تسديد اجورالمعايرة البالغة(١١٠٠٠)أحد عشر الف دينار فقط بموجب الوصل المرقم (١٥٤٧٧) في(٢٠١٩/٢/٢٠).
٢- نعتذر عن معايرة جهازي قياس تدفق الهواء والسوائل وذلك لعدم توفر الامكانية في الوقت الحاضر.

الاجهزة :-
مقياس ضغط عدد (١) بالرقم (PRE/117/2019)

مع التقدير........

المرافقات:-
شهادة معايرة عدد (١).

ع. مدير عام دائرة التقييس
حنان عبد الجليل عبد اللطيف
٢٠١٩/٧/٢٤

نسخة منه الى /
- الطالب (حيدر شاكر هادي صالح) /للعلم...مع التقدير.
- مكتب المدير العام/للعلم....مع التقدير.
- شعبة قياسات الكتلة والضغط / مختبر قياسات الضغط /مع الاوليات...لطفا.

العراق - بغداد - الجادرية - ص . ب (١٣٠٣٢) - البريد الالكتروني : www.cosqc.gov.iq
هاتف ٨٤ / ٨٣ / ٨٢ / ٨١ / ٧٧٨٥١٨٠ تليفاكس ٧٧٦١٩٨١ cosqc@cosqc.gov.iq

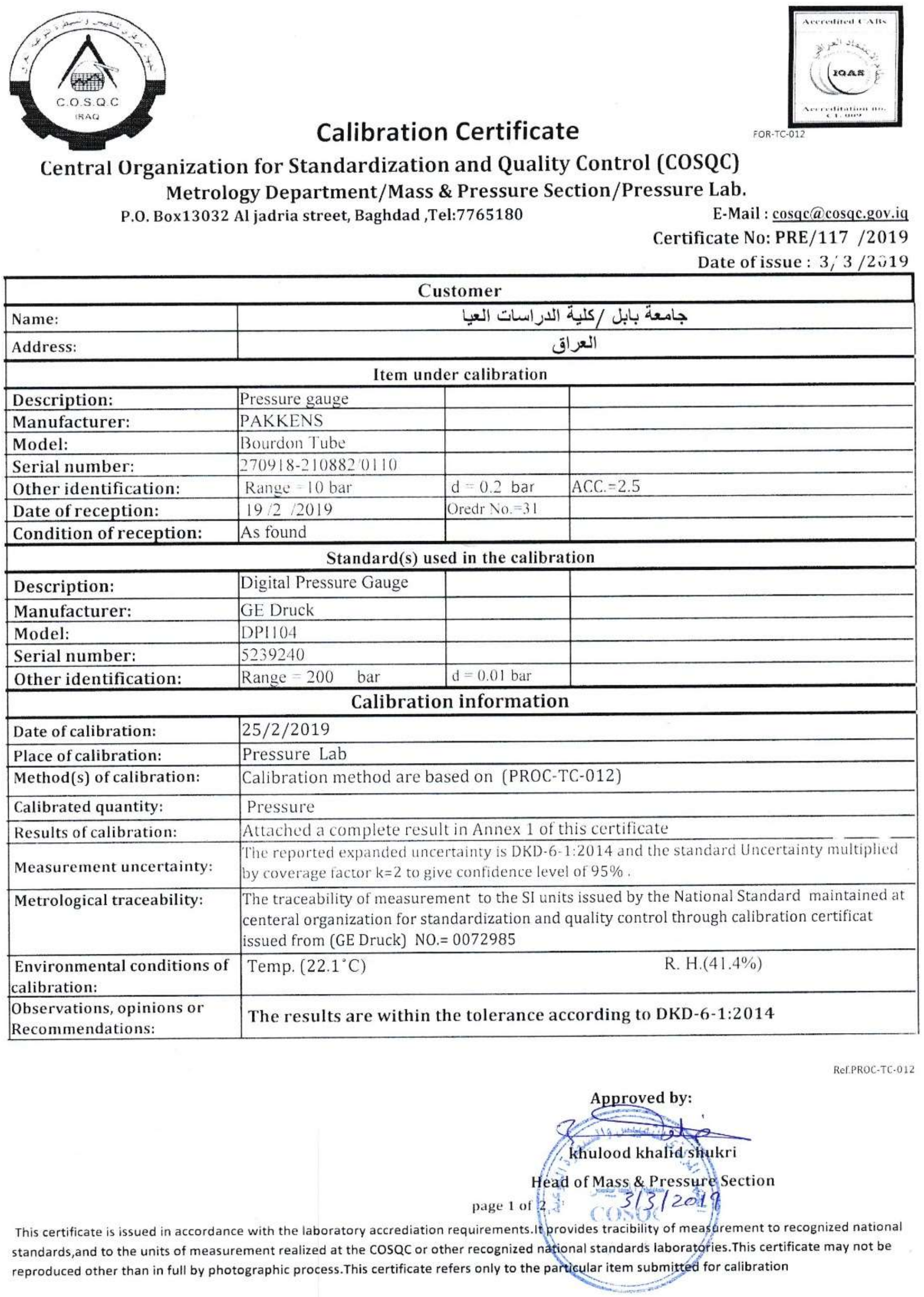

FOR-TC-012

Calibration Certificate

Central Organization for Standardization and Quality Control (COSQC)
Metrology Department/Mass & Pressure Section/Pressure Lab.
P.O. Box13032 Al jadria street, Baghdad ,Tel:7765180
E-Mail : cosqc@cosqc.gov.iq

Certificate No: PRE/117 /2019
Date of issue : 3/ 3 /2019

Customer

Name:	جامعة بابل /كلية الدراسات العيا
Address:	العراق

Item under calibration

Description:	Pressure gauge		
Manufacturer:	PAKKENS		
Model:	Bourdon Tube		
Serial number:	270918-210882/0110		
Other identification:	Range =10 bar	d = 0.2 bar	ACC.=2.5
Date of reception:	19 /2 /2019	Oredr No.=31	
Condition of reception:	As found		

Standard(s) used in the calibration

Description:	Digital Pressure Gauge		
Manufacturer:	GE Druck		
Model:	DPI104		
Serial number:	5239240		
Other identification:	Range = 200 bar	d = 0.01 bar	

Calibration information

Date of calibration:	25/2/2019
Place of calibration:	Pressure Lab
Method(s) of calibration:	Calibration method are based on (PROC-TC-012)
Calibrated quantity:	Pressure
Results of calibration:	Attached a complete result in Annex 1 of this certificate
Measurement uncertainty:	The reported expanded uncertainty is DKD-6-1:2014 and the standard Uncertainty multiplied by coverage factor k=2 to give confidence level of 95% .
Metrological traceability:	The traceability of measurement to the SI units issued by the National Standard maintained at centeral organization for standardization and quality control through calibration certificat issued from (GE Druck) NO.= 0072985
Environmental conditions of calibration:	Temp. (22.1˚C) R. H.(41.4%)
Observations, opinions or Recommendations:	**The results are within the tolerance according to DKD-6-1:2014**

Ref.PROC-TC-012

Approved by:
khulood khalid shukri
Head of Mass & Pressure Section
3/3/2019

page 1 of 2

This certificate is issued in accordance with the laboratory accrediation requirements.It provides tracibility of measurement to recognized national standards,and to the units of measurement realized at the COSQC or other recognized national standards laboratories.This certificate may not be reproduced other than in full by photographic process.This certificate refers only to the particular item submitted for calibration

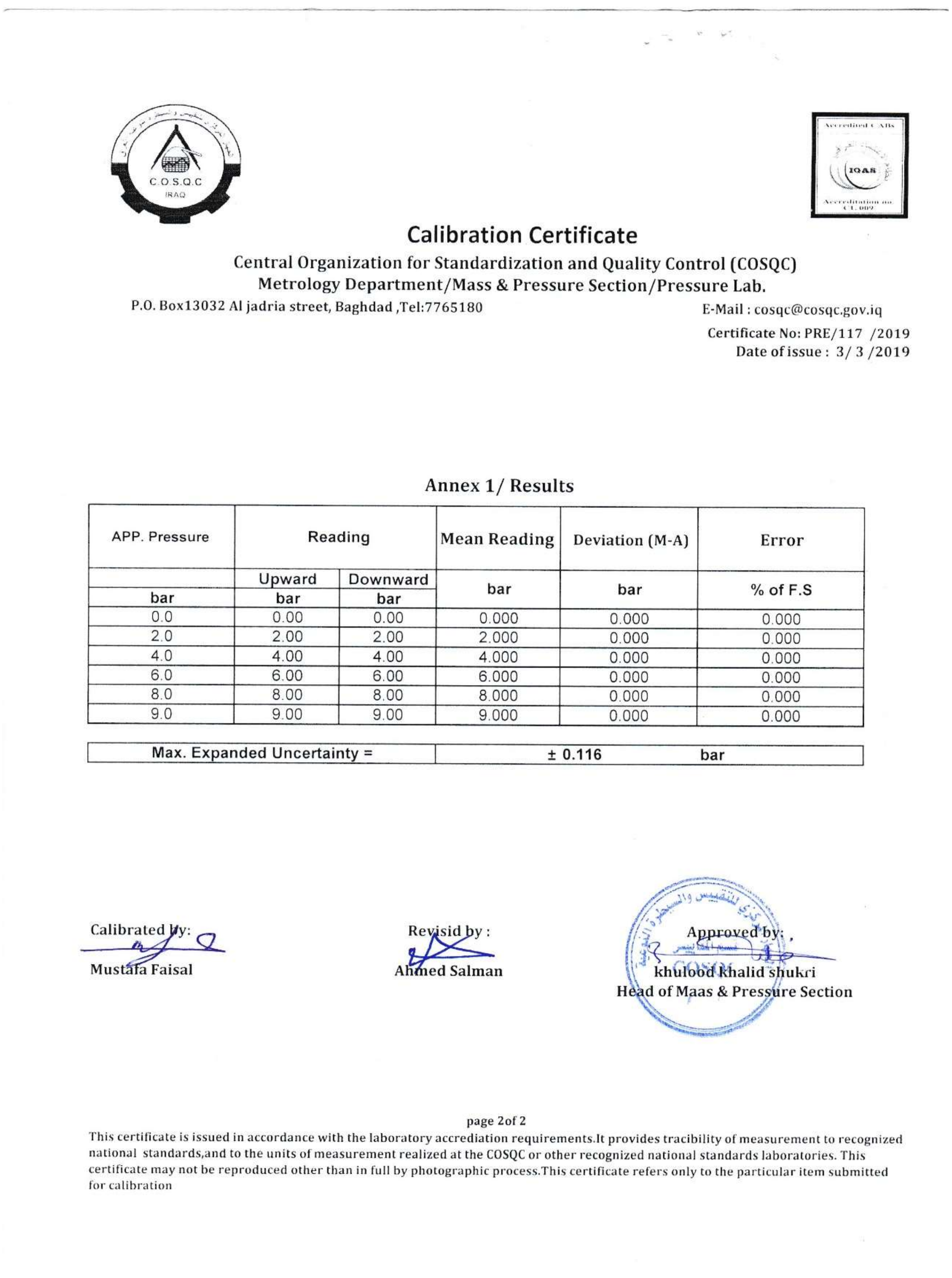

Calibration Certificate

Central Organization for Standardization and Quality Control (COSQC)
Metrology Department/Mass & Pressure Section/Pressure Lab.
P.O. Box13032 Al jadria street, Baghdad ,Tel:7765180
E-Mail : cosqc@cosqc.gov.iq

Certificate No: PRE/117 /2019
Date of issue : 3/ 3 /2019

Annex 1/ Results

APP. Pressure	Reading		Mean Reading	Deviation (M-A)	Error
	Upward	Downward			
bar	bar	bar	bar	bar	% of F.S
0.0	0.00	0.00	0.000	0.000	0.000
2.0	2.00	2.00	2.000	0.000	0.000
4.0	4.00	4.00	4.000	0.000	0.000
6.0	6.00	6.00	6.000	0.000	0.000
8.0	8.00	8.00	8.000	0.000	0.000
9.0	9.00	9.00	9.000	0.000	0.000

Max. Expanded Uncertainty =	± 0.116 bar

Calibrated by:
Mustafa Faisal

Revisid by :
Ahmed Salman

Approved by:
khulood khalid shukri
Head of Maas & Pressure Section

page 2of 2

This certificate is issued in accordance with the laboratory accrediation requirements.It provides tracibility of measurement to recognized national standards,and to the units of measurement realized at the COSQC or other recognized national standards laboratories. This certificate may not be reproduced other than in full by photographic process.This certificate refers only to the particular item submitted for calibration

Ministry of Higher Education and Scientific Research
University of Babylon
College of Engineering

وزارة التعليم العالي والبحث العلمي
جامعة بابل
كلية الهندسة
شعبة الدراسات العليا

Ref. no. :
Date : / /

العدد : ٢٥٥٣
التاريخ : ٨/ ٣/ ٢١ م

جامعة بابل / كلية الهندسة
الصادرة

الى/ كلية هندسة المواد/قسم البوليمر

م/ ابداء مساعدة

تحية طيبة. . .

يرجى تفضلكم بإبداء المساعدة الممكنة لطالب الدراسات العليا (الدكتوراه) في كليتنا/ قسم الهندسة الميكانيكية/ قدرة (مصطفى محمد جابر) لغرض اجراء الفحوصات الخاصة بأطروحته لغرض اكمال متطلبات البحث العلمي الخاص بالطالب اعلاه . . . شاكرين تعاونكم معنا . . .

أ. م. د. علي حسون نهاب
معاون العميد للشؤون العلمية والدراسات العليا
٢٠٢١\٣\٨

صورة عنه الى//

- قسم الهندسة الميكانيكية// اشارة الى هامشكم المثبت على أصل الطلب المقدم بتاريخ ٢٠٢١/٣/٤ للتفضل بالعلم. . مع الاحترام.
- شعبة الدراسات العليا . . . مع الاوليات.
- الاضبارة الشخصية الخاصة بالطالبة

Telephone number + 96430254387
P.O.Box No 4 Hilla - Iraq

E-mail : engineering@uobabylon.edu.iq

هاتف +٩٦٤٣٠٢٥٤٣٨٧
ص.ب. ٤ الحلة - محافظة بابل - العراق

www.uobabylon.edu.iq

Appendix C

Calibrations Tables & Curves

Table (C-1) for channel No.1 and table (C-2) for channel No.7. Figures (C-1) and (C-2) represent the calibration curve of channels No.1 and No.7 respectively.

Table (C-1): The temperature values of two devices for channel No.1.

No.	Reads of Data logger (°C)	Reads of Thermometer Device (°C)
1	26.2	27
2	37.5	38.5
3	45.7	46.9
4	58.9	59
5	64.6	65.5

Table (C-2): The temperature values of two devices for channel No.7.

No.	Reads of Data logger (°C)	Reads of Thermometer Device (°C)
1	23.7	24.5
2	33.4	35
3	42.5	43.5
4	54.9	55
5	61.6	62.5

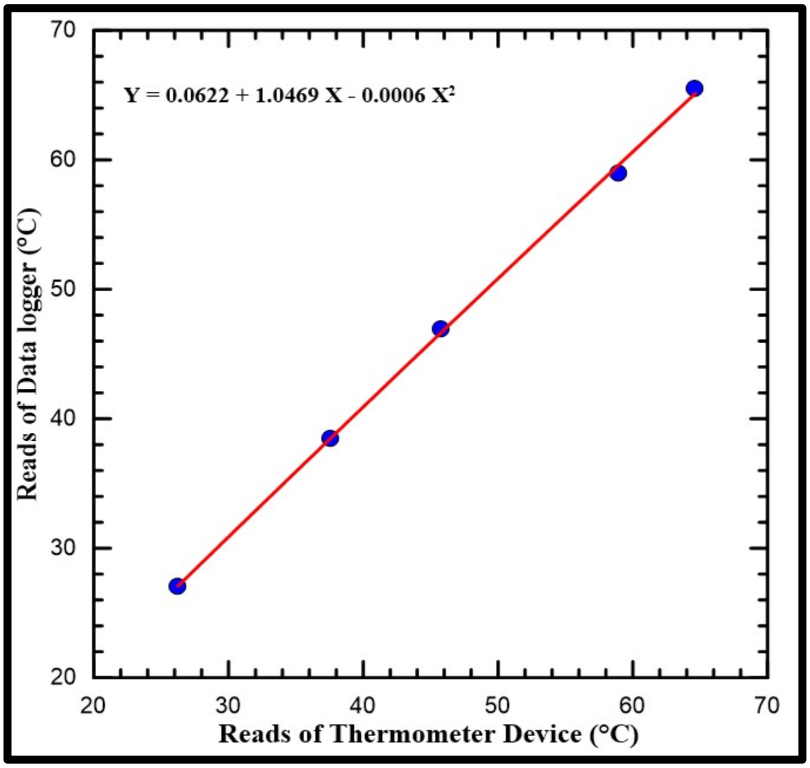

Figure (C-1): Calibration curve for channel No.1.

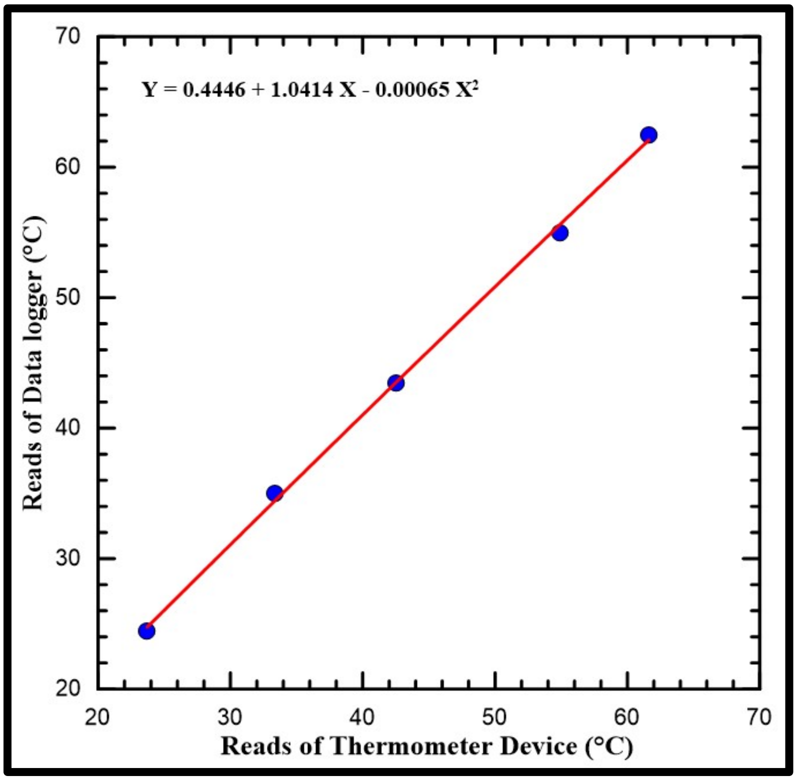

Figure (C-2): Calibration curve for channel No.7.

The calibration data for pressure taking from transducer and manometer at the same condition represents in table (C-3). Figure (C-3) presents the recorded values of the two devices.

Table (C-3): Pressure values of two devices

Manometer Reading (Kpa)	Pressure Sensor (Kpa)
1	0.97
1.5	1.55
2	1.932
2.5	2.587
3	2.91
3.5	3.608
4	3.84

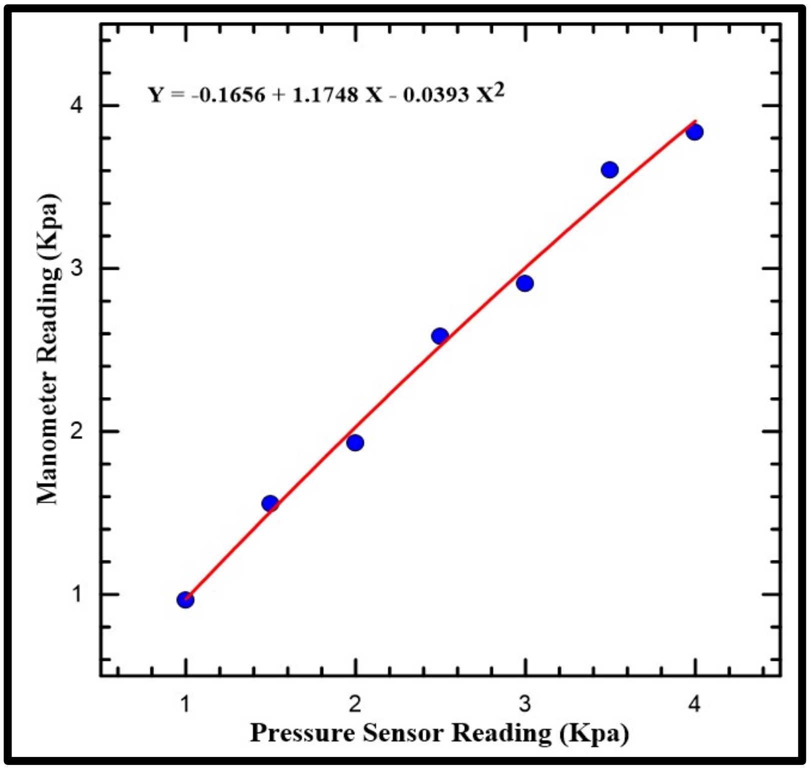

Figure (C-3): Calibration curve of pressure sensor.

The calibration data for water flow meter at the same condition represents in table (C-3). Figure (C-3) presents the recorded values of the two devices.

Table (C-4): Different values of the water discharge.

No.	Measured Discharge of water (L/min)	Measured Discharge of water by Flow Meter (L/min)
1	6.2	6
2	8.15	8
3	10.3	10
4	11.8	12
5	14.18	14
6	16.07	16
7	17.88	18
8	20.4	20

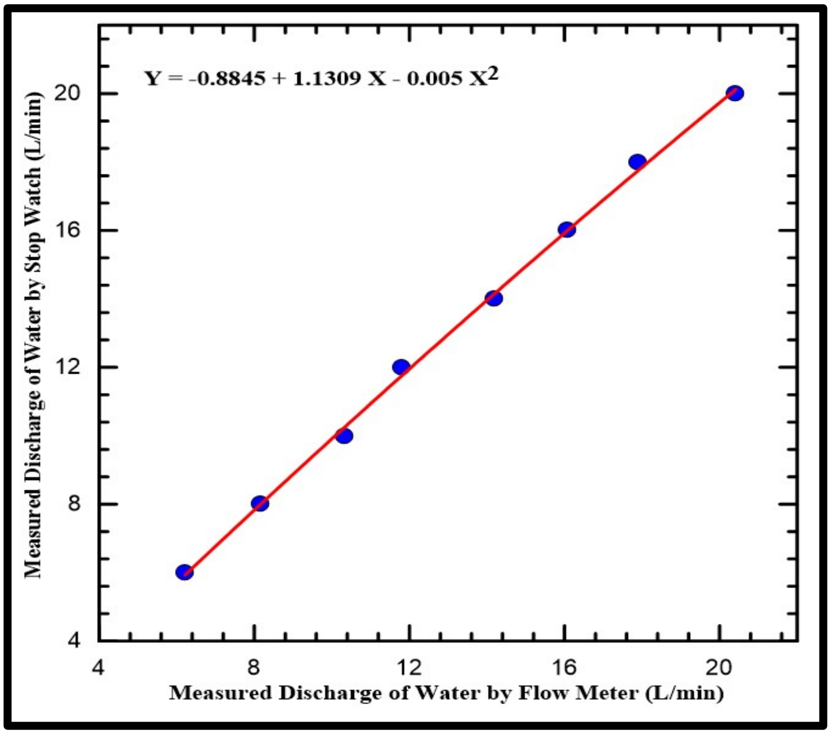

Figure (C-4): Flow meter accuracy reading.

The calibration data for air flow meter at the same condition represents in table (C-3). Figure (C-3) presents the recorded values of the two devices

Table (C-5): Different values of the air discharge.

o.	Measured Discharge of Air by orifice (L/hr)	Measured Discharge of Air by Flow Meter (L/hr)
	381.6	360
	451.2	480
	564	600
	763.2	720
	789.6	840
	1017.6	960

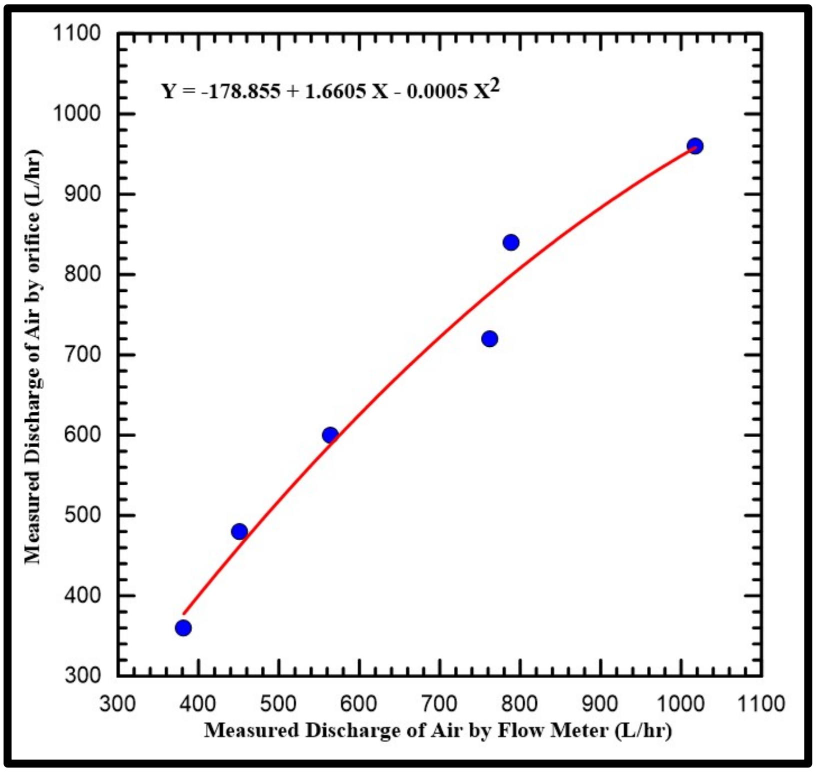

Figure (C-5): The calibration curve for air flow meter, which is used for different air flow rate.

Appendix D

Thermo-physical properties of (MgO-CMC/Water) Nanofluid

Thermo-physical properties of MgO nanoparticles presented in table (D-1).

Tables (D-1): Properties for MgO nanoparticle [59,94].

Material	**ρ (kg/m^3)**	**C_p (J/kg °C)**	**k (W/m.°C)**	**μ (kg/m.s) x10^{-3}**
MgO	**3580**	**955**	**48.4**	**0**

The mass of MgO nanoparticles presented in table (D-2) that need to distilled in pure water.

Table (D-2): Mass of each concentration add to thirty liters of distilled water.

φ%	0.125%	0.25%	0.5%	1%
Mass (gram)	136.05	272.44	546.25	1098.02

Thermo-physical properties of the water-MgO fluid presented in tables from (D-3) to (D-6) at temperature 50°C.

Table (D-3): Experimental and empirical results of density at 50 °c.

Material	Water-MgO fluid			
Nanoparticle's concentration (vol %)	0.125%	0.25%	0.5%	1%
Experimental results of density ρ (kg/m^3)	995.74	998.98	1005.46	1018.42
Empirical results of density ρ (kg/m^3)	991.24	994.48	1000.96	1013.92

Table (D-4): Experimental and empirical results of specific heat at 50 ºc.

Material	Water-MgO fluid			
Nanoparticle’s concentration (vol %)	0.125%	0.25%	0.5%	1%
Experimental results of Specific heat Cp (kJ/kg.K)	4166.446	4151.977	4123.32	4067.105
Empirical results of Specific heat Cp (kJ/kg.K)	4166.436	4151.967	4123.31	4067.095

Table (D-5): Experimental and empirical results of dynamic viscosity at 50 ºc.

Material	Water-MgO fluid			
Nanoparticle’s concentration (vol %)	0.125%	0.25%	0.5%	1%
Experimental results of dynamic viscosity μ (N.s/m2)	0.000587	0.000588	0.000589	0.000592
Empirical results of dynamic viscosity μ (N.s/m2)	0.000547684	0.000548368	0.000549735	0.00055247

Table (D-6): Experimental and empirical results of thermal conductivity at 50 ºc.

Material	Water-MgO fluid			
Nanoparticle’s concentration (vol %)	0.125%	0.25%	0.5%	1%
Experimental results of Thermal conductivity W/m.k	0.6528	0.6551	0.6598	0.6692
Empirical results of Thermal conductivity W/m.k	0.6463	0.6486	0.6533	0.6627

Thermo-physical properties of CMC particles presented in table (D-7).

Table (D-7): Properties for carboxymethyl cellulose (CMC) [96].

Material	ρ (kg/m^3)	C_p (J/kg °C)	k (W/m.°C)	μ (kg/m.s) x 10^{-3}
CMC	**1020**	**4.4**	**0.7**	**0.25**

The mass of CMC nanoparticles presented in table (D-8) that need to distilled in pure water.

Table (D-8): Mass of each concentration add to thirty litter of distilled water.

φ%	0.2 %	0.5%
Mass (gram)	60	150

The experimental thermo-physical properties of the water-CMC fluid presented in tables from (D-9) to (D-12) at temperature 50°C.

Table (D-9): Experimental results of density at 50 ºc.

Material	Water-CMC fluid	
CMC powder concentration (wet %)	**0.2%**	**0.5%**
ρ (kg/m^3)	988.37	991.5

Table (D-10): Experimental results of specific heat at 50 ºc.

Material	Water-CMC fluid	
CMC powder concentration (wet %)	**0.2%**	**0.5%**
Cp (kj/kg.k)	4181.878	4196.398

Table (D-11): Experimental results of dynamic viscosity at 50 ºc.

Material	Water-CMC fluid	
CMC powder concentration (wet %)	**0.2%**	**0.5%**
μ (N.s/m^2)	0.00103	0.001328

Table (D-12): Experimental and empirical results of thermal conductivity at 50 ºc.

Material	Water-CMC fluid	
CMC powder concentration (wet %)	**0.2%**	**0.5%**
k (W/m.K)	0.645	0.651

The experimental and empirical thermo-physical properties of the water-MgO-CMC fluid presented in tables from (D-13) to (D-16) at temperature 50°C.

Table (D-13): Experimental and empirical results of density at 50 ºc.

Material	Water-MgO-CMC fluid			
CMC powder concentration (wet %)	0.2%			
Nanoparticle's concentration (vol %)	0.125%	0.25%	0.5%	1%
Experimental results of density ρ (kg/m^3)	996.059	999.3	1005.778	1018.736
Empirical results of density ρ (kg/m^3)	991.609	994.85	1001.328	1014.286
CMC powder concentration (wet %)	0.5%			
Nanoparticle's concentration (vol %)	0.125%	0.25%	0.5%	1%
Experimental results of density ρ (kg/m^3)	999.185	1002.42	1008.89	1021.835
Empirical results of density ρ (kg/m^3)	994.735	997.971	1004.442	1017.385

Table (D-14): Experimental and empirical results of specific heat at 50 ºc.

Material	Water-MgO-CMC fluid			
CMC powder concentration (wet %)	0.2%			
Nanoparticle's concentration (vol %)	0.125%	0.25%	0.5%	1%
Experimental results of Specific heat Cp (kJ/kg.K)	4167.325	4152.858	4124.204	4067.993
Empirical results of Specific heat Cp (kJ/kg.K)	4167.315	4152.848	4124.1935	4067.983
CMC powder concentration (wet %)	0.5%			
Nanoparticle's concentration (vol %)	0.125%	0.25%	0.5%	1%
Experimental results of Specific heat Cp (kJ/kg.K)	4181.82	4167.338	4138.643	4082.348
Empirical results of Specific heat Cp (kJ/kg.K)	4181.816	4167.328	4138.633	4082.338

Table (D-15): Experimental and empirical results of dynamic viscosity at 50 ºc.

Material	Water-MgO-CMC fluid			
CMC powder concentration (wet %)	0.2%			
Nanoparticle's concentration (vol %)	0.125%	0.25%	0.5%	1%
Experimental results of dynamic viscosity µ (N.s/m2)	0.001056	0.001063	0.001074	0.001082
Empirical results of dynamic viscosity µ (N.s/m2)	0.00103	0.001032	0.001034	0.00104
CMC powder concentration (wet %)	0.5%			
Nanoparticle's concentration (vol %)	0.125%	0.25%	0.5%	1%
Experimental results of dynamic viscosity µ (N.s/m2)	0.00137	0.001382	0.001389	0.001396
Empirical results of dynamic viscosity µ (N.s/m2)	0.00133	0.001332	0.001335	0.001342

Table (D-16): Experimental and empirical results of thermal conductivity at 50 ºc.

Material	Water-MgO-CMC fluid			
CMC powder concentration (wet %)	0.2%			
Nanoparticle’s concentration (vol %)	0.125%	0.25%	0.5%	1%
Experimental results of Thermal conductivity W/m.k	0.6538	0.6561	0.6608	0.6702
Empirical results of Thermal conductivity W/m.k	0.6473	0.6496	0.6543	0.6637
CMC powder concentration (wet %)	0.5%			
Nanoparticle’s concentration (vol %)	0.125%	0.25%	0.5%	1%
Experimental results of Thermal conductivity W/m.k	0.7013	0.7037	0.7088	0.7189
Empirical results of Thermal conductivity W/m.k	0.6948	0.6972	0.7023	0.7124

Appendix E

Estimating Uncertainties

Uncertainty Equations

From **Holman [98]**

- **The Mean (x)**

$$\boldsymbol{\bar{x}_{mean} = x_{average} = \frac{\sum_1^n x_i}{n}}$$

Where:

x_i: is the values of each measurement.

n: is the total number of measurements of x.

- **The Standard Deviation (σ)**

The standard deviation of (x) denoted by (σ), given by.

$$\sigma = \sqrt{\frac{\sum_1^n (x_i - \bar{x})^2}{n-1}} \qquad \text{……………………………... (E.1)}$$

- **The standard error or the error in the mean (σ_m)**

The standard deviation of the mean. It is also called the standard error is denoted by (σ_m) given by:

$$\sigma_m = \frac{\sigma}{\sqrt{n}} \qquad \text{……………………………... (E.2)}$$

The true measured value of (*x*) given by.

$$\boldsymbol{x = \bar{x} + \sigma_m = \bar{x} \pm \frac{\sigma}{\sqrt{n}}} \qquad \text{……………………………... (E.3)}$$

The uncertainties

The error analysis in experimental measurements is important. So, the measured data by the temperature sensors for 3 experiments of 7 thermocouples and two pressure sensor is presented in Table (E-1).

After applying the above-mentioned equations to the measured data listed in Table (B-1), the mean (average value, standard deviation and the standard error will be obtained and tabulated also in Table (E-1).

Table (E-1) repeatability and Uncertainty Analysis of the experimental measured data

variable	Reading of parameter			x_m	σ	σ_m	x	Percentage uncertainty
	x_1	x_2	x_3					
T_1	50.4	50.2	49.9	50.17	0.25	0.14	50.31 50.02	±0.29%
T_2	25.3	25.1	24.9	25.1	0.2	0.11	25.21 24.98	±0.46%
T_3	24.8	25.2	25	25	0.2	0.11	25.11 24.88	±0.46%
T_4	33.1	32.3	31.6	32.33	0.75	0.43	32.76 31.9	±1.34%
T_5	50.3	50	49.8	50.03	0.25	0.14	50.17 49.88	±0.29%
T_6	38.1	39.6	38.7	38.8	0.75	0.43	39.23 38.36	±1.12%
T_7	23.5	23.5	23.5	23.5	0	0	23.5 23.5	0.00%
P1	2489.64	2467.9	2446.2	2467.91	21.72	12.54	2480.45 2455.373	±0.51%
P_2	430.85	415.47	402.14	416.15	14.36	8.29	424.44 407.85	±1.99%

Sample of The Uncertainty Calculation

There is no doubt that the maximum portion of errors in calculations referred essentially to the errors in the measured quantities. Hence, to calculate the error in the obtained results, Kline and McClintock method **[Kline and McClintock, 1934]** is used in this field.

Let the result R be a function of an independent variables v_1, v_2 … v_n

$R=R\ (v_1, v_2 \ldots\ldots\ldots v_n)$ …………………………….... (E.3)

For small variations in the variables, this relation can be expressed in a linear form as:

$$\delta R = \frac{\partial R}{\partial v_1}\delta v_1 + \frac{\partial R}{\partial v_2}\delta v_2 + \ldots\ldots\ldots + \frac{\partial R}{\partial v_n}\delta v_n$$ …………………………... (E.4)

Hence, the uncertainty interval (w) in the result can be given as

$$w_R = \left[\left(\frac{\partial R}{\partial v_1}w_1\right)^2 + \left(\frac{\partial R}{\partial v_2}w_2\right)^2 + \ldots\ldots\ldots\ldots + \left(\frac{\partial R}{\partial v_n}w_n\right)^2\right]^{1/2}$$ ……………..... (E.5)

Equation (B.5) is greatly simplified upon dividing by R to non-dimensionalize

$$\left(\frac{w_R}{R}\right)^2 = \left(\frac{\partial R}{\partial v_1}\frac{w_1}{R}\right)^2 + \left(\frac{\partial R}{\partial v_2}\frac{w_2}{R}\right)^2 + \ldots\ldots\ldots\ldots + \left(\frac{\partial R}{\partial v_n}\frac{w_n}{R}\right)$$ ……………..... (E.6)

The local Nusselt number equation can be written as follows

$$Nu = \frac{q.D}{(T_S - T_C)\ A\ \kappa}$$ ……………..... (E.7)

$$Nu = \frac{q\ D}{(T_h - T_C)\ A\ \kappa}$$ ……………..... (E.8)

The experimental error in the local Nusselt number calculation can be expressed in the following manner:

$$\frac{\partial Nu}{\partial q} = \frac{D}{(T_S - T_\infty)\ A\ \kappa}$$ ……………..... (E.9)

$$q = V\ I$$ ……………..... (E.10)

$$dq/dI = V$$ ……………..... (E.11)

$$dq/dV = I$$ ……………..... (E.12)

So,

$$\frac{\partial Nu}{\partial I} = \frac{VD}{(T_S - T_C)\, A\, \kappa} \qquad \text{……………...... (E.13)}$$

$$\frac{\partial Nu}{\partial D} = \frac{VI}{\Delta T A \kappa} \qquad \text{……………...... (E.14)}$$

$$\frac{\partial Nu}{\partial \Delta T} = -\frac{VID}{(\Delta T)^2 A \kappa} \qquad \text{……………...... (E.15)}$$

$$\frac{\partial Nu}{\partial A} = -\frac{VID}{\Delta T A^2 \kappa} \qquad \text{……………...... (E.16)}$$

$$w_{Nu} = \left[\left(\frac{\partial Nu}{\partial V} w_V\right)^2 + \left(\frac{\partial Nu}{\partial I} w_I\right)^2 + \left(\frac{\partial Nu}{\partial D} w_D\right)^2 + \left(\frac{\partial Nu}{\partial \Delta T} w_{\Delta T}\right)^2 + \left(\frac{\partial Nu}{\partial P} w_P\right)^2 + \left(\frac{\partial Nu}{\partial m} w_m\right)^2\right]^{\frac{1}{2}} \qquad \text{……………...... (E.17)}$$

or,

$$\left[\frac{w_{Nu}}{Nu}\right]^2 = \left[\left(\frac{w_V}{V}\right)^2 + \left(\frac{w_I}{I}\right)^2 + \left(\frac{w_D}{D}\right)^2 + \left(\frac{w_{\Delta T}}{\Delta T}\right)^2 + \left(\frac{w_P}{P}\right)^2 + \left(\frac{w_m}{m}\right)^2\right] \text{... (E.18)}$$

Where,

V: volt

I: current

D: inner pipe diameter

ΔT: Temperature difference

P: pressure

m: flow rate

Hence, the experimental errors that may happen due to the implementation of the variables are given in Table (E-2) which are taken from the measuring devices as follows in table (E-3).

Table (E-2) Uncertainties of Measuring Devices.

INDEPENDENT VARIABLES (V)	UNCERTAINTY INTERVAL "TAKEN FROM THE MEASURING DEVICES" (W) %
Temperature difference	± 0.004 ºC
Voltage of the heater	± 0.009 volt
Current of the heater	± 0.05425 Amp
diameter	± 0.0002 m
The pressure gauge	± 0.002 pa
Flow meter	±0.005 L/min

Table (E-3) Uncertainties of Nusselt number.

Hot fluid flow rate (L/min)	Air flow rate (L/hr)	Nusselt number	Percentage uncertainty
8	0	140.86	0.004%
10	0	146	0.0039%
12	0	148.9	0.0039%
14	0	154.27	0.0038%
8	480	148.81	0.0039%
10	480	153.3	0.0038%
12	480	157.44	0.0037%
14	480	162.08	0.0037%

Appendix F

Data Analysis

Experimental Calculation

1. **Overall heat transfer coefficient**

The average heat transfer rate (Q_{ave}) in a double pipe heat exchanger can be calculated with.

1. Heat transferred by Hot to Cold Water

$$Q_h = \mathring{m}_h \times C_{p.h} \times (T_{h.in} - T_{h.out}) \tag{F-1}$$

2. Heat Transferred by Cold to Hot Water

$$Q_C = \mathring{m}_c \times C_{p.c} \times (T_{c.out} - T_{c.in}) \tag{F-2}$$

3. Average Heat Transfer

$$Q_{ave} = \frac{Q_c + Q_h}{2} \tag{F-3}$$

4. Area of inner tube

$$A_i = \pi D_i L_i \tag{F-4}$$

5. Area of annulus tube

$$A_O = \pi D_o L_o \tag{F-5}$$

6. Logarithmic mean temperature deference

For parallel flow arrangement

$$LMTD_{PF} = \frac{\Delta T_1 - \Delta T_2}{ln\,[\Delta T_1/\Delta T_2]} \tag{F-6}$$

Where: $\Delta T_1 = T_{h.in} - T_{c.in}$; $\Delta T_2 = T_{h.out} - T_{c.out}$

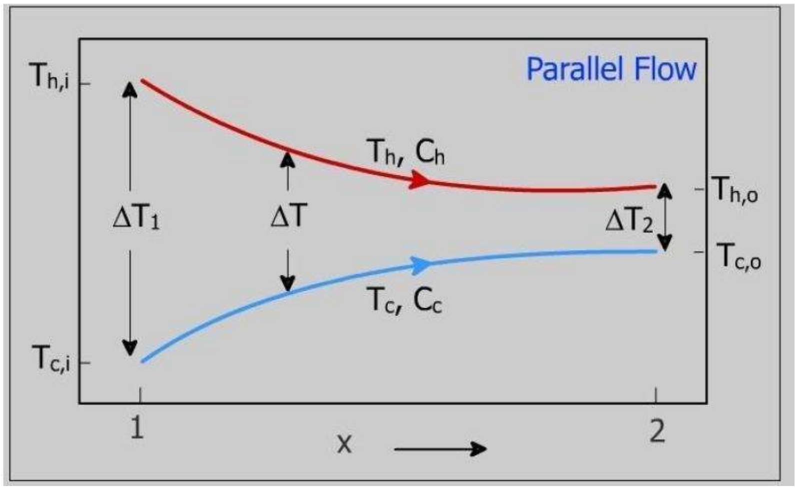

For counter flow arrangement

$$LMTD_{CF} = \frac{\Delta T_1 - \Delta T_2}{ln\,[\Delta T_1/\Delta T_2]} \tag{F-7}$$

Where: $\Delta T_1 = T_{h.in} - T_{c.out}$; $\Delta T_2 = T_{h.out} - T_{c.in}$

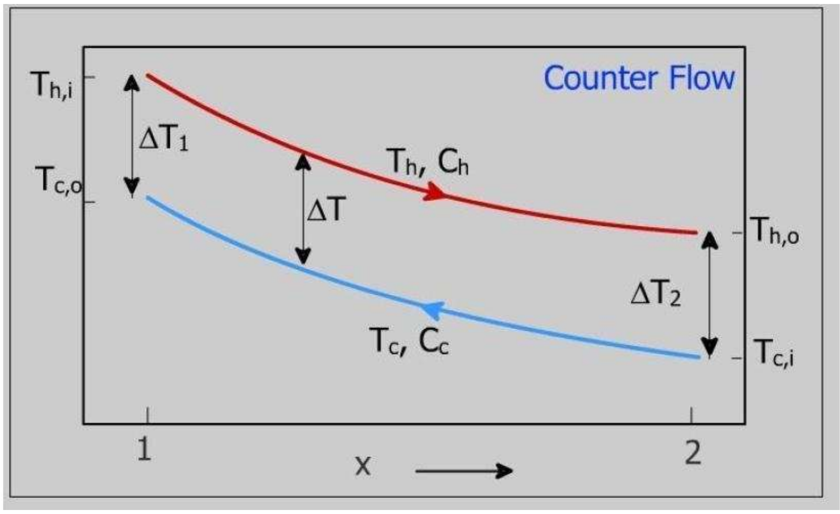

7. Overall heat transfer coefficient (annulus side)

$$U_o = \frac{Q_{ave}}{A_o LMTD} \tag{F-8}$$

8. Overall heat transfer coefficient (tube side)

$$U_i = \frac{Q_{ave}}{A_i LMTD} \tag{F-9}$$

For double pipe heat exchangers without considering the fouling factor term the below equation is used:

$$\frac{1}{U_i\, A_i} = \left[\frac{1}{h_o A_o}\right] + \left[\frac{ln(\frac{D_0}{Di})}{2\,\pi\, k\, L}\right] + \left[\frac{1}{h_i A_i}\right] \tag{F-10}$$

Where $\mathbf{U_o}$, $\mathbf{U_i}$ is the overall heat transfer coefficients for annulus side and tube side,

k is the thermal conductivity of tube material and L is the length of the heat exchanger.

The annulus heat transfer coefficient ($\mathbf{h_o}$) is calculated based on the **Gnielinski [21]** and the expression is given below:

$$Nu_0 = \frac{\left(\frac{f}{2}\right)(Re - 1000\,)\,Pr}{1.07 + 12.7\left(\frac{f}{2}\right)^{0.5}\ (Pr^{\,2/3} - 1\,)} \tag{F-11}$$

$\boldsymbol{f} = (\mathbf{1.58\,ln}(\boldsymbol{Re})\ \mathbf{3.82})^{-\mathbf{2}}$ 2300 < Re < 10^6 , 0.5 < Pr < 2000 for single phase

$\boldsymbol{f} = ((\mathbf{0.0925} * \mathbf{Re}^{-0.2534}) + ((\mathbf{13.98} * \mathbf{Re}^{-0.9501}) - (\mathbf{0.0925} * \mathbf{Re}^{-0.2534})))/$
$((\mathbf{1} + \left(\frac{\mathbf{Re}}{\mathbf{293}}\right)^{\mathbf{4.864}})^{\mathbf{0.1972}}$ for two-phase flow

The obtained Nusselt number value from Eq. (C-11) is used to calculate the annulus heat transfer coefficient and the expression is given below:

$$h_o = \frac{Nu_0 \times k_o}{D_h} \tag{F-12}$$

Where ***Dₕ*** is the hydraulic diameter and k_o is the thermal conductivity of annulus fluid.

$$D_{\mathrm{h}} = \frac{4A}{p} = (\,D_0 - D_i\ )$$

Where A is the flow area i.e., $A = \frac{\pi}{4}\left(D_0^2 - D_i^2 \right)$

The $\boldsymbol{h_o}$ value from Eq. (F-12) is substituted in Eq. (F-10) for obtaining the tube side heat transfer coefficient (h_i or h_{nf}). That is the only unknown value in the equation. The value of Nu_{nf} can be determined as follows:

$$Nu_{nf} = \frac{h_{nf} \times D_i}{k_{nf}} \tag{F-13}$$

The Reynolds number is based on the flow rate at the inlet of the tube.

$$Re_{nf} = \frac{\rho_{nf} v D_i}{\mu_{nf}} \tag{F-14}$$

The Prandtl number is calculated based on the specific heat, thermal conductivity, and viscosity of nanofluids at mean temperature of the fluid.

$$Pr_{nf} = \frac{cp_{nf}\mu_{nf}}{k_{nf}} \tag{F-15}$$

The experimental friction factor is calculated based on the pressure difference between the entrance and exit of the tube and the expression is given below:

$$f = \frac{\Delta P}{\frac{L_i}{D_i} \times (\frac{v^2 \rho_{nf}}{2})} \tag{F-16}$$

Where: ΔP (pressure drop) = $P_1 - P_2$

2. Effectiveness – NTU method

1. Number of transfer units:

$$NTU = \frac{U \times A}{C_{min}} \Longrightarrow NTU = \frac{Q}{(\Delta T)_{LMTD} \times C_{min}} \tag{F-17}$$

2. Heat capacity of tube side fluid:

$$C_h = \mathring{m}_h \times C_{p.h} \tag{F-18}$$

3. Heat capacity of annulus side fluid:

$$C_C = \mathring{m}_C \times C_{p.C} \tag{F-19}$$

Where C_{min} is the smaller of C_h and C_C

4. Effectiveness:

$$\varepsilon = \frac{1 - exp\,[-NTU\,(1 - Z)]}{1 - Z\,exp\,[-NTU\,(1 - Z)]} \tag{F-20}$$

Where:

$$\boldsymbol{Z} = \frac{\boldsymbol{C_{min}}}{\boldsymbol{C_{max}}} \tag{F-21}$$

3. Pumping Power Calculation

The pumping power which is needed to drive the nanofluid in double pipe heat exchanger is defined according [93] to as:

$$\text{Pumping power} = \Delta P \times Q \tag{F-22}$$

Where ΔP is the pressure drop along the inner pipe and $\dot{V}$ is the volumetric flow rate.

$$Z = \frac{C_h}{C_c}$$

$$\text{Effec} = \frac{1 - S}{1 - Z \cdot S}$$

$$S = \mathbf{exp}\left[- \text{NTU} \cdot (1 - Z)\right]$$

$$E_h = T_e \cdot \dot{m}_h \cdot C_{ph} \cdot \mathbf{ln}\left[\frac{T_{ho}}{T_{hi}}\right]$$

$$E_c = T_e \cdot \dot{m}_c \cdot C_{pc} \cdot \mathbf{ln}\left[\frac{T_{co}}{T_{ci}}\right]$$

$$E = E_h + E_c$$

$$e_{dimensionless} = \frac{E}{T_e \cdot C_{min}}$$

$$T_e = 25$$

$$vf = \frac{\dot{V}_a}{\dot{V}_a + \dot{V}_f}$$

Appendix G

Publication of the PhD Thesis

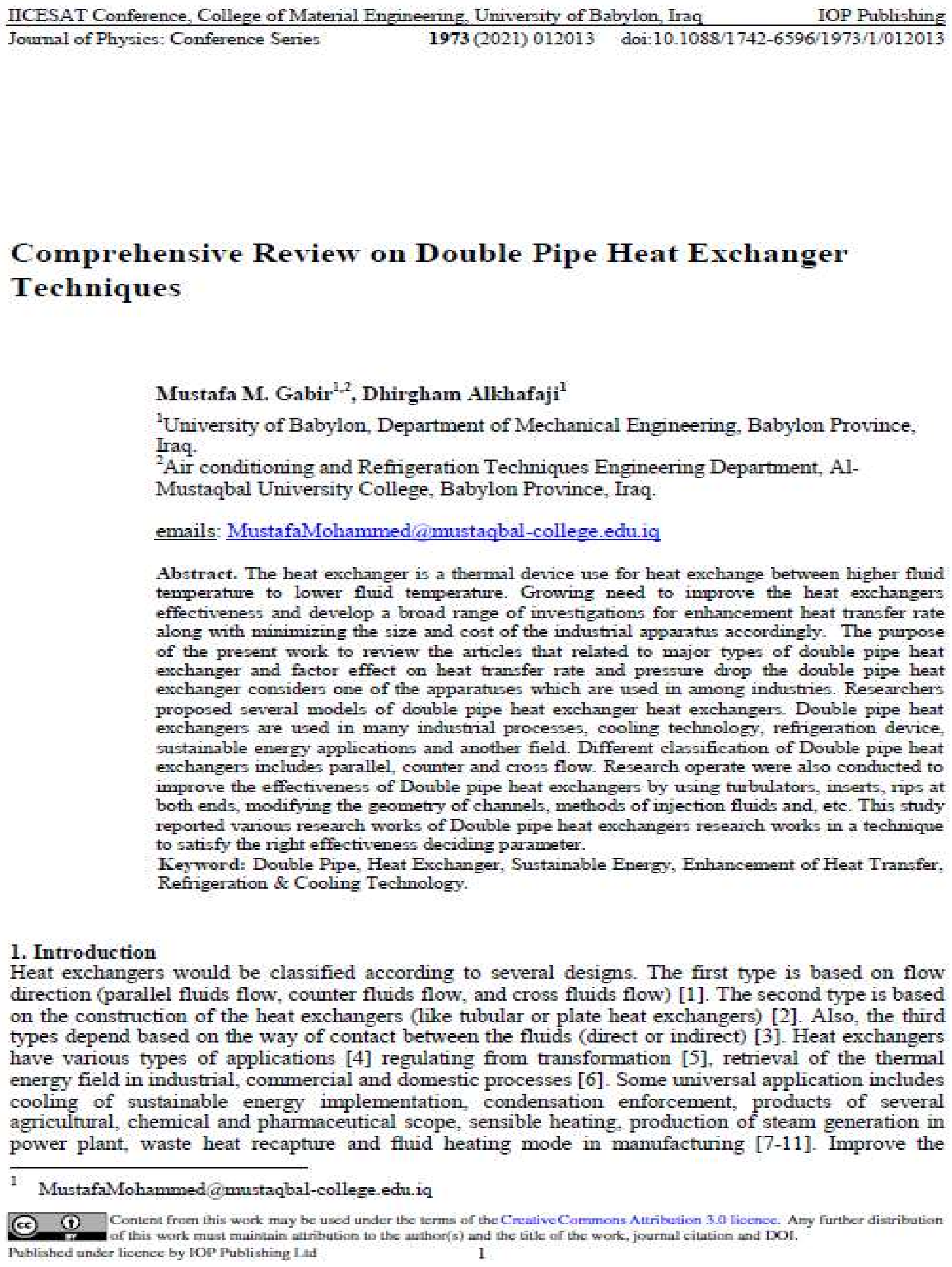

IICESAT Conference, College of Material Engineering, University of Babylon, Iraq IOP Publishing
Journal of Physics: Conference Series **1973** (2021) 012013 doi:10.1088/1742-6596/1973/1/012013

Comprehensive Review on Double Pipe Heat Exchanger Techniques

Mustafa M. Gabir[1,2], **Dhirgham Alkhafaji**[1]
[1]University of Babylon, Department of Mechanical Engineering, Babylon Province, Iraq.
[2]Air conditioning and Refrigeration Techniques Engineering Department, Al-Mustaqbal University College, Babylon Province, Iraq.

emails: MustafaMohammed@mustaqbal-college.edu.iq

Abstract. The heat exchanger is a thermal device use for heat exchange between higher fluid temperature to lower fluid temperature. Growing need to improve the heat exchangers effectiveness and develop a broad range of investigations for enhancement heat transfer rate along with minimizing the size and cost of the industrial apparatus accordingly. The purpose of the present work to review the articles that related to major types of double pipe heat exchanger and factor effect on heat transfer rate and pressure drop the double pipe heat exchanger considers one of the apparatuses which are used in among industries. Researchers proposed several models of double pipe heat exchanger heat exchangers. Double pipe heat exchangers are used in many industrial processes, cooling technology, refrigeration device, sustainable energy applications and another field. Different classification of Double pipe heat exchangers includes parallel, counter and cross flow. Research operate were also conducted to improve the effectiveness of Double pipe heat exchangers by using turbulators, inserts, rips at both ends, modifying the geometry of channels, methods of injection fluids and, etc. This study reported various research works of Double pipe heat exchangers research works in a technique to satisfy the right effectiveness deciding parameter.

Keyword: Double Pipe, Heat Exchanger, Sustainable Energy, Enhancement of Heat Transfer, Refrigeration & Cooling Technology.

1. Introduction

Heat exchangers would be classified according to several designs. The first type is based on flow direction (parallel fluids flow, counter fluids flow, and cross fluids flow) [1]. The second type is based on the construction of the heat exchangers (like tubular or plate heat exchangers) [2]. Also, the third types depend based on the way of contact between the fluids (direct or indirect) [3]. Heat exchangers have various types of applications [4] regulating from transformation [5], retrieval of the thermal energy field in industrial, commercial and domestic processes [6]. Some universal application includes cooling of sustainable energy implementation, condensation enforcement, products of several agricultural, chemical and pharmaceutical scope, sensible heating, production of steam generation in power plant, waste heat recapture and fluid heating mode in manufacturing [7-11]. Improve the

---

[1] MustafaMohammed@mustaqbal-college.edu.iq

IICESAT

Date: May 2, 2022
Paper ID: IICESAT_253

LETTER OF ACCEPTANCE

Dear Authors,

On behalf of the IICESAT | ICMAICT -22 Scientific Committee, and based on the reviewers' evaluation after double blind peer review Process and Guest Editors' Preliminary approval we are pleased to inform you that your paper entitled:

" Using Magnesium Oxide MgO Nanoparticles to Enhance Heat Transfer in a Double Pipe Heat Exchanger: A CFD study "

Written By

Mustafa M. Gabir, Dhirgham Alkhafaji

Has been accepted and will be processed for possible publication in AIP Conference Proceedings (ISSN: 0094-243X, 1551-7616). It is our pleasure to invite you to attend 4th International Scientific Conference of Engineering Sciences and Advances Technologies (IICESAT) will be held By Iraq Academic Syndicate on 7-8 May, 2022, to present your paper. We congratulate you for your achievement, the technical details about the publication will be informed later. Remember that, the paper should follow accurately our reviewer comments, and the technical notes which has been sent earlier. The publication of the accepted paper will be provided after passing the Internal Check of AIP Editors, and the paper should not contain plagiarism till that date more than 15%, and the content also follow our conference Guidelines and template. Publication time it depends on Publisher process and we will provide to your after we held our conference.

We Will encourage more quality submissions from you and your colleagues in future

Regards

Shubham Sharma

Prof. Dr. Shubham Sh. Sharma
IICESAT II ICMAICT Conference Guest Editor

CAUTION: This Acceptance Letter Made by IICESAT / ICMAICT Conference Guest Editors, All Approval and other Inquiries Should be addressed to Conference Editorial Board and Patrons Committee, as all Accepted Papers will Process for Possible Publication in AIP Conference Proceedings, and Final Decision upon Publish of your/s Paper will be Made by AIP Publication Editors Only after Review the Paper Contents and Writing Quality.

الخلاصه

يتم أختبار الموائع النانوية بتركيزات مختلفة من أكسيد المغنيسيوم (MgO) وكاربوكسي ميثيل السليلوز (CMC) في مبادل حراري مزدوج الانابيب والمصمم مع انحناء U ومثبت بصوره افقية لتحسين اداءه وحسب اتجاه الجريان المتوازي والمتعاكس تحت تأثير الجريان الأحادي والثنائي الطور. تمت الدراسة عند معدل تدفق حجمي (8، 10، 12 و14) لتر / دقيقة من الماء النقي، سائل (Water-CMC) بتراكيز وزنية من CMC (0.2٪ و0.5٪)، سائل (Water-MgO) بتراكيز حجمية من جزيئات MgO النانوية (0.125) ٪، 0.25٪، 0.5٪ و1٪) وسائل (Water-MgO-CMC) بنفس التركيزات السابقة.

تعرض هذه الدراسة تأثير الجريان ثنائي الطور بأنظمة جريان مختلفه في الجانب الحلقي للمبادل الحراري على معدل انتقال الحرارة. تم تشخيص ثلاثة أنواع من أنظمة الجريان ، الجريان الفقاعي (bubbly flow) و الجريان الدفعي (slug flow) و الجريان الطباقي (stratified flow)، عند حقنها 24 لترًا / دقيقة من الماء مع (360 ، 420 ، 460) لتر / ساعة من الهواء في الجانب الحلقي.

تم تنفيذ العمل التجريبي باستخدام مبادل حراري مزدوج الأنابيب مع انحناء U ، مصنوع من أنابيب متحدة المركز بطول 5 م. تم اختيار أنبوب نحاسي بقطر داخلي 20 ملم وقطر خارجي 22 ملم كأنبوب داخلي ، وأنبوب برسبيكس بقطر داخلي 45 ملم وقطر خارجي 50 ملم تم اختياره كأنبوب خارجي. تشمل الدراسة التجريبية أيضًا تحضير الموائع النانوية وقياس خصائص التوصيل الحراري للسوائل الساخنة واللزوجة والكثافة والحرارة النوعية.

تم بناء دراسة المحاكاة بتقنية CFD بناءً على نموذج حجم السائل (VOF) للجريان متعدد الأطوار باستخدام الكود التجاري ANSYS Fluent 2020 R1. تم استخدام هذا الكود للتنبؤ بدرجة الحرارة والضغط والسرعة وجزء الفراغ من الجريان ثنائي الطور على طول المبادل

الحراري للأنابيب المزدوجة على شكل حرف U. يتم تحقيق ذلك عدديًا من خلال حل مجموعة من المعادلات التفاضلية الجزئية، وهي الحفاظ على الكتلة والزخم والطاقة. هذه المعادلات خطية ومحددة ويتم حلها بطريقة الحجم المحدود في المحلل للحصول على حل مفصل، بما في ذلك الحدود المطلوبة في مجال الجريان، والتحقق من صحة البيانات التجريبية.

أشارت النتائج إلى أن معامل انتقال الحرارة بالحمل الحراري (h) قد زاد بزيادة التراكيز الوزنية لجسيمات CMC والتراكيز الحجمية لجسيمات MgO ومعدل جريان السائل الساخن الحجمي. يتحسن معامل انتقال الحرارة بالحمل الحراري من (2532.4) عند 8 لتر / دقيقة إلى (2771.71) 14 لتر / دقيقة وبعد إضافة (1% MgO vol.+0.5% CMC wt.) ازداده من (5062.57) عند 8 لتر / دقيقة إلى (5545.24) 14 لتر / دقيقة. زاد معامل الاحتكاك مع زيادة التراكيز الوزنية لجسيمات CMC، والتراكيز الحجمية لجسيمات MgO، وينخفض مع زيادة معدل جريان السائل الساخن الحجمي.

اعتمادًا على تأثير الجريان ثنائي الطور ومعدل الجريان الحجمي ، عندما يزداد معدل جريان الهواء الحجمي يؤدي الى زيادة معامل انتقال الحرارة بالحمل الحراري حوالي 8٪. عندما زاد معدل جريان الهواء أدى لزيادة قيمة فعالية المبادل الحراري حوالي 9٪. معامل انتقال الحرارة الإجمالي للجريان المتعاكس أعلى بنسبة 4-6٪ من الجريان المتوازي عند إضافة (1% MgO vol.+0.5% CMC wt.) إلى الماء النقي.

أخيرًا، تم إجراء مقارنة بين النتائج العددية والتجريبية للسائل النيوتوني (ماء نقي) بمعدل تدفق 8 و10 و12 و14 لتر/دقيقة. هناك اتفاق ممتاز بين النتائج العددية والتجريبية (بحد أقصى انحراف 7٪ في رقم نسلت) للعمل الحالي إلى جانب اتفاقيات جيدة جدًا في اتجاهات وقيم النتائج المستخرجة من محاكاة CFD للعمل الحالي مع ما حصل عليها باحثون مهمون.

وزارة التعليم العالي والبحث العلمي
جامعة بابل
كلية الهندسة
قسم الهندسة الميكانيكية

تحسين أداء مبادل حراري مزدوج الانبوب بأستخدام مائع نانوي (MgO-CMC/ماء) مع جريان ثنائي الطور

أطروحة
مقدمة الى كلية الهندسة / جامعة بابل كجزء من متطلبات نيل درجة دكتوراه فلسفة في الهندسة / الهندسة الميكانيكية / قدرة

من قبل

مصطفى محمد جابر رديد

بإشراف

الأستاذ الدكتور ضرغام الخفاجي

1444هـ **2023 م**